PUBLICATIONS
OF
DEBRECEN
HELIOPHYSICAL OBSERVATORY
OF THE
HUNGARIAN ACADEMY OF SCIENCES

VOLUME 7

THE DYNAMIC SUN

Proceedings of the EPS 6th European Solar Meeting
held in Debrecen, May 21–24, 1990

DEBRECEN
1990

PUBLICATIONS
OF
DEBRECEN
HELIOPHYSICAL OBSERVATORY
OF THE
HUNGARIAN ACADEMY OF SCIENCES

VOLUME 7

THE DYNAMIC SUN

Proceedings of the 6th European Meeting on Solar Physics
held in Debrecen, May 21-24,1990

The meeting was organized by the
Solar Physics Section of the European Physical Society
in co-operation with the
Debrecen Heliophysical Observatory
under the sponsorships of the
Hungarian Academy of Sciences and its Debrecen Academy Committee

DEBRECEN
1990

EDITOR:

L. D E Z S Ő

Heliophysical Observatory
Hungarian Academy of Sciences
H-4010 D E B R E C E N
HUNGARY

ISSN 0209-7567

(Publ.Debrecen Obs., Volume 7, pages 312)

CONTENTS

PREFACE

The Sixth European Meeting on Solar Physics was organized by the Solar Physics Section /of the Astronomy and Astrophysics Division/ of the European Physical Society (EPS). The 1989 Board of the Section was acting as the Scientific Organizing Committee of the meeting:

W.Mattig, Freiburg (Chairman)
A.O.Benz, Zürich (Secretary and Treasurer)
P.Ambrož, Ondřejov
F.Chiuderi-Drago, Firenze
L.Dezső, Debrecen
F.-L.Deubner, Würzburg
G.Godoli, Firenze
D.O.Gough, Cambridge
P.Hoyng, Utrecht
E.R.Priest, St.Andrews
A.Righini, Firenze
B.Schmieder, Meudon
G.Trottet, Meudon

The Board decided to hold its sixth triennial meeting in the eastern part of Europe in order to facilitate and encourage new scientific contacts and co-operations among solar physicists from the whole of Europe.

The previous five European meetings organized by the EPS Solar Physics Section were as follows:

No	Year	Place	Title	Local Organizer	Sponsors & co-sponsors
1	1975	Firenze	First European Solar Meeting	Oss.Astrofis. di Arcetri, Firenze	Consiglio Nazionale delle Richerche
2	1978	Toulouse	Highlights in Solar Physics	Obs.Toulouse et du Pic du Midi	Centre National de la Recherche Sci.
3	1981	Oxford	Solar Activity	Oxford Univ.Depts; Rutherford-Appleton Lab.	Royal Astronomical Society
4	1984	Noordwijkerhout	Hydromagnetics of the Sun	Obs.Sonnenborgh; Space Res.Lab., Utrecht	R.Netherlands Acad.; European Space Ag.; Utrecht Univ.
5	1987	Titisee	Solar and Stellar Phys.	Kiepenheuer-Inst. für Sonnenphys., Freiburg	D.Forschungsgemeinsch.; Ministerium für Wiss. Baden-Würtenberg

The Board asked the Debrecen Heliophysical Observatory to act as the local organizer of the 6th EPS solar meeting.

The staff of the Debrecen Heliophysical Observatory considered it a great honour that the local organization of this meeting was put into their hands.

The meeting was held in Debrecen from 21 to 24 May,1990, at the headquarters of the Debrecen Academy Committee, not far from the site of the Heliophysical Observatory, which is located on the university campus, in spite of the fact that the Heliophysical Observatory, with its observing station in Gyula, formally belongs to the Astronomical Research Institute of the Hungarian Academy of Sciences, Budapest.

Since in the last years Hungary has been in a very grave economic situation, the Hungarian Academy of Sciences could give only very limited financial assistance to the meeting. Therefore, it was necessary to cover the expenses practically from the registration fees collected. Waiver of registration fee could be assigned only to six participants. Otherwise there were no funds available to give aid to young participants either. No doubt this was the reason why the number of participants was about half as large as was expected from the affirmative answers to the First Announcement. Although there is no hindrance in travelling any more, the financial problem grew even worse after the great political changes of 1989 in the East European countries. Finally, the total number of participants was 97 (one from Mexico, all the others from Europe).

For the meeting a broad scientific programme had been proposed under the general theme THE DYNAMIC SUN in order to cater to a large fraction of the solar community. The range of the selected scientific topics was very broad focusing on those of current interest in the structure and dynamics of the solar atmosphere. Research in this area is actively being pursued across Europe with important recent progress and consequently, it was a very appropriate theme for this conference. It was clearly not possible to focus on every aspect of solar physics, therefore the processes in the Sun's interior and also the solar wind have been excluded as these have been adequately covered in recent meetings.

The meeting passed off without any formal ceremony. In place of this at the beginning a few words were said by Béla Szeidl, Director of the Astronomical Research Institute, who extended a welcome to the participants and by Wolfgang Mattig, who as Chairman declared the meeting open.

The programme was divided into six half-day sessions, each consisting of one or two invited reviews, a small number (3-5) of oral contributions and poster contributions with a brief (in general 2-minute) oral presentation, which could also be illustrated with one slide or transparency. The poster-exposition, in the coffee area, was open all day long during the whole 4-day meeting.

The six sessions were organized by their chairmen and were specified as follows:

Session	T O P I C	C h a i r m a n
1	Large-Scale Motions	P.Ambrož
2	Patterns of Activity	H.Wöhl
3	Magnetohydrodynamic (MHD) Processes	E.R.Priest
4	Particle Acceleration and Non-Thermal Emissions	A.O.Benz
5	Spectroscopy of the Upper Atmosphere	Ph.Lemaire
6	Waves in Active Regions	J. Staude

Contributions accepted by the chairmen for presentation at the meeting, well in advance (by 3-4 months), fit into one of the six half-day sessions listed above. In order to do so one--page abstracts of contributions have been submitted to the chairman of the appropriate session, who selected the oral and poster contributions. However, for the final versions of the papers, published in this Proceedings, the authors bear all responsibility (even for the English used). A paper is included in this volume only if the author, or one of its co-authors presented it at the meeting and the camera-ready paper reached the editor not later than August 3,1990. (Conference proceedings can only command interest if they are published in a short time, but this requirement can only be met through the dead--line given.)

The present Proceedings unfortunatelly do not contain in full all 10 invited reviews given at the meeting. (Herewith you find 7 complete review papers and the extended abstracts of 3 others.) The number of the presented oral and poster contributions was altogether 77 and 70 of them are included in this volume. An oral contribution fills in print generally 4 pages, while a poster paper (with five exceptions) 2 pages.The content of the often intense discussions of oral presentation could not be included in the Proceedings.

The six half-day sessions practically filled out three whole days of the 4-day meeting. On the third day an all day excursion was organized to Eger, to visit, among other things, the remnant of the prematurely miscarried university observatory of the 18 century, which at present is, in some respects, patronized by the Debrecen Heliophysical Observatory. The excursion and, on the other days, the pre-ordered common meals for participants were mainly organized with a view to give possibilities for detailed extra and informal discussions.

All participants were invited to the Open Business Meeting of the EPS Solar Physics Section. It was held on the second meeting day in the evening. As the last item of the Business Meeting (of 2-hour duration) some new Board members were also elected.

Kluwer Academic Publishers (Dordrecht, The Netherlands) offered a prize for outstanding work in the field of solar physics. The prize consists in the form of a free subscription to the journal *Solar Physics* for three years. The Board of the Solar Physics Section had decided to select the prize winner from the young contributors to the 6th European Meeting on Solar Physics. A sub-committee of the Board, consisting of C.Chiuderi,W.Mattig and Y.D.Zhugzhda, undertook the task to select the winner. They considered three authors equally worthy of the award and made known their decision at the closing of the meeting. By courtesy of the Publishers all three honoured were granted the prize. The list of awards: Lidia van Driel-Gesztelyi (Debrecen-Utrecht), Peter J.I.De Bruyne (St.Andrews) and Bernhard Fleck (Würzburg).

On behalf of all Participants grateful acknowledgements are due to the scientific organizers of the meeting and especially to the session chairmen: P.Ambrož, H.Wöhl, E.R.Priest, A.O.Benz, Ph.Lemaire and J.Staude, who took the main burden of the scientific organization for quite a time before the meeting, as well as during the sessions stimulating the discussion periods.Their effort was crucial to the success of the meeting, but non the less important was the contribution of those who prepared and delivered the reviews: H.Wöhl, I.Tuominen, C.Zwaan, C.Chiuderi, G.Trottet, L.Vlahos, J.Sylwester, H.E.Mason, F.Kneer and Y.D. Zhugzhda. Sincere thanks are due to them, too.

The scientific personnel of the Debrecen Heliophysical Observatory was acting as the Local Organizing Committee and, as its chairman, I express my thanks to them and to the whole staff of the Observatory sharing in the arrangement of the meeting.

Last but not least, my special thanks are due to Arnold O. Benz for his valuable and continuous assistance in all sorts of problems from the very beginning of the organizing period, as well as during and even after the meeting up till now.

This volume was prepared to press by Ágnes Kovács.

Debrecen, August 3,1990

L.Dezső

LIST OF PARTICIPANTS

ABOUDARHAM, Jean, Observatoire de Paris, Meudon
ABUZEID, Bashir, Astr.Dept.,Univ., Budapest and Benghazi
ALTAS, Levent, Kandilli Observatory, Istanbul
ALY, Jean-Jacqes, Service d'Astrophys.,CEN-Saclay, Gif-sur-Yvette
AMBROŽ, Pavel, Astr.Inst.,Acad., Ondřejov
ARENA, Placido, Arcetri Astrophys.Obs., Firenze
AUFFRET, Hervé, Observatoire du Pic-du-Midi
BALLESTER, Jose Luis, Phys.Dept.,Univ.Balears, Palma de Mallorca
BARANYI, Tünde, Heliophys.Obs.,Acad., Debrecen
BELVEDERE, Geatano, Astr.Inst.,Univ., Catania
BELY-DUBAU, Francoise, Observatoire de Nice
BENZ, Arnold O., Astr.Inst.,ETH, Zürich
BONANDER, Kjell, Stockholm Obs., Saltsjöbaden
BUMBA, Vaclav, Astr.Inst.,Acad., Ondřejov
CHIUDERI, Claudio, Astr. and Space Sci.Dept.,Univ., Firenze
CHIUDERI-DRAGO, Franca, Astr. and Space.Dept.,Univ., Firenze
CSEPURA, György, Heliophys.Obs.,Acad., Debrecen
CUGNON, Pierre, Observatoire R. de Belgique, Bruxelles
DE BRUYNE, Peter J.I., Maths.Dept.,Univ., St.Andrews
DEUBNER, Franz-L., Astr. and Astrophys.Inst.,Univ., Würzburg
DEZSŐ, Loránt, Heliophys.Obs.,Acad., Debrecen
DUMITRACHE, Christiana, Astr.Inst.,Acad., Bucuresti
EDWIN, Patricia, Maths.Dept.,Univ., St.Andrews
ERDÉLYI, Róbert, Astr.Dept.,Univ., Budapest
FAUROBERT-SCHOLL, Marianne, Observatoire de Nice
FIEDLER, Russel, Maths.Dept.,Univ., St.Andrews
FLECK, Bernhard, Astr. and Astrophys.Inst.,Univ., Würzburg
FLUDRA, Andrzej, Mullard Space Sci.Lab.,Univ., Dorking
FOING, Bernard H., Space Sci.Dept.,ESA/ESTEC, Noordwijk
GABRIEL, Alan, Inst.Astrophys.Spatiale, Verrières-le-Buisson
GALINDO TREJO, Jesus, Astr.Inst.,Univ., Mexico

GALSGAARD, Klaus, Astr.Obs.,Univ., København
GARCIA DE LA ROSA, J.Ignacio, Astrophys.Inst.Canarias, La Laguna
GERLEI, Ottó, Heliophys.Obs.,Acad., Debrecen
GREIMEL, Robert, Astr.Inst.,Univ., Graz
GURTOVENKO, Eric R., Astr.Obs.,Acad., Kiev
GYŐRI, Lajos, Obs.Station,Heliophys.Obs.,Acad., Gyula
HANSLMEIER, Arnold, Astr.Inst.,Univ., Graz
HEINZEL, Petr, Astr.Inst.,Acad., Ondřejov
HERMANS, Dirk F.M., Maths.Dept.,Univ., St.Andrews
HOFMANN, Axel, Solar Obs.,Acad., Potsdam
HOOD, Alan, Maths.Dept.,Univ., St.Andrews
KÁLMÁN, Béla, Heliophys.Obs.,Acad., Debrecen
KARABIN, Mirjana, Astr.Inst.,Univ., Beograd
KLIEM, Bernhard, Astrophys.Inst.,Acad., Potsdam
KNEER, Franz, Univ.Obs., Göttingen
KOVÁCS, Ágnes, Heliophys.Obs.,Acad., Debrecen
KRÜGER, Albrecht , Astrophys.Inst.,Acad., Potsdam-Babelsberg
KURT, Victoria, Nucl.Phys.Inst.,Univ., Moscow
KURTHS, Jürgen, Astrophys.Inst.,Acad., Tremsdorf
LANTOS, Pierre, Observatoire de Paris, Meudon
LEMAIRE, Philippe, Inst.Astrophys.Spatiale, Verrières-le-Buisson
LUDMÁNY, András, Heliophys.Obs.,Acad., Debrecen
MALTBY, Per, Inst.Theor.Astrophys.,Univ., Oslo
MANN, Gottfried, Astrophys.Inst.,Acad., Tremsdorf
MARIK, Miklós, Astr.Dept.,Univ., Budapest
MARMOLINO, Ciro, Phys.Dept.,Univ., Napoli
MASON, Helen E., Dept.Appl.Math. and Theor.Phys.,Univ., Cambridge
MATTIG, Wolfgang, Kiepenheuer-Inst., Freiburg
McCLEMENTS, Kenneth G., Rutherford Appleton Lab., Didcot
MESSEROTTI, Mauro, Astr.Obs., Trieste
MOURADIAN, Zadig, Observatoire de Paris, Meudon
MULLER, Richard, Observatoire du Pic-du-Midi
NAGELIS, Janis, Radioastr.Obs.,Acad., Riga
NAGY, Imre, Heliophys.Obs.,Acad., Debrecen
NESIS, Anastasios, Kiepenheuer-Inst., Freiburg
NORDLUND, Åke, Astr.Obs.,Univ., København

OLIVER, Ramón, Phys.Dept.,Univ.Balears, Palma de Mallorca
ONCICA, Adrian, Astr.Inst.,Acad., Bucuresti
PETROVAY, Kristóf, Astr.Dept.,Univ., Budapest
PETTAUER, Thomas, Solar Obs.Kanzelhöhe
PINTÉR, Teodor, SCAA, Hurbanovo
POHJOLAINEN, Silja, Helsinki TechnUniv., Espoo
POQUÉRUSSE, Michel, Observatoire de Paris, Meudon
PRIEST, Eric R., Maths.Dept.,Univ., St.Andrews
RIGAUD, Dominique, Observatoire de Paris, Meudon
RUŠIN, Vojtech, Astr.Inst.,Acad., Tatranska Lomnica
RUTTEN, Robert J., Astr.Inst.,Univ., Utrecht
RUŽDJAK, Vladimir, Observatory, Hvar
SCHMIEDER, Brigitte, Observatoire de Paris, Meudon
SCHOLL, Hans, Observatoire de Nice
SEEHAFER, Norbert, Astrophys.Inst.,Acad., Potsdam-Babelsberg
SKULJAN, Jovan, Astr.Inst.,Univ., Beograd
STAUDE, Jürgen, Solar Obs.,Acad., Potsdam
STEELE, Colin D.C., Maths.Dept.,Univ., St.Andrews
STEINEGGER, Michael, Astr.Inst.,Univ., Graz
SYLWESTER, Janusz, Space Res.Centre,Acad., Wroclaw
SZEIDL, Béla, Konkoly Obs.,Acad., Budapest
TROTTET, Gerard, Observatoire de Paris, Meudon
TUOMINEN, Ilkka, Univ.Obs., Helsinki
VAN DRIEL-GESZTELYI, Lidia, H.Obs.,Acad.,Debrecen-Astr.Inst.,Univ., Utrecht
VLAHOS, Loukas, Phys.Dept.,Univ., Thessaliniki
VULETIĆ, Milan, Astr.Inst.,Univ., Beograd
WÖHL, Hubertus, Kiepenheuer-Inst., Freiburg
ZHUGZHDA, Yuzef D., IZMIRAN, Troitsk
ZLOBEC, Paolo, Astr.Obs., Trieste
ZWAAN, Cornelis, Astr.Inst.,Univ., Utrecht

SESSION 1

May 21, Monday (a.m.)

LARGE-SCALE MOTIONS

Chairman: P. AMBROŽ
Astronomical Institute of the Czechoslovak Academy of Sciences
Ondřejov

Invited reviews:

H. WÖHL
Large-Scale Motions in the Solar Photosphere
(Observational Aspects)

I. TUOMINEN
Solar Differential Rotation and its Variations

and 12 (oral and poster) contributions

LARGE - SCALE MOTIONS IN THE SOLAR PHOTOSPHERE *

(observational aspects)

H. Wöhl

(Kiepenheuer-Institut für Sonnenphysik, Schöneckstr. 6, D-7800 Freiburg, F.R.G.)

1. Introduction

The topic of this session are motions in the photosphere of the Sun on a scale exceeding the supergranules. This part of the review shall include only observations. Within the last few years several reviews on this topic or smaller or wider views of it were given in journals, conference proceedings and books (citations only after 1984), e.g. Schröter (1985), Howard (1985), Ribes (1986), Gilman (1986), Bogart (1987), Rüdiger (1989) and Stix (1989a,b).

The aim of this review is first to repeat rather briefly the known data concerning the solar rotation, its differential rotation, possible meridional and large - scale motions and torsional oscillations. I include also my personal view, but try to separate it clearly from the review. In a second part some still controversial results are given. The third and final part concentrates on some new observational and data reduction projects, their needs and constraints as well as a few preliminary results.

The limited time available does not allow a very detailed description, therefore - especially in the second and third part - I will give a rather personal view of the controversial results and new projects.

2.1. Equatorial rotation

The Mt. Wilson solar plasma rotation and magnetic field measurement project is the main source for solar equatorial plasma rotation data. In the first publication by Howard and Harvey (1970) the most interesting result were daily variations of the equatorial velocity up to 10 percent. Perez Garde et al. (1981), Küveler and Wöhl (1983) and Lustig and Wöhl (1989a) aimed in comparing their data with those from Mt. Wilson and Stanford, respectively. Although daily variations were found, no correlation of those measured in Europe and the United States could be established. By extensive averaging of many measurements in April 1981 and May 1982 using a twodimensional diode array as the detector Küveler and Wöhl (1983) found rms errors within their observing periods of 3 m/s and 4 m/s, respectively, while the yearly means - from their very short periods - differed by 35 m/s, which is significant.

Similar results were obtained from the Mt. Wilson data after several technical improvements (Howard, 1983, private communication). The dramatic improvements of the Mt. Wilson data since the end of 1982 can be clearly seen in the Fig. 3 of Snodgrass

* Mitteilung aus dem Kiepenheuer-Institut Nr. 326

(1984), where he gives the fit-determined coefficients of the rotation.

Attempts to determine variations of the equatorial plasma rotation velocity depending on the solar cycle were not very successful up to now : Although Howard (1976) claimed that he found a variation of the solar rotation velocity depending on the activity cycle, Gilman and Howard (1984) were no longer convinced and explained this e.g. with their Figure 1 and the comparison with the sunspot data.

The Table 1 and Figure 1 given by Lustig and Wöhl (1989b) show still strange variations around a mean value of about 1970 m/s and within the declining phase of the solar activity from 1983 until 1986 a comparison of data from Capri, Stanford and Mt. Wilson shows no significant differences (Lustig and Wöhl, 1989a) and therefore these authors conclude, that all cyclic variations - if existing at all - are below one percent. Bogart and Scherrer (1986) give an equatorial rotation velocity of 2000 m/s with an error of about 10 m/s and a maximum change of 2 m/s/year.

For the sunspots e.g. Gilman and Howard (1984), Balthasar et al. (1986a), Lustig (1983) and Lustig and Schroll (1989) found a higher equatorial rotation velocity during the activity minimum as compared to the maximum. The difference between the maximum and minimum of the rotation velocity for the period 1902 until 1976 as given by Balthasar et al. (1986a) was about 0.25 deg/day or just a little more than 30 m/s, which is not significant.

It should be kept in mind, that most results for the equatorial rotation of tracers are determined from an extrapolation of data obtained within a broader equatorial belt.

2.2. Differential rotation

The differential rotation of the solar photosphere was detected for the sunspots in principle already by Scheiner (1630), although a first law of the differential rotation was only given by Carrington (1863). Within this century also many data were collected for the differential rotation of the photospheric plasma. The data for other structures e.g. polar faculae or coronal holes are much less abundant in the literature. A typical list of results is given by Stix (1989b) in his Table 1. I also repeat his comment, that the close coincidence of the results from the total amount of the Greenwich data and those from Mt. Wilson is remarkable. A general trend seems to be, that the gradient of the differential rotation is smaller for larger structures.

Only some years ago earlier findings, that the differential rotation profile of sunspots changes within the activity cycle could be established more clearly by analyzing the full data from Greenwich (Balthasar et al., 1986a) and Mt. Wilson (Howard et al., 1984), respectively. Some discussions about the different results from the Greenwich data and the Mt. Wilson sunspot data are given e.g. by Tuominen and Virtanen (1987).

The solar magnetic field pattern shows a differential rotation law, which differs up to about + 100 m/s to the plasma velocity as reported e.g. by Stenflo (1974). Within the last decade the magnetic field rotation was determined e.g. by Snodgrass (1983), by Sheeley et al. (1987) and more recently again by Stenflo (1989), who combined the rotation law of Snodgrass (1983) - for the surface - and of himself - for the bottom of

the convection zone - to derive the depth dependence of the rotation of magnetic fields. Bumba and Hejna (1987) pointed out too, that the strong background field rotates rigid, while the weak magnetic fields rotate differential.

2.3. Meridional motions

Although first remarks about meridional motions of sunspots were already given by Carrington (1863), they were only mentioned to indicate an error source for the determination of the solar rotation axis. A first detailed analysis of meridional motions was performed by Tuominen (1942) using the Greenwich data about 50 years ago. He found a mean motion of sunspots to the equator within a belt of $\pm$ 16 degrees in latitude. Later e.g. Becker (1954) using also the Greenwich data found some differences in the details. Important is the discussion about the significance, which was claimed by Tuominen (1961) but questioned by Ward (1964, 1973) and also by Balthasar et al. (1986a).

The meridional motions determined for the plasma by Doppler methods in general show poleward flows of the order of 10 to 20 m/s (Duvall, 1979; LaBonte and Howard, 1982b; Snodgrass, 1984), but there is also a finding of an equatorward motion of about 30 m/s by Perez Garde et al. (1981).

Some years ago Andersen (1984) reported about meridional plasma motions of up to 80 m/s in high latitudes. Pierce and LoPresto (1987) found even 120 m/s towards the equator at about 60 deg to 67 deg. Meridional velocities of up to + 80 m/s and - 40 m/s are also found in the most recent reduction of the Mt. Wilson data by Ulrich et al. (1988), but they claim, that a lot of these changes may be caused by instrumental changes and possible giant cells.

Within a special observing project lasting some weeks each year from 1982 until 1986 Lustig and Wöhl (1990a) could show, that such results can be obtained for short periods, but that the - not-significant - mean over the whole period mentioned is below 10 m/s. The direction of the mean flow was towards the equator below 30 deg latitude and towards the poles in higher latitudes.

From my point of view any meridional motions reported are not significant: For the plasma this limit is about 10 m/s and for the sunspots 1 m/s to 2 m/s depending on the sample. There are two arguments that the last result is also an upper limit for the plasma : The plasma motions in general determined by Doppler measurements are strongly influenced by spectral line asymmetries and shifts and in some cases by magnetic fields. Since Balthasar et al. (1982) found a braking of stable recurrent sunspots down to the rotation velocity of the plasma and Lustig and Wöhl (1990b) find a tendency for a decreasing of meridional motions with aging of recurrent spots it seems evident that the sunspot meridional motions give the upper limits also for the plasma.

It should not be forgotten, that the detection of real meridional motions at least from solar observations within periods of a few months is probably not possible, because wrong solar rotation elements are used (Balthasar et al., 1986b, Balthasar et al., 1987).

The search for meridional motions is - from the point of theoreticians - still important, because they hope to use any result for a discrimination between the diverse models of

the solar plasma motions (Stix, 1989b).

2.4. Large - scale motions

Besides the mentioned motions many attempts were performed to find patterns of large - scale motions. Of course the Mt. Wilson data should be best suited for such attempts. Unfortunately there was - as already mentioned - a big scatter in their results for many years and it is still not clear how the magnetic fields have influenced the results. Nevertheless this large sample was several times used to search for large - scale patterns of motions: LaBonte et al. (1981) found upper limits of 3 m/s and 12 m/s for the longitudinal wavenumbers of 40 and 1, respectively. Snodgrass and Howard (1984) give even a limit of 1 m/s for wavenumbers higher than 10.

Some years ago Yoshimura et al. (1985) reported about the detection of global convective wave flows on the Sun. The different interpretation of results by H. Yoshimura and the other colleagues at Stanford led to a very personal paper of Yoshimura (1987) concerning global convection on the Sun detected from Stanford Doppler data. Also Bumba (1987) reported, that large magnetic field structures rotate slower than the photospheric differential rotation and are uninfluenced by it.

Special searches for large - scale motions near the solar poles were performed by Beckers (1978), Cram et al. (1983) and Durney et al. (1985). The final result of the last two papers was, that no long-lived velocity patterns could be found with amplitudes bigger than 5 m/s.

Short period observations of large - scale motions using an optical resonance spectrometer showed coincidences of velocity fields with active regions, but no systematic steady patterns within the limits of the method used, which was about 15 m/s rms (Robillot et al., 1984).

Within special projects Schröter et al. (1978) and Perez Garde et al. (1981) searched for large - scale motions in the solar photosphere (Schröter et al., 1978, searched also for large - scale motions of Ca^+ mottles). Although the results in the second project were analyzed e.g. by sophisticated programs used to detect patterns of proper motions of stars no convincing result was obtained.

From my point of view no large - scale velocity pattern covering a large part of the solar photosphere could be detected up to now. The limit of the velocities in such a pattern - if it exists at all - must be below 10 m/s.

2.5. Torsional oscillations

Changing local patterns of motions, which are called the torsional oscillations were first reported by Howard and LaBonte (1980). Their deviation from the local rotation is of the order of 3 m/s. Different results for these patterns by different analyzing methods and slightly changing samples of data were found by LaBonte and Howard (1982a,b) and Snodgrass (1985) and Snodgrass and Howard (1985). Keeping in mind the strange daily variations in the Mt. Wilson rotation data until 1982 (see Snodgrass, 1984), the impor-

tant changing of spectral line positions by magnetic fields e.g. reported by Livingston (1982), and the possible influences of terrestrial blends on the spectral line used, e.g. by Livingston and Wallace (1985), the existence of the torsional oscillations was in question for some years. The improved data from Mt.Wilson within the last decade seem to support the earlier findings and give new details (Ulrich, 1990, private communication). Detailed correlations of the torsional oscillations with the activity cycle were performed by Snodgrass (1987).

3. Controversial results

Some observers think that the torsional oscillations may be a signature of giant cells (Snodgrass and Wilson, 1987), but this is not yet an established fact. Unfortunately no other observations of the torsional oscillations of the solar plasma except those obtained at Mt.Wilson are performed. The similar measurements at Stanford do not show them, because the observing aperture of 3 arcminutes is too big (Bogart, 1990, private communication).

While Tuominen et al. (1983) detected comparable effects as the torsional oscillations in sunspot motions, Gilman and Howard (1984) did not find systematic meridional drifts of the fast and slow zones.

Ribes at al. (1985) reported about a systematic meridional motion of young sunspots in the years 1969 and 1972 from analyzing of spectroheliograms taken at the Paris observatory. Following this suggestion Wöhl (1988) tried to find similar motions using the Greenwich data for a selected group of spot types. Although identical spots could be compared, any similar result to that of Ribes et al. (1985) could not be found for the years 1940 until 1976. The motions of the sunspots were not systematic and the mean errors bigger than the mean for any year.

Since Eddy et al. (1976) published their finding of a different rotation of sunspots within the 17th century by reducing observations published by Hevelius (1647) as compared to modern results and although this result could not be repeated by Abarbanell and Wöhl (1981) and Yallop et al. (1982) several new attempts were performed to gain informations about the motions on the Sun - and other parameters, e.g. the diameter - in that time: Ribes et al. (1987) reported that the differential rotation of sunspots observed by La Hire during the end of the 17th and the begin of the 18th century was steeper and the equatorial rotation slower than today. The assumed precision of the optics was criticized by O'Dell and Van Helden (1987), but there is no independent reduction of these sunspot position data known. How uncertain the possibilities are to detect real changes of the solar rotation velocity decades ago even if two sets of data exist, can be found from the discussions by Balthasar and Fangmeier (1988) and Wöhl and Balthasar (1989) concerning the higher rotation velocity determined from sunspots observed about 100 years ago as compared to the velocity after 1902.

Becker (1955) reported about the rotation of sources of sunspots on the Sun, which should rotate about two to three degrees per rotation faster than the sunspots. Some years ago Gaizauskas et al. (1983) and Castenmiller et al. (1986) also investigated 'nests'

of sunspots. Castenmiller et al. (1986) claim, that there is no higher rotation velocity as compared to sunspots, but that these structures rotate more rigid.

Within several papers the problem of the braking of sunspot rotation was discussed within the last years: While e.g. Zappala and Zuccarello (1989) find a linear decreasing of the rotation velocity of young sunspots with time during the first 9 days of their existence, Tuominen and Virtanen (1987) show a decreasing of the braking effect for young and old sunspots with time.

Possible relations of solar motions and large - scale magnetic fields are in discussion. For instance Ambroz (1987) reported about a relation of motions of filaments and locations of solar activity.

4. Further observations and reductions

The Mt. Wilson daily solar magnetic and velocity field measurement project is indeed still an important source for solar photospheric large - scale motions. The Stanford data can be used as an additional reference, although they seem in general more affected by scattered light and their spatial resolution is lower. On the other side new twodimensional detectors allow to collect so many more data in much shorter time, that it is possible to do special projects of motion analysis now, which were not possible with the single detector area scanning equipments. An example can e.g. be seen in the contribution by Wöhl and Ye (1990) concerning the differential rotation at the solar poles: They find a persistent velocity pattern on the differential rotation within the polar regions from observations in summer 1989 and spring 1990.

Even more promising is the work with sunspot positions : The well known Greenwich Photoheliographic Results are continued by the Debrecen Photoheliographic Results and the last ones seem to have even a better quality, as e.g. shown by Dezsö and Kovacs (1987). Other observations of this kind are also performed and allow to do direct comparisons of spot motions. Lustig and Wöhl (1990b) show in their contribution a comparison of the meridional motions of recurrent sunspots 1949 until 1976 from the Greenwich and the Kanzelhöhe data and find now for the first time, that indeed meridional motions obtained from different observations agree very well for many spots, while there are some differences for others. The total rms motions are nearly four times as high as the rms motions of the differences for their samples of 39 recurrent sunspots of types H and J taken from the Greenwich data and the Kanzelhöhe data, respectively.

I hope that the Debrecen Photoheliographic Results for the last decade will soon be available for similar investigations. It could speed up our reductions a lot, if they also would be published in a computer - readable form.

Acknowledgements

I thank Drs. H. Balthasar and G. Lustig for reading a preliminary version of the manuscript and for fruitful cooperations and discussions on many topics of it during the last years.

References

Abarbanell, C., Wöhl, H. : 1981, Solar Phys. **70**, 197
Ambroz, P. : 1987, Bull.Astron.Inst.Czechosl. **38**, 110
Andersen, B.N. : 1984, Solar Phys. **94**, 49
Balthasar, H., Schüssler, M., Wöhl, H. : 1982, Solar Phys. **76**, 21
Balthasar, H., Vazquez, M., Wöhl, H. : 1986a, Astron.Astrophys. **155**, 87
Balthasar, H., Lustig, G., Stark, D., Wöhl, H. : 1986b, Astron.Astrophys. **160**, 277
Balthasar, H., Stark, D., Wöhl, H. : 1987, Astron.Astrophys. **174**, 359
Balthasar, H., Fangmeier, E. : 1988, Astron.Astrophys. **203**, 381
Becker, U. : 1954, Z.Astrophys. **34**, 129
Becker, U. : 1955, Z.Astrophys. **37**, 47
Beckers, J.M. : 1978, Astrophys.J. **224**, L143
Bogart, R.S., Scherrer, P.H. : 1986, Bull.Am.Astron.Soc. **18**, 848
Bogart, R.S. : 1987, Solar Phys. **110**, 23
Bogart, R.S. : 1990, private communication
Bumba, V. : 1987, Solar Phys. **110**, 51
Bumba, V., Hejna, L. : 1987, Solar Phys. **110**, 109
Carrington, R.C. : 1863, Observations of the Spots on the Sun from November 9, 1853, to March 24, 1861, made at Redhill, (Williams and Norgate, London, Edinburgh
Castenmiller, M.J.M., Zwaan, C., van der Zalm, E.B.J. : 1986, Solar Phys. **105**, 237
Cram, L.E., Durney, B.R., Guenther, D.B. : 1983, Astrophys.J. **267**, 442
Dezsö, L., Kovacs, A. : 1987, in Hejna, L., Sobotka, M. (eds.), 10th European Regional Astronomy Meeting of the IAU, Proceedings vol.1, Publ. Astron. Inst. Czechoslovak Academy of Sciences No. 66, 81
Durney, B.R., Cram, L.E., Guenther, D.B., Keil, S.L., Lytle, D.M. : 1985, Astrophys.J. **292**, 752
Duvall, T.L. : 1979, Solar Phys. **63**, 3
Eddy, J.A., Gilman, P.A., Trotter, D.E. : 1976, Solar Phys. **46**, 3
Gaizauskas, V., Harvey, K.L., Harvey, J.W., Zwaan, C. : 1983, Astrophys.J. **265**, 1056
Gilman, P.A., Howard, R. : 1984, Astrophys.J. **283**, 385
Gilman, P.A. : 1986, The Solar Dynamo : Observations and Theories of Solar Convection, Global Circulation, and Magnetic Fields, in Sturrock, P.A., Holzer, T.E., Mihalas, D.M., Ulrich, R.K. (eds.): Physics of the Sun, Vol. I, 95 (Reidel, Dordrecht)
Hevelius, J. : 1647, Selenographia: sive, Lunae Descriptio; atque accurata, tam macularum ejus etc. praesertim autem macularum Solarium etc. (Typis Hünefeldianis, Gedani)
Howard, R., Harvey, J.W. : 1970, Solar Phys. **12**, 23
Howard, R. : 1976, Astrophys.J. **210**, L159
Howard, R., LaBonte, B.J. : 1980, Astrophys.J. **239**, L33
Howard, R., 1983 (private communication)
Howard, R., Gilman, P.A., Gilman, P.I. : 1984, Astrophys.J. **283**, 373
Howard, R. : 1985, Report to the International Astronomical Union comm. 12, in R.M. West (ed.) : IAU transactions vol. XIXA, (Reidel, Dordrecht)
Küveler, G., Wöhl, H.: 1983, Astron.Astrophys. **123**, 29
LaBonte, B.J., Howard, R., Gilman, P.A. : 1981, Astrophys.J. **250**, 796
LaBonte, B.J., Howard, R. : 1982a, Solar Phys. **75**, 161
LaBonte, B.J., Howard, R. : 1982b, Solar Phys. **80**, 361
Livingston, W.C. : 1982, Nature **297**, 208
Livingston, W., Wallace, L. : 1985, Solar Phys. **95**, 251
Lustig, G. : 1983, Astron.Astrophys. **125**, 355
Lustig, G., Schroll, A. : 1989, Variations in solar rotation with the sunspot cycle, in v.d.Lühe, O. (ed.) : Proceedings of the 10th Sac Peak Summer Workshop 'High Spatial Resolution Solar Observations', 545
Lustig, G., Wöhl, H. : 1989a, Astron.Astrophys. **218**, 355

Lustig, G., Wöhl, H. : 1989b, Equatorial rotation velocity of the Sun from 1983 to 1986, in v.d.Lühe, O. (ed.): Proceedings of the 10th Sac Peak Summer Workshop 'High Spatial Resolution Solar Observations', 540
Lustig, G., Wöhl, H. : 1990a, Astron.Astrophys. **229**,224
Lustig, G., Wöhl, H. : 1990b, this volume
O'Dell, C.R., Van Helden, A. : 1987, Nature **330**, 629
Perez Garde, M., Vazquez, M., Schwan, H., Wöhl, H. : 1981, Astron.Astrophys. **93**, 67
Pierce, A.K., LoPresto, J.C. : 1987, Bull.Am.Astron.Soc. **19**, 935
Ribes, E., Mein, P., Mangeney, A. : 1985, Nature **318**, 170
Ribes, E. : 1986, Adv. Space Res. **6**, 221
Ribes, E., Ribes, J.C., Barthalot, R. : 1987, Nature **326**, 52
Robillot, J.M., Bocchia, R., Fossat, E., Grec, G. : 1984, Astron.Astrophys. **137**, 43
Rüdiger, G. : 1989, Differential Rotation and Stellar Convection (Akademie-Verlag, Berlin)
Scheiner, C. : 1630, Rosa Ursina sive Sol ex admirando Facularum et Macularum suarum Phaenomeno Varius etc. (Andream Phaeum Typographum Ducalem, Bracciani)
Schröter, E.H., Wöhl, H., Soltau, D., Vazquez, M. : 1978, Solar Phys. **60**, 181
Schröter, E.H. : 1985, Solar Phys. **100**, 141
Sheeley, N.R. Jr., Nash, A.G., Wang, Y.-M. : 1987, Astrophys. J. **319**, 481
Snodgrass, H.B. : 1983, Astrophys. J. **270**, 288
Snodgrass, H.B. : 1984, Solar Phys. **94**, 13
Snodgrass, H.B., Howard, R. : 1984, Astrophys.J. **284**, 848
Snodgrass, H.B. : 1985, Astrophys.J. **291**, 339
Snodgrass, H.B., Howard, R. : 1985, Solar Phys. **95**, 221
Snodgrass, H.B. : 1987, Solar Phys. **110**, 35
Snodgrass, H.B., Wilson, P.R. : 1987, Nature **328**, 696
Stenflo, J.O. : 1974, Solar Phys. **36**, 495
Stenflo, J.O. : 1989, Astron.Astrophys. **210**, 403
Stix, M. : 1989a, The Sun (Springer, Berlin, Heidelberg)
Stix, M. : 1989b, The Sun's Differential Rotation, in Klare, G. (ed.) : Reviews in Modern Astronomy 2, 248 (Springer, Berlin, Heidelberg)
Tuominen, J. : 1942, Z.Astrophys. **21**, 96
Tuominen, J. : 1961, Z.Astrophys. **51**, 91
Tuominen, J., Tuominen, I., Kyröläinen, J. : 1983, Monthly Notices Roy. Astron. Soc. **205**, 691
Tuominen, I., Virtanen, H. : 1987, Solar Rotation Variations from Sunspot Group Statistics, in Durney, B.R., Sofia, S. (eds.): The Internal Solar Angular Velocity, Proceedings of the 8th National Solar Observatory Summer Symposium, Sunspot 1986, 83 (Reidel, Dordrecht)
Ulrich, R.K., Boyden, J.E., Webster, L., Snodgrass, H.B., Padilla, S.P., Gilman, P., Shieber, T. : 1988, Solar Phys. **117**, 291
Ulrich, R.K. : 1990, private communication
Ward, F. : 1964, Pure Appl. Geophys. **58**, 157
Ward, F. : 1973, Solar Phys. **30**, 527
Wöhl, H. : 1988, Solar Phys. **116**, 199
Wöhl, H., Balthasar, H. : 1989, Astron.Astrophys. **219**, 313
Wöhl, H., Ye, B. : 1990, this volume
Yallop, B.D., Hohenkerk, C., Murdin, L., Clark, D.H. : 1982, Q.J.R.Astron.Soc. **23**, 213
Yoshimura, H., Scherrer, P.H., Bogart, R.S., Hoeksema, J.T. : 1985, Bull.Am.Astron.Soc. **17**, 639
Yoshimura, H. : 1987, The Detection of Global Convection on the Sun by an Analysis of Line Shift Data of the John M. Wilcox Solar Observatory at Stanford University, in Durney, B.R., Sofia, S. (eds.): The Internal Solar Angular Velocity, Proceedings of the 8th National Solar Observatory Summer Symposium, Sunspot 1986, 89 (Reidel, Dordrecht)
Zappala, R.A., Zuccarello, F. : 1989, Astron.Astrophys. **214**, 369

Solar differential rotation and its variations

I. Tuominen
Observatory and Astrophysics Laboratory, University of Helsinki
Tähtitorninmäki, SF-00130 Helsinki, Finland

Abstract: The generation of the solar differential rotation by the effects of rotation on the turbulent motions is discussed. Besides the direct observations of differential rotation by Doppler measurements and tracers, helioseismological results and the behaviour of the solar dynamo give further constraints on the turbulence models. In addition, cyclic variations of the rotation law can be used as a means of probing the solar dynamo.

1 Solar turbulent convection zone

The solar convection zone is very probably in a highly turbulent state. The Rayleigh number Ra within it is large, probably of the order of 10^{20}. This situation can be compared with the experimental results of Libchaber and his group at the University of Chicago for Rayleigh-Bénard convection (Castaing *et al.*, 1989). In their experiments the fluid heated from below is described by the Nusselt number (ratio of heat transported by convection to that transported by conduction). The flow undergoes several transitions with increasing Nusselt number. In the beginning a regular convection pattern developes. Subsequent increases of Nusselt and Rayleigh numbers causes the flow to become temporally chaotic. After a transition phase the flow reaches a state where, in addition to temporal, also a spatial chaos occurs, which the authors call soft turbulence. With still higher Nusselt and Rayleigh numbers a regime of hard turbulence is reached. Soft and hard turbulence differ in several respects, e.g. the distribution of temperature fluctuations is Gaussian in the former case and exponential in the latter. The Rayleigh number reached in the experiment is about 10^{11}. Comparing this to the solar value (10^{20}), it can be concluded that we are rather far from the real solar situation; our models describe in a sense a "toy" sun.

2 Reynolds stresses

The highly turbulent state of the solar and stellar convection zones leads us to the mean-field concept, especially if we want to understand the solar global behaviour, e.g. the differential rotation and the magnetic cycle. In the mean-field framework we separate the physical quantities in the simplest way, into two parts - a mean slowly varying or steady large-scale part and a fluctuating part. The mean should be in principle be the

expectation value. In practice, when we try to interpret observations, temporal and/or spatial averages must be used.

In hydrodynamics the mean-field approach leads to Reynolds stresses and in dynamo theory to the α-effect and turbulent diffusivities. The form of the Reynolds stresses, in other words the correlation tensor $\langle u_i' u_j' \rangle$ together with the turbulent heat flux $\langle u_i' T' \rangle$, are the essential quantities in the theory of differential rotation. In the situation in which there is no preferred direction other than the angular velocity vector, angular momentum is transported according to the classical Boussinesq relations

$$Q_{r\phi} = -\nu_t r \sin\theta \frac{\partial \Omega}{\partial r} \tag{1}$$

$$Q_{\theta\phi} = -\nu_t \sin\theta \frac{\partial \Omega}{\partial \theta} \tag{2}$$

where ν_t is eddy viscosity and $Q_{ij} = \langle u_i' u_j' \rangle$. For anisotropic turbulence however, when the radial direction is a preferred, new terms appear in the correlation tensor

$$Q_{r\phi} = -\nu_t r \sin\theta \frac{\partial \Omega}{\partial r} + \Lambda_V \sin\theta \Omega \tag{3}$$

and

$$Q_{\theta\phi} = -\nu_t \sin\theta \frac{\partial \Omega}{\partial \theta} + \Lambda_H \cos\theta \Omega \tag{4}$$

with

$$\Lambda_V = \nu_t (V^{(0)} + V^{(1)} \sin^2\theta + V^{(2)} \sin^4\theta) \tag{5}$$

and

$$\Lambda_H = \nu_t (H^{(1)} \sin^2\theta + H^{(2)} \sin^4\theta), \tag{6}$$

the so-called Λ-effect (Rüdiger, 1989). They act in a non-diffusive way as they do not vanish for Ω =constant, thus preventing the existence of uniform rotation.

Support for the existence for the non-diffusive part of the horizontal stress $Q_{\theta\phi}$ comes from the statistics of the sunspot proper motions (Ward, 1965; Gilman and Howard, 1984). Observations give for the correlation a positive value (in the northern hemisphere) whilst for vanishing $H^{(1)}$ it should be negative. Furthermore, several statistical properties of the sunspot motions (Tuominen and Virtanen, 1988) can be understood if the youngest groups reflect the motions deep in the convection zone. Figure 1 gives the latitudinal profiles for groups of different age (Virtanen, 1989). In fact, the youngest groups give a horizontal correlation about three times larger than the old recurrent groups. This gives the possibility of estimating the radial profile of the stress and, because $H^{(1)}$ already for dimensional reasons depends on the inverse Rossby number, i.e.

$$H^{(1)} \sim (\tau_{\rm corr}\Omega)^2, \tag{7}$$

we can estimate the depth dependence of the scale of the motions which produce the horizontal stress. The suggested radial dependence is steeper than for a giant flow pattern

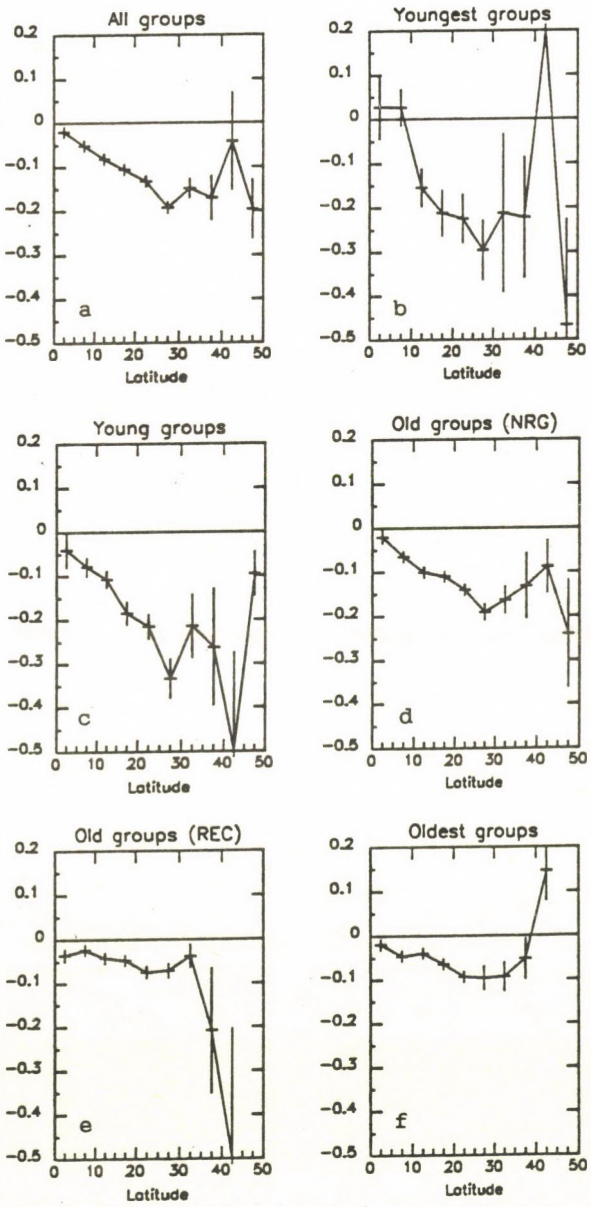

Figure 1: The latitudinal profiles for horizontal velocity correlation $\langle u'_\theta u'_\phi \rangle$ for all groups and for groups of different age in $(\mathrm{deg/day})^2$ from Greenwich Photoheliographic Results for the years 1874–1976. The sign corresponds to the southern hemisphere.

but less steep than that obtained from the mixing length theory. We have expressed the stress as

$$Q_{\theta\phi} = \nu_t \Omega(r) w_1 (1 + \frac{w_2}{w_1} \sin^2\theta + ...) \cos\theta \sin^2\theta. \quad (8)$$

Figure 2 gives the latitudinal profile of $Q_{\theta\phi}$ derived from all groups and fitted to the formula (8) with the ratio w_2/w_1 being 5.6.

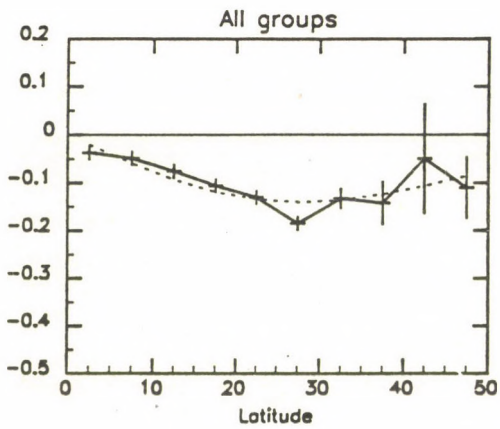

Figure 2: The same as in Figure 1 for all groups. The observations have been fitted to the formula (8) with $w_2/w_1 = 5.6$.

Another method of investigating the correlation tensor is by 3D numerical simulations. An example is given by Pulkkinen et al. (1991). They calculated compressible convection in the solar convection zone using a modified code by Nordlund and Stein (1989). The simulations were done in a three dimensional box with 31^3 meshpoints. The box could be situated at different latitudes allowing the angle between the angular velocity vector and gravity to be varied. The Rayleigh and Taylor numbers were 30 000 and 10 000, respectively. The Rossby number was near unity and compatible with value near the bottom of the convection zone. Temporal averages of the velocity correlations were calculated from about 1000 time instants after every 100 time steps of the integration. We mention here only the results for the latitudinal profiles. The absolute value and the radial dependence of the correlation is more difficult to deduce from the simulations. The latitudinal profile

of the horizontal correlation in the southern hemisphere is given in the Figure 3. The continuous line gives the fit to the formula (8). The remarkable result is that the best fit is obtained with the ratio $w_2/w_1 = 5$, which is very close to the value obtained from the sunspot statistics.

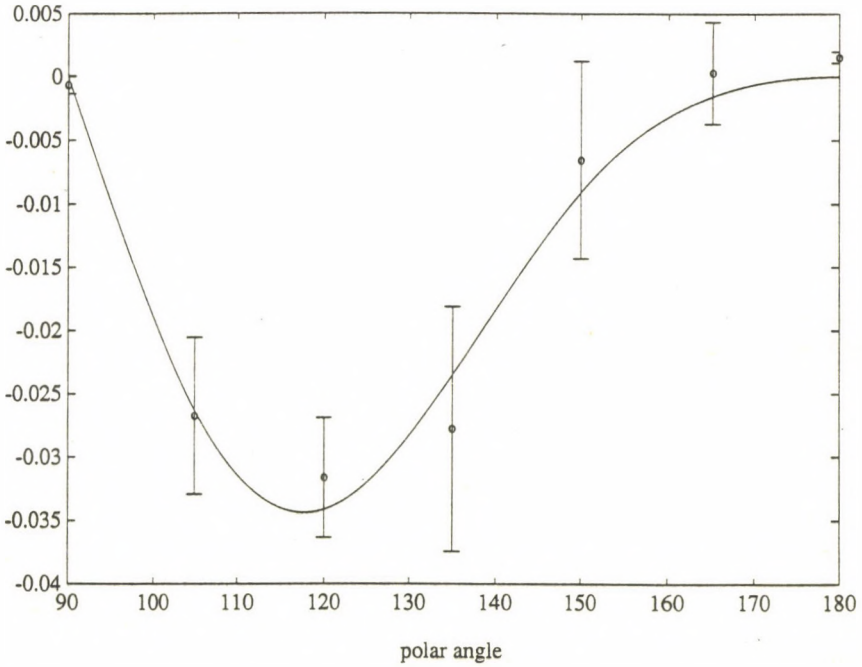

Figure 3: The horizontal velocity correlation $\langle u'_\theta u'_\phi \rangle$ from 3D simulations of compressible convection. The solid line is the fit with $w_2/w_1 = 5$ and the circles denote the values from simulations. Bars give the uncertainties of the mean values derived from the simulations.

For the $Q_{r\phi}$ the same calculation also give values near those expected. The coefficients $V^{(0)}$ and $V^{(2)}$ are negative and $V^{(1)}$ is positive at all depths of the box. Similar signs of the parameters give reasonable models for the solar differential rotation (see Tuominen and Rüdiger, 1989).

3 Solar differential rotation

During the last years helioseismological observations have shed new light on the rotation law inside the solar convection zone. Although many uncertainties exist in the observations and inversion methods (see e.g. Goode, 1991) the basic result seems to be that the latitudinal differential rotation is roughly independent of depth through the convection zone but in the lower part decreases rapidly (Dziembowski et al., 1988, Christensen-Dalsgaard and Schou, 1988, Schou, 1989). Roughly speaking the Ω-contours are cylindrical close to the equator, radial at middle latitudes and disk-like at the poles (cf. Fig. 2 in Libbrecht, 1988). They differ markedly from an over-all cylidrical structure.

The result that the differential rotation decreases towards the bottom of the convection zone is also obtained by using tracers. Stenflo (1989) has used the pattern of solar magnetic fields to determine the rotation law. If the rotation law is determined from a cross-correlation analysis of daily Mt. Wilson magnetograms (Snodgrass, 1983), a latitudinal profile similar to that derived from Doppler measurements is obtained. In contrast, if the rotation rate is determined by autocorrelation analysis, using the places where new flux appears as tracers, the position of which is measured in consecutive meridian passages, a different law is obtained. The rotation period reaches a maximum at a latitude 50-55° , with a tendency for a small polar spin-up. According to Stenflo's interpretation, his reduction gives the angular velocity in deep layers. The angular velocity is also slightly higher than that at the surface.

A similar result is also obtained from sunspot statistics (Tuominen and Virtanen, 1988). The youngest spots give a similar latitudinal profile to Stenflo's, also with a higher angular velocity than given by the old recurrent groups. Similarly to the case of the horizontal correlations, it is tempting to make the interpretation that the young spots carry information from the deep layers of the convection zone. Inward increase of angular velocity in the lower part of the convection zone, even near equator, before the region of strong decrease of latitudinal differential rotation, may not be in conflict with the helioseismological inversions (see Dziembowski et al., 1989; Schou, 1989).

The emerging picture gives constraints to the possible turbulence models in the solar convection zone. Some attepts to describe the observations by a linearized theory of differential rotation have been presented by Tuominen and Rüdiger (1989), Rüdiger and Tuominen 1990, 1991) and Rüdiger and Kichatinov (1990), based on the Λ-effect formalism. The models demonstrate a mechanism whereby the relatively smooth observed angular velocity profile can be reproduced. It is also probable that nonlinear effects in Reynolds stresses are important, limiting the amplitude of the Λ-effect by nonlinear feedback, and influencing the angular momentum balance. A first attempt to this direction has been described by Brandenburg et al. (1990).

4 Time variations

An important finding concerning the solar dynamo was that of Howard and LaBonte (1980), namely that the solar rotation varies with the solar cycle. This result was derived

using Mt. Wilson Doppler measurements over many years and clearly represents the variation of the mean flow. It has also a period of eleven years and it is spatially closely related to the mean magnetic field. These basic observations clearly show that it is a feedback effect by the mean Lorentz force of magnetic field. The observations and interpretation have been discussed in detail by Rüdiger et al. (1986) and Tuominen et al. (1990) who give further relevant references.

5 Final remarks

As a conclusion we can return to the beginning and make some remarks about the solar turbulence. The mixing length concept suggests that the turbulent flow in the Sun consists of rising and falling bubbles which eventually dissolve to exchange heat with their surroundings. A quite different picture, however, seems to emerge from computer simulations of solar and stellar convection. The dominant feature here is fast filamentary downdrafts in a background of more gentle ascending fluid (Stein & Nordlund, 1989). Such filamentary downdrafts may cause large anisotropies in the fluid which crucially determine properties of the Λ-effect. Recently, Vincent & Meneguzzi (1990) have performed simulations of homogeneous turbulence at high resolution (240^3 mesh points). Their results suggest that turbulence consists of a hierachy of vorticity tubes (see also She *et al.*, 1990). This makes it evident that small scale structures are inherently connected with large scale features, because vortex tubes are thin and can be very long. Thus, the whole spectrum of different length scales is represented already in a single tube. There is no separation of length scales. This result certainly poses challenges for mean-field theories.

Acknowledgements: Any defects of this review may be at least partially explained by the arrangements necessary for the IAU Colloquium on the Sun and Cool Stars in Helsinki July 1990. The author thanks all friends and collaborators for arranging a lively summer at Helsinki Observatory before, during, and after the meeting, day and night. Prof. L. Dezsö is acknowledged for his gentle pressure and patience in awaiting the manuscript.

References

Brandenburg, A., Moss, D., Rüdiger, G., Tuominen, I.: 1990, "The nonlinear solar dynamo and differential rotation: A Taylor number puzzle?" *Solar Phys.* (in press)

Castaing, B., Gunaratne, G., Heslot, F., Kadanoff, L., Libchaber, A., Thomae, S., Wu, X.-Z., Zaleski, S., Zanetti, G.: 1989, "Scaling of hard thermal turbulence in Rayleigh-Bénard convection," *J. Fluid Mech.* **204**, 1-30

Christensen-Dalsgaard, J., Schou, J.: 1988, "Differential rotation in the solar interior," in *Proc. Symp. Seismology of the Sun and Sun-like Stars*, ed. E. J. Rolfe, ESA SP-286, p. 149-153

Dziembowski, W. A., Goode, P. R., Libbrecht, K. G.: 1989, "The radial gradient in the Sun's rotation," *Astrophys. J. Letters* **337**, L53-L57

Gilman, P. A., Howard, R.: 1984, "On the correlation of longitudinal and latitudinal motions of sunspots," *Solar Phys.* **93**, 171-175

Goode, P. R.: 1991, "The Sun's Differential Rotation from Seismology," in *The Sun and cool stars: activity, magnetism, dynamos*, IAU Coll. 130, Helsinki July 1990, eds. I. Tuominen, D. Moss & G. Rüdiger, Lecture Notes in Physics, Springer-Verlag

Howard, R., LaBonte, B. J.: 1980, "The sun is observed to be a torsional oscillator with a period of 11 years," *Astrophys. J. Letters* **239**, L33-L36

Libbrecht, K.G.: 1988, "Solar p-mode frequency splittings," in *Proc. Symp. Seismology of the Sun and Sun-like Stars*, ed. E. J. Rolfe, ESA SP-286, p. 131-136

Nordlund, Å., Stein, R.F.: 1989, "Simulating Magnetoconvection," in *Solar and Stellar Granulation*, eds. R. Rutten & G. Severino, Kluwer Acad. Publ.

Pulkkinen, P., Tuominen, I., Brandenburg, A., Nordlund, Å, Stein, R. F.: 1991, "Simulation of rotational effects on turbulence in solar convective zone," in *The Sun and cool stars: activity, magnetism, dynamos*, IAU Coll. 130, Helsinki July 1990, eds. I. Tuominen, D. Moss & G. Rüdiger, Lecture Notes in Physics, Springer-Verlag

Rüdiger, G.: 1989, *Differential rotation and Stellar Convection: Sun and solar-type stars*, Gordon & Breach, New York

Rüdiger, G., Kichatinov, L. L.: 1990, "On the turbulent stresses in the theory of solar torsional oscillations," *Astron. Astrophys.* (in press)

Rüdiger, G., Tuominen, I., Krause, F., Virtanen, H.: 1986, "Dynamo-generated flows in the Sun, I. Foundations and first results," *Astron. Astrophys.* **166**, 306-318

Rüdiger, G., Tuominen, I.: 1987, "Horizontal Reynolds stress and radial rotation law of the Sun," in *The Internal Solar Angular Velocity*, eds. B. R. Durney & S. Sofia, D. Reidel, Dordrecht, p. 361-370

Rüdiger, G., Tuominen, I.: 1990, "Generators of solar differential rotation and implications of helioseismology," in *Solar Photosphere: Structure, Convection and Magnetic Fields*, ed. J. O. Stenflo, Kluwer Acad. Publ., Dordrecht, p. 315-320

Rüdiger, G., Tuominen, I.: 1991, "The key question in the theory of the solar differential rotation," in *The Sun and cool stars: activity, magnetism, dynamos*, IAU Coll. 130, Helsinki July 1990, eds. I. Tuominen, D. Moss & G. Rüdiger, Lecture Notes in Physics, Springer-Verlag

Schou, J.: 1989, "Helioseismic inversion methods and the determination of the rotation in the solar interior," Dissertation, University Århus

She, Z.-S., Jackson, E., Orszag, S. A.: 1990, "Intermittent vortex structures in homogeneous isotropic turbulence," *Nature* **344**, 226-228

Snodgrass, H. B.: 1983, "Magnetic rotation of the solar photosphere," *Astrophys. J.* **270**, 288-299

Stenflo, J.O.: 1989, "Differential rotation of the Sun's magnetic field pattern," *Astron. Astrophys.* **210**, 403-409

Stein, R.F., Nordlund, Å.: 1989, "Topology of convection beneath the solar surface," *Astrophys. J. Letters* **342**, L95-L98

Tuominen, I., Rüdiger, G.: 1989, "Solar differential rotation as a multiparameter turbulence problem," *Astron. Astrophys.* **217**, 217-228

Tuominen, I., Virtanen, H.: 1988, "Variation of the solar rotation at the surface and deep in the convection zone," *Adv. Space Sci.* **8**, (7)141-145

Tuominen, I., Rüdiger, G., Brandenburg, A.: 1990, "Torsional oscillations and the solar dynamo regime," in *Solar Photosphere: Structure, Convection and Magnetic Fields*, ed. J. O. Stenflo, Kluwer Acad. Publ., Dordrecht, p. 387-390

Vincent, A., Meneguzzi, M.: 1990, "The spatial structure and statistical properties of homogeneous turbulence," *J. of Fluid Mech.*, in press.

Virtanen, H.: 1989, *Solar observational hydrodynamics from the sunspot group statistics*, Licentiate thesis, submitted to University of Helsinki

Ward, F.: 1965, "The general circulation of the solar atmosphere and the maintenance of the equatorial acceleration," *Astrophys. J.* **141**, 534-547

ACTIVE REGIONS AND SOLAR ROTATION

by Z. Mouradian and I. Soru-Escaut
Observatoire de Paris-Meudon, DASOP, URA 326

1 – Introduction

The observations of Deubner and Vasquez [1975] show that the differences from the mean solar rotation [Howard and Harvey, 1970] are of the order of ± 2% which is equivalent to 20° of longitudinal shift over one rotation (at $\varphi = 30°$). Also, McIntosh and Wilson [1985] find that the line of zero differential rotation stretches out over a broad band of latitudes. This type of difference with respect to the classical differential rotation can also be found in the measurements by magnetic tracers. We studied the case of filament rotation (prominences), for which the classical law was established by L. and M. d'Azambuja [1948]. We found that the majority of filaments do not obey this law, and that, during successive rotations (25.4 days), some of these filaments superimpose upon each other, while others pivot about a point on the surface called a "pivot point" (PP). We then found that the PPs have a real physical meaning. The positions of some of them indicate regions of magnetic flux emergence in the form of Active Regions [Mouradian et al., 1987]. The existence of these pivot points, revealed at Meudon in 1984 [Soru-Escaut et al., 1986] has been confirmed by Bumba and Gesztelyi [1987], and found again in another type of measurement, by McIntosh and Wilson [1985]. Ambrož [1987] identified regions in rigid rotation by the movement of the large-scale magnetic fields. It should be noted that filaments are used as tracers for the polarity reversal line of the large-scale magnetic fields.

2 – Characteristics of Pivot Points

(i) When filaments of two successive rotations "cross", to form a PP, they do so in one of two ways. Either one of the filaments passes into a gap of the preceding one, or they both come to occupy the same "corridor". The superimposition occurs with a precision better than 3', and calls for a time resolution corresponding to the Carrington rate mentioned above. We consider that a PP is detected if at least three filaments in succession pass through the same point. This rule may be violated if the magnetic field map indicates a $B_{//} = 0$ line without filament, at the location of the PP [Mouradian, Soru-Escaut, 1989c].

(ii) The rotation of the filaments about the PP follows the sense but not the value of the differential rotation. That is, the end of the filament located near the equator rotates faster than the Carrington rate, and the poleward end more slowly.

(iii) All the PPs on the solar surface form a network in rigid rotation.

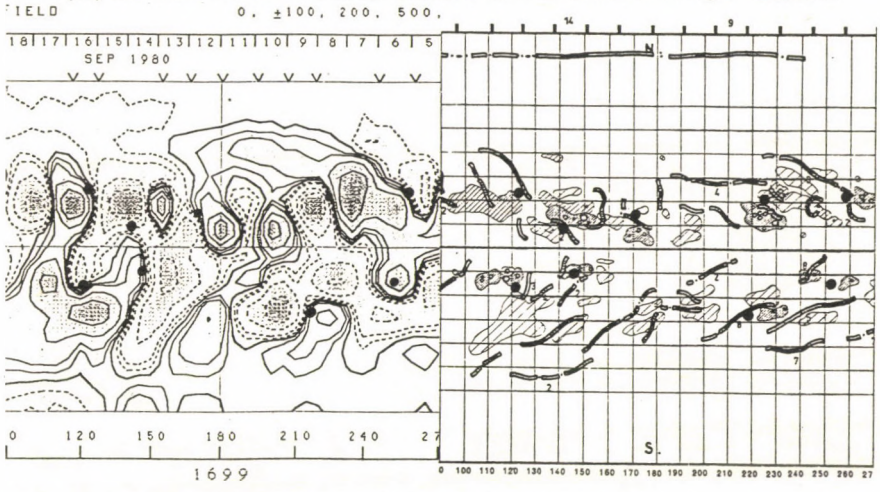

Fig. 1 Portion of the Meudon Synoptic Map (on the right) and of the Stanford magnetic field map, showing the positions of the pivot points (●).

(iv) The PPs are localized on the $B_{\parallel} = 0$ line of the Stanford magnetic field maps (Fig. 1), which can be interpreted as proof that these structures are anchored deep in the convective zone.

(v) Also, in a recent paper, Mogilevski [1989] proposes the existence of a local dynamo anchored deep in the convective zone, to explain the magnetic flux emergence of the PPs. At the base of two convective cells, a toric structure increases the weak magnetic field, then the Rayleigh–Taylor instability brings the resulting field to the surface.

3 – Active Regions and Pivot Points

(i) Active Regions (AR) emerge in the immediate vicinity of the Pivot Points. Figure 2 illustrates the formation of a PP (arrow) during four rotations (1682 to 1685), and the emergence of an AR during rotation 1685. When the PP is inside an AR, then the AR appears as a parasitic polarity [Mouradian and Soru-Escaut, 1989b], one of whose polarities is the same as the surrounding polarity. When a flare occurs in a AR including a PP, the flaring arches start from the PP and connect back into an area of opposite polarity [Mouradian et al., 1989].

(ii) PPs are areas that are highly productive of flares [Soru-Escaut et al. 1985]. In Fig.2 (bottom,right),is shown the distribution of the number of flares in the AR.

(iii) When sunspots have their own movement, if they meet a PP, they change direction and avoid it [Martres et al., 1986].

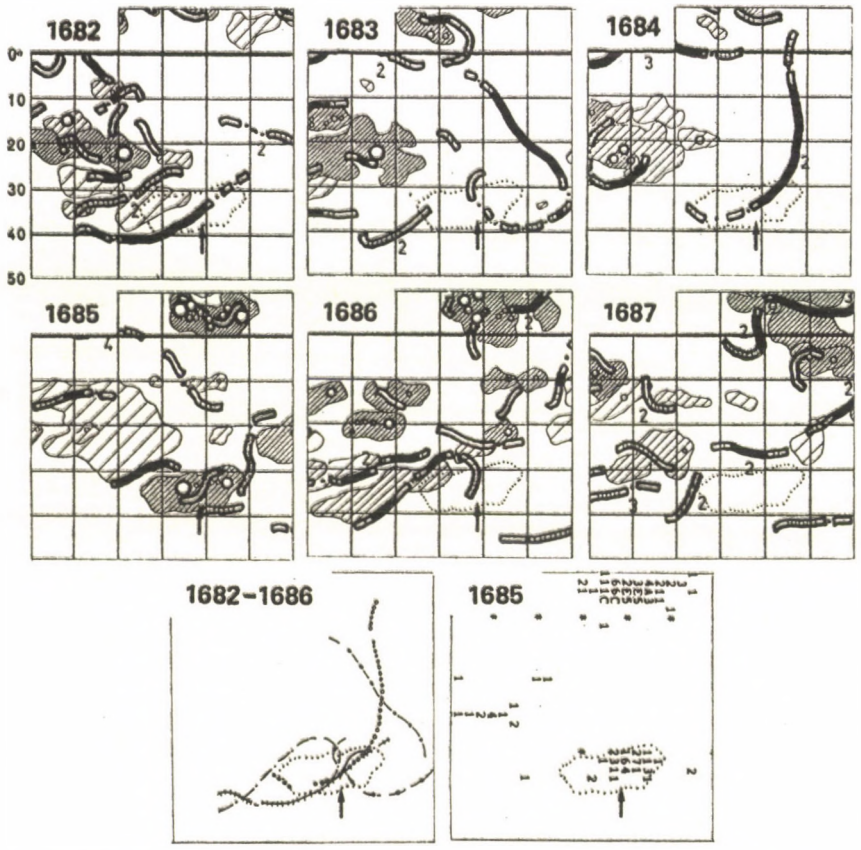

Fig. 2 Formation of a pivot point (Meudon Synoptic Maps), that preceded the emergence of an Active Region (34S 188, rotation 1685). The AR is outlined by a dotted line. The arrows indicate the pivot-point.The composite drawing (bottom,left),illustrates the "crossing" of filament traces at the location of the pivot point. The number of flares is maximum at that point (bottom,right).

4 – Filaments and Pivot Points.

When a filament suddenly disappears (DB), if the foot of the prominence is in a PP, then the DB is due to the heating of the plasma (ionization). After it cools, the filament becomes visible in H_α line again. When the prominence has no PP, then the DB is final [Mouradian, Soru-Escaut, 1989a].

References.

-Ambrož, P.: 1987, Bull. Astron. Inst. Czechosl., **38**, 110.
-Bumba, V., Gesztelyi, L.: 1987, Bull. Astronom. Inst. Czechosl., **38**, 351.
-d'Azambuja, L., d'Azambuja, M.: 1948, Ann. Obs. Paris, **VI**, fasc. VII,151.
-Deubner, F.L., Vasquez, M.: 1975, Solar Phys. **43**, 87.
-Howard, R., Harvey, J.: 1970, Solar Phys. **12**, 23.
-Martres, M.-J., Mouradian, Z., Soru-Escaut, I.: 1986, Astron. Astrophys. **161**, 376.
-McIntosh,P.S., Wilson, P.R.: 1985, Solar Phys. **97**, 59.
-Mogilevski, E.I.: 1989, in Solar Magnetic Fields and Corona (in memory of V.E.Stepanov), Vol.1, p.72.
-Mouradian, Z., Martres, M.-J., Soru-Escaut, I., Gesztelyi, L.: 1987, Astron. Astrophys. **183**, 129.
-Mouradian, Z., Soru-Escaut, I.: 1989a, Astron. Astrophys. **210**, 410.
-Mouradian, Z., Soru-Escaut, I.: 1989b, I.A.U. Coll. No.104, Stanford Univ., California, Poster Papers (B.M.Haisch, M.Rodono eds.) p.227.
-Mouradian, Z., Martres, M.-J., Soru-Escaut, I., Simnett, G.M.: 1989, Astron. Astrophys. **224**, 267..
-Mouradian, Z., Soru-Escaut,I.: 1989c, Solar Phys. **123**, 79.
-Soru-Escaut,I., Martres, M.-J., Mouradian, Z.: 1985, Astron. Astrophys. **145**, 19.
-Soru-Escaut,I., Martres, M.-J., Mouradian, Z.: 1986 in P.A. Simon, G.Heckman, M.A. Shea(eds.) Solar-Terrestrial Predictions, Proc. Workshop Meudon, France, june 18-22, 1984, p.186.

A COMPREHENSIVE FILE OF FILAMENT DISAPPEARANCES AND STATISTICAL RELATIONSHIP WITH "MAGNETIC CLOUDS"

M. Poquérusse, Observatoire de Meudon, FRANCE
P.S. McIntosh, NOAA/ERL/SEL, Boulder, USA

1. Introduction

Solar energetic events are dominated by flares and coronal mass ejections. A comprehensive file of optical flares is produced by NOAA; using reports from many observatories around the world, they generate a single synthetic file by grouping the various reports concerning a same event into a single "grouped" report. The NOAA file is an invaluable tool for statistical studies involving large numbers of flares. Such a comprehensive file did not exist until now for CMEs, which considerably limited the statistical study of these events and their relationship with other aspects of solar activity.

In fact, it is difficult to produce a file of CMEs as these events can only be observed from space. In addition, they are best observed near the limb of the Sun, and for this reason they cannot be located accurately, nor can their possible interplanetary effects be well observed at Earth.

But CMEs are well correlated with eruptive prominences, which are seen as sudden filament disappearances on the disc. Filament disappearances may also happen without the eruption of the filament, for various reasons; however, the fraction of filament disappearances truly related to eruptive prominences and (disc) CMEs is high enough for a systematic file of filament disappearances to be highly desirable. This is what motivated us to undertake the generation of a such a computer file, by using existing (partial) files and doing the synthesis of as many of them as possible.

2. Grouping various files into a synthetic file of filament disappearances

2.a Source files

We compiled all the filament disappearances reported over the 31 years from 1957 to 1987, in the following sources of information:
- "Cartes Synoptiques de la Chromosphere Solaire et Catalogues des Filaments et des Centres d'Activité", of Paris-Meudon Observatory (this series was initiated by the d'Azambujas, who discovered the phenomenon and named it "Disparition Brusque" in French) → 2 184 events;
- "Annotated Atlas of Hα Synoptic Charts for Solar Cycle 20", by McIntosh (1979) → 1 549 events;
- Solnechnye Dannye (throughout the issues) → 117 events;
- a private list from Karen Harvey ("double-ribbon" events) → 90 events;
- NOAA computer diskets of filament activity (H. Coffey), collecting reports from various origins: Culgoora Observatory → 401, Catania Observatory → 269, and SOON (Solar Optical Observation Network) stations: Holloman → 149, Palehua → 135, Ramey → 112, Learmonth → 76, San Vito → 30.

The first 4 lists are in printed form, and we entered all the events they contain one by one on the computer. The last list is already in a digital form, and we could treat it directly on the computer. We sorted out the reports into 11 computer files, one file for each origin. This way we expect the data within a given file to be relatively homogeneous, in particular the detection thresholds, and we can compare the observations from different observatories.

Each report in each file is made up of a time and its uncertainty (often ±12 hours), a position in Carrington coordinates, and a 1-digit coefficient of "importance", plus eventual remarks. We made some conversions from the original values in order to get comparable parameters in the different files, with similar conventions and units, as best as we could.

In particular, we converted importances into a normalized scale defined by $I_0 = -2 \log N$, where $N =$ is the average number of events with importance $I \geq I_0$ per day. This is a convenient scale, covering occurrence frequencies of 1 event per day to 1 event per century with 1-digit numbers. All events currently reported fit within this scale.

2.b Clustering of reports

We considered all the reports from all the observatories together, and ordered them according to the time of the events. Reports which are close in time and in position probably concern the same physical event and are to be grouped into a single synthetic report. To do so, we defined the following "distance" between 2 reports i and j, in the 3-dimensional space with coordinates time t, longitude λ and latitude φ:

$$d_{ij}^2 = \left[\frac{t_j - t_i}{(dt_i + dt_j + 1\text{h}) \times 2}\right]^2 + \left[\frac{\lambda_j - \lambda_i}{20°}\right]^2 + \left[\frac{\varphi_j - \varphi_i}{10°}\right]^2$$

where dt is the uncertainty on the time. We chose the parameters in this definition so that the probability for 2 reports i and j to concern the same physical event is $p_{ij} \sim 0.5$ for $d_{ij}^2 \sim 0.5$; then we have:

$$p_{ij} \sim exp(-2\ln 2 \times d_{ij}^2)$$

. We did a first, crude clustering into clusters of less than about 20 events, based on the criterion that the distance between 2 reports in 2 different clusters must be > 3. Then we divided up every one of these "pre-clusters" further by taking the most probable clustering in the sense of the combined probabilities of all the pairs of events; this particular clustering is the one for which the following quantity is maximum:

$$P = \prod_{\substack{i,j \text{ in} \\ \text{same cluster}}} p_{ij} \quad \times \quad \prod_{\substack{i,j \text{ in} \\ \text{different clusters}}} (1 - p_{ij})$$

Inside each final cluster, we averaged the parameters with weights depending on the estimated uncertainties in the individual reports, and came up with a single "synthetic" report for each physical event. Starting from a total of 5112 individual reports we ended after clustering with a synthetic file of 4184 physical events.

3. Statistical properties of reported filament disappearances

The synthetic file of filament disappearances we just described covers almost 3 solar cycles (maximum of cycle 19 to the beginning of cycle 22). It contains an average of about 0.4 event per day. It is certainly less homogeneous than the individual files we used to generate it, but it is much more complete than any one of them: it contains twice as many events as the Meudon file which is the largest individual file. For this reason, it is interesting to study the statistical distribution of events in this file. We will just give 2 examples here.

Fig. 1 shows the distribution of the events as a function of their distance to the central meridian. This distribution is significantly dissymetrical, with more events on the east of the central meridian than on the west. This means that the detection threshold is on the average a little lower for events east of the central meridian. There is a similar effect, albeit smaller, for flare reports. It seems likely to us that this reflects the slightly greatest interest of observers for that part of the solar disc which they will be able to follow for the longest time. We must keep this in mind when doing statistical studies.

Fig. 2 shows the distribution of events in the 2-dimensional time-latitude space. We recognize a butterfly diagram similar to, albeit somewhat less dramatic than, the one observed with sunspots.

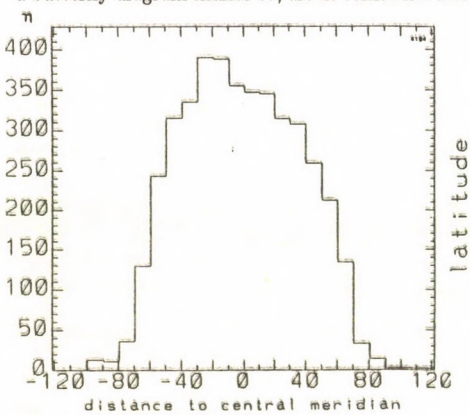

Fig. 1

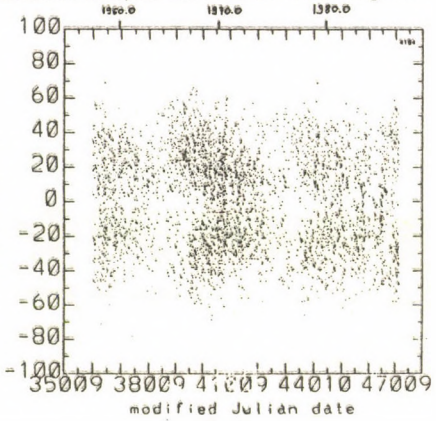

Fig. 2

4. Correlation between filament disappearances and magnetic clouds

It has been suggested that so-called "magnetic clouds" observed in the solar wind (Klein, Burlaga: 1982) are the trace of CMEs in the solar wind, but only case studies involving few events have been presented so far (e.g. Marubashi: 1989), whose statistical significance was difficult to assess. In order to know whether the observed associations are due to chance or are physical associations we have to carry out a systematic, selection free analysis between the 2 kinds of events. This is what we did with the synthetic file of filament disappearances, and a file of 176 magnetic clouds. We will describe elsewhere how we generated the latter file from existing lists and from our own inspection of King's Interplanetary Medium Data Books.

The crosscorrelation function of the occurrence times of filament disappearances and magnetic clouds exhibits two peaks centered on time delays of −1 and 0 solar rotation. It is likely that these 2 peaks are not random fluctuations, but correspond to physical associations. On the average there are ∼1.7 filament disappearances per time intervals 4 days wide, but there are ∼2.0 of them for time intervals centered on the occurrence of magnetic clouds or 27 days later. This increase in the occurrence frequency of filament disappearances at these specific times is rather small compared with the average occurrence frequency, and could only be discovered through the statistical treatment of a very large number of events.

The peak at -1 solar rotation is almost half a rotation wide. We interpret it the following way. The corona is subject to large scale instability processes which start high in the corona, above filaments, and slowly proceed towards lower and lower altitudes, to end up about a month later with the most spectacular phase to earth observers, the eruption of the filament. The typical time scale of the whole process is determined by coronal parameters and is of the order of one solar rotation just by chance. Several times during the whole process, coronal masses are ejected into the interplanetary medium where they result in magnetic clouds; but most of the time, and especially at the beginning of the process, these masses are too high above the Sun and too tenous to be observable as such.

When finally the underlying filament erupts, it is accompanied by a dense CME which will be observable if far enough from the center of the disc; it is followed within hours by the formation of a magnetic cloud in the solar wind. These filament disappearance – magnetic cloud pairs produce the $\Delta t = 0$ peak. Fig. 3 shows that this peak grows sharply out of the random fluctuations as we select only filament disappearances within a specific angular distance to the center of the disc or above a given importance level, while the $\Delta t = -27$ days peak does not exhibit the same tendency. This is readily explained in the suggested scenario.

Fig. 4 allows us to compare the histograms of the longitude difference in filament disappearance – magnetic cloud pairs, between random (background) pairs and pairs whose time difference is within the $\Delta t = 0$ peak. We see that magnetic clouds occur mostly 20° to 30° east and west of the center of the disappeared filament. This is reminiscent of the frequent property of CMEs to take the shape of large arches supported by 2 "legs" on either side. We suggest that magnetic clouds form in these legs.

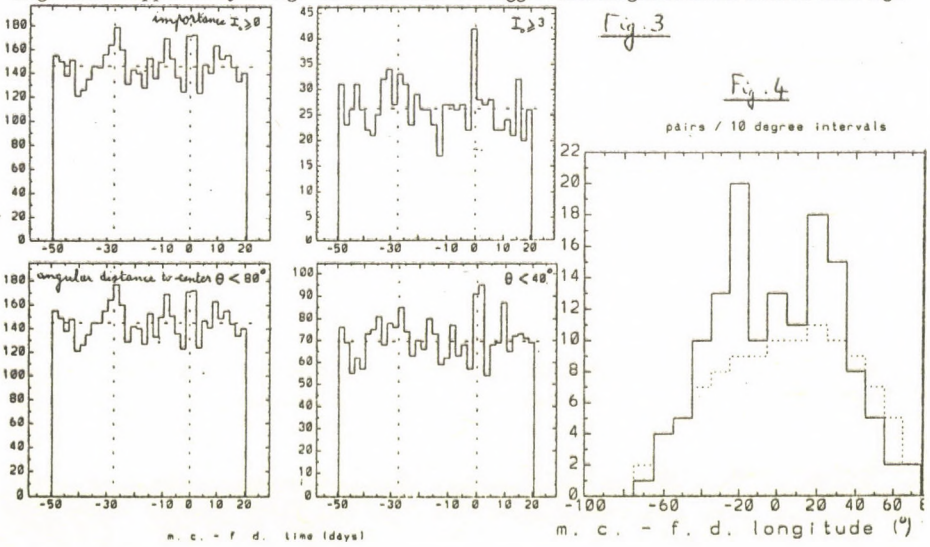

5. Conclusion

We have generated a computer file of more than 4000 filament disappearances over a 30 years period, by synthesis of many different observations. This file will allow us to carry out statistical studies involving a large number of filament disappearances.

As a first application, we bring the first solid statistical evidence of a physical link between filament eruptions and magnetic clouds observed in the solar wind.

STRUCTURE AND EVOLUTION OF THE LARGE SCALE GRANULATION FLOW PATTERN

R. Muller, Th. Roudier, J. Vigneau
Pic du Midi Observatory, France
Z. Frank, R. Shine, T. Tarbell, A. Title
Lockheed Palo Alto Research Laboratory, USA
G. Simon
Air Force Geophysical Laboratory, Sunspot, USA

A granulation movie has been performed at the Pic du Midi Observatory on September, 20, 1988. It combines spatial resolution (close to the diffraction limit of the 50cm refractor at 5750 Å : 0"23), a large field of view (100"x70") and a duration of 3 hours. The movie was digitized with a 1024x1024 CCD camera at Lockheed Palo Alto Research Laboratory (LPARL). The images were compressed to 512x512 frames to be processed with movie processing developped at NSO Sunspot and LPARL (November et al., 1986 ; Title et al., 1986, 1988, Simon et al., 1988, Brandt et al. 1988). It consists of alignement of consecutive frames, destretching for atmospheric distorsion, and a 4km sec^{-1} subsonic filtering which removes the 5 minute oscillations. Video disk movies of the full 3 hours, as well as a 57 min segment of the best quality were assembled. Time averaged plots of the velocity vectors were made. An example is shown in Figure 1, representing the velocity pattern derived from the 57 min best segment. The motions related to the evolution of granules are suppressed by the averaging, revealing a steady flow pattern. The Pic du Midi granulation movie contains an additional important piece of information : the location of magnetic flux tubes can be detected through the identification of the associated Network Bright Points (NBPs) which form the photospheric network (Stenflo and Harvey, 1985 ; Muller, 1985). All NBPs which appeared during a period of 20 minutes are plotted in Figure 1. A single large cell, suggesting a supergranule, is prominent in the right side of the plot. The accumulation of NBPs at the boundary supports the supergranule nature of this cell.

Many regions of divergence are visible within the cell boundaries, which can be considered to be mesogranules (Simon et al., 1988 ; Title et al., 1989) ; such regions are also visible outside the supergranular cell. The regions of convergence are more prominent outside the large cell than inside. Surprisingly, there is no vortex visible in the movie, although the field of view is 15 times larger and the duration 25 times longer than the La Palma movie, where such a flow pattern was discovered (Brandt et al., 1988).

Figure 1 shows where magnetic flux tubes, which produce NBPs, tend to accumulate. As we have already noticed, the main accumulation occurs at the supergranule boundaries. There are, in addition, several concentrations of NBPs in isolated convergence areas. It is also remarkable that very few magnetic features are visible inside the supergranule and that they completely avoid the centers of divergence. There is a concentration of Network

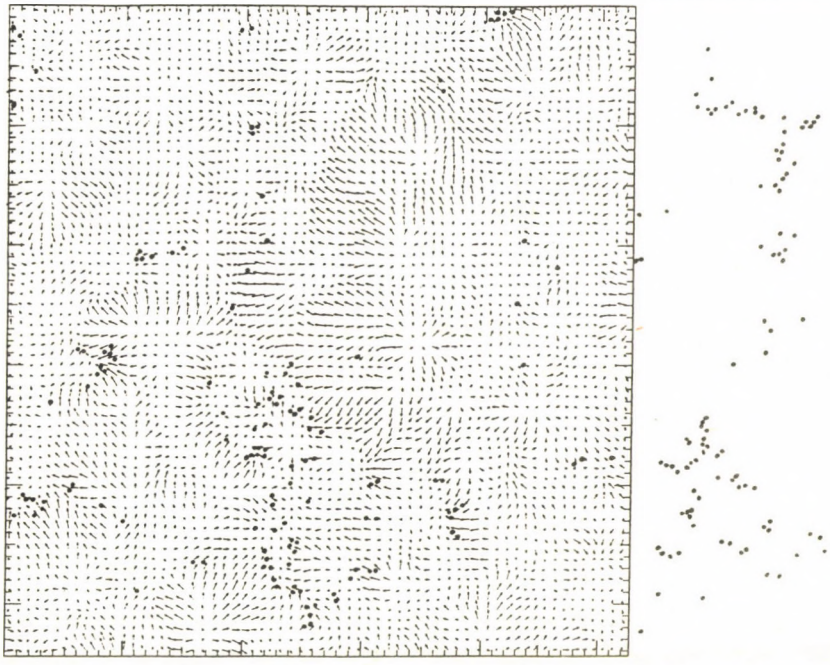

Figure 1 : Granulation flow pattern on 64x64 grid, averaged over 57 minutes. The position of the Network Bright Points (NBPs) identified during a 20 minute segment are plotted ; many of them have been identified outside the processed area. The divisions represent 1".

Bright Points in the lower part of the field of view ; it corresponds to a region of abnormal granulation produced by the remnant of an active region or a small plage. It is interesting to note that there is a small area of divergence inside this plage, which is free of NBPs. The amplitude of the vectors is small in the plage area, which is compressed between large amplitude inward flows ; they probably contribute to stabilize the plage area.

Figure 2 is a 33 minute time average of the flow pattern. It was derived from the 3-hour movie and represents a slightly different area than in Figure 1 ; its dimension is 58"x48". Five successive frames were produced in order to analyse the change of the flow pattern. The supergranule is stable over the 3-hour duration of the movie. The divergence areas are noted as overlayed contour maps of the average flow vectors ; their position is shown at the beginning and at the end of the sequence. Their motion toward the supergranular boundary is evident, especially when they are located away from the cell center. The translational velocities range from 0.0 km/s to 0.7km/s, with a mean velocity of 0.3 - 0.4 km/s ; this is consistent with the horizontal velocities derived in supergranules from Dopplergrams. Asymmetry in the granular flow pattern also suggests a mesogranular flow to the boundary of the

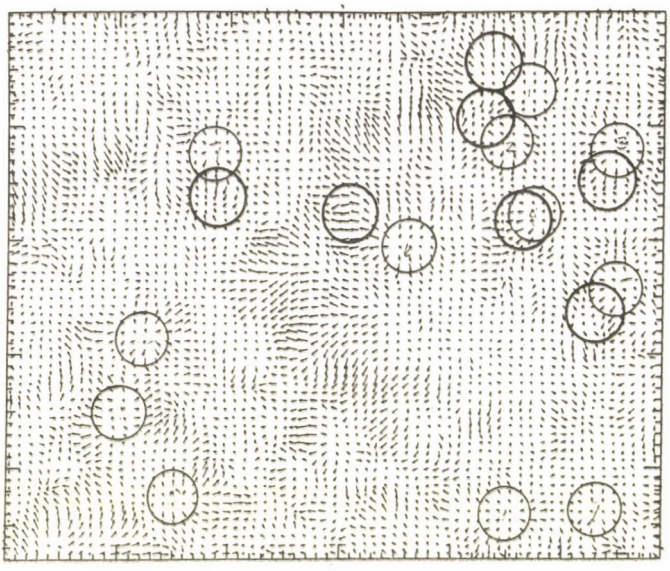

Figure 2 : Granulation flow pattern on a 64x64 grid, averaged over 33 minutes. Initial positions of divergence regions are marked by a thin circle ; their positions 2.5 hours later are marked by a thick circle.

supergranular structure. Velocity arrows are longer on one side of the mesogranules, indicating motion in that direction : the supergranular flow sweeps the mesogranular cells to its boundary. There are 7 to 8 diverging regions in the supergranule cell at any time. One of these regions will appear or disappear every 33 minutes, which implies a mesogranule lifetime of about 3 hours. Outside the supergranule, the diverging regions move at random and their lifetime is shorter, two hours in average.

Our observational results about the flows on the surface of the sun are in good agreement with the predictions of the 3-D numerical simulation of solar convection, recently performed by Stein and Nordlund (1989). They describe the horizontal flow in terms of a hierarchy of cell sizes ; pressure fluctuations induced by large scale cells can reach the surface, driving horizontal flows which in turn advect smaller cells.

References

Simon, G., Title, A., Topka, K., Tarbell, T., Shine, R., Ferguson, S., Zirin, H. and The SOUP Team : 1988, Astrophys. J. 327, 964.

Title, A., Tarbell, T., Topka, K., Ferguson, S., Shine, R. and The SOUP Team : 1989, Astrophys. J. 336, 475.

Stein, R. and Nordlund, A. : 1989, Astrophys. J. 342, L95.

Brandt, P., Scharmer, G., Ferguson, S., Shine, R., Tarbell, T. and Title, A. : 1988, Nature 335, 238.

ON MOTIONS OF MAGNETIC FIELDS AND INDUCTION OF ACTIVITY CENTERS

I. Sattarov
Astronomical Institute of the Uzbekistan Academy of Sciences,
700052, Tashkent, USSR

V. Bumba
Astronomical Institute of the Czechoslovak Academy
of Sciences, 251 65 Ondřejov, Czechoslovakia

Abstract: The problem of the existence of an agent exciting the appearance of activity centers connected with the action of Active Longitudes is discussed.

During June-July 1984 we observed, in a recurrent active region, two sunspot groups both fully developed on the visible solar disk in which their leading spots seem to be genetically related. The second leader developed in the position in which the first would have been located during its westward motion, if it had not disappeared earlier. Of course, we have to take into account the substantially slower motion of aging spots (Van Driel-Gesztelyi 1990). The same has been observed in another July 1984 group with a revival of activity: the new leading spot joined the rapidly diminishing westward moving old spot as soon as the older preceeding spot reached the place where the new one was growing, to continue both jointly in their westward motion. At the same time the motions of the following spots of all four groups were very vague. The observations raise a problem: Is the agent exciting the development of these groups common to all of them?

If we observe the consecutive development of the individual active regions in a heliographic longitudinal interval belonging to a certain Active Longitude (A.L.) (See for example Fig. 1 for Carrington's rotations Nos 1745-1749), we again see that the first groups start to form close to the eastern border of the A.L. interval and the formation of further new active regions is gradually shifted more and more

westward.

The westward shift of the A.Ls during their development from one rotation to the next shows a very remarkable feature: if an A.L. meets the region of an older, already almost exhausted activity, very often this activity is revived. For example, during five Carrington's rotations in 1984 we found about ten such renewals of activity connected with the shift of one single A.L.. We have to mention that the velocity of the westward shift of the A.L. front is of the order of about 30 m/sec.

This continuous successive revival of activity can be observed on successively mounted magnetic synoptic charts from the Kitt Peak Observatory also if only a weak and old field existed in the area the front of the A.L. had crossed before the new activity appeared.

In this way we believe it is demonstrated that such an agent exciting or inducing the formation of active regions observed morphologically in the form of a moving A.L. front very probably exists. The question remains: what is the physical reason for such a process?

Reference:

Van Driel-Gesztelyi 1990 PHD Thesis, Ondřejov, 28.

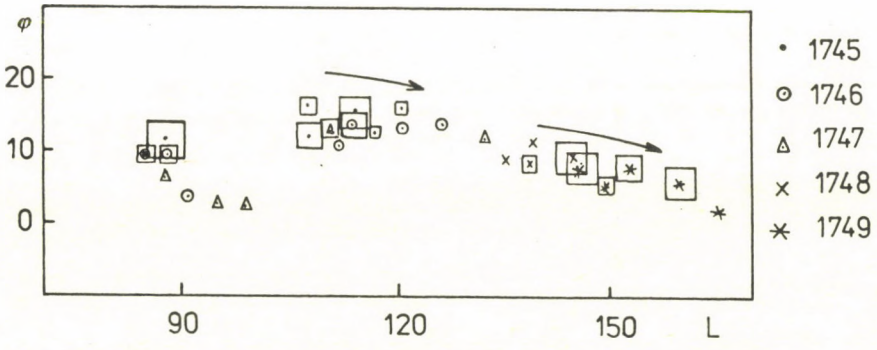

Fig. 1 Successive development of new active regions during subsequent Carrington's rotations in the interval of heliographic longitudes L = 90^{o} - 150^{o}.

THE SOLAR GLOBAL VELOCITY FIELD INFERRED FROM DEVELOPING LARGE-SCALE MAGNETIC FIELD STRUCTURES

Pavel A m b r o ž
Astronomical Institute of the Czechoslovak Academy of Sciences
251 65 Ondřejov, Czechoslovakia

Changes created during the development of large-scale background magnetic fields are used for the horizontal velocity field determination. A computer algorithm to determine transverse velocities in the photosphere has been developed. The algorithm is based on local cross correlation. The first results are presented as well as usefulness of the method is discussed. The examples of photospheric velocity maps are shown.

This paper describes the application of a very fast method for computing the displacement map between two similar synoptic charts of large-scale distribution of the solar magnetic field.

This field may be described by 2D array of the radial component of magnetic induction vectors. Values of vectors are calculated using the spherical harmonic function method (Altschuler and Newkirk, 1969) in the Carrington coordinate system. Calculations are made for two following rotations from harmonic coefficients which are determined from observations by Hoeksema and Scherrer (1986). Existing difference between both synoptic charts (arrays) is supposed to be affected mainly by horizontal velocity field. We assume that the velocity is responsible for local changes of the magnetic field strenght (Ambrož 1987).

A computer algorithm to measure transverse velocities of apparent displacements of intensity structures is based on the local cross correlation techniques described in detail by November (1986). Our correlation algorithm computes the Local Absolute Difference Function according Darvann et al. (1990).

The displacement map calculated by the above mentioned method is presented in Fig. 1. Arrows indicate local horizontal velocity vectors responsible for the horizontal displacement of magnetic field structures. We suppose that they represents the horizontal plasma velocity field. Arrows with circles in the origin represents the velocity which surpasses the used graphical scale. Typical velocities in both directions corresponds to about 20 to 30 m s^{-1}.

The radial velocity field may be inferred from divergence calculations. For the selected time periode, a more enhanced flow is detected in the southern hemisphere.

The mean value of the meridional velocity averaged over the whole solar surface is nearly 2 m s^{-1}. However, a specific structure and organization in the velocity field distribution are observable. This is probably a reason why the nearly negligible mean meridional circulation and the time dependent differential rotation are measured. The structure and organization of the global convection are not yet sufficiently clear. The map which show as a contour plot the values of rot v indicates a nearly

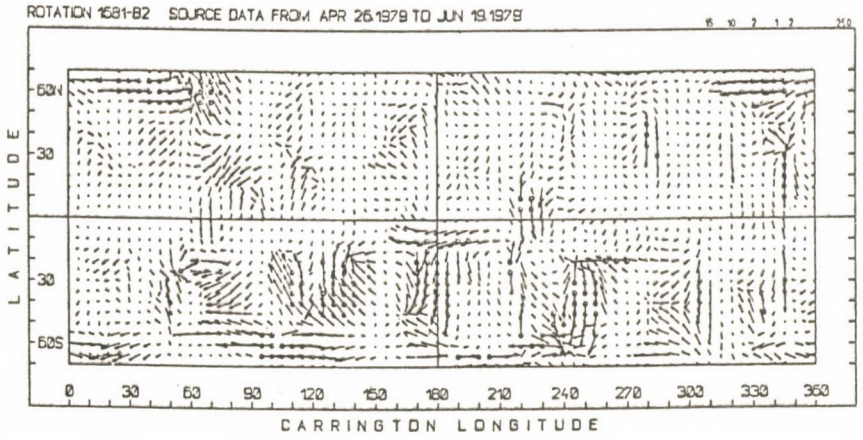

Fig. 1. Horizontal velocity vectors field generated by comparing numerically pairs of magnetic synoptic charts. Arrows with circles in the origin represent the velocity which exceed the used linear graphical scale.

random distribution of regions with positive and negative values. But when a more broader convolution window is used and a higher spatial averaging process is applicated then we obtain a simpler and more regular system of patterns. Distinct boundaries in the heliographic latitude between $\pm$(50 - 60) degrees then exist. A 60 degree period of the pattern occurrence is also present in longitude. Both these characteristics indicate a specific organization of the large-scale convection on the Sun. The work in this field is in progress.

References

Altschuler, M.D. and Newkirk, G.: 1969 Solar Phys. 9, 131
Ambrož, P.: 1987 Bull. Astron. Inst. Czechosl. 38, 110
Darvann, T.A., Koutchmy, S. and Zirker, J.B.: 1990, preprint Proc. IAU Coll No. 117, Hvar obs. Bull. (ed. V. Ruždjak)
Hoeksema J.T. and Scherrer, P.H.: 1986, The Solar Magnetic Field 1976 Through 1985, Report UAG-94
November, L.J.: 1986 Appl. Opt. 25, 391

THE DIFFERENTIAL ROTATION LAW OF THE SOLAR PLASMA NEARBY THE POLES

Hubertus Wöhl and Binxun Ye

(Kiepenheuer-Institut für Sonnenphysik, Schöneckstr. 6, D-7800 Freiburg, FRG)

One mode of large-scale motions of the solar plasma, the differential rotation, was determined as a generally accepted law by Howard and Harvey (1970) two decades ago. But how reliable is this law, which was determined globally, for the solar poles ? Taking into account earlier attempts e.g. by Beckers (1978) and Cram et al. (1983) the deviations are determined quantitatively. In addition a search for large scale velocity patterns nearby the solar poles was performed.

Traditional spectroscopic methods were used to perform this task using the Echelle spectrograph of the German 60 cm Vacuum Tower Telescope located at Izaña, Tenerife. A CCD detector recorded the profile of the Fe 6302.5 line along with the nearby terrestrial oxygen lines for simultaneous wavelength references (Schleicher et al; 1989). Observations were performed mainly during the period of 27th June to 2nd July,1989. In addition data obtained in May 1989 and April 1990 during test phases could be used. In total, more than 300,000 spectra from 1,230 CCD images were obtained over the area from the heliographic latitude of 75° to the poles.

Data frames were flat-fielded by a frame derived from the data frames itself. For further reducing the fringe effects caused by the thinned CCD structure, a 2nd-order Butterworth filter was run over the data frame in its frequency domain. The final accuracy for the determination of velocity was kept within 1.5m/s. Spectral limb shift and scattered light effects were also derived from the area very near to the central meridian and individual data were corrected with it.

Our results show a slightly steeper gradient of the differential rotation law as compared to Howard and Harvey(1970), the standard deviation to that law being about 9 m/s. In addition a persistent velocity pattern within 10° latitude around the poles was found : A lower velocity of about 200 m/s as compared to the Howard and Harvey (1970) expression from 83° to 85° and a higher velocity of about 100 m/s from 86° to 89°.

The full details of this investigation will be published in a paper, which is submitted to Astron.Astrophys.

References

Beckers, J.M. : 1978, Astrophys.J. **224**, L143

Cram, L.E.,Durney, B.R., Guenther, D.B., : 1983, Astrophys. J. **267**, 442

Howard, R., Harvey, J.W.: 1970, Solar Phys. **12**, 23

Schleicher, H., Wittmann, A.D., Wöhl, H., Ye, B. : 1989, : Astronomische Gesellschaft Abstract Series **3**, 18

MERIDIONAL MOTIONS OF RECURRENT SUNSPOTS - A COMPARISON OF GREENWICH AND KANZELHÖHE DATA *

G. Lustig, Institut für Astronomie, Karl-Franzens-Universität, Universitätsplatz 5, A-8010 Graz, AUSTRIA

H. Wöhl, Kiepenheuer-Institut für Sonnenphysik, Schöneckstr.6, D-7800 Freiburg, F.R.G.

From the Greenwich Photoheliographic Results and the Kanzelhöhe sunspot observations identical recurrent sunspot groups with at least eight observations per passage and at least two passages of type H or J were selected. The total number of these groups - mainly single spots - is 44 for the period of overlapping observations from 1948 until 1976.

The meridional motions were determined by two methods for each group.
(a) from linear fits of the latitudes depending on the passage time (= PM = passage motion)
(b) from mean latitudes at about central meridian passages of recurrencies (= RM = recurrent motion).
Average values of these meridional motions, mean latitudes and mean dates of the existence were computed.
The main result is a very small non-significant mean value of the meridional motions of the RM data, well below a motion of one meter per second. The correlation of the PM and RM-data is about + 0.4.

In general the PM values are about twice as big as the RM values. The same holds for the rms errors. There is a non-significant southward motion of the spots from the PM data, as already found for all spots by several authors.
Attempts were performed to determine latitude and cycle dependencies of the motions.

* submitted to Astronomy and Astrophysics

LATITUDE-TIME DEPENDENCE OF THE 530.3 nm SOLAR CORONA ROTATIONAL CHARACTERISTICS OVER CYCLE 21

V. Dermendjiev[1], V. Rušin[2], M. Rybanský[2], G. Buyukliev[1]

1 Department of Astronomy and NAO, 72 Lenin Blvd, 1784 Sofia, Bulgaria
2 Astronomical Institute, Slovak Academy of Sciences, 059 60 Tatranská Lomnica, Czechoslovakia

1. INTRODUCTION

A problem of coronal rotational characteristics and their latitude-temporal dependence is still under discussion. There are also some discrepancies in the results of different authors. Nevertheless, an unanimous conclusion was obtained that the short-term variations in the time series of different coronal indexes are associated with the evolution and rotation of active photospheric areas, controlled by magnetic fields.

In this paper, we study the shortest cyclic variations in the data set of the 530.3 nm coronal line, representing its rotational rate at given latitudes and depenging of the solar cycle phase.

2. OBSERVATIONAL DATA AND METHOD OF ANALYSIS

Average values of 530.3 nm coronal line intensities (Rybanský, 1975) for a given latitude were used in the period 1977-1986.

A method similar to that proposed by Hansen et al. (1969) for establishing the synodic rotation period for different bands of latitude was used. The data are divided into yearly intervals and then averadeg into bands of latitude (each 15^{o} in extent) centered on latitudes 75^{o}, 60^{o}, 45^{o},30^{o}, and 15^{o} in each hemisphere, and the solar equator.

The data series had any significant long-term trend removed before calculations of the ACF. The lag τ_{*} of the first positive interpolated by parabola maximum of ACF, was taken to be the estimate of the synodic rotation period. The underlying assumption in such an interpretation is the observational fact that coronal structures persist at least 27 days and give rise to a local maximum in the ACF as they appear across the central meridian on successive solar rotations.

The corresponding 15^{o} and 30^{o} wide latitude bands are formed to be symmetrically situated in relation to the solar equator. Each band averaged four seven 5^{o}, in a position angle separated intensity values in a such way, that its first value is the last value of the preceding band. In other words, the consecutive latitude bands overlap 5^{o}.

3. RESULTS AND DISCUSSION

The averaged synodic rotation period at 15^{o} centered latitudinal bands as a function of latitude is shown in Figure 1.The 90 % error bars are also indicated. For comparison, the synodic rotation periods (crosses) for the same corona and period, but observed at the height of 1.15 $R_{\odot}$ (Sime et al., 1989) are given. Our estimates of the rotation periods are smaller that than of them, and show the N/S asymmetry. The yearly average synodic rotation period as a function of year for the interval 1977-1986 is shown in Figure 2.

The crosses indicate similar Sime's data. Again, our data are smaller (the green corona rotated faster) in comparison with their data and show a cyclic behaviour. It follows from Figure 2 the height-temporal dependence (± 0.5-1.0 day) of the green corona rotation rate over cycle 21. A very complicated picture of its rotation rate over cycle 21, but very closely to these both results, was obtained by a FTT method (Rušin and Zverko, 1989).

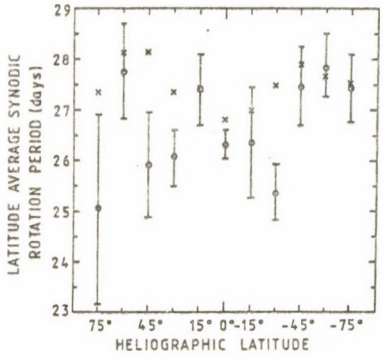

Figure 1. The averaged synodic rotation period vs latitude.

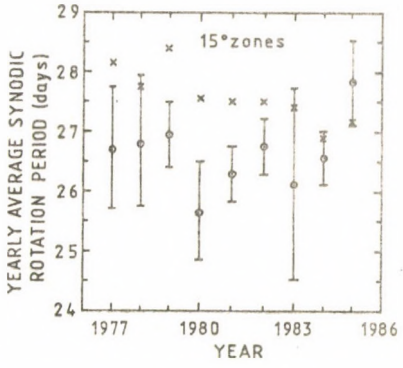

Figure 2. The averaged synodic rotation period vs cycle.

An interesting result can be traced in the isoplete map (Figure 3). It represents the value of $(P_{i,b} - \bar{P})/\sigma$, where σ is the standard deviation as a function of heliographic latitude and time respectively, for 5^o and 15^o latitude zones taken asymmetrically to the equator. Two years after the 21th solar cycle maximum (1983) in the high latitudes of the N-hemisphere the green corona shows its faster rotation. This effect is repeated also in 1985 in the same latitudes. We suppose it could be a result of the appearance of a new convective roll structure of the global extended cycle.

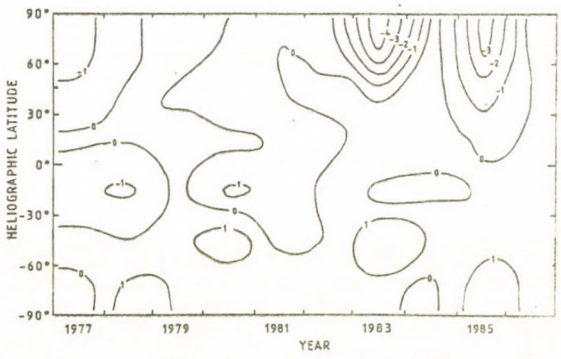

Figure 3.
Isoplete map of $(P_{i,b} - \bar{P})/\sigma$

References

Hansen, R. T., Hansen, S. F., Loomis, H.: 1969, Solar Phys. **10**, 135
Rybanský, M.: 1975, Bull. Astron. Inst. Czechosl. **26**, 367
Rušin, V., Zverko, J.: 1989, Solnechnyje magnitnije polja i korona, Nauka, Novosibírsk, Sib. otdelenije, p. 350
Sime, D. G., Fisher, R. R., Altrock, R. C.: 1989, Astrophys. J. **336**, 454.

ON THE APPEARANCES, INTENSITIES AND MOTIONS OF SOLAR MICROWAVE LOW TEMPERATURE AREAS

S.Pohjolainen[1], R.Brajša[2], S.Urpo[1], H.Teräsranta[1], B.Vršnak[2], V.Ruždjak[2] and S.Jurač[2]

[1]Metsähovi Radio Research Station, Helsinki University of Technology, 02150 Espoo, Finland

[2]Hvar Observatory, 58 450 Hvar, Yugoslavia

ABSTRACT: Solar microwave sources at 37 GHz have been observed at Metsähovi since 1978. The solar maps have revealed the existence of low temperature regions (LTR), i.e. areas where the brightness temperature is typically 100-400 K lower than the quiet Sun level, throughout the solar cycle. We have investigated the appearances, intensities and motions of these temperature depressions and compared them with the activity features in the optical part of the spectrum.

The sun has been monitored at 37 GHz since 1978 using the 13.7 m diameter telescope at Metsähovi with a beam size of 2.4 arc minutes. In the temperature scale the resolution is better than 100 K, depending on changes in atmospheric attenuation. The mean quiet sun at 37 GHz is estimated to have a brightness temperature of 7800 K in all maps. The contour lines in Figure 1 represent the temperature increase (thin lines) or decrease (bold lines) compared to the quiet sun level whereas number 1 denotes the crossmarker, 2- enhancement of radiation, 3- belt of low temperature regions, 4- low temperature area, 5-active region, respectively.

LTR are areas where the brightness temperature is usually 100-400 K below the quiet sun level, though temperature drops as high as 900 K have been recorded. The regions appear at all latitudes between 0-55 degrees at both solar hemispheres. The positions of temperature minima within the LTR, superposed on the synoptic maps of the inferred maps from SGD are presented as an example in Figure 2. About 90 % of the LTR were on the SGD inversion lines of the photospheric magnetic field and the same holds for the Solnečneye Dannye inversion lines. Only about 1 % of LTR were not associated neither to SGD or SD inversion lines. About 60 % of LTR were associated with filaments. However, since filaments occupy a considerable length of magnetic inversion lines, this association could be partly accidental.

The tracers used for an estimate of the differential rotation were determined to be points with the lowest brightness temperature in the LTR. We excluded from the original sample the objects which were measured only two times during the disc passage, as well as the objects for which the coefficient of correlation for the linear least square fit was less than 0.99 in the central meridian distance maps used for the determination of the rotation rates. The average rotations rates in 10 degree intervals of latitude are presented in Figure 3 together with the standard deviations.

In conclusion we can say that the differential rotation curve for LTR representing the pattern of large scale magnetic fields, fits very well to the standard differential rotation low. It implies that the height of LTR is low, since otherwise it would show higher rotation rates due to projection effects. Furthermore a very strong association of the LTR and magnetic inversion lines has been established. The possible association with filaments needs further study.

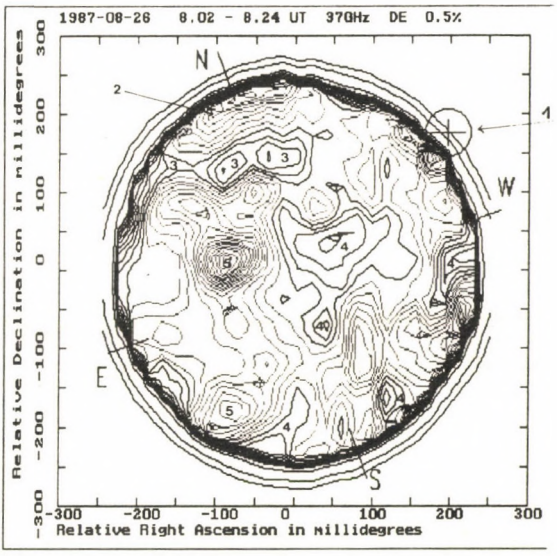

Fig. 1

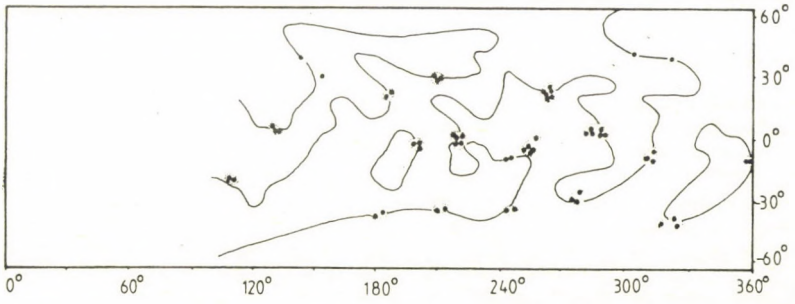

Fig. 2

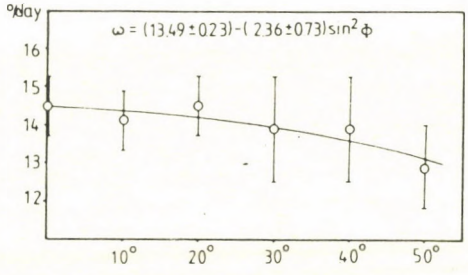

Fig. 3

PROPER MOTIONS IN HALE REGIONS 18405 AND 18511 (2-14 JUNE, 4-16 AUGUST 1982)

G.Csepura and I.Nagy
Heliophysical Observatory, Debrecen

Abstract

Between June 2-14 and August 4-16 1982 there were two active regions on the north hemisphere of the Sun (Hale regions 18405 and 18511). We investigated the first and third rotation of these regions. We found an about eighteen-day-long torsional oscillation of sunspot umbrae exists.

Introduction

In this article we present the study of the sunspots proper motions in a large activity complex over four solar rotations. These four solar rotation were from June to September 1982 (Hale Region 18405, 16474, 18511 and NOAA 3885, 3886) and the active regions were between L:307-305, B:7-22. Two of these four active regions have already been written up [1,2]. In our work we try to write up the first and the third rotation of these regions.

Discussion

In our work we investigated the motions of the umbrae in the Carrington system and a few rotations of the umbrae.
The HR 18405 sunspot group was well developed when it appeared. Different polarities of the umbrae occurred in the P part of this group for example spot 3,4 and 6 are northern and the others were southern in Fig.2. The leading umbra of the June group consisted of 2 main parts (3 , 4). In the beginning these 2 umbrae moved toward each other. After clashing one of them turned back.
In the third rotation the leading spot became compact and this sunspot group stretched 26 degrees in the Carrington system. The P part motions of the third rotation of the sunspot group is shown in Fig.3. We fitted an ellipse around the umbra spot A. We studied the angular of the major axis of this ellipse in the Carrington system. The result is shown in Fig.5. The P part of third rotation divided into two main parts in the fourth rotation. This region has been published [1].

We found the following result:

- the direction of this rotation changed. We think the P part performed a torsional oscillation which had about an 18 day-long period.

Reference

1./ G.Csepura and I.Nagy: 1987, *Publ. Astr. Inst. Czechoslovak Acad. Sci.* No. 66, p. 157-160
2./ B.Kálmán and I.Nagy: 1988, in V.N. Obridko, G.Ya. Smolkov (eds.), *Solar Maximum Analysis*, Novosibirsk, p. 47-50

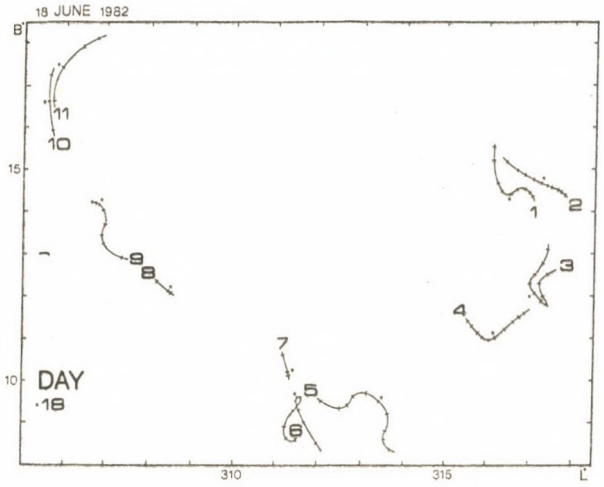

Figure 2.

Figure 1.

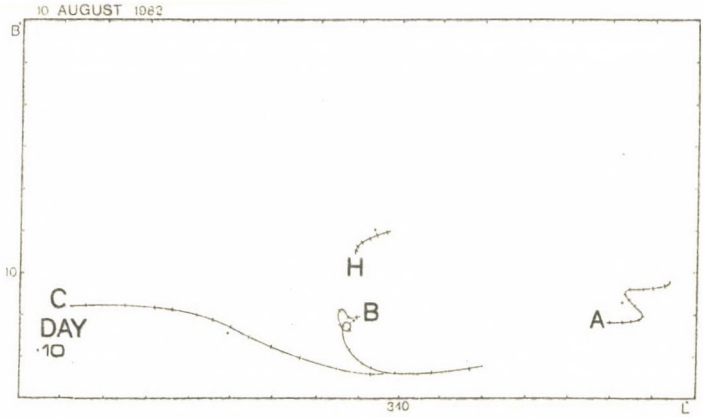

Figure 3.

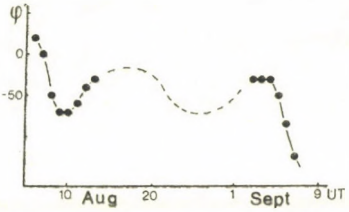

Figure 5.

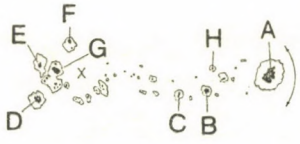

Figure 4.

DERIVATION OF THE PARAMETERS NECESSARY TO DETERMINE THE NORTH DIRECTION OF A HELIOGRAM

L. Győri

Heliophysical Observatory of the Hungarian Academy of Sciences, Gyula Observing Station, 5701 Gyula, P.O.Box 93, Hungary

Abstract. The accurate determination of the north direction of a heliograph is of basic importance to measure global motion on the Sun. If the alignment of the heliograph is not perfect the north direction of the heliogram changes relative to a fix direction in the image plane of the heliograph. This change depends partly on the alignment errors of the heliograph. Here we propose a method to determine the pole distance and hour angle of the hour axes of the heliograph which are the alignment errors of the heliograph.

To measure global motion on the Sun´s surface with high accuracy we must know the accurate north direction of the heliogram (Smart, 1977). If the alignment of the heliograph is not perfect that direction changes relative to a fix direction in the image plane of the heliograph according to the formula

$$DP_o^{\substack{E\\W}} = (\pi/2-|\alpha|)\,\mathrm{sign}(\alpha) + \lambda\sin(t-\varphi)\sec(\delta)\pm \pm[\omega\sec(\delta)-\varepsilon\tan(\delta)] \qquad (1)$$

(Győri, 1989).
The meaning of notations in (1) are: ΔP_o, the angle between the north direction of the image plane and image of a thread located in the primary image plane of the heliograph; α, angle between the imagened image of the declination axis and the image of the thread; λ, pole distance of the hour axis of the heliograph; φ, the hour angle of the hour axis; ω, the angle between the declination axis and hour axis of the heliograph is $\pi/2+\omega$; ε, the angle between the declination axis and optical axis of the heliograph is $\pi/2+\varepsilon$; δ, the declination of the Sun; t, hour angle of the Sun; the plus sign before the last term in (1) stands for the east position (E) of the heliograph and the minus sign for the west position (W).

We propose a method to determine parameters λ and φ. We make use of that well known effect that if the alignment of the heliograph is not perfect the image of a sunspot is continuously being shifted along the north direction of the image plane as the time proceeds (the heliograph is clamped in declination and rotated around the hour axis so that the center of the Sun´s image be on the line containing the centre of the image plane and representing the north direction). The shift d of a sunspot measured from a fiducial point along the north direction can be decribed by formula

$$d=\lambda\left[\cos(\varphi-t)-\cos(\varphi-t_o)\right] \qquad (2)$$

where t_o is the hour angle of the fiducial point.

To get equation (2) λ is supposed to be small ($1 < 1°$).

At deriving formula (2) the effect of the refraction and change of the Sun's declination were not taken into account. If one corrects the measured shift for refraction and the change of the declination of the Sun one can fit the curve determined by formula (2) to the corrected shift versus hour angle of the Sun and the parameters λ and φ can be determined.

As an example we provide Figure 1 which shows the corrected shift of a sunspot (*) as the function of the hour angle of the Sun and the curve fitted to them (lam=λ, fi=φ, in degrees).

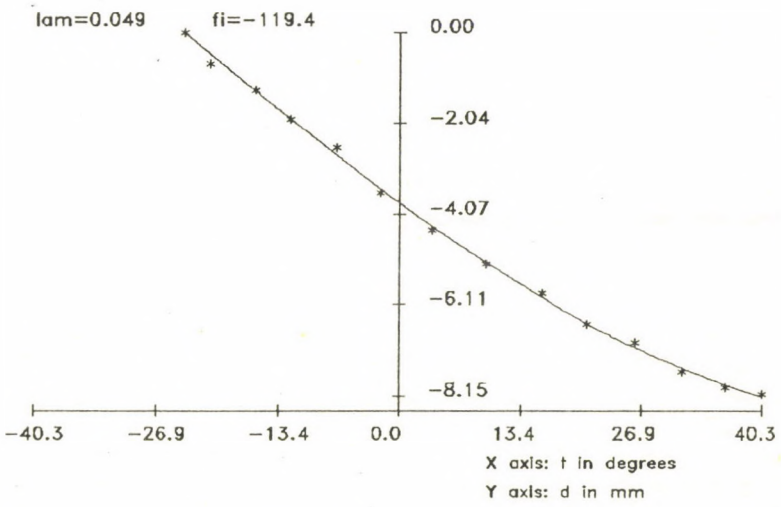

Fig. 1. d vs t. (*) denotes the corrected shift of a sunspot, continuous line is the fitted curve to them (lam=λ, fi=φ, in degrees).

References

Smart, W. M.: 1977, Textbook on Spherical Astronomy, Cambridge University Press, Cambridge.

Győri, L.: Solar Physics **120** (1989) 421-430.

THE KANZELHÖHE PHOTOHELIOGRAPH

Thomas Pettauer
Sonnenobservatorium Kanzelhöhe

The heliograph is of the classical design with an enlarging lens and cross-hairs in the prime focus for orientation.

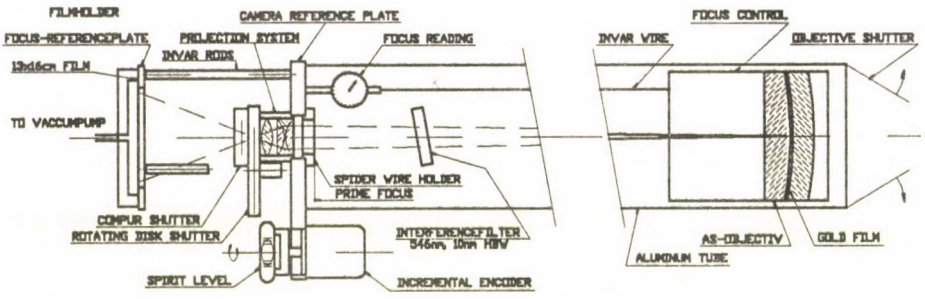

The front element of the Jena AS-objective lens (13/195cm) is coated with a transparent goldfilm, to get, with full aperture, exposure times in the millisecond range and to prevent eccessive heatload on the interference filter . The goldfilm, evaporated in high vacuum on the air gap side of the front lens transmits 9% in the green. With this method no additional optical element is necessary, and the soft film is well protected against mechanical damage. Goldfilms are very stable in the atmosphere and have additionally a sharp cut-off in transmission in the green to longer wavelength.

The interference filter of image quality has a HBW of 10nm at 546nm. It is placed about 15cm in front of the prime-focus with a small tilt, to reflect the offband ligth to the well blackened (3M black velvet) and baffled telescope tube.

The "camera-unit" with the magnifying lens and shutter is screwed to the telescope tube. The alignement of the camera in respect to the telescope tube is given by a ground steel plate, which defines a reference plane and a mechanical (=optical) axis. Exactly centered on this axis are: the cross hairs necessary for precision position measurements and the magnifying lens, a modified orthoscopic eyepiece. This magnifying lens has considerable distortion and will be replaced. The diameter of the enlarged solar image is 8,7cm. Three invar rods define the film plane parallel to the reference plate (and focal-plane) better than +/-0.02mm, therefore plate tilt is neglible. Vacuum film holders prevent wrapping of the 13 x 16cm film (Kodalith Ortho 3).

The shutter unit consits of a commercially available magnetic Compur-shutter and a rotating disk shutter. The latter defines the exposure time and has a trapezoidal shutter profil with appr. 80% complete opening. A microprocessor is used for the correct timing of the shutter sequence and control of the motor speed of the disk shutter. The exposure time is set manually or measured electronically.

The cross-hairs in the prime focus serve as reference marks on the heliograms. To get accurate positions, the orientation of one of the cross-hairs on the sky has to be known very precise. Normally the daily motion of the sun is used for this purpose. With this heliograph a simple and accurate orientation method is used.

If one cross-hair is exactly in the east-west direction, than the angle it includes with the horizon is the parallactic angle (eta in the Debrecen notation). In practice the cross-hair deviates from the east-west direction due to errors in telescope alignment, mounting of the camera etc. The orientation error at the time of exposure is obtained by comparing the true, measured angle of the cross-hair with the calculated angle. The device to measure the inclination of the cross-hair consists of a spirit level (20" sensitivity per part) mounted on an incremental encoder to measure the angle with one arc minute resolution. The "P-meter" is firmly attached to the reference plate of the camera and forms a compact unit with the cross-hairs.

The instrument is completly calibrated in the laboratory with the camera mounted on an exactly leveled granit-table with a horizontal camera axis. First the cross-hair is aligned in the east-west direction to a few tens of a degree, than the cross-hair is brought into a perfect horizontal position by turning the whole camera around its axis. This position defines the zeropoint of the P-meter.

The true angle cross-hair/horizon on the instant of exposure is obtained by interpolation of P-meter readings before and after the exposure. The times of the P-meter readings and exposure are automatically registered and are accurate to 1 second.

Errors of the P-meter: 1. The axis of the spirit level is not normal to the rotation axis of the angle measuring device. - If the rotation axis was horizontal during calibration, the correction is proportional to tan(elevation). By reading the P-meter in the normal and reverse position it is possible to measure this correction directly.

2. The rotation axis of the encoder is not parallel to the optical axis of the heliograph. - This error can be determined by reversing the telescope (if possible). There is an error component in declination and hourangle. It is possible to determine both errors in the laboratory.

With the P-meter the orientation of a single heliogram is known to an accuracy of 1 minute of arc. A detailed describtion of this device with the calibration procedure and error analysis is in preparation (Mitteilungen des Sonnenobservatoriums Kanzelhöhe).

This instrument was brought into routine operation in August 1989, to supplement the sunspot observations for the Debrecen Photoheliographic Results (see Dezsö et. al. 1987: Debrecen Photoheliographic Results for the year 1977).

The author thanks Prof. Dezsö and Dr. Kovacs of the Debrecen Observatory for many valuable, stimulating discussions, for providing a test-target and the first distortion determination of the heliograph. The mechanical part of the instrument was built by Ing. Freislich with great skill and precision. Part of the instrument was supported by the Austrian National Bank under project number 2932.

SESSION 2

May 21, Monday (p.m.)

PATTERNS OF ACTIVITY

Chairman: H. WÖHL
Kiepenheuer-Institut für Sonnenphysik
Freiburg

Invited review:

C. ZWAAN
Patterns of Activity

and 15 (oral and poster) contributions

PATTERNS OF ACTIVITY

Cornelis Zwaan
Sterrekundig Instituut
Postbus 80 000
3508 TA Utrecht, The Netherlands

1. Introduction

In this review, patterns in the occurrence of bipolar active regions in the solar atmosphere are discussed: entire active regions are the building blocks of the patterns considered here.

Large-scale patterns in the occurrence of active regions have been known for some time. The observers compiling the *Greenwich Photoheliographic Results* distinguished "revivals", or "growths" of active regions from recurrent sunspots. The frequent appearance of a new active region nearby an existing one has been pointed out by d'Azambuja (1955). The term "complexes of activity" was used by Bumba and Howard (1965) to describe active regions emerging in each others proximity and the tendency of remnants of active regions to merge. Dodson and Hedeman (1968) used "families" of plages to describe the clustering tendency of active regions in space and in time. The term "active longitude" has a long history.

The type of patterns that stands out depends entirely on the presentation of the magnetic data. If one concentrates on large features in magnetograms of low resolution then complexes of activity are found as defined by Bumba and Howard (1965), which are long-lived, steadily expanding features. The patterns are large because remnants of originally isolated active regions merge as the result of differential rotation and "diffusion". If one focuses on loci of the highest magnetic flux density, the young active regions or sunspots, then a different type of patterns is defined. It is instructive to compare in the Kitt Peak synoptic magnetic maps the panels labeled FLUX, which bring out the strong field concentrations, with the panels labeled POLARITY, which display long-lived patterns in the magnetic field, irrespective of the field strength. The structures in the two sets look quite different (for an explanation of the construction of the magnetic synoptic maps, see in Gaizauskas *et al.* (1983), their Figure 1 and the description in the text).

This review focuses on the patterns in the *flux emergences*, i.e., on patterns seen in young active regions or in sunspots. The reason is that these may yield the most direct information on the dynamo action in the convection zone. Particular attention is paid to studies that try to describe *quantitative aspects* of the patterns of activity.

2. Harmonic Mode Analysis

In principle the patterns in the solar atmosphere can be treated in a rigorously quantitative fashion by harmonic mode analyses. Stenflo and coworkers analysed 25 years of magnetograms in this way (see Stenflo and Vogel 1986, Stenflo and Güdel 1988).

In the rotationally symmetric modes ($m = 0$, hence ignoring patterns in longitude) a strong resonance is found for $P = 22$ years, but only for uneven degree l, i.e. in patterns that are anti-symmetric with respect to the equator. The period of the activity cycle $P = 22$ years does not show up for even l.

The features in the non-axisymmetric modes are hard to analyse, probably because of the superposition of the pattern in the emergence of new magnetic flux on top of the effects of differential rotation and diffusion acting on old flux. For the time being the applicability of harmonic mode analysis in the study of activity patterns seems limited.

3. Patterns in Recently Emerged Magnetic Flux

The first successful attempt to demonstrate the occurrence of clusters in the appearances of sunspots in the longitude L - latitude ϕ - time t space has been published by Becker (1955). For many solar cycles Becker plotted sunspot appearances in longitude - time diagrams for narrow ranges in latitude. By a straightforward graphical procedure Becker demonstrated the reality of alignments in the L - t diagram. He showed that the corresponding L - ϕ areas on the solar surface, within which the sunspot groups are born, are quite small if a differential rotation is allowed for. Those sites he called "Sonnenfleckenherde", which I can only translate as "loci". We have chosen the term *nest* for such a locus where active regions (or sunspots) are born. Because of the limitations of his method Becker discovered only the largest sunspot nests of the longest duration.

Gaizauskas *et al.* (1983) used the FLUX displays in the synoptic magnetic maps derived from Kitt Peak magnetograms. Strips corresponding to the activity belt on one hemishere were then arranged chronologically in vertical columns to form L - t diagrams. The nests, called "complexes" by Gaizauskas and coworkers, stand out very clearly. These diagrams suggest that nests are much more common than appears from Becker's work. For one thing, the majority of the nests appear to have lifetimes up to 6 Carrington rotations, which is the minimum lifetime postulated by Becker. Moreover, also small active regions that never show real sunspots may occur in activity nests; one such "'simple' complex of activity" is described by Gaizauskas *et al.* One more striking feature brought out by the study of the magnetic maps is that many of the complexes consist of two or more branches.

Prompted by the differences between the results obtained by Becker (1955), Bumba and Howard (1965), and Gaizauskas *et al.* (1983), Castenmiller *et al.* (1986) investigated the clustering tendency in the spot group appearances during the period August 1959 - December 1964,

that is the same period that had been investigated by Bumba and Howard (1965). Castenmiller and coworkers indentified possible sunspot nests by eye in the two-dimensional projections of the L - ϕ - t space. They compared the results with those obtained from concocted samples in which the latitude ϕ and the time t are copied from the real sample but the longitude L is picked at random from the longitude range at the visible hemisphere. It is a sobering experience to see that in these concocted samples some surprisingly real-looking "nests" show up.

Castenmiller and coworkers found a real clustering tendency in the appearances of sunspots which involves at least 30 % of the spots. Moreover, it was found that the complexes identified by Bumba and Howard are different patterns, made up of one or more of the then "alive" sunspot nests, plus old remnants of previous nests and of single active regions.

The shortcoming in the study of Castenmiller and coworkers is the subjective identification of the nests in the L - - t by eye. Hence Brouwer and Zwaan (1990) repeated the analysis of the same 1236 spot groups but now with a mathematical technique of cluster analysis to trace the clusters in the data.

4. Sunspot Nests Traced by a Cluster Analysis

From experiments with various clustering methods it appeared that the *single-linkage hierarchical clustering method* is a convenient technique for tracing sunspot nests. The clustering criteria were derived from the results of previous studies. Each sunspot appearance i is characterized by one data point $\{ L_i, \phi_i, t_i \}$, the components longitude, latitude, and time are determined midway the visibility period during the disk crossing. Two sunspot appearances i and j are linked if the mutual distance on the solar disk satisfies

$$(\Delta L'/x)^2 + (\Delta\phi/y)^2 < 2 , \qquad (1)$$

where $L' = | L_i - L_j - v \times (t_i - t_j) |$, i.e. the distance in longitude as corrected for an adjustable differential rotation:

$$v = a - b \sin^2\langle\phi\rangle . \qquad (2)$$

The latitude-dependent quantities in (1) and (2) are

$$\Delta\phi = \phi_i - \phi_j \quad \text{and} \quad \langle\phi\rangle = (\phi_i + \phi_j)/2 .$$

Furthermore, the time gap t between two subsequent spot groups in one nest is bounded by the condition:

$$\Delta t = | t_i - t_j | < \tau . \qquad (3)$$

The clustering conditions (1) - (3) contain 5 adjustable parameters: the distance parameters x and y; the rotation parameters a and b; and the maximum time gap τ. These clustering parameters were determined such that the smallest intrinsic scale in the clustering of the real sample remains well visible, and that the clustering by chance is minimal (for the detailed procedure see Brouwer and Zwaan 1990). The outcome is:

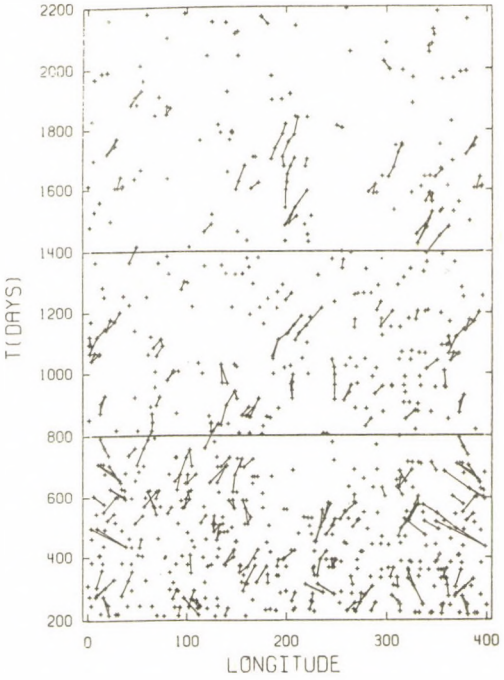

Figure 1.

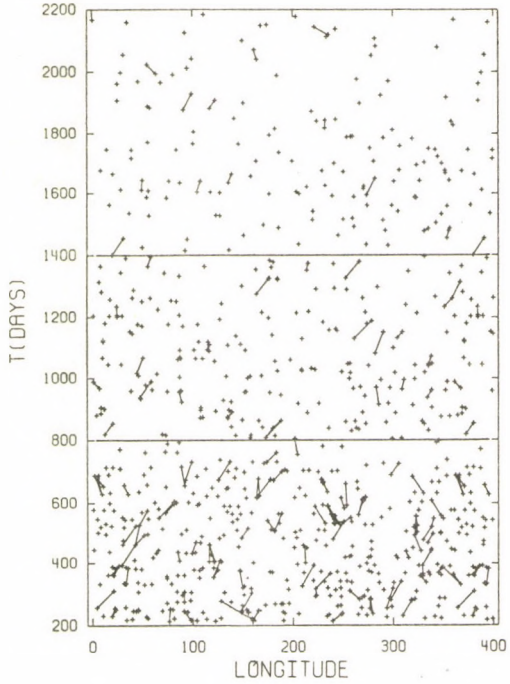

Figure 2.

Fig.1. Longitude-time diagram for the appearances of sunspot groups on the northern hemishere during Carrington rotations 1417 to 1488. Each cross marks a spot group appearance. Spot groups which belong together according to the clustering criteria are connected. Note that seemingly nearby data points may differ substantially in latitude.

Fig.2. Longitude-time diagram for a concocted sample with randomized data points for the northern hemishere. Compare with Fig.1.

$x = 2y = 4°$ (which corresponds to 40 Mm on the photospheric surface);
$a = 0.25\ °d^{-1}$ and $b = 3.0\ °d^{-1}$, i.e., as for recurrent sunspots; and
$\tau = 2.5 * 28\ d = 70\ d$.

A cluster is the collection of data points in which every point is connected with at least one other point of that collection. Figure 1 brings out the clusters traced on the northern hemisphere with the above criteria, and Figure 2 shows the clusters in a corresponding concocted sample with randomized longitudes, identified with the same clustering criteria. Although more and richer clusters are found in the real sample, some clusters are identified in the concocted samples as well. This serves as a warning that some of the clusters traced in the original sample may result from coincidences per chance, without a real physical cause behind it.

Clearly, the chance that a cluster is a real intrinsic nest increases with the "membership" M, i.e. the number of individual sunspot groups that are linked into that one cluster according to the adopted clustering criteria. The fraction of the the sunspot groups appearing in genuine nests may be estimated as follows: assume two populations of sunspot groups. Population I contains all the spot groups that appear in real nests. Population II comprises the groups that show up stochastically, but that may cluster per chance. Assume that all the loose data points, i.e. the points that are not linked to any other point according to the clustering criteria, belong to Population II. Then the total number of spot groups in population II may be estimated by reducing the number of data points in the concocted sample until the number of loose points ($M = 1$) agrees with the number of loose points in the real data. The distribution $N(M)$ for the thus reduced concocted sample, indicated by the broken line in Figure 3, is then subtracted from the distribution of the number of groups $N(M)$ contained in clusters of membership M in the real data. The difference, shown by the hatched area in Figure 3, estimates the number of spot groups contained in intrinsic clusters of various membership $M \geq 2$.

The histogram approximating Population II is made up by taking means, and the uncertainties in those means, of five concocted samples, with the reduced number of data points as explained above. For details on the procedure I refer to Brouwer and Zwaan (1990).

Note that the number of loose points probably leads to an overestimate of the number of spot groups that are not members of genuine nests, since cluster members may have emerged without being recorded separately, or even without being noticed,for instance on the invisible solar hemisphere. Hence Brouwer and Zwaan probably underestimated the fraction of sunspot groups that occur in nests.

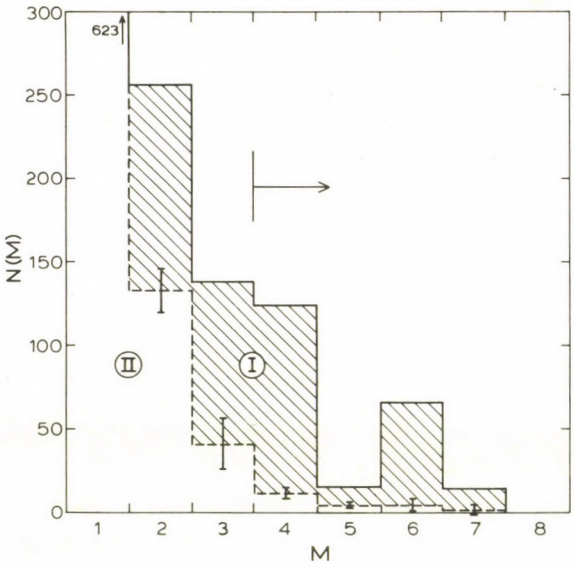

Fig.3. Histogram showing the number of clusters N(M) against membership M. The solid top line shows the distribution for the real data. The dashed bottom line represents the the average found for 5 adjusted sets of data with randomized longitudes. The columns for M = 1 (not shown) have the same height N(1) = 623. The hatched part represents the estimated values for physical clusters that are not produced by chance.

Over the entire investigated period about one third of the spot groups belonged to a genuine nest. The fraction appears to to depend on the period and on the hemisphere: e.g., during the last two years of the investigated time span, shortly before sunspot minimum, about half of the groups on the northern hemisphere belonged to real nests (see Figure 1, the top part).

Figure 3 shows that the probability that a cluster traced by the cluster analysis technique is a real sunspot nest increases strongly with increasing membership. For $M = 2$ about 50 % of the clusters are real, but about one third of these are listed as recurrent spot groups. For $M = 3$ at least 70 % of the clusters are genuine nests, and for $M \geq 4$ more than 90 % must be real. Hence for the determination of the properties of nests Brouwer and Zwaan used the 47 clusters with four or more members.

5. Some Properties of Nests

Some basic properties of nests do not depend critically on the choice of the clustering criteria. Within a wide range of criteria the very existence of nests is confirmed, and the conservative estimate of the fraction of spot groups belonging to nests turns out to be one third.

The number of active regions (or sunspot groups) occurring within one nest is underestimated. There are active regions emerging on the invisible hemisphere. Moreover, many regions emerging in the proximity of a still existing region are not recorded as new regions in the standard data compilations. For instance, in the Great Complex discussed by Gaizauskas *et al.*(1983) during its lifetime of 6 Carrington periods 13 emerging active regions are listed in *Solar-Geophysical Data*, whereas 29 major active regions are counted on the the magnetograms.

The detailed properties of nests do depend on the precise selection criteria that are inserted in the relations (1) - (3). Brouwer and Zwaan aimed for the smallest scale of clustering in the spot group appearances, such that the clusters in the real sample stand out most clearly against the coincidental clustering in the concocted samples with randomized longitudes. The bonus of the objective clustering technique is that it appears to trace the fine structure in the clustering much better than the human eye can do.

Figure 4 shows the distributions of the spreads in latitude and longitude, as measured relative to the average latitude and the linear regression line in the L - t plane, respectively. The nests are very compact indeed: allowing for a linear displacement in Carrington longi-tude with time the centroids of the members scatter within the area typical for a small active region, or over about a supergranular diameter. Since nests are even more sharply bounded in latitude than in longitude, the term "active longitudes" is a misnomer if applied to structure on the solar surface.

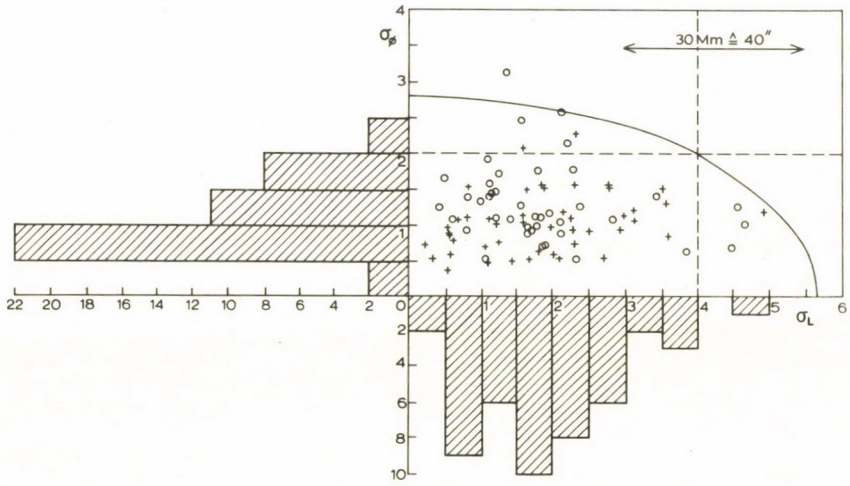

Fig.4. Scatter plot and histograms for the spreads in longitude σ_L *and in latitude* σ_ϕ *for the 47 clusters with M 4 in the real sample (crosses). For comparison the scatter plot for the 41 clusters in the total of 3 concocted sets of data is shown as well.*

The lifetimes of the individual nests with $M \geq 4$ ranges from slightly more than one Carrington rotation period (by definition) to slightly over half a year. This result agrees very well with the findings by Gaizauskas *et al.* (1983).

Emergence of magnetic flux is intermittent at a large range of scales (see Zwaan 1978). Sunspot nests demonstrate the intermittence at large scales. Brouwer and Zwaan found several nests producing four or more spot groups within two Carrington periods; apparently these groups were oustanding enough to be listed separately in the *Greenwich Photoheliographic Results*. Note that such concentrations within one cluster do not occur in concocted samples, so it is a genuine solar feature. On the other hand, in many nests no spots are visible for an interval of more than one Carrington period - the number of spot groups in nests is increased substantially by the allowance for time gaps (relation (3)).

For each cluster the rotation velocity v_L relative to the Carrington rotation rate is defined by the linear regression in the L - t plane. Figure 5 shows these rotation rates for the 47 clusters with membership $M \geq 4$ found in the analysis by Brouwer and Zwaan. The rotation rates v_L closely follow the relation (2), with a = 0.25 °d^{-1} and b = 3.0 °d^{-1} as

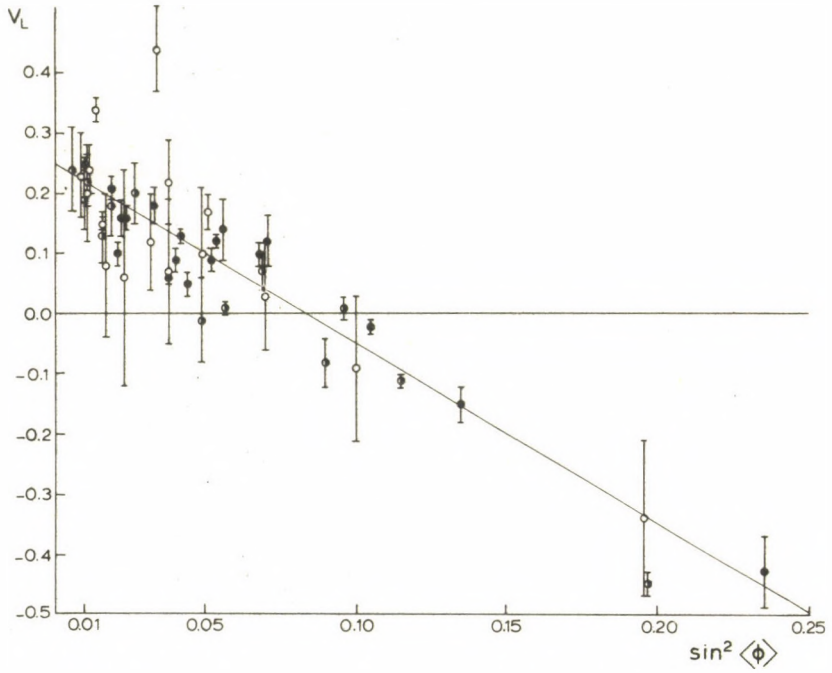

Fig.5. Rotation rates v_L with respect to Carrington rotation against latitude given as $\sin^2\phi$ for the clusters with $M \geq 4$. The solid inclined line represents the rotation rate assumed in the clustering criteria.

used in the clustering criteria. This is not quite a self-fulfilling prophesy. Brouwer and Zwaan varied the parameters a and b in the clustering parameters, and they found two reasons to choose the rotation rate relation v_L ($\sin^2$) within a narrow sheaf about the line defined by a = 0.25 and b = 3.0: (1) to bring out the fine structure in the clustering in the best possible way; and (2) to let the rotation rates of the eventual individual clusters be close to the rotation rate adopted in the clustering criteria.

Note that there is a truly intrinsic scatter in the rotation rates v_L but this is within about 0.1 $^\circ d^{-1}$, or within 15 m s^{-1}.

The displacements in latitude are very small. The peculiar motions are less than 5 m s^{-1}, and large-scale flows in latitude must be extremely small: less than 3 m s^{-1}. Note that this virtual absence of meridional flow has been found from nests during a small time span and, thence, for a limited range of latitudes. Most of the 47 nests occurred at latitudes smaller than 20°, and a few between 20° and 30°.

There is a clear tendency for the nests to cluster once again in *compo-*

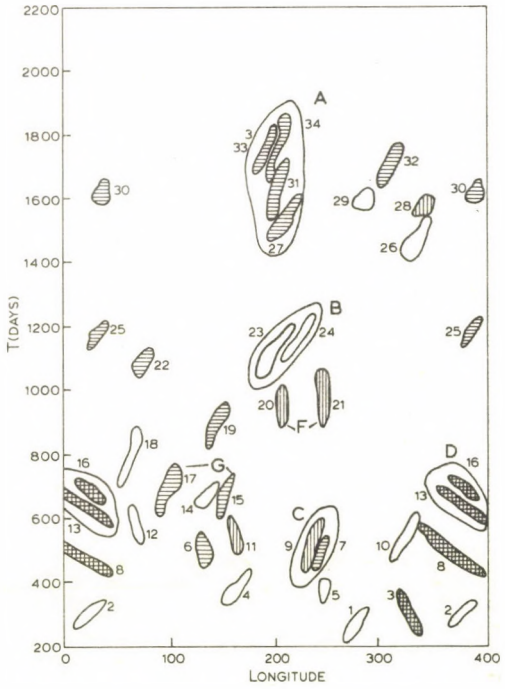

Fig.6. Longitude-time diagram showing the 34 clusters with $M \geq 4$ traced on the northern hemisphere. Latitude zones are indicated by different shading: white: $\langle\phi\rangle < 10^\circ$, horizontally hatched: $10^\circ < \langle\phi\rangle < 15^\circ$, vertically hatched: $15^\circ < \langle\phi\rangle < 20^\circ$, cross-hatched: $20^\circ < \langle\phi\rangle < 30^\circ$. Composite nests are indicated by capital letters (and encircled).

site nests, see Figure 6. The properties of these composite nests are: the latitude of the component nests differ by less than 2.5°; the components overlap strongly in time; and the longitudes differ by less than 60°. These composite nests appear in the real sample only; they are never seen in concocted samples with randomized longitudes. The composite nests stand out very clearly in the study by Gaizauskas *et al.* (1983) where they are called activity complexes with more "branches".

Some of the composite nests live much longer than any of their components: the composite nest labelled A in Figure 6 is present for more than 12 Carrington rotation periods.

The occurrence of composite nests and the difficulty to distinguish these from single nests explain differences in results of the various studies. For instance, several of the nests listed in the study of Castenmiller *et al.*(1986) turn out to be composite nests. This explains why in that study the histograms, for spreads in longitude and in latitude, and for lifetime, are less regular and much broader than the corresponding histograms in Brouwer and Zwaan (1990). Becker (1955) required a minimum lifetime of 6 rotations for his Sonnenfleckenherde, hence he recorded composite nests of long duration.

The composite nests come in a large variety of complexity and of lifetimes. This emphasizes once more the need to trace the component nests of the smallest size. It appears to be the bonus of the mathematical clustering technique that it can trace these component nests in places where the human eye fails.

The properties of the clusters at the smallest scale appear to be well defined: for the size and lifetime parameters one finds histograms of a simple and narrow shape. This suggests that these clusters are fundamental features in solar magnetism - they may be called *elementary nests*. These elementary nests are then the building blocks of the next level of clustering in *nested nests* or *composite nests*.

6. Some New Aspects of the Activity Cycle

In this section I report on recent rsults obtained by Karen Harvey in her study of 29 Carrington periods selected from Kitt Pak magnetograms obtained between 1974 and 1986. She studied the data set of *all* active regions that were seen from emergence to maximum development, including very small active regions, from areas of 2.5 square degrees and larger (2.5 square degrees corresponds to 373 Mm^2, or to 125 10^{-6} of the visible hemisphere).

Two principles underlie Harvey's study:

1. In matters of counts and statistics area-dependent *corrections for incompleteness* of the sample have been applied for limited visibility and for data gaps.

2. The active regions are *counted only once*, and the area is determined at the *time of maximum development*. The time of maximum development is when all magnetic flux in the active region has emerged. The area of the region is a monotonic measure of its total magnetic flux.

Some of the results of Harvey's comprehensive study are summarized below.

The *size distribution* $N(A)$: the number of active regions per unit area

as a function of area A at maximum development, has *a constant relative shape* at all times (after averaging over several Carrington rotation periods). This constancy of shape also applies in the comparison of various areas on the photospheric surface, except for some dependence on latitude (which is mentioned below).

The constancy of the shape of $N(A)$ implies that during the cycle the number of active regions in any of the size bins varies by the *same* factor. This factor is found to be 5.7. (Note that this factor may not be applicable to ephemeral active regions).

The constancy of the relative shape of the size distribution also implies that no significant phase shifts occur between the cyclic variations in the counts of active regions of different size bins. (I do not know yet whether the number of ephemeral regions varies in phase with the number of larger regions).

The relative shape of the size distribution is virtually the same for active regions emerging inside existing active regions and for those emerging outside existing regions. The probability of emergence (per unit area at the solar surface) within an existing active region is higher by a factor of at least 25, however. Clearly, this is another manifestation of the clustering in the appearance of active regions. During minimum activity the clustering tendency is largest: then the emergence probability inside existing active regions is larger by a factor of 40. (Recall that Section 4 mentions an enhanced probability of the occurrence of spot groups in nests near the time of minimum activity).

Harvey noticed one significant size-dependent effect: for active regions in the smallest size bin ($2.5 < A < 5.0$ square degrees) the latitude distribution is broader than the latitude distribution for the larger active regions. This implies that the size distribution $N(A)$ depends slightly on latitude at the side of the smallest active regions.

7. Discussion

In the studies reviewed by this paper, active regions are considered around maximum development, shortly after the emergence of magnetic flux. The advantage is evident: clear patterns appear which are the apparently clean products of the dynamo machine in the solar interior. They are well visible before the steady erosion by convection diffuses the crisp features, and before the spreading magnetic patches merge with existing fields.

The patterns visible in recently emerged flux convey information on the magnetic structure and processes in the solar interior. The slightly inclined, nearly E - W orientation of active regions, as formulated in one of Hale's polarity laws, indicates that the toroidal magnetic field must exceed the equipartition field strength, or 10^4 gauss near the bottom of the convection zone (Zwaan 1978). Karen Harvey's (1990) discovery of the constant shape of the size distribution for active regions throughout the cycle and over large parts of the solar surface holds a clue to the processes controlling the emergence of flux from the toroidal flux ropes in the interior.

The compactness of nests and the sharp boundary of a nest throughout its lifetime provide more clues to the emergence processes. The magnetic flux emerges and disappears within the nest, *in situ*, very locally.

During the nest's lifetime the rate of emergence and the rate of disappearance are roughly equal, and in some cases very high. In the Great Complex described by Gaizauskas *et al.* (1983) the total flux present at any time was more than 10^{23} Mx. Since more than 29 major active regions emerged in that complex which lasted for six Carrington periods it is clear that an enormous amount of flux had been processed through that complex; 10^{24} Mx is a conservative estimate. If that total flux were stored at a field strength of 10^{4} gauss the necessary cross section would be [100 Mm]^2.The largeness of these figures suggest that in one nest the *same* magnetic flux is reprocessed several times, with a time constant of no more than a few weeks. So it seems that the Sun knows a trick to let magnetic flux loops shuttle up and down at a rapid rate. In other words, in addition to magnetic bouyancy we should consider possibilities to prompt magnetic flux loops to sink.

The magnetic structure within a nest may become quite complex, which indicates that the processes producing and maintaining active nests may not proceed smoothly and independently. In fact, it is probable that these processes in the solar interior are responsible for the build up of the most powerful flares. Despite the irregularities in the transport of magnetic flux, the nest remains sharply defined and compact, until the flux emergence stops altogether.

Finally let us try to sketch a picture as a speculative attempt to relate some of the features with rather dim notions on the structure and processes in the solar interior.

In the interior - presumably near the bottom of the convection zone - there appear to be three stages in the organization of toroidal magnetic flux ropes and their emergence into the atmosphere:

1. A bipolar active region and - if enough flux is available - with its sunspots lay prepared in the toroidal flux rope, as a flower in its bud. The active region unfolds during the rise of the flux loop and its emergence into the atmosphere. The complete emergence and the adjustment to the atmospheric conditions take no more than a few days. If the flux loop rises from the bottom of the convection zone at the Alfvén speed according to the equipartition field strength then the rise time would be a few weeks.

2. Elementary nests are formed by some process that causes magnetic flux loops to rise from a very local source region for several months. In some nests two or more bipolar active regions are present at the same time and at a very short mutual distance. Such regions probably originate from adjacent strands in the toroidal flux system. Note that subsequent bipolar regions within one nest may be re-emergences from the same flux bundle. A time gap in the appearance of active regions would mean that the previous flux loop has been retracted, and that the next loop has not yet surfaced.

3. In composite nests two or more elementary nests appear with a long overlap in time. The substantial separation in longitude suggests that they may be formed by loops that occur in about the same bundle of flux tubes, in the fashion of a sea serpent. So a suggestion above concerning the reprocessing of flux may be extended to the proposal that in a

composite nest we see the same magnetic flux rope processed in more than one simultaneous loop, and reprocessed in a series of subsequent loop emergences.

In any case, the surprisingly clear patterns in the solar activity,hidden in the seeming complexity of the atmospheric structure, must hold clues for basic mechanisms in solar activity.

Acknowledgement

I wish to thank Karen Harvey for permission to quote from her work before publication, and Brian Murphy for improving the text.

References

Becker, U.: 1955, *Z. Astrophys.* **37**, 47
Brouwer, M.P., and Zwaan, C.: 1990, *Solar Phys.*, in press
Bumba, V. and Howard, R.: 1965, *Astrophys. J.* **141**, 1502
Castenmiller, M.J.M., Zwaan, C., and van der Zalm, E.B.J.: 1986, *Solar Phys.* **105**, 237
d'Azambuja, M.: 1955, *Cartes Synoptiques de la Chromosphère Solaire*, 1, No. 10, p.31 (Obs. de Paris)
Dodson, H.W., and Hedeman, E.R.: 1968, in K.O. Kiepenheuer(ed.): IAU Symp. **35**, *Structure and Development of Solar Active Regions*, p.56
Gaizauskas, V., Harvey, K.L., Harvey, J.W., and Zwaan. C.: 1983, *Astrophys. J.* **262**, 1956
Harvey, K.L.:1990, in preparation
Stenflo, J.O., and Güdel, M.: 198., *Astron. Astrophys.*
Stenflo, J.O., and Vogel,M.: 1986, *Nature* **319**, 285
Zwaan, C.: 1978, *Solar Phys.* **60**, 213

The figures in this review paper are, with some adaptations, from Brouwer and Zwaan (1990).

THE ROLE OF ACTIVITY COMPLEXES IN THE DISTRIBUTION OF SOLAR MAGNETIC FIELDS

J.I. García de la Rosa
Instituto de Astrofísica de Canarias, 38200 La Laguna, Tenerife, Spain

and

R. Carlos Reyes
Seminario de Astronomía y Astrofísica. UNM San Marcos, Lima, Peru

1. Introduction

According to Zwaan (1987), *...there are no reports on the relationship between coronal holes and active nests* (complexes of activity), *but probably both patterns reveal fundamental processes in solar magnetism.* The present study is devoted to the search of that relationship.

Using published data on the large-scale distribution of solar activity, we conclude that the long-lived coronal holes are formed and maintained by the unbalanced magnetic flux which develops at both extremes of the complexes of activity.

2. Data

Different data sources were used to cover the studied period, 1970 to 1990.

(1) **Coronal Holes**: Pre-Skylab observations were obtained from Underwood and Broussard (1977) and Skylab observations from several sources (e.g. Hundhausen, 1977, pg. 235). From January 1982, coronal hole estimates using HeI λ 10830 line have been published in the *Solar-Geophysical Data Bulletins.*

(2) **Complexes of Activity**: Mount Wilson Synoptic Charts of Solar Magnetic Fields, published in the *Quarterly Bulletin on Solar Activity*, were used to study the distribution of activity.

Some 150 complexes of activity have been studied.

3. Results

Besides the well known characteristics of the complexes of activity, reported by Bumba and Howard (1965) and by Gaizauskas et al. (1983), other prominent features were observed:

(i) The Active Regions (ARs) of the complex are roughly aligned and show comparable magnetic flux.

(ii) The ARs of the complex are separated by a typical wavelength.

(iii) The whole complex is tilted towards the equator with the preceeding part at a lower latitude.

(iv) The ARs of the complex show interconnecting loops at the coronal level.

Some results on the use of complexes as a trace of the internal source of the photospheric magnetic fields have been presented in Garcia de la Rosa (1989).

In this case, for the sake of brevity, we shall restrict ourselves to show a single typical example of a long-lived complex of activity.

The selected complex covered the longitude interval 90°-270° of the Southern Hemisphere during the Carrington Rotations (CRs) 1603 to 1621.

The reason for this choice is double. On the one side, the availability of several X-ray images of the Sun during this period, and on the other, the simplicity of the large-scale distribution of solar activity during the decay of the Cycle.

Through several steps, an alignment of emerging ARs evolves into two unbalanced unipolar magnetic regions located at both extremes. Fig 1a shows one of the bursts of activity of the long-lived complex.

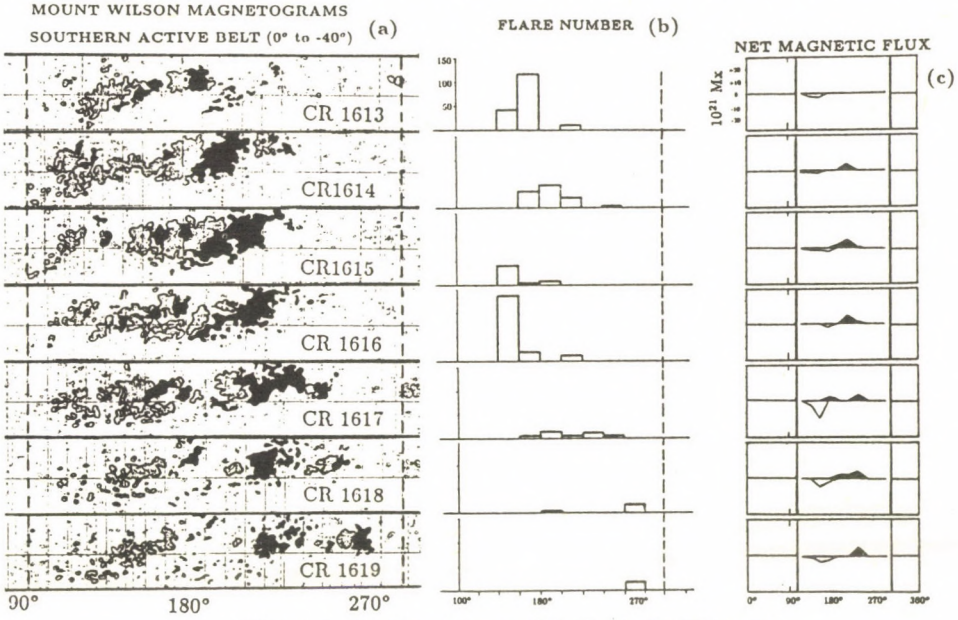

Figure 1. (a) Magnetograms of the burst of activity. (b) Number of flares and subflares. (c) Net magnetic flux (sum + and -) in the Southern Hemisphere.

Step 1. *Flares and subflares are restricted to the longitude interval of the complex*

This expected result is presented in Fig. 1b. with a histogram of the total number of flares and subflares in 20° wide sectors.

Flares preferentially take place near the limits of emerging active regions. This suggests that the reconnections between neighbouring ARs take place soon after their emergence, in agreement with several studies on the formation of connecting coronal loops (e.g. Sheeley et al, 1975)

Step 2. *The magnetic flux located inside the complex is removed from the photosphere at a very fast rate*

Using Mount Wilson Synoptic Charts we made a rough estimate of the magnetic flux of the active regions. The estimation was carried out by measuring the area of each gauss level of the magnetogram.

At a typical rate of 3 10^{21} Mx/day, the magnetic flux is removed from the photospheric level. If all the coexisting complexes on the Sun were taken into account, the rate of flux disappearance would easily reach the large figure reported by Howard and LaBonte (1981). The flux is observed to disappear far from the neutral lines, in agreement with more detailed observations (e.g. Wallenhorst and Topka, 1982).

Step 3. *After the decay of the central flux of the complex, only two unipolar magnetic regions remain at both extremes of the complex*

Although obviously the whole complex is magnetically balanced, i.e. same amount of flux of each polarity, the fact that all ARs show a comparable flux allows the annihilation of opposite polarities from neighbouring ARs. This process leaves two unbalanced magnetic poles at both extremes of the complex. Fig 1c shows the evolution of the net magnetic flux (algebraic sum of positive and negative polarities) during successive CRs.

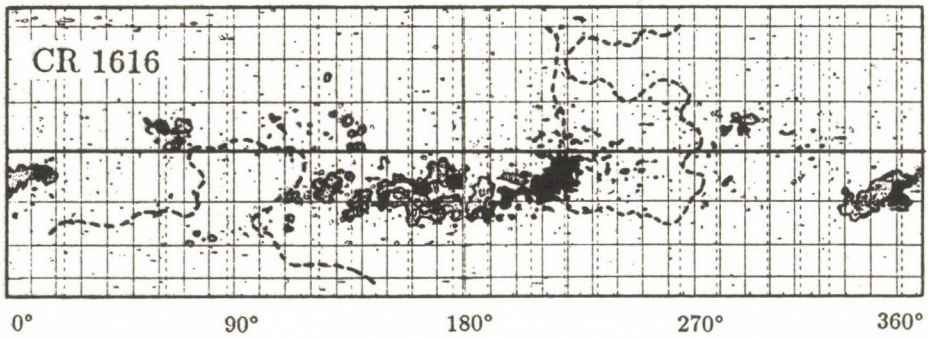

Figure 2. Contours of Coronal Holes (CHs) superimposed on full (N and S) Synoptic Magnetogram. CH1 at 250° from Underwood and Broussard (1977). CH2 at 90° from Hundhausen (1977).

In CR 1619 the *unbalanced* magnetic poles are located at Carrington Longitudes (CLs) 160° and 240°, with the last one 10° closer to the equator. The new AR which emerges at CL 270° will just extend the unbalanced p-part to larger CLs ($\sim$ 290°).

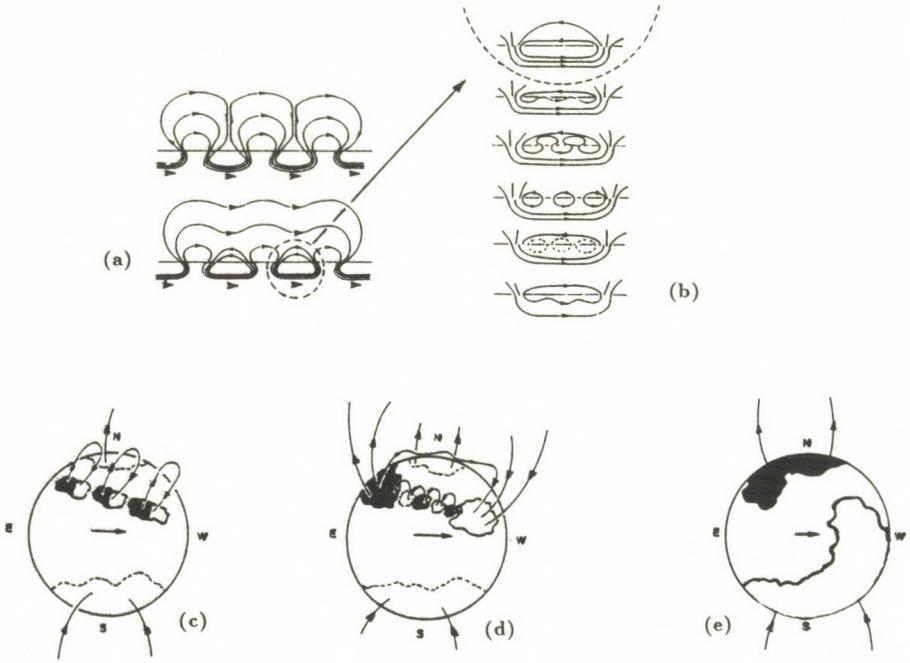

Figure 3. (a) Reconnection of closely packed active regions. (b) Process of U-loop escape according to Spruit et al. (1987). (c) and (d) Evolution of the magnetic flux in a complex of activity. (e) Contribution to the maintenance of Coronal Holes.

Step 4. *The unbalanced unipolar extremes of complexes of activity are the source of long-lived coronal holes*

Fig 2 shows the location of two transequatorial coronal holes; CH1, at CL 250°, stretches out from the North Polar Cap to the unbalanced p-extreme of the complex. A similar configuration appears for hole CH2, located at CL 90°. The repeated emergence of new bursts of activity supplies new flux to the coronal holes.

4. Discussion

Besides the observational support, each step of the previous section is also supported by theoretical considerations.

Step 1. According to Parker (1984), the expansion above the surface of **closely packed** upward arching loops (Fig 3a) produces a very high rate of reconnection, resulting in the field topology of Fig3b. Long distance arches connect both extremes of the complex, while several U-loops are left below.

Step 2. Spruit et al (1987) suggest a process which combines buoyancy, reconnection and ohmic disipation to annihilate those U-loops, without the need of bodily motions of magnetic features towards the neutral line (see Fig 3c).

Step 3. The magnetic regions located at both extremes of the complex are essentially different to the others (Fig 3c,d). They are not obstructed to spread out as it happens in the closely packed interior of the complex. In addition, the bouyancy and the solar wind will eventually stretch out the long arch which connects both extremes, giving them virtually *open* magnetic configurations.

Step 4. Studies by Levine (1977) show that a local predominance of one magnetic polarity is not sufficient to produce a coronal hole. The magnetic configuration should also be open. The unbalanced extremes of the complex show those two characteristics and can contribute to the formation and maintenance of the long-lived coronal holes (Fig 3e).

References

Bumba, V. and Howard, R.: 1965, *Astrophys. J.* **141**, 1502

Gaizauskas, V., Harvey, K.L., Harvey, J.W. and Zwaan, C.: 1983, *Astrophys. J.* **265**, 1056.

Garcia de la Rosa, J.I.: 1989, in the Proceedings of the *XI European Regional Astronomy Meeting.* Tenerife, July 1989. Cambridge University Press.

Howard, R. and LaBonte, B.J.: 1981, *Solar Phys.* **74**, 131.

Hundhausen, A.J.: 1977, in *Coronal Holes and High Speed Wind Streams.* ed. J.B. Zirker. Colo. Ass. Univ. Press, pg 225.

Levine, R.H.: 1977, in *Coronal Holes and High Speed Wind Streams.* ed. J.B. Zirker. Colo. Ass. Univ. Press, pg 103.

Parker, E.N.: 1984, *Astrophys. J.* **281**, 839.

Sheeley, N.R., Jr., Bohlin, J.D., Brueckner, G.E., Purcell, J.D., Scherrer, V.E. and Tousey, R.: 1975, *Astrophys. J.* **196**, L129.

Spruit, H.C., Title, A.M. and Van Ballegooijen, A.A.: 1987, *Solar Phys.* **110**, 115.

Spruit, H.C. and Van Ballegooijen, A.A.: 1982, *Astron. Astrophys.* **106**, 58.

Svalgaard, L. and Wilcox, J.M.: 1975, *Solar Phys* **41**, 461.

Underwood, J.H. and Broussard, R.M.: 1977, *Atlas of Coronal Hole Boundaries from Observations Prior to the Skylab Mission,* Aerospace Rep. No. ATR-77(7405)-2.

Wallenhorst, S.G. and Topka, K.P.: 1982, *Solar Phys.* **81**, 33.

Zwaan, C.: 1987, *Ann. Rev. Astron. Astrophys.*, **25**, 83.

PHOTOMETRY OF THE INTERNAL STRUCTURE OF A LARGE UMBRA

V. Bumba, M. Sobotka, S. Šimberová
Astronomical Institute of the Czechoslovak Academy
of Sciences, 251 65 Ondřejov, Czechoslovakia

Abstract: An analysis of a high-resolution white-light photograph of an umbra of a large complex main spot, taken in the region 590 +3 nm with a 205 mm refractor, was performed. Digital image processing methods were used. The umbra was observed as a very inhomogeneous structure with large differences in intensities of the individual elements (dark cores, bright dots, light bridge, etc.). The temperatures of these elements were derived (Tab. 1). It is demonstrated that the intensity of the individual bright umbral dots is related to the intensity of their dark surroundings.

OBSERVATIONS

During June 1979 special series of experimental movie pictures were obtained (Bumba et al. 1973). Using the photometric scale we were able to make the photometric calibration of these pictures. The following photograph was chosen for the investigation: June 2, 1979, film no 417, picture No 1916, taken at 6^h19^m UT. It represents the main part of an anomaly and very fast developing sunspot group No 250 (Solnechnye Dannye), $\varphi = +19^o$ L = 180.5; which was still relatively close to the eastern limb of the Sun ($r/R \cong 0.8$). It appeared at the limb in its initial stage of development, reached its maximum during June 3 and disintegrated since then.

The target of our investigation is the largest spot of the group which, according to the polarity of its magnetic field (S, 0.21 T), belongs to the following part of the group.

DATA REDUCTION

The image of the photosphere was digitized by a PHOTOMATION - 1700 device (Optronics, USA) with 25 μm sampling in two coordinates and quantization of transparency in a relative scale of 0-255.

Digital image processing was carried out using a special

system for image analysis, the PERICOLOR 2001. The imput image was reduced to an intensity scale according to specific nonlinear transformation given by the H-D calibration curve. The intermediate image in relative intensities was thus obtained.

In our case, the level of stray light was very low and the dominant degradation influence was caused by the optical system of the telescope, i.e. by its instrumental function. We described the optical system by the 2-D impulse response (Airy's pattern). The transfer function of the system is given by the 2-D Fourier transform of the impulse response.

To restore the image spatial filtering was used, i.e. inverse filter restoration (Pratt 1984). The inverse filter is given by the inverse transfer function and the restored image was obtained by using the inverse Fourier transform of the degraded image multiplied by the inverse filter.

THE RESULTS

The image restoration did not reveal new details below the resolution limit, but increased the contrast and sharpness of marginally resolved structures substantially. At the same time, the relative intensity of umbral dark cores decreased below 0.05 at λ = 590 nm.

In the restored image of the umbra, six dark cores with $I \leq 0.05$ were found with a general area of 2% of the total umbral areas. The relative area of the region with $0.05 < I \leq 0.1$ was 23% and the brighter regions with $0.10 < I \leq 0.15$ occupied 35% of the umbral area. The boundary of the umbra was defined at I = 0.30, where the steepest intensity gradient was observed.

The light bridge has a granular structure with relative intensity ranging from 0.30 - 0.50 in the background to 0.85 in the bright grains.

In the restored image, 10 central and 10 peripheral umbral dots (u.d.) were detected. Their sizes are comparable with the resolution limit of the telescope. The difference between the peak and background intensity ΔI is, roughly estimated, 0.05 - 0.10 for the central u.d. and 0.10 - 0.20 for the peripheral

u.d. Moreover, their relative contrast referred to the background remained practically constant. Some simple numerical simulation showed that this effect is probably not caused by the limited resolution of the telescope and that there exists a connection between the peak and background intensities of u.d.

In order to obtain more detailed information on the photometry of some significant fine-structure elements in the umbra, four photometric profiles were derived. The profiles intersect 11 various features (4 dark cores, 1 bright region, 3 umbral dots and 3 grains of the light bridge), which are summarized in Table 1 together with their peak intensity I centr, difference ΔI between I_{centr} and the local background intensity (for u.d.) and size. The intensity unit is the intensity of the undisturbed photosphere; the size (in arc seconds) is defined as FWHM in case of u.d. or as the width at I = 0.50 in the case of the bright grains of the light bridge.

Moreover, for each I_{centr} a corresponding parameter $\Delta\theta$ and temperature at unit optical depth $T/\tau_{500} = 1$ / are displayed. The model parameter, defined as

(1) $$\Delta\theta = 5040/\ T/\tau/ - 5040/T_{ref}/\tau/\ ,$$

where $T_{ref}/\tau/$ is the temperature distribution of a reference model atmosphere, may describe the temperature structure $T/\tau/$ of the element under investigation, assuming the validity of LTE and radiative equilibrium (Obridko 1985). If we accept the undisturbed photosphere (e.g. Maltby et al. 1986) as the reference model, we may, following Obridko (1985), derive the model parameter from the monochromatic intensity $I/\lambda/$, expressed in units of intensity of the undisturbed photosphere:

(2) $$\Delta\theta = -\frac{\lambda.5040}{1.439.10^7}\ \ln\ I\ /\lambda/$$

where wavelength λ is in nanometers. Naturally, this method only yields a rough estimate of the model parameter and temperature (derived from (1)), as we have no guarantee that u.d., light bridges, etc., are really in LTE and radiative equilibrium.

REFERENCES

Bumba V. Ranzinger P. Suda J. 1973 Bull. Astron. Inst. Czechosl. 24, 22

Maltby P. Avrett E.H. Carlsson M. Kjeldseth-Moe O. Kurucz R.L. Loeser R. 1986 Astrophys. J. 306, 284

Obridko V.N. 1985 Solnechnye pyatna i kompleksy aktivnosti, Nauka, Moskva

Pratt W.K. 1978 Digital Image Processing, New York, 283

Table 1

No.	Element	Observed image					Restored image				
		I_{centr}	ΔI	Size	$\Delta\theta$	$T(\tau=1)$ [K]	I_{centr}	ΔI	Size	$\Delta\theta$	$T(\tau=1)$ [K]
	dark cores										
1	central d.c.	0.09			0.50	3960	0.02			0.81	3180
2	d.c.	0.11			0.46	4090	0.03			0.74	3330
3	d.c.	0.10			0.48	4020	0.03			0.73	3350
4	periph. d.c.	0.09			0.49	3990	0.04			0.66	3520
5	*bright region*	.18- -.21			.35- -.32	4490- -4610	.13- -.18			.42- -.35	4220- -4490
	umbral dots										
6	central u.d.	0.14	0.03	0.7"	0.41	4260	0.13	0.08	0.8"	0.42	4220
7	periph. u.d.	0.23	0.06	0.5"	0.30	4700	0.23	0.14	1.0"	0.30	4700
8	periph. u.d.	0.20	0.05	0.7"	0.33	4570	0.17	0.10	0.8"	0.37	4410
	light bridge										
9	bright grain	0.63		0.7"	0.10	5770	0.85		0.7"	0.03	6280
10	bright grain	0.83		1.4"	0.04	6200	0.83		0.9"	0.04	6200
11	bright grain	0.49			0.15	5460	0.48			0.15	5460

Remark: Photospheric $T(\tau=1)$ = 6520 K. Size in arc seconds.

INTERACTION BETWEEN BIPOLAR SUNSPOT GROUPS

G. Csepura[1], L. van Driel-Gesztelyi[1,2], I. Nagy[1],
O. Gerlei[1], B. Schmieder[3], and J. Rayrole[3]

[1] Heliophysical Observatory of the Hungarian Academy of Sciences, P.O. Box 30, H-4010 Debrecen, Hungary
[2] Sterrenkundig Instituut, Rijksuniversiteit te Utrecht, Postbus 80.000, 3508 TA Utrecht, The Netherlands
[3] Observatoire de Paris, Section d'Astrophysique, 92195 Meudon, France

Abstract

We find some evidence for the interaction of two close-by developing sunspot groups: (i) the proper motions of the principal preceding spots of both groups show quite similar patterns; although they had different ages, they moved almost parallel and changed the direction of their motion on the same day at almost the same heliographic longitude; (ii) after the emergence and fast divergence (shearing motions) of new spots in both groups, a filament formed between them; (iii) the fast development of the new group was followed by new flux appearance (faster area increase) in the older, larger one; two periods in which the area of the larger sunspot group increased were followed by periods in which the area of the smaller group decreased.

Introduction

Solar active regions tend to appear near other active region(s) (see e.g. Zwaan, 1990), and the question arises if there is any sign of a possible link between sunspot groups developing close to each other. This question was investigated by Martres (1970), who found some effects of a possible interaction in the area development and proper motions of the involved sunspot groups. In connection with the lifetime of active regions, Sheeley (1981) stated that bipolar magnetic regions might annihilate one another within a few days if they emerged in a suitable configuration.

In the period of 11-18 June 1980 we observed two bipolar sunspot groups of different ages developing very close to each other. Their longitudes were almost identical ($L \approx 280°$) and their separation in latitude was only 5° (N17.5° and N12.5°). These active regions gave an excellent opportunity to study the characterictics of a possibly disturbed sunspot group development, and to search for any sign of interaction between these sunspot groups.

Observations

At the Heliophysical Observatory of the Hungarian Academy of Sciences in Debrecen (Gyula Observing Station) 387 white-light full-disk photoheliograms were obtained between 9-20 June 1980, which we could use for a study of the motion and evolution of the sunspot groups in this period. The method of observation, position measurements and computation of heliographic coordinates is described in detail in the Introduction to the "Debrecen Photoheliographic Results" by Dezső *et al.* (1988).

For this study we also used a few Hα filtergrams which were obtained in Debrecen with a 53 cm Nikolsky-type coronograph, equipped with a 0.5 Å Halle filter.

Between 13-15 June 1980, 8 magnetic maps were taken at the Observatoire de Meudon. The data processing of the Meudon magnetograph is described in a previous paper (Rayrole, 1981).

Signs of Interaction in the Development of the Active Regions

Hale region 16898 rotated onto the disk on 8 June 1980 as an older-looking bipolar sunspot group (Mt.W. 21517), hereafter referred to as Group 1 in this paper (Fig. 1). On 11 June new flux emerged 5 heliographic degrees south of it, which had formed a smaller bipolar group by the next morning (Mt.W. 21526), named Group 2 (Fig. 1).

In the middle part of Group 1 new activity emerged in several waves: on 11, 13 and 16 June. At first in both sunspot groups the *p* (N polarity) spots moved westward (towards the

W-SW) faster than the f(S polarity) spots moved eastward (to the E-NE), showing the ordinary behaviour of a young, developing bipolar active region (Fig. 2). Then the principal p umbrae of Group 1 and Group 2 stopped on 15 June and changed the direction of their motion, and both moved towards the NE till the end of the observing period, 20 June (or in case of Group 2 till 18 June, when it died out, see Fig. 2). Taking into account their different ages, this parallel proper motion and the subsequent simultaneous change in the direction of the motion of the main p spots can be a sign of some kind of connection between the sunspot groups, or perhaps of the mutual influence of the sunspot groups on each other. It may be that these sunspot groups are different branches of the same flux tube, and that the behaviour of the common flux tube root is displayed in the common features of their proper motions. But on the other hand we can not exclude the possibility that the simultaneous turn of the principal preceding spots could also be an indication of the existence of large-scale flows in the vicinity of the close-by developing active regions, which influence the motion of these spots. A possible influence of large-scale flows on sunspot motions was described previously by Marquette and Martin (1988).

A pair of young opposite polarity spots (N2, S3, S4 and S5) produced a sheared velocity field in the centre of Group 2 on 13 June (c.f. Figs. 1 and 2). The velocity of their divergence was 350 m s^{-1}. The location of this sheared velocity field became the end-point of a new filament

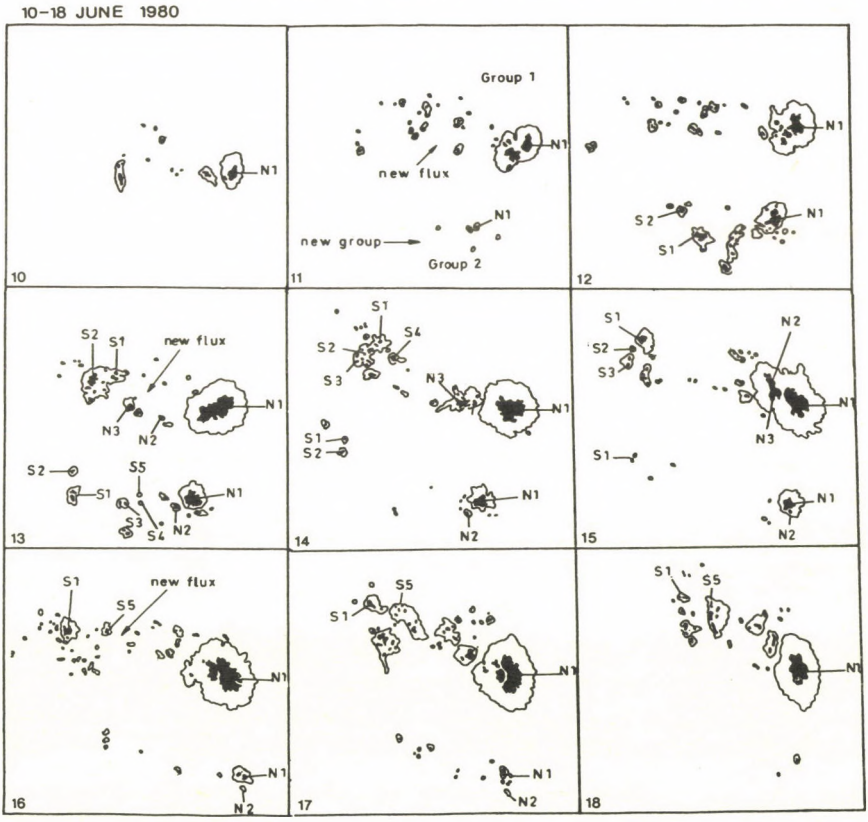

Figure 1. *The sunspot groups in Hale region 16898 between 10-18 June 1980. The denotations of umbrae show their magnetic polarity: N and S means north and south polarity, respectively; numbers are given in order of appearance of the spots.*

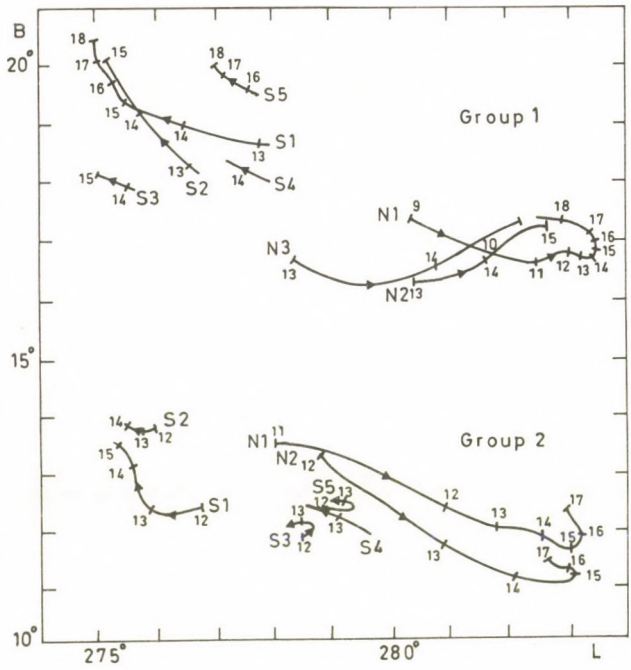

Figure 2. *Proper motions of umbrae in Group 1 and in Group 2 between 9-20 June 1980. The preceding umbrae are marked with the letter N and the following umbrae with the letter S, showing their magnetic polarity, and also with different numbers in order of appearance (c.f. Fig. 1)*

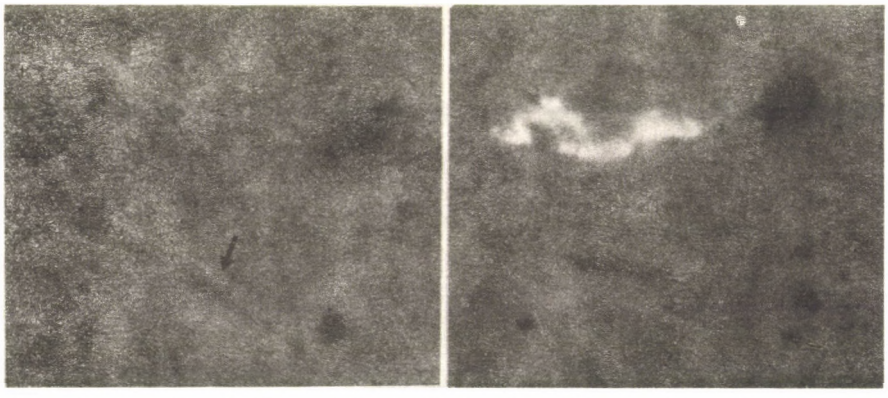

Figure 3. *Formation of a filament observed in the channel between Group 1 and Group 2 on 13 June 1980 at 14:10 UT in Hα -0.5 Å and on 14 June at 06:32 UT in Hα+0.5 Å.*

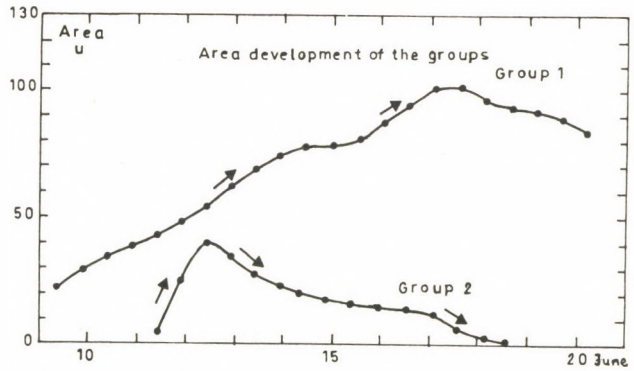

Figure 4. *Development of the global umbral area of Group 1 and Group 2 between 9-20 June 1980.*

which formed in the channel between Group 1 and Group 2 in the afternoon of 13 June (Fig. 3). At the same time there were also fast moving, diverging spots in Group 1 (Fig. 2), which were associated with the most intense (non-thermal) radio source of the whole region (Chiuderi-Drago *et al.*, 1987). These shearing motions could create favourable conditions for the formation of a filament, as proposed by Rompolt and Bogdan (1986).

A third possible sign of the interaction of the sunspot groups can be found in the development of their area (Fig. 4). The fast development of the new Group 2 was followed by the appearance of flux (faster increase in area) in the older, larger Group 1. Two periods in which the area of the larger Group 1 increased were followed by periods of decreasing area of Group 2. When Group 2 disappeared, Group 1 showed a "resurgence" of activity, and flares were again observed in it at the west limb. The disappearance of Group 2 seemed to lead to an instability of Group 1. This sign of interaction of sunspot groups developing close-by was already mentioned by Martres (1970), Sheeley (1981), and Martres *et al.*, (1986).

Acknowledgements

We would like to thank L. Győri for the photospheric observations, and J. Moity for the magnetic observations. We are grateful to Dr. M.J. Martres for her useful comments and to Dr. W. van Driel for a critical reading of the paper. One of us (L.v.D.-G.) would like to thank the Observatoire de Paris for financial support during her visits there.

References

Chiuderi-Drago, F., Alissandrakis, C., and Hagyard, M.: 1987, *Solar Phys.* **112**, 89.
Dezső, L., Gerlei, O., and Kovács, Á.: 1988, "Debrecen Photoheliographic Results" *Publ. Debrecen Obs. Heliographic Series* **No. 1.** 11.
Marquette, W.H., Martin, S.F.: 1988, *BBSO Preprint*, No. 0290.
Martres, M.J.: 1970, *Solar Phys.* **11**, 258.
Martres, M.J., Mouradian, Z., Soru-Escaut, I.: 1986, *Astron. Astrophys.* **161**, 376.
Rayrole, J.: 1981, *Proc. Japan-France Seminar on Solar Phys.* p. 258.
Rompolt, B., and Bogdan, T.: 1986, in A.I. Poland (ed.) *'Coronal and Prominence Plasmas'*, NASA Conference Publ. 2442, p. 81.
Sheeley, N.R.: 1981, in F.Q. Orrall (ed.) *"Solar Active Regions"* Colorado Assoc. Univ. Press, p. 17.
Zwaan, C.: 1990, this issue

SOLAR ACTIVE LONGITUDES AND THEIR POSSIBLE RELATION TO THE REGULAR LARGE-SCALE PATTERNS OF THE SOLAR MAGNETIC FIELDS

V. Bumba
Astronomical Institute of the Czechoslovak Academy of Sciences, 251 65 Ondřejov, Czechoslovakia

L. Hejna
Department of Computer Techniques of the Faculty of Mathematics and Physics, Charles University, Ke Karlovu 3, 121 16 Praha 2, Czechoslovakia

Abstract: Four groups of solar active longitudes with different synodic rotation periods are discussed. The dynamics of their formation is studied on the longitudinal distribution of highly integrated Stanford magnetic charts. An attempt is made to relate them with the regular large-scale features of the background fields visible around the time of the recent two minima of solar activity.

ACTIVE LONGITUDES KNOWN AS YET

Recently, evaluating newly acquired observational data from a number of papers investigating concentrations of solar activity in its longitudinal distribution, we found that the 27-day maximum of its recurrency has a fine structure consisting in the low latitude zone ($\pm 20^{o}$) at least of two active longitudes (A.Ls) rotating faster than Carrington's rotation. Their synodic rotation values are: 26,77 and 27,16 days (Bumba and Hejna 1990). The summary graph of all these active longitudes shows that, although they belong to different activity phenomena and were discovered by different authors, they overlap to a relatively high degree and run at least through three eleven-year cycles. As many authors have shown (for example, Vitinskij 1969) we also have to add to the known A.Ls the one rotating at Carrington's rotation rate.

There also exists a fourth A.L. acting differently at low ($\pm 20^{o}$) and higher ($\pm(20^{o}-40^{o})$) latitudes, the synodic rotation value of which is 28-29 days (for example, Bumba and Hejna 1981).

Although the three main solar A.Ls are reflected in the distribution of the interplanetary magnetic fields (Svalgaard and Wilcox 1975) and although their existence has been demonstrated by many authors, we are still trying to find more facts about the reality of the A.Ls and about the physical processes behind the formation of these phenomena.

LONGITUDINAL DISTRIBUTION OF INTEGRATED MAGNETIC FIELDS

As a part of this effort we reduced all synoptic magnetic maps from the Wilcox Observatory (Hoeksemo and Scherrer 1986) to the scale used in our earlier quoted paper (Bumba and Hejna 1990) integrating the magnetic fields following their polarity in three latitudinal strips, 20^{o} wide. For each longitudinal interval we drew the predominating polarity. We carried out this procedure separately for weak (all) fields and for higher intensity ($\triangleq \pm 200$ MicroTesla) fields. We also used our older data obtained from the McIntosh maps (Bumba and Hejna 1986). In this way we obtained the longitudinal distribution for both magnetic field polarities for cycles Nos 20 and 21 in latitudinal zones: $\pm 20^{o}$ and $\pm(20^{o}-40^{o})$.

We have not yet succeeded in evaluating fully all the relevant graphs, but the following preliminary results may be presented: The distribution of weak fields of both polarities in the equatorial zone does not reflect the stage of the activity cycle. The distribution of both weak polarities in low latitudes is strikingly regular, each one forming long strips inclined parallel to the direction given by the synodic 26,7 -26,8-day rotation with small deviations. The strips formed from the positive polarity are more continuous and longer. But in both graphs it is not possible to estimate which strip belongs to the A.L.

In the stronger field distribution some strips are more outstanding. These may be associated with A.Ls. The positive polarity strips again develope continuously running strips, while the negative polarity strips are discontinuous. If we combine the weak and strong field distributions into one graph (Fig. 1), we see that both distributions may be combined.

Comparing the positions of the large-scale morphological features formed from magnetic fields during the final and initial stages of the two last eleven-year cycles (Bumba 1987) with the regularities of the magnetic field longitudinal distribution, we see that they are bound to the main strips of the stronger fields or to the A.Ls.

At higher latitudes ($\pm(20^{o}-40^{o})$) the distribution of both polarities resembles the one at low latitudes, only the inclination of its strips is reversed. It has two mean rotational periods: 27,456 and 28,242 days.

If we compare the longitudinal distributions found at low and higher latitudes, in the weak as well as in the stronger fields, we see that there exists a relatively strong coupling between both latitudinal zones.

CONCLUSION

Our expectation that more evidence of A.Ls will be found in our integrated graphs was not fulfilled. These graphs became too schematic, and all details visible on synoptic maps, which are so important for the visualization of A.Ls, were lost. But we have to continue our studies because, if we study the 26.77 day A.L., several times overlaped, found earlier to the present days, we see that it is still active, producing many active regions.

REFERENCES

Bumba V. 1987 Bull. Astron. Inst. Czechosl. 38, 92
Bumba V. Hejna L. 1981 Bull. Astron. Inst. Czechosl. 32, 349
Bumba V. Hejna L. 1986 Studia Geoph. et geod. 30, 158
Bumba V. Hejna L. 1990 Bull. Astron. Inst. Czechosl. 41, (in press)
Hoeksemo J.T. Scherrer P.H. 1986 World Data Center A for Solar-Terr. Physics, Report UAG-94
Svalgaard L. Wilcox J.M. 1975 Solar Phys. 41, 461
Vitinskij J.I. 1969a Solar Phys. 7, 210

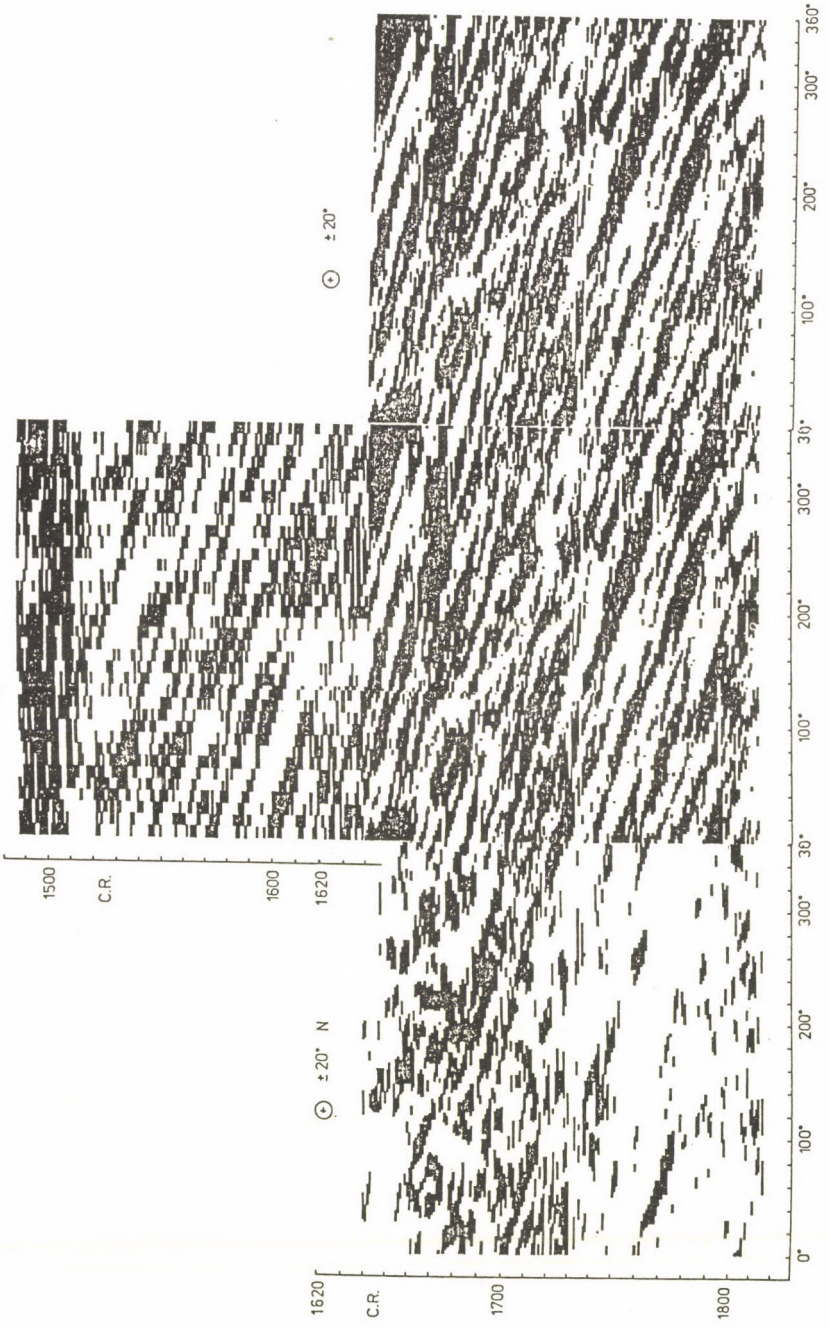

Fig.1.

SUNSPOT AND PLAGE PHOTOMETRY FOR SOLAR IRRADIANCE VARIATIONS IN AUGUST/SEPTEMBER 1980

M. Steinegger[1], P.N. Brandt[2], W. Schmidt[2]

[1] Institut für Astronomie, Universitätsplatz 5, A-8010 Graz, Austria
[2] Kiepenheuer-Institut für Sonnenphysik, Schöneckstraße 6, D-7800 Freiburg, FRG

1. Introduction

Solar irradiance variations on active region time scales are due to the combined effect of sunspot blocking and facular excess radiation and up to now were described by the Photometric Sunspot Index (PSI) and Photometric Facular Index (PFI) models (e.g. Foukal, 1981; Willson et al., 1981). To test the reliability of the PSI and PFI concepts we started a detailed photometric analysis of sunspot pictures and Ca-spectroheliograms. We present the results of the sunspot photometry for the period Aug. 19 to Sep. 4, 1980, and give some preliminary results of the Ca-analysis for the same period.

2. Sunspot Observations and Data Reduction

Photographs ($\lambda\,550 \pm 50\,nm$) of all visible spots were taken on a daily basis with the $40\,cm$ Vacuum Newton Telescope (Izaña, Tenerife). From the digitized photographs intensity vs. area histograms have been derived, normalized to the mean intensity of the adjacent quiet photosphere, and corrected for 5% straylight. For each intensity bin the temperature was calculated and converted into radiation. The normalization factor α as introduced by Willson et al. (1981), was determined taking into account the relative area of the bin. Finally the irradiance deficit of the spots in ppm of the quiet Sun irradiance was derived and the result was compared with the ACRIM measurements and the PSI results. Additionally the umbra-penumbra area ratios r_{up} have been calculated. A more detailed description of the reduction procedure is given in Steinegger et al. (1990).

3. Results of the Sunspot Photometry

1) In order to have a direct comparison with the $\alpha = 0.32$ of the PSI model, values of α were calculated using mean temperatures for umbra and penumbra. They vary from $\alpha \simeq 0.24$ to $\alpha \simeq 0.28$ for small and large spots, resp. (Fig. 1).

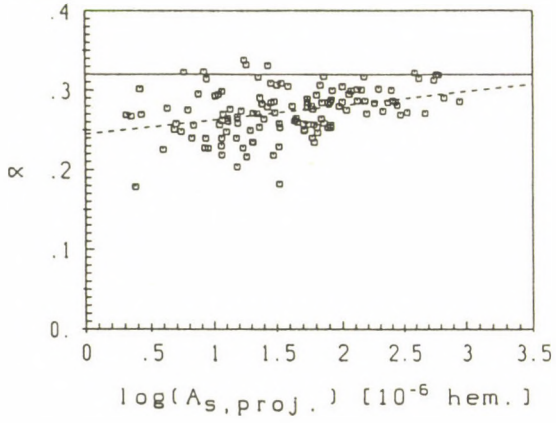

Fig. 1.: Irradiance deficit factors α as function of the projected sunspot area. The full line represents constant value $\alpha = 0.32$ assumed in the PSI model.

2) The trend of the irradiance deficit derived from our analysis agrees well with the ACRIM measurements. In general the PSI model yields larger deficits, which is mainly due to its larger α value (cf. Steinegger

et al., 1990).

3) The area ratio r_{up} varies from approx. 0.1 to 0.5, with an average value of 0.32 for large spots, as compared to the value of 0.21 assumed in the PSI model. A linear fit to the data yields a slope of approx. 1.10, which again demonstrates that r_{up} is not constant (cf. Brandt et al., 1990).

4. Preliminary Results of the Ca–Analysis

For the Ca–analysis we used spectroheliograms from Sacramento Peak Obs., which were digitized and converted into relative intensities. In order to obtain the quiet Sun center-to-limb variation (CLV) the following procedure was applied: 1) The intensity profiles on circles with constant μ were determined and the mean intensity along this profile was computed. To eliminate the effect of bright Ca features, all values higher than this mean were replaced by the mean itself. After several iterations a stable value for the quiet Sun Ca intensity at this μ was obtained. 2) A second order polynomial fit through these quiet Sun values as a function of μ then yielded the desired CLV. Fig. 2 shows the CLV for 21 August 1980, in comparison to the result of White and Suemoto (1968). After normalization to the quiet Sun CLV, intensity vs. area histograms have been derived analogous to the sunspot analysis.

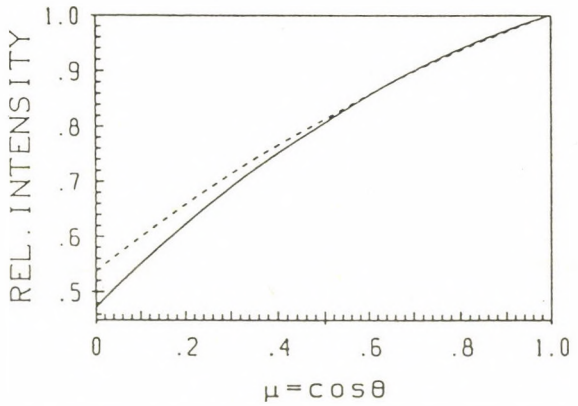

Fig. 2: CLV for spectroheliogram of 21 Aug. 1980 (full line) in comparison to the result of White and Suemoto (dashed line).

5. Concluding Remarks

The photometric analysis of our sunspot data has shown that the umbra–penumbra area ratio is a function of the sunspot area. Therefore, it seems inadequate to assume a constant value for this ratio which could represent 'all' sunspots.

The irradiance deficit value α varies with spot size and was found to be always smaller than the value adopted by Willson et al. (1981).

Acknowledgement

M.S. greatfully acknowledges the support of the Austrian *"Fonds zur Förderung der wissenschaftlichen Forschung"*, grant P7500/PHY.

References

Brandt, P.N., Schmidt, W., Steinegger, M.: 1990, *Solar Phys. Lett.*, in press

Foukal, P.: 1981, in L.E. Cram and J.H. Thomas (eds.), *The Physics of Sunspots*, Sacramento Peak Observatory, Sunspot, NM, p. 391

Steinegger, M., Brandt, P.N., Pap, J., Schmidt, W.: 1990, *Astrophys. Space Sci.*, in press

White, O.R., Suemoto, Z.: 1968, *Solar Phys.* **3**, 523

Willson, R.C., Gulkis, S., Janssen, M., Hudson, H.S., Chapman, G.A.: 1981, *Science* **211**, 700

AN INVESTIGATION OF SUNSPOT NESTS DURING SOLAR CYCLE No. 20

Bashir K. Abuzeid[1,2] and Kristóf Petrovay[1]

[1]Eötvös University, Department of Astronomy, Budapest, Kun Béla tér 2, H-1083 Hungary

[2]Garyonis University, Physics and Astronomy Department, P.O. Box 9480, Benghazi, Libya

Abstract. The space-time distribution of sunspot groups in the time interval 1965-1977 was studied using cluster analysis. (Data were taken from the Greenwich and Debrecen Heliographic Results.) Results for the 8–10 groups/cluster level of clustering are presented.

1. Introduction

Sunspot nests are the clusters that appear to dominate the heliographic longitude–time (L–t) distribution of sunspot groups if only spots in a given 10° latitude interval are regarded. They were studied by Becker (1955) and Castenmiller, Zwaan and van der Zalm (1986). On average they consist of 8–10 spot groups. Their size was found by Castenmiller et al. to be $\Delta L \sim 10°$–$20°$, $\Delta t \sim 6$–8 rotations.

The main purpose of our investigation was to determine the rotational rate of the nests. Our basic data were taken from the Greenwich Heliographic Results for the years 1965–1976 and from the Debrecen Heliographic Results for the year 1977. Only spot groups that were (probably) born on the visible hemisphere of the Sun were included. For each group we used the position and time data of the first observation. The cluster analysis was performed with a Bayes iteration procedure that is particularly well suited for sorting out nonspherical, elongated clusters. A description of this procedure, well known in mathematical statistics, may be found e. g. in Dempster et al. (1977).

TABLE I

Belt	Latitude	Groups	$\omega - \omega_C$ (deg/rot)
N7	30° –	47	-1.19 ± 0.39
N6	25° – 35°	109	-1.61 ± 1.44
N5	20° – 30°	212	-4.43 ± 3.45
N4	15° – 25°	343	-6.09 ± 2.70
N3	10° – 20°	409	-8.16 ± 1.38
N2	5° – 15°	370	-6.24 ± 2.07
N1	0° – 10°	224	-2.66 ± 1.61
0	-5° – 5°	113	-2.65 ± 0.81
S1	-10° – 0°	209	-4.21 ± 0.86
S2	-15° – -5°	378	-6.14 ± 2.47
S3	-20° – -10°	372	-5.35 ± 2.78
S4	-25° – -15°	255	-3.53 ± 2.10
S5	-30° – -20°	157	-1.69 ± 0.21
S6	-35° – -25°	75	-1.45 ± 0.40
S7	– -30°	27	+0.252 ± 4.08

2. Results

For the study of the 8–10 gr/cl level of the clustering "tree" we divided the sample into overlapping 10° latitude belts, as usual. The values of the cycle-averaged rotational rates for each belt are shown in Table I and Figure 1. It is found that *the cycle- and latitude-averaged rotation rate of the nests is slightly but significantly smaller than the Carrington rate*: $\omega_S - \omega_C = -3.7 \pm 1.7$ deg/rotation. This also proves the significance of the non-random character of the distribution: clearly, in a random sample the relative rotation rate should not be significantly different from zero.

From Figure 1 it is apparent that *the differential rotation of the nests is strongly reduced*: only a variance of ~8–9 deg/rot (2–3 %) is found within the whole sunspot belt. A curious *bimodality* is also apparent in Figure 1: intermediate latitudes (10°–20°) on both hemispheres seem to rotate somewhat slower than both the equator and the higher latitudes. The effect is small but significant. The data also suggest a (not significant) 2–3 % time dependence with *somewhat slower rotation near and immediately following the sunspot maximum* and a somewhat faster rotation in the later phases of the cycle and near minimum. When coupled with the butterfly diagram, this effect (if real) may partly or wholly explain the bimodality of the latitude dependence.

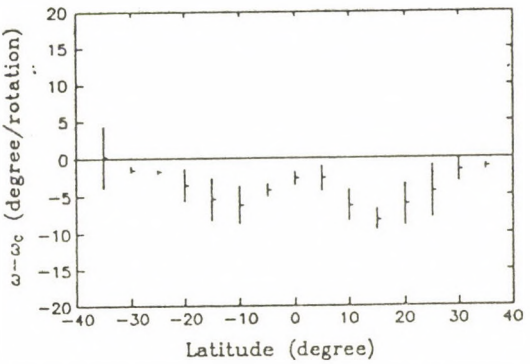

Fig. 1 The cycle-averaged rotational rate of the sunspot nests as a function of heliographic latitude

Acknowledgement

We are grateful to Dr. Lajos Balázs who kindly provided us with his Bayesian iteration computer code and to the Debrecen Heliophysical Observatory staff for their hospitality during part of this work.

References

Becker, U.: 1955, *Z. Astrophys.*, **37**, 47.

Castenmiller, M. J. M., Zwaan, C. and van der Zalm, E. B. J.: 1986, *Solar Phys.*, **105**, 237.

Dempster, A. P., Laird, N. M. and Rubin, D. B.: 1977, *J. Roy. Stat. Soc., Series B*, **39**(1), 1.

A SHORT TERM PERIODICITY NEAR 155 DAY IN SUNSPOT AREAS

M.Carbonell and J.L.Ballester
Departament de Fisica
Universitat de les Illes Balears
E-07071. Palma de Mallorca
Spain

ABSTRACT
We present evidence of a nearby 155 days periodicity in the historical record of sunspot areas from 1904 to 1976, rotation by rotation, covering cycles 14 to 20. This suggests that earlier periodicities around 155 days found in other indicators of solar activity during the last three cycles could be connected to this one presented here. Due to the fact that the amount of emerging magnetic flux is directly proportional to sunspot areas, this result also suggests the existence of a periodicity in the emergence of magnetic flux through the solar photosphere. Another peak around 510 - 540 days, pointed out in solar flares by several authors, is also present in our results, however, is not significant at all, because it remains below the level of the "null continuum".

DATA AND METHOD

The Greenwich Photoheliographic Results from 1874-1976 provides with the mean area of visible sunspots (umbra plus penumbra and pores included) per Carrington rotation, together with the number of days with observations during each rotation. This mean area comes separated by hemispheres, corrected for foreshortening. We have constructed three different time series for the total sunspot areas per Carrington rotation, northern hemisphere, southern hemisphere and whole disk. In order to preserve the homogeneity, we have constructed our time series with the data from 1904 till 1976, solar cycles 14 to 20, since during this period of time the rotations have had a number of observed days equal or greater than 26. To look for periodicities, we have performed Blackman-Tukey power spectrum (Blackman and Tukey, 1958) using as "null" continuum the Markov "red noise".

RESULTS

In the northern hemisphere significant peaks, above 99% confidence level, at 3.5 and approximately 2 rotations are present. The prominent peak at 5.75 rotations corresponds, approximately, to 153 days, remaining slightly below the 99% confidence level, while the peak around 2 rotations corresponds to 54 days, perhaps the third harmonic of 153 days. A peak around 20 rotations can be seen but it is below the level of the red noise, this must be the same peak detected by Akioka et al.(1987) and should be related with the peaks at 564 and 552 days detected by Bai et al. (1987) and Ozgüç et al. (1989) in solar flares. In the southern hemisphere, the most prominent

peak occurs at 5 rotations, approximately 135 days. Other significant peaks in the power spectra of southern hemisphere are at 2.8 rotations and 2.5 rotations (second harmonic of 5 rotations). The peak around 20 rotations is weaker than in the northern hemisphere. For the whole disk, the most prominent peak remains at 5.75 rotations.

CONCLUSIONS

Our aim has been to look for the existence of the short periodicities around 155 and 540 days in one of the key features of solar activity, sunspot areas. The results show that during cycles 14 - 20 a significant peak around 155 days is present in the power spectra when we consider the whole disk or the northern hemisphere, while in the southern hemisphere is not significant at all. However, a significant peak at 2.8 rotations, probably corresponding to the second harmonic of 5.75 rotations, is present in the the southern hemisphere. The peak at 20 rotations is present in the Blackman-Tukey power spectra, exactly at the same position as in the power spectra computed via FFT, for the whole disk and northern hemisphere but it is not significant at all because it remains below the "red noise" level. On the other hand, there is observational evidence which suggests that many H_α flares seem to occur when new flux emerges, within pre-existing magnetic regions, and reconnects with the old flux (Martin et al., 1984). Theoretical models have been set up to explain how the emergence of new flux through the photosphere could give rise to small flares and, even, to trigger large flares (Priest, 1986). It follows that the presence of this short periodicity in the most characteristic feature of solar activity, which is a measure of the emerging flux, could point out the existence of a periodicity in the emergence of magnetic flux,which could produce the similar one found in solar flares. This result together with the fact that sunspot areas have presented a clear North-South asymmetry (Vizoso and Ballester, 1990) during most of the period considered here, allow us to conclude that the emergence of magnetic flux is asymmetric between hemispheres, and present short-term periodicities.

REFERENCES

Akioka,M.,Kubota,J.,Suzuki,M.,Ichimoto,K. and Tohmura,I.:1987, Solar Phys., 112, 313
Bai,T.,Sturrock,P.A.:1987,Nature,327, 601
Blackman, R.B., Tukey, J.W. : 1958, The Measurement of Power Spectra, Dover, New York
Carbonell,M.,Ballester,J.L.: 1990, Astron.Astrophys. (In press)
Martin,S.F.,Bentley,R.D.,Schadee,A.,Antalova,A.,Kucera,A.,Dezso L.,Gesztelyi,L.,Harvey,K.L.,Jones,H.,Livi,S.H.B.,Wang,J.: 1984, Adv.Space Res., 4, 61
Ozgüç,A.,Ataç,T.:1989,Solar Phys., 123, 357
Priest,E.R.:1986,Adv.Space Res., 6, 73
Vizoso,G.,Ballester,J.L.:1990,Astron.Astrophys. 229, 540

INFLUENCE OF MAGNETIC FIELDS ON TEMPERATURE INHOMOGENEITIES

Hanslmeier, A.[1], Mattig, W.[2]

[1]Institut f. Astronomie, Graz, [2]Kiepenheuer Inst., Freiburg

Most solar phenomena are directly associated to the presence of magnetic fields or are influenced by them in a substantial way. In this paper we studied the influence of magnetic fields on the temperature variations. For this purpose we used a spectrum, obtained with the 45 cm Gregory Coudé telescope at Izaña, Tenerife. The spectra covered about 144 arcsec on the solar disk and were recorded photographically. Magnetically active regions were defined as regions with enhanced Ca^+ emissivity. A detailed description of the observation and reduction can be found e.g. in Hanslmeier and Mattig (1990). In Table 1 the observed line and some important line parameters are given.

Table 1: Observed photospheric lines and their parameters

Line	Element	λ(Å)	W_λ(mÅ)	Height[2]	Height[1]
I	CaI	6499.654	81	255	–
II	FeI	6498.945	43	215	–
III	BaII	6496.908	98	490,310	–
IV	FeI	6496.472	69	190	200
V	FeI	6495.740	42	–	135
VI	FeI	6494.994	165	535	500
VII	FeI	6494.499	34	64	105
VIII	CaI	6493.788	133	335	–

[1]Nesis et al. (1987), [2]Wiehr et Kneer (1988)

Intensity fluctuations generally correspond to temperature variations. In order to get information about the height dependence of these variations, we calculated the line core intensity rms fluctuations at the respective line cores. This was carried out for a selected magnetically non active (NAR) and active (AR) region. We found a substantial reduction of the rms line core intensity fluctuations in active regions. The difference between these fluctuations in NAR and AR is given in Fig. 1. A decrease of the difference up to 170km can be seen, followed by an increase up to 490km.

The value at 535km occurs near the temperature minimum. The increasing difference can be explained by a faster decrease of the temperature inhomogeneities with height at the presence of magnetic activity.

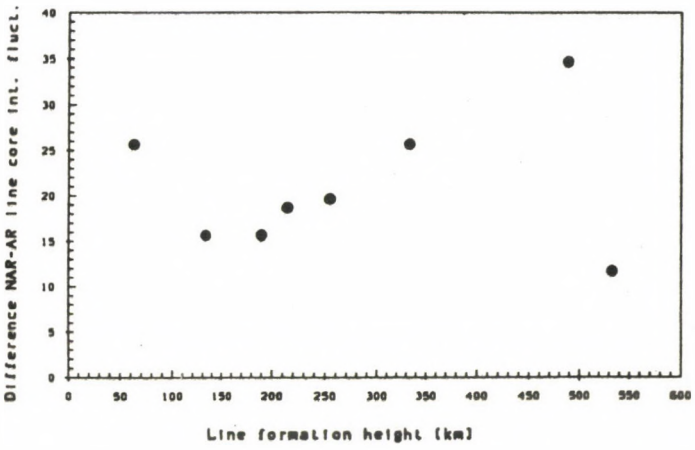

Fig.1.: Difference in % between line core intensity fluctuations in Ca^+ non active and active regions.

REFERENCES

Hanslmeier, A., Mattig, W.: 1990, XI ERAM, Astrophys. and Space Science, in press.

Nesis, A., Mattig, W., Fleig, K.H., Wiehr, E.: 1987, Astron. Astrophys. 182, L5.

Wiehr, E., Kneer, F.: 1988, Astron. Astrophys. 195 ,310.

ACTIVITY CYCLE VARIATION OF SOME PHOTOSPHERIC LINES

M. Karabin*, A. Kubičela**, J. Skuljan*, I. Vince**

The long term spectral lines monitoring program started in August 1987 at the Belgrade Astronomical Observatory. Full disk observations of selected photospheric lines have been done using the solar spectrograph (Arsenijević et al, 1988). Measurements from August 1987 till May 1990 cover the rise from minimum to maximum of 22^{nd} Solar cycle. The data were analized by the software for flat field reduction, normalization to the continuum level and numerical integration. For ten spectral lines (530.74nm $\leq \lambda \leq$ 568.82nm) equivalent width has been measured to find possible changes during the activity cycle. In order to remove systematic errors, appropriate corrections were made (Fig. 1).

A linear least squares fit to the data is drawn for each line, from where the trend of equivalent width W' is estimated. Out of ten lines, four do not show any change with time, and six show steady change. The results of those activity-sensitive lines are presented in Fig. 2.

Three lines show steady decrease: MnI 539.47nm (−4.1% per year), ScII 552.68nm (−4.4% per year) and FeI 557.61nm (−2.4% per year). But the other three lines show increase: TiII 533.68nm (+3.5% per year), CaI 560.13nm (+2.2% per year) and NaI 568.82nm (+6.2% per year). All the results are above 2σ-level.

It may be worth pointing out that all the lines which increase with activity are those that are strengthened in the spot spectrum too. Our results confirm that equivalent width of some lines are sensitive to the activity i.e. to changes in photospheric conditions (temperature, l/H, E.P., microturbulence etc.). Similar results were obtained by Stepanyan and Scherbakova (1979), also by Livingston and Holweger (1982) and Kokhan (1987).

REFERENCES

1) Arsenijević, J. at al.: 1988, *Bull. Astron. Obs. Belgrade,* **138,** 1.
2) Kokhan, E. K.: 1987, *Izv. GAO,* **204,** 81.
3) Livingston, W. and Holweger, H.: 1982, *Ap. J.,* **252,** 375.
4) Stepanyan, N. and Scherbakova, Z.: 1979, *Izv. Krim. Ast. Obs.,* **59,** 91.

*) Institute of Astronomy, Mathematical faculty, University of Belgrade, Studentski trg 16, 11000 Beograd, Yugoslavia
**) Astronomical Observatory, Volgina 7, 11000 Beograd, Yugoslavia

The activity cycle variations of photospheric lines (full disk observations)

Fig.1. Systematic error elimination: W'=(W−b)/a

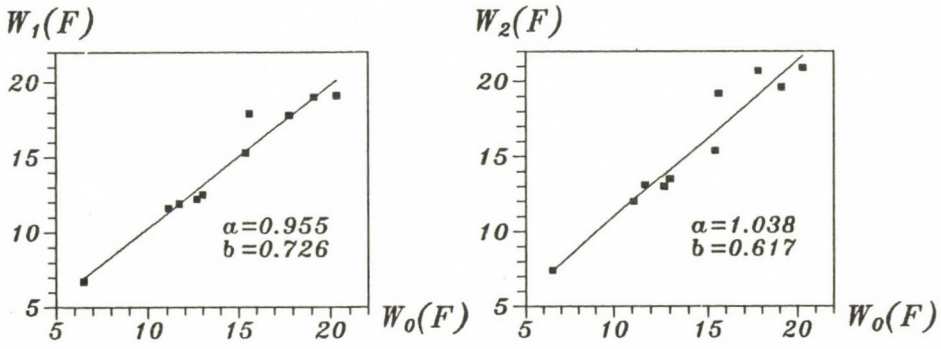

Fig.2. Equivalent width trend for selected lines

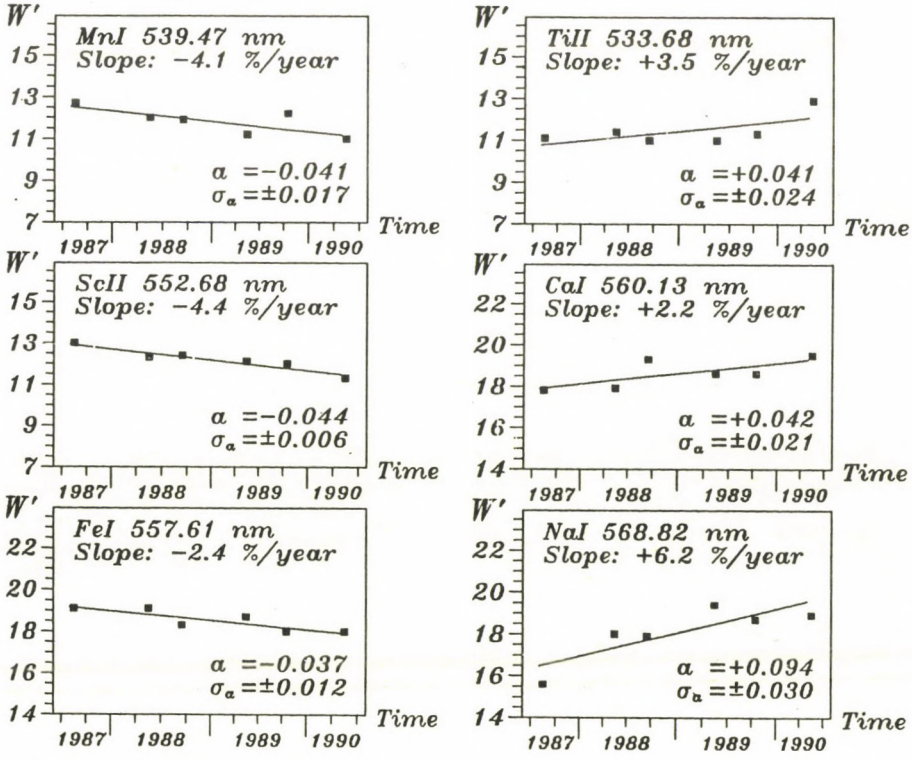

CHANGES IN RESIDUAL POLARIZATION OF THE CORONA AND THE SOLAR ACTIVITY CYCLE

M. Vuletić,[1] P. Cugnon,[2] J. Arsenijević[3]

1) INTRODUCTION

The variation of the general shape of the Solar corona with the Solar activity cycle is a well known phenomenon (Allen, 1946 and Van de Hulst, 1950). More recent works (Dzubenko, 1983; Koutchmy and Nitschelm, 1984; Loucif and Koutchmy, 1989) confirmed that the flattening of the corona is highly correlated with the phase of the Solar cycle. Our purpose in this short preliminary paper is to examine the behavior of another global quantity, the residual polarization of the corona in white light, because there are reasonable chances – owing to very simple geometrical considerations – that the two parameters characterizing the phenomenon (percentage and angle of polarization) also show dependance on the Solar cycle.

2) THE OBSERVATIONS

Calculations were based on photographic observations made during the total eclipses of 1973 and 1980 (Kenya) and of 1983 (Indonesia) by three Belgian expeditions.

During the totality of three eclipses photographic images of the corona were taken on a Kodak PLUS-X emulsion, using a reflex camera at the focus of an 1 meter focal length and 7 cm aperture refractor. The analyzer was a polaroid filter put a little in front of the film which could be oriented in three directions (0°, 60° and 120°) (Fessenkov 1935, Arsenijević 1961, Clette et al. 1985).

The measured densities were converted into intensities using the calibration curve of the film established for our specific conditions. However, for the case in which we are interested here, no absolute calibration is necessary, so that only relative intensities were computed.

The residual polarization was then computed in two steps : a) For each network from a set of observations, the summations of the intensities inside rings of different external radii (from 1.5 to 2.2 solar radii), the inner one being always 1.2 solar radius. b) The calculation of the percentage p of polarization and of the position angle θ of the electric vector and the north pole of the Sun, using the classical Fessenkov formulae :

$$p = \frac{2\sqrt{I_1^2 + I_2^2 + I_3^2 - I_1 I_2 - I_2 I_3 - I_1 I_3}}{I_1 + I_2 + I_3}, \qquad \tan 2\theta = \frac{\sqrt{3}(I_2 - I_3)}{2I_1 - I_2 - I_3}.$$

3) RESULTS

Table I shows, for the case of the total eclipse of 1983, the evolution of the degree of polarization with the outer radius of the rings. We observe a slow asymptotic decrease,

[1] Institute of astronomy, Mathematical faculty, University of Belgrade, Studentski trg 16, 11000 Belgrade, Yugoslavia

[2] Observatoire Royal de Belgique, Av. Circulaire 3, 1180 Bruxelles

[3] Astronomical Observatory, Volgina 7, 11000 Belgrade, Yugoslavia

for which we have, up to now, no fully satisfying explanation; it is to be noted that such a situation is not present for the eclipse of 1973. This point will be investigated in a more detailed paper.

In Table II the results for the three eclipses, together with other data, are sumarized: the phase of the eclipses in the solar cycle, the daily sunspot number (Zurich, Brussels) and the flattening index ε of the corona (taken from our data), defined as: $\varepsilon = R_{eq}/R_{pol} - 1$, the degree and angle of polarization.

Table I

$R_{max}(R_\odot)$	1.5	1.6	1.7	1.8	1.9	2.0	2.1	2.2
P (%)	17.2	16.9	16.5	16.2	16.0	15.8	15.7	15.6

Table II

Eclipse	Phase	Wolf number	Flattening index	Degree of polarization	Angle of polarization
Jun 30, 1973	-0.40	33	0.176	22%	21°
Feb 16, 1980	-0.97	163	0.080	3%	not significant
Jun 11, 1983	-0.40	73	0.180	16%	1°

4) DISCUSSION – CONCLUSIONS

This preliminary investigation shows that the residual polarization is much higher for the two eclipses of 1973 and 1983, which occured both in the decreasing phase of the cycle, than for the maximum eclipse of 1980. It is interesting to note that for exactly the same phase, the flattening indexes of the corona are also the same. Moreover, as a consequences of the high level of residual polarization, the angle of polarization (electric vector refered to the polar direction) is well defined in both cases (estimated error: 3°). On the contrary, for the eclipse of 1980, this angle is found to be erratic and hence without significance.

As expected, the geometry of the corona seems to play a fundamental role. Indeed, the flattening observed in 73 and 83 makes the contributions to residual polarization of the western and eastern parts higher than northern and southern contributinos, the local polarization being weighted by the local intensity. Moreover, this local polarization is also lower in the polar directions. It is also important to note that the lower the daily sunspot number, the higher the residual polarization is. It is however prematurate to infer from this short discussion that residual polarization should be a good indicator of solar coronal activity; more investigations are needed to conclude on firm ground.

REFERENCES:

Allen, C. W., 1947, *M.N.R.A.S.* **107,** 426
Arsenijević, J., 1969, *Bulletin Astr. Obs. Belgrade,* **XXVII, 2,** 24
Clette, F., Cugnon, P., Koeckelenbergh A., 1985, *Solar Phys.* **98,** 163
Dzubenko, N. I., 1984, *Solnechnye Dannye* No 6
Fessenkov, B.,1935, *AJ USSR,* **XII,** 4
Koutchmy, S., Nitschelm, C., 1984, *Astron. Astrophys.* **138,** 161
Loucif, M. L., Koutchmy, S., 1989, *Astron. Astrophys. Suppl.* **77,** 45
Van de Hulst H. C., 1950, *Bull. Astron. Inst. Neth.* **410, (11),** 135

THE INFLUENCE OF THE GRANULATION ON THE ABSORPTION LINES I. NONACTIVE REGIONS

A. Nesis[1] A. Hanslmeier[2] R. Hammer [1] R. Komm[1] and W. Mattig[1]
[1]Kiepenheuer-Institut für Sonnenphysik, Schöneckstr. 6, D-7800 FREIBURG, F.R.G.
[2]Institut für Astronomie, Universitätsplatz 5, A-8010 GRAZ, Austria [1]

The hydrodynamical state of the photospheric layers depends sensitively on the decay process of the granulation and on secondary motions such as turbulence and waves which are induced by this process. The hydrodynamical state of the deep photospheric layers controls the process of line formation; especially, the broadening of the absorption lines.

It is the aim of this investigation to find the functional interdependence between the granular intensity fluctuations I_i and the line width W_i of the absorption lines, calculated as FWHM (full width at half maximum) at any step i (i=1...900) along the slit of the spectrograph. Here, the intensity fluctuations are used as "control data" and the line width serves as a diagnostic tool for the response of the plasma to the intensity fluctuations of convective origin. A functional dependence between I_i and W_i could provide insight into the hydrodynamical state of, especially, the granulum and intergranulum. The method which we use is the mathematical regression.

We used 3 spectrograms taken on July 20, 1987, with the 45 cm Gregory-Coudé vacuum telescope at Izaña (Tenerife; Spain). The spectrograms include the wavelangth range λ: 6494.499 – 6496.472 mÅ, which contains absorption lines of different strength reflecting different heights of the photosphere (100, 200 and 500 km above $\tau_{5000} = 1$).

Fig. 1 demonstrates the results of the regression anlalysis: The three columns correspond to three different spectrograms, sp2, sp4 and sp3. Spectrogram 2 (sp2) was included to demonstrate the influence of the *seeing*. A separate investigation has shown that the rms of the continuum intensity of this spectrogram is a factor of 4 smaller than the rms of the spectrograms 3 and 4 (sp3 and sp4, respectively). This fact explains the different behaviour (positive slope b) of the regression line of sp2 compared to the regression lines of sp3 and sp4.

The three rows show the regression lines for three different heights in the photosphere (100, 200 and 500 km). In sp4 and sp3 we realize the following:

1) a negative slope b of the regression line and

2) a decrease of b with height in the photosphere.

The *negative slope* of the regression lines indicates an increase of the FWHM at low intensity value, which corresponds to the intergranular space, compared to the bright granular regions. The increase of the FWHM amounts to 20 mÅ for the deeper layers (100 km) and 16 mÅ for the higher layers (200 km). We attribute this increase of the FWHM in the intergranular space to enhanced nonthermal velocities (microturbulence) due to the decay process of the granulation associated with the dark regions (cf. Komm et al. 1990).

The *decrease of the slope* b with height on the other hand signifies a decrease of the difference of the line width W_i between granulum and intergranulum with height. We interpret this as a decrease of the nonthermal velocities or microturbulence with height in the photosphere (cf. Komm et al. 1990; Canfield and Beckers 1975). In conclusion, the *negative slope* of the regression lines and its *decrease* with height visualize the sensitivity of the week absorption lines to the nonthermal velocities (microturbulence) associated with the *intergranular regions.*

[1]Mitteilungen aus dem Kiepenheuer-Institut Nr.331

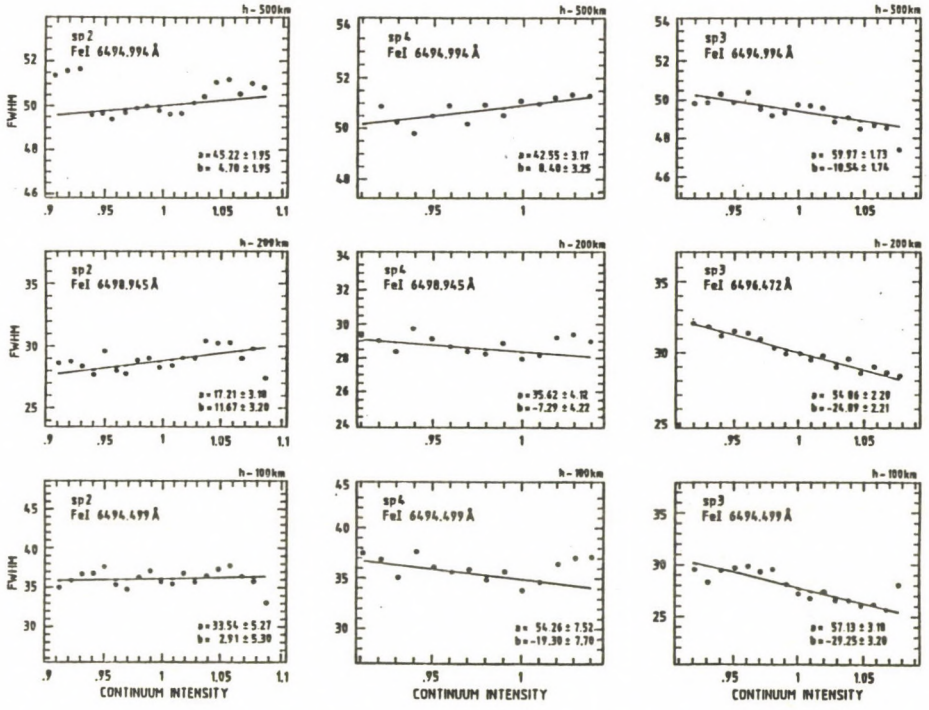

Figure 1: Regression lines of FWHM on the continuum intensity I. The columns represent three different spectrograms (sp2, sp4, sp3). The rows represent three different heights in the photosphere (100, 200 and 500 km). The dots show averaged binned data.

References

Canfield, R. C. and Beckers, J. M.: 1975, in Motions in the Solar Atmosphere, eds. J. M. Beckers, and R. C. Canfield, Sacramento Peak Observatory

Komm,F., Mattig,W. and Nesis,A: 1990, to published in Astron. Astrophys.

THE ANALYSIS OF SOLAR ACTIVITY FEATURES BY MEANS OF THE BASIS DIGITAL IMAGING SYSTEM

M. Messerotti, L. Lampi, S. Furlani, P. Zlobec

Astronomical Observatory, Via G.B. Tiepolo 11, Trieste (Italy)

Abstract CCD-based digital imaging systems are powerful tools for the analysis of solar activity features in real-time or as post-processing. Despite the actual sensor-limited resolutions of low-cost systems, interesting projects can be carried out such as, for instance, the tracing of photospheric motions, in principle also in automatic mode. With regard to that BASIS, a digital imaging system for the Sun operated at Trieste, will be briefly described. Possible applications as mentioned above will be discussed with emphasis on photospheric and chromospheric patterns.

INTRODUCTION A flexible, PC-based digital imaging system for solar observations is currently near completion at the Basovizza observing station, branch of the Trieste Astronomical Observatory. A brief technical description of this system will be given in the following, pointing out its peculiarities with regard to automatic tracing of photospheric and chromospheric activity features.

THE BASIS SYSTEM The Basovizza Solar Imaging System (BASIS) (Messerotti, 1990) is based on a PC-AT compatible personal computer, which is hosting a real-time digitizer card (Matrox mod. PIP1024B) and two controller cards (Matrox i2s Interface Kit, MIIK), which generate all the relevant timing signals to drive two monochromatic CCD cameras (i2s mod. IAC 562 BC). The first camera is coupled to a refractor telescope with aperture D=75mm and focal length F=500mm to get a full disk image of the Sun in white light via a full aperture rejecting filter (FULL DISK MODE, FDM). The second camera is attached to a refractor telescope with aperture D=165mm and focal length F=2100mm to get a 14.4x10.9 arcmin image in white light (ACTIVE REGION TRACKING MODE, ARTM). In near future a narrow-band H-alpha filter will be used for chromospheric observations. The cameras have an interline transfer CCD sensor with a resolution of 493 (horiz.) x 575 (vert.) pixels; the pixel shape is rectangular (17x11 microns). This constitutes the major drawback of the system, because for most applications the digitized image must be rebinned before further processing. The spectral response ranges from 400 to 1100 nm and the sensitivity is 3.5 lux, while the declared S/N ratio is 55 dB. Due to the actual optical arrangement and to the CCD sensor specification the resolving power is sensor-limited. In FDM it is 7.4 arcsec/pixel (horiz.) and 4.7 arcsec/pixel (vert.), while in ARTM it is 1.7 and 1.1 arcsec/pixel respectively. Through the MIIK controllers, programmable via software, the cameras allow two operating modes for image acquisition: 1. a TV mode, which provides 50 fields/s with the exposure locked to the TV synchronization (fixed exposure time = 40 ms/field); 2. a MONOSHOT mode, where the

exposure is variable from 1 to 32767 ms. The latter mode is quite useful to acquire sequences of images of fast evolving phenomena or to compensate for low luminosity in monochromatic images. The images generated by the cameras are digitized by the PIP1024B card, which is a frame grabber with a resolution of 512x512, 8 bits/pixel, 3 software selectable video inputs. The frame buffer of this card can store one 1024x1024, four 512x512 or sixteen 256x256 pixels images with 8 bits/pixel. The card video output is 8 bits IN/24 bits OUT, which means 256 intensities available from a 16.7 million colour palette. Hence the images are displayed on a high resolution multisync colour monitor with RGB input. An extensive low-level software library is provided with the card, which permits the full control of the digitizing process and allows some basic image processing. The images can be stored on disk in compressed (run-length encoding) or uncompressed format for archival purposes. Using the native card library an interactive control program was prepared in FORTRAN language, which continuously displays the status of the system on the PC screen as a control panel with on-off buttons and selection gadgets to be managed via the mouse to define all the parameters relevant to a particular observing mode. The computing power of the used card is relatively limited and suitable only for basic filterings in the space domain, but the association with an array processor card can overcome the problem for computing intensive real-time procedures. This approach will be tested in near future. It is interesting to note that a minimal system can be composed by a portable PC-AT computer, which hosts the controller and the digitizer card, a CCD camera and the connection cable. Such a system can be easily moved to different instruments, perhaps in sites with a better seeing to adequately test software procedures inplemented at the home institution.

AUTOMATIC ANALYSIS OF SOLAR ACTIVITY FEATURES The possible applications of a similar system range from the automatic analysis of spot motions to the evolution of flares, filaments and prominences via a set of dedicated software procedures to control the acquisition process. Moreover, once individuated the relevant parameters to be derived from a series of images, the post-processing can be done in batch mode without the intervention of the operator. With regard to that an automatic procedure was recently developed at the Trieste Observatory, which, given a white light full disk solar image as input, is capable to identify the sunspots and the groups, providing as output the location and area of groups and the Wolf number in an absolutely objective way. The future development of this program (which is actually under test) will be the automatic classification of groups. Such software techniques can be easily applied to mark a tracer on the photosphere/chromosphere and follow its motion/evolution during the transit on the disk in a uniform series of observations.

REFERENCES Messerotti, M.: 1990, OAT Internal Report (in prep.).

ACKNOWLEDGEMENTS Prof. A. Righini (Univ. of Florence), Prof. L. Paterno' (Univ. of Catania), Drs. V. Ruždjak and B. Vršnak (Univ. of Zagreb) are gratefully acknowledged for many fruitful discussions on this topic.

CURRENTS AND ENERGY BUILD-UP IN A FLARING CURLED FIELD CONFIGURATION

A. Hofmann[1] and B. Kálmán[2]

[1] Zentralinstitut für Astrophysik, Sonnenobservatorium Einsteinturm, Telegrafenberg, DDR-1560 Potsdam, G.D.R.
[2] Heliophysical Observatory of the Hungarian Academy of Sciences, H-4010 Debrecen, Hungary

One aim of observation of flaring activity complexes is to determine the field configurations in which flares occur, how these configurations form and how the energy is stored in them.

We analysed vector magnetic field observations of an active region (NOAA 4263, July-August 1983) at a location of repeated flaring. In the field configuration under study the positive (northern) polarity footpoints of the field lines were concentrated in a sunspot rotating counterclockwise with a fairly constant angular velocity of approximately 40 deg/day. Vector magnetic field measurements show that the photospheric magnetic field was strongly curled in this spot. The twist of the magnetic field due to the rotation of the spot was the basic mechanism of energy build-up. The maps of vertical current densities calculated from the vector magnetograms show an area with a strong downward current flowing antiparallel to the field. From these maps we derived the following net current densities and net currents:

Date	j_z	I_z
1983 July 30	$-27.5*10^{-2}$ Am^{-2}	$-2.3*10^{12}$ A
1983 July 31	$-30.5*10^{-2}$ Am^{-2}	$-2.6*10^{12}$ A

The free energy stored by a current I flowing in a magnetic field is given by $E_f=0.5*L*I^2$, where L is the inductance of the magnetic field system. Using $L=1*I=9.7*H$ ($1\approx 6.5*10^7$m, $I=1.7*10^{-7}$ Hm^{-1}) we can estimate the free energies associated with the currents observed:

E_f^{bs}(July 30) $\approx 2.6*10^{27}$ Joules
E_f^{bs}(July 31) $\approx 3.3*10^{27}$ Joules

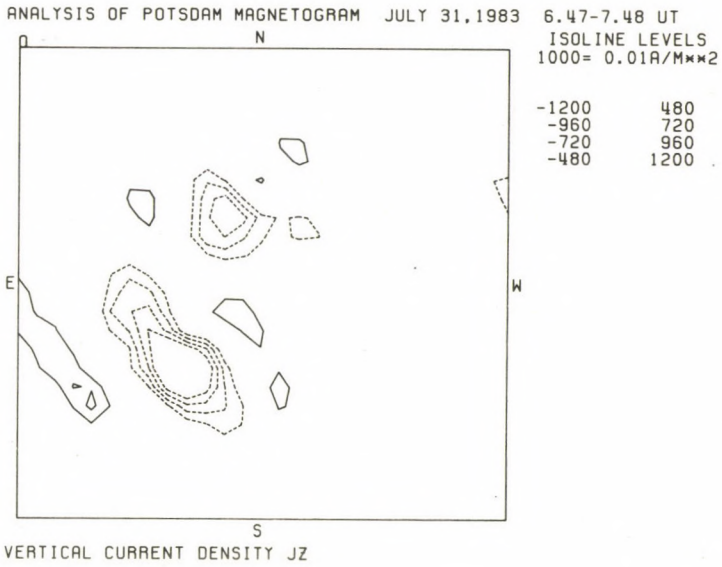

Example of a current-density map (1983 July 31). The intense current area labeled as UF is situated in a sunspot just at that place where umbral flare ribbons of repeated flares were observed

In a simple model we approximated the field configuration by a thick flux-tube twisted by rotational motion at one end.In doing so we obtain current or energy build-up rates of $5*10^{11}$ A/day or $1.2*10^{24}$ Joules/day,respectively. This means that the rotation of the sunspot had to begin about 4.5 days before the first observation to explain the currents and associated energies observed. Indeed the continuous rotation of the spot was observed from July 29 as the spot was already far enough from the limb to allow such observations.The observed current build-up of $I^{obs} \approx 3*10^{11}$ A agrees very well with $I=3.5*10^{11}$ A calculated from this model for $t^{obs}=0.7$ days.

Our observation gives a good possibility to carry out a quantitative analysis of energy build-up in the field. The observed energy build-up is effective enough to enable repeated flaring as observed.

ORIENTATIONS OF NEW SUNSPOT GROUPS

Baranyi T., Ludmány A.

Heliophysical Observatory
of the Hungarian Academy of Sciences
H-4010 Debrecen P.O.Box. 30.

ABSTRACT We have studied the tilts between the direction of the rotation and the magnetic axes of the emerging active regions in the year 1977. We have examined the distribution of orientations in comparison with possible subsurface velocity fields by seeking recognizable patterns of distribution.

The data of the Debrecen Photoheliograph Results 1977 were used, (Dezső et al.1987). We considered only those sunspot groups, for which the catalog recorded both the appearance and the formation of the bipolar character within three days except the groups belonging to the previous cycle, this means 76 sunspot groups in 1977. Let the tilt be positive if the preceding part is nearer to the equator than the following one, on either hemispheres. We characterize the tilts by appropriate weights: if the sunspot group has an angle α_i and area $A_i=U+P$ on the i-th day of its existence, then let its weight:

$$W=(\Sigma\alpha_i(A_i)^{.5})/10 \quad (i=1,2,3).$$

52 cases are positive and 24 negative in the given material. It is impossible to recognize any pattern in the distribution of the angles in the Carrington coordinate system, therefore we assumed that the angular distribution is related to a certain subsurface formation of unknown angular velocity. So far the only published internal longitudinal structural pattern is the so-called "banana-roll" system (Glatzmaier,1984, Gilman,Miller, 1986) which takes the shape of a banch of bananas, so that the material ascends (expands) in the border of two given "bananas" and it descends (contracts) in the consecutive border, resulting positive or negative Coriolis-turns respectively.

We took hypothetical internal sector structures with given wavenumbers (l). If the position of a sunspot group of positive (negative) weight coincided with a positive (negative) sector (allowing a ±2°5 overlap between two sectors), then the absolute value of its weight was added to a sum of weights (ΣW), if not, then it was dropped, so this sum of weights characterizes the coincidence of the given sunspot group tilts with the supposed sector structure. We changed the $\Delta\omega$ differences between the internal and Carrington rotation rate in the range of $-3.2<=\Delta\omega<=4.1$ (deg/day) by 0.01 (deg/day) steps. The position of the sector structure in the Carrington system was shifted through the range of two sectors (one wave) by 2° steps in order to find the best coincidence. The possible curvatures of the sectors were computed by the formula: $Z*4*\sin^2 B$, where the Z changed from 0 to 36 by steps of 2. For the wavenumber l=11 the largest values of ΣW have been chosen for all $\Delta\omega$ values and they are plotted in the Figure 1. above $\Sigma W=1207$ (this is the average of ΣW plus its stand.dev.)

The most remarkable feature of the Figure 1. is the band of high maxima around $\Delta\omega$=-0.35 deg/day, the other maxima are of much less importance and they are probably spurious peaks. All maxima of the main band are characterized by small curvatures of sectors. The same procedure was carried out also with wavenumbers l=9-15, but they gave no similar remarkable peaks.

The above findings are consistent with a practically not bended north-south roll system having the longitudinal wavenumber l=11 (there are theoretical and also observational hints for this l see. e.g. by Glatzmaier,1985, Gilman,Miller,1986). This system would rotate slower than the Carrington rate by $\Delta\omega$=0.35 (deg/day) in accordance with the results of Abuzeid and Petrovay,1990.

Further details of this study will be published elsewhere.

REFERENCES

Abuzeid B., Petrovay K.(1990) this proceedings.
Dezső L., Kovács Á., Gerlei O.(1987): Debrecen Photoheliographic Results 1977, Publ.Debrecen Obs. Heliogr.Ser.No.1.
Gilman P.A.,Miller J.(1986): Ap.J.Suppl., Vol.**61.**, pp.585-608.
Glatzmaier G.(1984): J.Comp.Phys.,Vol.**55.**, p.461.
Glatzmaier G.(1985): Ap.J., Vol.**291.**, pp.300-307.

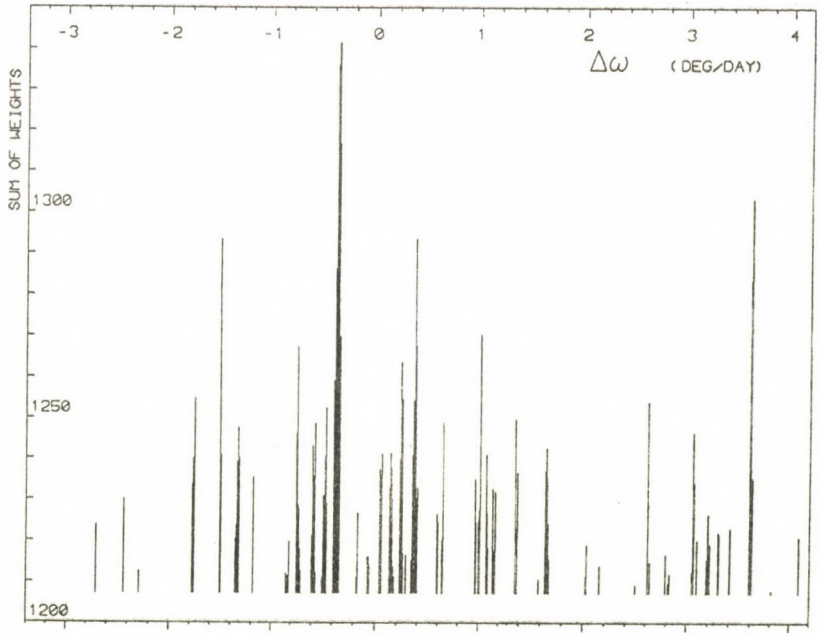

Figure 1. Sums of weights characterizing the coincidence of sunspot group orientations with the corresponding sectors of a supposed north-south roll system of longitudinal wavenumber l=11 as a function of $\Delta\omega$ (difference of the internal and Carrington rotation rate)

"A DIAGNOSTIC METHOD FOR VECTOR MAGNETIC FIELD AND PLASMA VELOCITY MEASUREMENT IN SUNSPOTS THROUGH THE ANALYSIS OF SPECTROPOLARIMETRIC PROFILES"

P. ARENA[1], E. LANDI DEGL' INNOCENTI[2], G. NOCI[2].

[1] *Osservatorio Astrofisico di Arcetri*

[2] *Dipartimento di Astronomia e Scienza dello Spazio, Università di Firenze*

Largo E. Fermi n.5 - 50125 Firenze - Italia.

Several methods for the measurements of the Stokes profiles of magnetic sensitive lines, to deduce the magnetic field vector, have been developed in recent times. The quantity of information contained in the Stokes profiles is considerable, therefore the application of the spectropolarimetric analysis can bring a decisive contribution to the knowledge of the physics of photospheric active regions.

Our diagnostic method for magnetic field vector and plasma motion measurements uses an analytical solution of the transfer polarized equations for an interpretation of the observed Stokes profiles through an inversion routine based on a non-linear least squares fit.

The analytical solution employed in this analysis is the one given by Unno and extended by Rachkowsky to account for magneto-optical effects. This solution is based on very schematic approximations and rely on the following physical assumptions: a) - the sunspot atmosphere is plane-parallel, unidimensional and static; b) - the magnetic field is constant in intensity and direction in the region of line formation; c) - the Planck function depends linearly on the optical depth τ: $B(\tau) = B_o + B_1\tau$; d) - the ratio η_o between the absorption coefficient at line center and that in the continuum is constant with τ; e) - the profile of the absorption coefficient is constant and equal for all the Zeeman components; f) - there is no atomic polarization. Magneto-optical effects (Faraday-Voigt effect) and damping effects have been introduced in the calculation.

By using this analytical solution, an inversion routine has been devised which calculates theoretical profiles, dependent on eight parameters and compares them with observed profiles; the routine iteratively changes the values of the parameters until the best fit with the observed profiles is obtained. The 8 parameters present in the analytical solution are: 1) - η_o, the absorption coefficient at line center referred to the continuum absorption coefficient; 2) - $\Delta\lambda_H$, the Zeeman splitting, connected to the intensity of the magnetic field by the relation: $\Delta\lambda_H = 4.67 \cdot 10^{-10}\lambda_o^2 gB$; where B is in gauss when $\Delta\lambda_H$ is in mÅ, λ_o, the value of wavelength at the spectral line center, is in Å and g is the Landé factor; 3) - $\Delta\lambda_D$, the Doppler width; 4) - ψ, the inclination angle between B and the line of sight; 5) - φ, the azimuth angle of B measured from the East-West direction in the counterclockwise direction; 6) - γ, the damping constant; 7) - k, containing the Planck function parameters; 8) - λ_o, the wavelength at line center.

The inversion routine has been tested with simulated profiles, obtained by a numerical solution of the transfer polarized equation; the result of the test is that the magnetic field parameters calculated with the inversion routine differ from those used to obtain the simulated profiles for some % at the most; the accuracy therefore is satisfactory. In our case the best fit procedure has been applied to the magnetic sensitive line at λ6302.502 of FeI. This spectral line is the most used in solar spectropolarimetry and has a Landé factor $g = 2.5$.

The spectropolarimetric profiles which are the object of our analysis have been recorded on a sunspot on 15 September 1980 in Sacramento Peak Observatory, through the spec-

tropolarimeter (Stokes II) of the High Altitude Observatory of National Center for Atmospheric Research, sponsored by the National Science Foundation.

The profiles were recorded with the flyback system in a raster of 25 x 25 points, the distance between two such points being some 5 arcsec, in both Right Ascension and Declination; in the data reduction, 85 wavelength points for each Stokes profiles have been considered, corresponding to an interval of 903.55 mÅ. The time employed by the instrument to record the whole raster was of some 30 min .

The maximum value of linear polarization obtained is 18 %, that for the total polarization 27 %; we have applied the inversion routine to the raster points with total polarization greater than 2%; 214 of the 625 spatial points observed are above this limit.

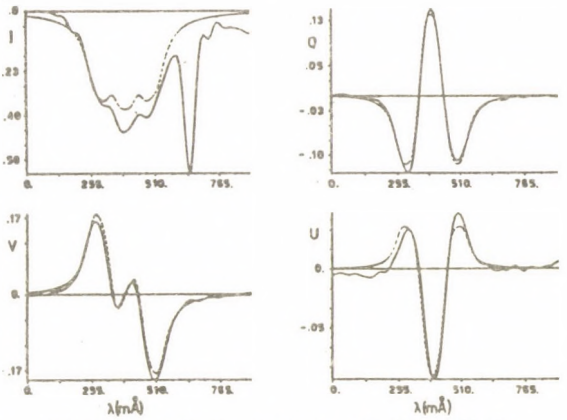

The Stokes profiles for raster point at R. A. = -328", Dec. = -277". The full curves refer to the observation, the dashed ones to the profiles obtained with the fitting procedure.

For the application of our routine to the observed data, ten sets of initial values of the eight parameters α_j, generated at random, within reasonable limits of the parameter values, have been used; the repetition of the calculation with different initial values of the parameters is necessary to avoid secondary minima of χ^2, which in some cases (irregularity and asymmetries in the observed profiles) are obtained with a single input set.

The fits between the calculated profiles and the observed ones are very good in 40% of the cases (see Figure), notwithstanding the noise and the asymmetries that the observed profiles present. The asymmetries which can be seen in some profiles might be caused by velocity gradients and/or by instrumental effects. It must be remembered that the spatial resolution is such that the data correspond to averaging over an area of some 13. million km^2.

Information on the plasma motions can be obtained from the shifts of the central wavelength of the observed line. We have determined the Doppler shifts in the region with total polarization $\geq$ 2% by calculating the differences of the values of λ_o^{fit} from the mean value over the observed region. The absolute value of the wavelengh of the spectral line cannot be used as a reference because the data have no absolute calibration in wavelength.

In conclusion we believe that the diagnostic method which we have used for the analysis of the spectropolarimetric profiles appears to be capable of giving a good measurement of the magnetic field vector and of the velocity field, although it is necessary to remember the limitations contained both in the data and in the analysis, in particular the fact that the physical assumptions which are imposed by the Unno-Rachkowsky analytical solution of the transfer equation are certainly far from describing the real situation of the solar atmosphere.

For an extensive discussion about our method and the results obtained, see "VELOCITIES AND MAGNETIC FIELDS OBSERVED IN A SUNSPOT" : 1990 *Salar Phys.*, in press, by the same authors.

SESSION 3

May 22, Tuesday (a.m.)

MHD PROCESSES

Chairman: E. R. PRIEST
Department of Mathematics, University of St.Andrews
St. Andrews

Invited review:

C. CHIUDERI
MHD of Solar Activity

and 20 (oral and poster) contributions

MHD OF SOLAR ACTIVITY

Claudio Chiuderi
Department of Astronomy and Space Science
University of Florence (Italy)

ABSTRACT

After a short overview of the subject, the general trends of the present efforts of modelisation of solar activity by means of MHD theory are discussed. Such trends are illustrated with the help of a few examples.

1. INTRODUCTION

Solar activity is a very large subject with a great variety of aspects. It includes the generation and the cyclic evolution of the solar magnetic field, the structure and evolution of sunspots, the formation, development and death of active regions, the appearance and disappearance of prominences, the occurrence of flares, bursts, mass ejections and other dynamical phenomena.

Therefore a comprehensive definition of "solar activity" must necessarily by a very general one, based on some unifying aspect of the above list of observed features. One possible definition is the following: the solar activity is the effect of the interaction of fluid motions and magnetic fields.

If we accept this as a working definition, we immediately see why magnetohydrodynamics (MHD) is the most natural theorstical scheme to interpret solar activity.

In this scheme, in fact, plasma is described as a fluid in the simplest possible way, namely as a single fluid (no distriction between electrons and ions). Moreover, the MHD regime corresponds to the maximal fluid-field interaction. In fact, if U, L, τ are the typical values of the fluid velocity, and of the spatial and temporal scales of variations of the magnetic (and electric) fields, then in the MHD regime, $U = L/\tau$.

MHD theory works fairly well, sometimes even beyond expectations. It has been applied virtually to every aspect of solar activity with reasonable success (Priest 1982). Even in those cases where explanations based on MHD theory seem to fail, we tend to interpret those failures as due to some neglected effect rather than to the inappropriateness of the MHD scheme.

The apparent capability of MHD to tackle successfully the problems posed by solar activity explains the very large amount of papers produced in recent years. Rather than trying to go through a very large (but necessarily incomplete) list of recent papers, I shall try to underline the general trends and to il-

lustrate them by means of a few selected examples. The list of references will also be a very reduced one.

Essentially, we are now in a phase where we have moved from the initial basically simple theories, with a limited degree of realism and limited possibilities of meaningful comparison with observations, toward more realistic modelisations with better capabilities of being directly checked against observations. This type of evolution is essential to match the continuous improvement in observational resolution.

Such a progress comes partially from the availability of faster and larger computers and of more performant numerical methods. It is however important to remark that, at the same time, analytic progress has also been achieved, which is very comforting on the human side.

Among the various aspects of solar activity, one of the most intensively studied subjects has been the structure and evolution of coronal loops. Coronal loops are the hottest components of the solar corona, as evidenced by X-ray observations, that show the corona as essentially composed by loops. They can be thought as the "building blocks" of the solar corona and therefore they appear as the preferential sites to test the various heating theories. They also bear some resemblance to plasma configurations encountered in fusion devices, a feature that allows to use, with proper care, results, or ideas, from laboratory plasmas.

Another central problem of MHD theory of solar activity is that of coronal heating and the related one of formation of small spatial scales. Here too we have progressed from such relatively simple-minded problems as the dilemma between wave heating or current heating to more profound and physically subtle questions like the existence or non-existence of equilibrium states or the role of non-uniformities in the process of energy dissipation.

The illustrative examples to be discussed belong to the above mentioned areas.

2. DYNAMICS OF CORONAL LOOPS

As already mentioned, coronal loops represent probably the most important single feature of solar corona. In a sense a proper understanding of the dynamics of coronal loops would clarify many basic aspects of solar activity.

The way in which the study of coronal loops has proceeded is a good representative example of the general evolution of MHD theories of solar activity. As a first step, coronal loops have been modelled as magnetic configurations whose geometry was either one-dimensional or that of a straight cylinder. In most cases the field was assumed to be force-free and gravity was, as a rule, neglected. In spite of the crudeness of the approximations adopted, this first generation of studies has been extremely useful to understand the basic physics of the loops and has produced a considerable insight in the problem of stability, a central one in plasma physics.

Loops, in fact, are relatively stable structures that seem to remain essentially in the same configuration for times much longer than the typical timescale for the most destructive instabilities. These are the so-called ideal instabilities, directly tied to the geometrical structure of the magnetic field. If $c_A = B(4\pi\rho)^{-\frac{1}{2}}$ is the Alfvén velocity, the typical timescale for the growth of ideal instabilities is the Alfvén crossing time, $\tau_A = a/c_A$, where a is a typical lenght of the structure, for example the radius of the loop. In the solar corona τ_A is of the order of seconds. Therefore coronal loops must be ideally stable. On the other hand, loops are the sites where flares start, so that they must be subject to other types of instability, capable of transforming the stored magnetic energy into the observed thermal, particle and radiative energy.

Given the geometrical similarity between loops and laboratory devices (a loop looks just as a half tokamak) and the extensive work done on the stability of fusion plasmas, it is quite natural to use analogies. Straightforward extrapolations are however dangerous. In the laboratory, in fact, stability is achieved with an extended use of the appropriate hardware, like external coils, perfectly conductive walls, etc. None of these being, of course, available in the solar atmosphere, one has to think about substitutes.

We are thus lead to modify the initial oversimplified models by adding new features, more closely related to the actual coronal situations. For example, if one considers the loops as current carrying structures, but represents the field outside the loops as a potential (current free) one, stability is considerably improved (Chiuderi and Einaudi 1981). Another, and most important, stabilizing effect comes from the fact the magnetic field lines are effectively anchored in the dense photospheric plasma and this fact strongly opposes the development of a certain number of instabilities. In this scheme the currents can be thought as being generated by the observed photospheric motions that twist and distort the original potential field. Apart from the ideal instabilities there are many others that originate from various dissipative terms. These include thermal instabilities that are essentially due to the interplay between the destabilizing effect of radiation losses and the stabilizing one of thermal conduction. Resistive (and viscous) instabilities are responsible for the transformation of magnetic energy into heat. Finally, fluid motions sensibly modify the behaviour and the stability properties of coronal plasmas.

Typically, the study of non-ideal instabilities started by considering each of them separately and adopting the simplest possible field geometry. The gross effect of the energy equation, foe example, can be estimated by projecting all the MHD equations along field lines. At the equilibrium level, this procedure gives use to the so-called scaling laws that have been widely used in the interpretation of the observations of loops. Resistive instabilities have been initially studied in the infinite cylinder configuration and only relatively recently in the line tied situation (Einaudi and Van Hoven 1981,1983; De Bruyne and Hood 1989a,b and references therein).

The above "historical" description outlines the general trend of MHD studies as applied to solar activity. In spite of the increasing degree of realism, however, there is still a basic approximation present in almost all treatments of loops. This concerns the interface of loops with the underlying photosphere. It is quite clear that what happens in the coronal part of the loop is the direct consequence of the forces that the dense lower solar atmosphere applies to the base of the loop itself. In other words, the problem is a global one. It is also a very complicated one, so the standard technique has been to deal only with the coronal part of the loop and to compress the (scarce) knowledge on the photospheric part in more or less appropriate boundary conditions at the loop's base. These conditions, therefore, should mimic the entire action of the atmosphere underlying the loop. It is quite clear that a better description of the loop-plus-photosphere system is highly desirable.

The first serious attempt toward a global description has been the ingenious "equivalent circuit" theory by Ionson (1982, 1984). By a proper averaging technique, Ionson reduced the set of MHD equations to those for a forced oscillating RLC circuit. This method has produced a number of interesting results, notably the fact that the energy dissipation rate does not depend on the particular dissipating mechanism (i.e. it is independent of R in the equivalent circuit language), a well-known feature of resonantly oscillating systems. This result has been confirmed in a number of more specific calculation that do not make use of the circuit analogy.

More recently, an interesting paper by Chen (1989) contains a number of results that show how important it is to consider the loop together with the underlying atmosphere. In Chen's paper the loop is represented by a system of currents that close at the photospheric level, or below. The coronal part of the loop is modelled as part of a circular torus. The submerged part of the torus is not precisely described. Here again, its influence is contained in a parameter, ε, that can be thought as a rough measure of the relative "size" of the loop above the photosphere and the entire current structure. Gravity is neglected, but the complete effect of "toroidal forces" is included.

The stability properties of such a system can be expressed in terms of ε by means of a simple equation for δZ, the variation of the height Z of the apex of the loop with respect to the photosphere:

$$\frac{d^2(\delta Z)}{dt^2} = \Gamma(\varepsilon)\delta Z, \qquad (1)$$

where $\Gamma(\varepsilon)$ is a complicated function of ε. It is clear from Eq.(1) that $\Gamma(\varepsilon) > 0$ corresponds to the growth of perturbations, whereas $\Gamma < 0$ represent: oscillatory motions.

From a study of $\Gamma(\varepsilon)$ it is seen that it exists a critical value of ε, ε_c, such that $\Gamma \gtrless 0$ according to $\varepsilon \lessgtr \varepsilon_c$. Thus, the new emergent flux situation, $0 \cong \varepsilon < \varepsilon_c$, corresponds to growth.

During linear expansion, that is for small δZ, the growth speed of unstable loops depends on the toroidal current I_t: structures with larger I_t grow faster. Always in the linear phase, the dynamical evolution corresponds to a decrease of the poloidal magnetic energy and to an increase of the toroidal magnetic energy and of the kinetic energy. The latter is partly transformed into heat by the effect of the viscous drag provided by the surrounding medium. In other words, the expansion is associated with an untwisting of the field and a heating of the rising loop.

This is confirmed by the numerical solution of the non-linear evolution equations, where Z is allowed to have large amplitude variations and the effect of the viscous drag on the upward moving loop is included. Although different temporal patterns are possible, continuous acceleration, saturation or oscillations, one very interesting general conclusion can be drawn: the time behaviour depends on the submerged structure.

This implies that loops almost identical in the visible part, but with different ε's (in Chen's modellisation) behave differently. One should not be too surprised therefore if loops that are morphologically indistinguishable have diverse time evolutions, these being simply the visible manifestation of differences in the (invisible) submerged part.

To conclude, we may expect that in the future loop models will become more and more realistic and that a greater attention will be paid to the problem of the electrodynamical coupling of the loops with the photosphere.

3. FORMATION OF SMALL SPATIAL SCALES

One of the outstanding problems of solar physics is that of coronal heating. In spite of the many efforts and of the great amount of ingenuity spent, the problem is still an unsolved one. This does not mean that progress has not been achieved. I believe that we have now pinpointed the basic problem and that a number of possible solutions are in sight. I will also like to remark that the very definition of the problem has undergone an evolution and that it is now recognized that coronal heating poses very fundamental questions, whose answers will be of extreme importance not only for solar physics, but for the whole MHD theory.

The basic idea for coronal heating is the following. Subphotospheric and photospheric motions drag around the footpoints of the magnetic field lines that extend upwards in the corona. As a result of such motions, stresses are induced in the otherwise potential magnetic field, so that electric currents start to flow in the corona. In a large number of circumstances, these currents are field-aligned, so that the resulting magnetic field is force-free. The currents dissipate through various possible mechanism, like resistivity or viscosity, with local production of heat.

The physical distinction between current (DC) heating and wave (AC) heating becomes immaterial since the propagating disturbances on field lines can be equally well thought of as cur-

rents or waves, the distinction being only related to the frequency. Photospheric motions taking place with velocities slower there c_A produce disturbances that are better described as currents, those faster than c_A generate various types of MHD waves.

Let's try to estimate the heating rate, E_H (ergs $cm^{-3}s^{-1}$) needed to produce a loop. The observations provide us with an estimate of the energy flux, F, necessary to make up for all the various coronal energy losses. F turns out to be of the order of 10^7 ergs $cm^{-2}s^{-1}$. Therefore

$$E_H \cong 2\,F/L$$

where L is the typical lenght of a loop, $L \cong 10^{10}$ cm. Using the observed estimate for F we get $E_H \cong 2 \times 10^{-3}$ ergs $cm^{-3}s^{-1}$. If the heating is the product of ohmic dissipation, $E_H = j^2/\sigma$, where σ is the electrical conductivity of the plasma.

At coronal temperatures of about 2×10^6 K, $\sigma \cong 6 \times 10^{16}$ s^{-1}, if classical conductivity is assumed. We can conclude that, in order to provide the necessary energy input, the current densities in the loops must be of the order of $j \cong 10^7$ esu.

In the general scheme previously outlined we must think that those current densities are produced by the continuous stressing of the original magnetic field. From a dimensional analysis of the equation

$$j = (c/4\pi)\,\nabla \times B\,,$$

we get $j \cong (c/4\pi)\,B/l$, where l is the scale of the variation of B transverse to the original field (for instance produced by a twisting motion). Using the previous estimate for j we finally arrive at

$$l\ (cm) \cong 200\,B\ (G)\,.$$

Therefore, even for the largest admissible B's, we conclude that $l << L \cong 10^{10}$ cm.

The above simple argument shows that the problem of coronal heating is closely tied with that of the formation of small transverse scales. At this stage we must ask ourselves how such small scales are formed and we must distinguish between slow and fast photospheric motions.

For the first type of motions we are faced with the following problems. How does the field respond to the slow, random, large scale motions of the photospheric footpoints? Can the field relax to an equilibrium state?

It is clear that if the answer to the second question is negative the application of the very concept of "equilibrium" to the solar corona would be highly doubtful.

These problems have been thouroughly investigated by Parker. The "loop" model he employs consists simply of an initially uniform field, whose lines have their endpoints anchored in two perfectly conducting, rigid plates that represent the two photospheric boundaries of the loop (Parker 1972). The endpoints are

subject to slow, random motions that cause an increased complexity in the field structures between the endplates (braiding of the field lines). According to Parker, no equilibrium state is possible unless the perturbed field has a structure which is translationally invariant along the direction of the original field. Since such a structure is unlikely to be produced as a result of random motions, Parker concludes that the plasma will never be in a state of equilibrium.

The braiding of the field lines produces discontinuous variations in the field intensity in neighbouring points, namely tangential discontinuities or, equivalently, current sheets. The corona would thus contain a very large number of regions where locally the field varies on a very small scale and these regions would be the seat of very rapid reconnection processes that would ultimately produce the necessary amount of heat (Parker 1983,1986).

The proposed scenario is certainly a very appealing one. In fact, it overcomes two of the major problems of theories of coronal heating: the steady character of the heating process and the heat transport across field lines. In Parker's theory the idea of continuous energy supply is replaced by that of the cumulative effect of many small events (micro- or nano-flares). We do not see the single event essentially for lack of temporal and/or energy resolution. The difficulty with heat transport could also be a false problem. We do not need to transport the heat: we simply produce it in a very large number of small regions. Again, the lack of spatial resolution does not allow us to see the "elementary" phenomenon.

However, the basic conclusion on which Parker's theory is based, the non-existence of equilibrium states, has been vigorously challenged in recent years by van Ballegooijen (1988). Starting from the same model used by Parker, he closely analyses the effect of random motions of the footpoints and concludes that the magnetic field can develop tangential discontinuities only if the motions of the footpoints at the endplates are themselves discontinuous. If continuous random motions are imposed at the photosphere the field remains continuous, but smaller and smaller transverse scales are generated.

Therefore, even if the two theories contrast at the mathematical level, this appears to be rather irrelevant from a physical point of view. After all, we don't need infinitely small scales, but simply very small ones. Thus, also van Ballegooijen's theory includes all be desirable features of Parker's one.

The nature of the process that causes the appearance of smaller and smaller scales has been further examined by van Ballegooijen by assuming that the velocity fields at the endplates are statistical, homogeneous, isotropic and time-independent variables. He has been able to prove that if l_v is the typical scale length of the velocity field, the scale of the magnetic field at the time t, $l_B(t)$ is given by

$$l_B(t) \sim l_v \exp(-\mu t).$$

We therefore have a cascade toward smaller scales and we will eventually reach the values needed to produce the right amount of heat.

The time evolution predicted analytically by van Ballegooijen has been brillantly confirmed by a numerical experiment by Mikic et al.(1989). By applying the prescribed velocity pattern at the footpoints of an homogeneous field they have been able to directly verify the existence of a cascade and to evaluate the rate of transformation of magnetic energy into other forms. Their paper thus gives further confidence in the validity of the model of coronal heating just described.

Turning finally to the case of fast photospheric motions, that, as already remarked generate propagating MHD waves, new indications on the possibility of creating small transverse spatial scales, come from the consideration of the non-uniformity of the solar corona.

Since a long time Alfvén waves have been considered as potentially interesting candidates for coronal heating since they are copiously produced by photospheric agitation. However, if the medium through which the waves propagate is homogeneous the energy damping rate is exceedingly small. This is easily understandable since in this case the only transverse scale available is the horizontal wavelength, so that the damped waves propagate almost horizontally.

In the non-homogeneous case, new possibilities of forming small scales arise because of the coupling between the perturbations and the variation of the background medium.

If we consider a one-dimensional model field, $\mathbf{B}_o = B_o(w)\,\mathbf{e}_z$, and we assume that the variation of the field is concentrated in a finite region so that $\mathbf{B}_o$ becomes constant when $|x|$ tends to infinity, it easy to show that the asymptotic well-behaved solutions of the fourth order resistive incompressible MHD equations separate into two pairs.

The first pair (the "ideal solutions") behave as if resistivity was absent

$$\Phi_{id} \sim \exp(-k|x|),$$

where as the second pair (the "resistive" ones) vary on a spatial scale that depends explicitly on the resistivity, η.

$$\Phi_{res} \sim \exp(-\lambda|x|), \quad \lambda \sim \eta^{-\frac{1}{2}}.$$

The asymptotically ideal solution, Φ_{id}, develop singularities at special points where

$$\omega = k\,c_A(x), \tag{2}$$

if resistivity is neglected everywhere. Therefore, in the vicinity of those points we must take into account the effect of finite plasma conductivity to avoid singularities.The resulting solution describes the so-called resonant absorption phenomenon on which an extensive literature exists. Even if the singularity disappears, in the vicinity of the "resonant layers", Eq.(2), the magnetic field develops strong gradients,i.e.small spatial scales.

The asymptotically resistive solutions, Φ_{res}, on the other hand, have no resonances, but show a rapidly oscillating behaviour, with a spatial scale of the order of $\eta^{-\frac{1}{2}}$, concentrated in the region where the field varies (Califano et al.1990). At this stage it is not yet clear what is the interplay between the two tapes of solutions, nor the effects of compressibility. The new mode reminds another process capable of forming strong localized gradients, the "phase mixing" proposed by Heyvaerts and Priest (1983) even if the polarizations are different in the two cases.

4. CONCLUSIONS

In this short review I have been trying to emphasize the evolution of the MHD models of solar activity rather than follow to a certain degree of detail the explanations for one or another aspect of this many-faced problem.

The most evident trend is the effort to produce more realistic models. This increased "realism" cannot be taken too literaly. In some cases new geometrical or physical effects have been explicitly introduced in order to make the theoratical models more adherent to physical reality. In other cases the models are still primitive in terms of their capacity of reproducing the real world, but new insight has been achieved in the understanding of basic physical processes.

The use of faster computers and the refinement of simulation techniques now allows the planning and execution of real numerical experiments, that may prove to be the substitutes of those laboratory experiments that are not feasible in astrophysics.

MHD theory has demonstrated its capability of dealing quite successfully with activity problems and we can expect a further flourishing of this field in the years to come.

REFERENCES

Califano,F.,Chiuderi,C. and Einaudi,G.: 1990, Astrophys.J., to appear.
Chen,J.: 1989, Astrophys.J. 338, 453.
Chiuderi,C. and Einaudi,G.: 1981, Solar Phys. 73, 89.
De Bruyne,P. and Hood,A.W.: 1989a, Solar Phys. 119, 87.
De Bruyne,P. and Hood,A.W.: 1989b, Solar Phys. 123, 241.
Einaudi,G. and Van Hoven,G.: 1981, Phys.Fluids, 24, 1092.
Einaudi,G. and Van Hoven,G.: 1983, Solar Phys. 88, 163.
Heyvaerts,J. and Priest,E.R.: 1983, Astron.Astrophys. 117, 220.
Ionson,J.A.: 1982, Astrophys.J. 254, 318.
Ionson,J.A.: 1984, Astrophys.J. 276, 357.
Mikic,Z.,Schnack,D.D. and Van Hoven,G.: 1989, Astrophys.J. 338, 1148.
Parker,E.N.: 1972, Astrophys.J. 174, 499.
Parker,E.N.: 1983, Astrophys.J. 264, 642.
Parker,E.N.: 1986, Geophys.Astrophys.Fluid Dynamics, 135, 243.
Priest,E.R.: 1982, *Solar Magnetohydrodynamics* (Dordrecht,Reidel).
van Ballegooijen,A.A.:1988, Geophys.Astrophys.Fluid Dynamics, 41, 181.

A NORMAL POLARITY QUIESCENT PROMINENCE MODEL

A W Hood[1] and U Anzer[2]

[1] Department of Mathematical and Computational Sciences,
St Andrews University, KY16 9SS, U.K.

[2] Max-Planck Institut für Astrophysik, D-8046 Garching bei München, FRG

Abstract

A class of simple 2-D non-isothermal models for quiescent prominences with normal polarity are presented. These extended the Kippenhahn-Schlüter and Menzel models by smoothly matching the prominence region onto an external, force-free coronal field. In addition, the field component along the prominence is an integral part of the solution and modifies the internal structure.

1. Introduction

The main aim of prominence models is to explain how cool dense material is supported against gravity for timescales greatly exceeding the free-fall, Alfvén and sound timescales. Obviously the coronal magnetic field is responsible for the support mechanism. Two classic prominence models are due to Menzel (1951) and Kippenhahn and Schlüter (1957). Menzel obtained a 2-D model but, due to the assumption of a cool isothermal atmosphere, the periodic solutions were unphysical. Kippenhahn and Schlüter suggested that the prominence is confined to an infinitely thin current sheet surrounded by a potential magnetic field. Their classic model is really an attempt to describe conditions inside the current sheet.

The present model builds on both of the above models by relaxing the isothermal assumption of Menzel (1951) and self consistently matching the current sheet region to an external force-free magnetic field to reproduce the classic cartoon model of a Kippenhahn-Schlüter prominence.

2. Basic Equations

To seek solutions to the magnetohydrostatic equation

$$\nabla p = (\nabla \times \mathbf{B}) \times \mathbf{B}/\mu - \rho g \hat{\mathbf{e}}_z, \tag{1}$$

we follow Menzel and set

$$\begin{aligned} \mathbf{B} &= (X(x),\ Y(x),\ Z(x))e^{-kz} \\ p &= P(x)e^{-2kz}, \quad T = T(x), \end{aligned} \tag{2}$$

where x is the horizontal coordinate, y an ignorable coordinate, z is the vertical height and μ the

magnetic permeability. The pressure p, temperature T, and density ρ, are linked by the gas law

$$p = \rho \mathcal{R} T / \tilde{\mu}, \tag{3}$$

where $\mathcal{R}$ is the gas constant and $\tilde{\mu}$ is the mean molecular weight. In the coronal plasma $\tilde{\mu}$ is taken as 0.5 but in the prominence plasma, which is mainly neutral hydrogen, $\tilde{\mu}$ is unity. Using (2), $\nabla \cdot \mathbf{B} = 0$ gives

$$X' = kZ \tag{4}$$

and (1) reduces to

$$2\mu P + X^2 + Y^2 + Z^2 = 2\mu P_T = \text{constant} \tag{5}$$

$$Y = \alpha X \tag{6}$$

$$XZ' = k\left\{\left(1 - \frac{1}{2kH}\right)Z^2 + \frac{1}{2kH}(2\mu P_T - X^2 - Y^2) - 2\mu P_T\right\}, \tag{7}$$

where α is a constant and the pressure scale height is defined by

$$H = \mathcal{R} T(x) / \tilde{\mu} g. \tag{8}$$

Equations (4)-(7) can be solved numerically for any given temperature profile.

Following Hood and Anzer (1990) analytic progress can be made if the prominence and corona consist of two uniform temperatures so that

$$H(x) = \begin{cases} H_{cool} & 0 < x < x_{prom} \\ H_{hot} & x > x_{prom} \end{cases} \tag{9}$$

where x_{prom} is the prominence width. A first integral can be obtained giving a phase plane for X' in terms of X as

$$(X')^2 = k^2(2\mu P_T - (1 + \alpha^2)X^2 + DX^{2-1/kH}), \tag{10}$$

where D is a negative constant of integration. In a prominence, $2 - 1/kH$ is negative and the solution curves are closed contours giving periodic solutions as found by Menzel (1951). However, if the temperature rises to coronal values before one period is completed and $2 - 1/kH$ is positive the contours are open.

3. Typical Prominence

As typical quiescent prominence values we take $H_{cool} = 180\,km$, $n_{prom} = 2 \times 10^{17} m^{-3}$, $X(0) = X_0 = 5G$, $Y(0) = 12G$. The latter two values give the angle between the field and prominence of 22.6°. The former two give $P(0) = P_0 = 0.167$ in units of the magnetic pressure $X_0^2/2\mu$. For the corona we take $H_{hot} = 6 \times 10^4\,km$ and select $k = 1/2H_{hot}$. These are all the values needed for the model but we can test the model's predictions of other coronal values by comparing with a typical corona (see Hood and Anzer, 1990). Results for this typical prominence are shown in Figure 1.

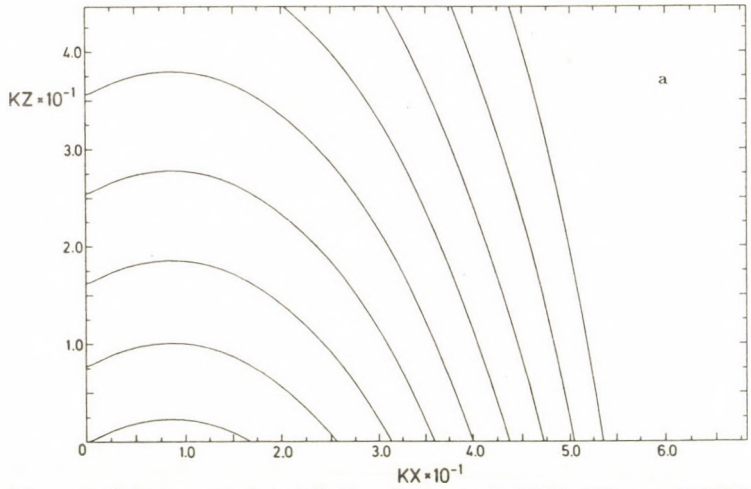

Fig 1a. Magnetic field lines for $k = 1/2\,H_{hot}$, $kx_{prom} = 0.0125$, $kH_{cool} = 0.0015$ and other parameters as defined in the text. The half- prominence lies between 0 and kx_{prom} and the edge of the arcade is at $kx_{edge} \approx 0.7$.

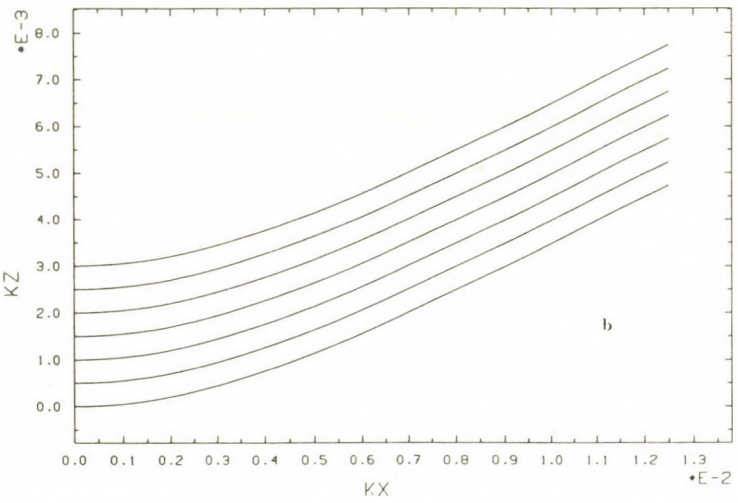

Fig 1b. The magnetic field inside the prominence. Parameters as in Fig 1a.

4. Discussion

The above model shows how it is possible to construct a self-consistent solution that matches the internal current sheet solution to a force-free coronal solution. Sensible results are obtained when typical prominence values are used. One of the main features is that the y

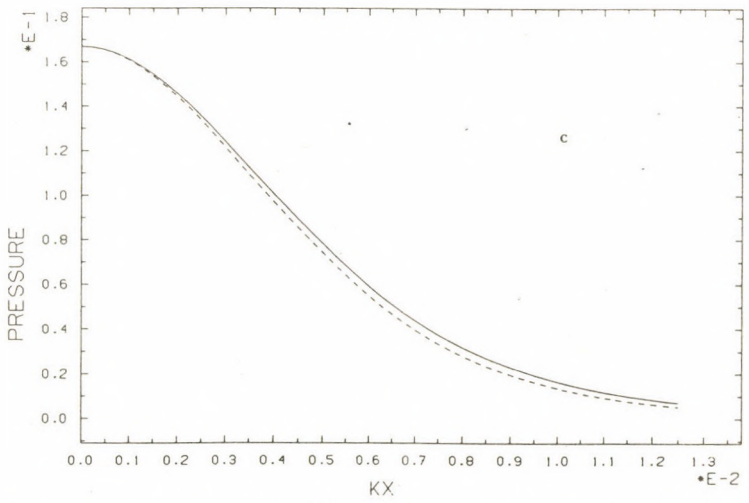

Fig 1c. The gas pressure, in limits of X_0^2/μ, inside the prominence. The solid curve gives the numerical solution and the dashed curve shows the Kippenhahn-Schlüter for comparison.

component of the magnetic field is included initially, rather than as an afterthought as in previous models, and can actually influence the internal prominence structure. For example, increasing α decreases the dip in the field by reducing the vertical field component B_z. The condition for a dip is approximately

$$\beta_0 = \frac{P_0}{1+\alpha^2} > \frac{H_{cool}}{H_{hot}}. \qquad (11)$$

Extensions to this basic model require detailed numerical calculations. These have been performed by Fiedler and Hood (1990a and 1990b). The magnetic field, as expected, dips in the dense, cool plasma region and matches smoothly onto the hot coronal plasma above, below and to the sides of the prominence.

Having obtained an equilibrium, it is essential to test the stability of the prominence to MHD disturbances. De Bruyne and Hood (1990), while finding stable configurations, find localised instabilities for many parameter values. These are almost certainly due to the fact that there is no shear in the model. How these instabilities develop is uncertain but one possibility is that these localised modes produce the fine-scale structure frequently observed in prominences.

References

De Bruyne, P and Hood, A W : 1990 in preparation.
Fiedler, R and Hood, A W : 1990a these proceedings.
Fiedler, R and Hood, A W : 1990b in preparation.
Hood, A W and Anzer, U : 1990 *Solar Phys.* **126**, 117.
Kippenhahn, R and Schlüter, A : 1957 *Z. Astrophys* **43**, 36.
Menzel, D : 1951 Proc. Conf. on Dynamics of Ionised Media, University College, London.

GENERATION OF MAGNETIC FIELD ALIGNED ELECTRIC CURRENTS

N. Seehafer and K.-H. Rädler
Zentralinstitut für Astrophysik, Rosa-Luxemburg-Str. 17a,
Potsdam, 1591, G.D.R.

Abstract. Reliable magnetic field measurements are still restricted to the photosphere and information on chromospheric and coronal magnetic fields stems mainly from the extrapolation of measured photospheric fields. The comparison of extrapolated force-free magnetic fields with chromospheric and coronal observations indicates that in active regions the electric current helicity, $H_C=\mathbf{B}\cdot\nabla\times\mathbf{B}$, is predominantly negative in the northern and positive in the southern hemisphere. This corroborates the conjecture that the generation of atmospheric electric currents is ultimately caused, via Coriolis forces, by the rotation of the Sun.
There is a simple relation between current helicity and the turbulent α-effect. In order that the α-effect can amplify a mean magnetic field it is necessary that (1) both fluctuating and mean magnetic fields possess current helicities, (2) the current helicities of fluctuating and mean magnetic fields have opposite signs and (3) the modulus of the first one exceeds that of the second one.
The magnetic fields and currents of active regions as a whole may be considered as fluctuations in the sense of a mean-field theory of the global field of the Sun. Alternatively, the fields of individual active regions may be decomposed into mean and fluctuating parts. Both possibilities are discussed with reference to the relation between current helicity and the α-effect and the sign rule for the current helicity.

1. Introduction

In the theories of the solar magnetism, which are mean-field theories, helicities are of fundamental importance. With $\mathbf{v}$, $\mathbf{B}$, $\mathbf{A}$ and $\mathbf{j}$ denoting fluid velocity, magnetic induction, magnetic vector potential and electric current density, the densities per unit volume of kinetic, magnetic and current helicity are defined by

$$H_K=\mathbf{v}\cdot\nabla\times\mathbf{v}; \quad H_M=\mathbf{A}\cdot\mathbf{B}; \quad H_C=\mathbf{B}\cdot\nabla\times\mathbf{B}. \tag{1}$$

In this paper we pay particular attention to current helicity. Helicities arise as a consequence of the rotation of the Sun. It is generally accepted that rotation is the cause for the global magnetic field of the Sun. But the solar rotation also may be the ultimate cause for the generation of dc currents in the atmosphere. Such currents are presumably the energy source for flares. They also may play a role for the non-flare heating of the atmosphere, either via some kind of micro-flaring or due to anomalous resistivity caused by kinetic plasma instabilities.

2. Predominant Signs of the Current Helicity

Since the magnetic energy density dominates over all other energy densities, the magnetic field in the solar chromosphere and corona must be nearly force-free (except for times of explosive events), i.e., electric currents, if present, must be aligned with the magnetic field and we have

$$\nabla \times B = \alpha_{ff} B, \tag{2}$$

where α_{ff} denotes a pseudo-scalar function of position. The current helicity and α_{ff} are related by the equation

$$H_C = \alpha_{ff} B^2. \tag{3}$$

Reliable magnetic field measurements are still restricted to the photosphere and information on chromospheric and coronal fields stems mainly from the extrapolation of measured photosperic fields.
Now the comparison of force-free magnetic fields calculated from photospheric magnetograms with chromospheric and coronal observations, mainly in Hα and EUV lines, indicates that α_{ff} and, consequently, the current helicity are predominantly negative in the northern and positive in the southern hemisphere (Seehafer, 1990). This corroborates the theoretical conjecture that the generation of atmospheric electric currents has to do with the rotation of the Sun.

3. Current Helicity and α-Effect

There is a simple relation between the current helicity and the turbulent α-effect (Rädler and Seehafer, 1990):
In mean-field electrodynamics it is usual to decompose all quantities into mean and fluctuating parts. Accordingly the mean value of the current helicity can be represented as the sum of the two contributions resulting from the mean and fluctuating magnetic fields, respectively,

$$\langle B \cdot \nabla \times B \rangle = \langle B \rangle \cdot \nabla \times \langle B \rangle + \langle B' \cdot \nabla \times B' \rangle. \tag{4}$$

Angular brackets always indicate averages and a prime fluctuations.
Magnetic and velocity fluctuations lead to a mean electromotive force

$$\mathcal{E} = \langle v' \times B' \rangle, \tag{5}$$

which is of crucial importance for mean-field dynamo theory. For a wide range of assumptions, $\mathcal{E}$ can be written in the form

$$\mathcal{E} = \alpha \langle B \rangle - \beta \times \langle B \rangle \tag{6}$$

with coefficients α and β which are in general tensors. The first term describes the α-effect.

Under the assumtions that

(i) $\langle v \rangle = 0$,

(ii) v' describes a homogeneous, steady and isotropic turbulence,

(iii) no higher than second order correlations of v' are taken into account

α and the current helicity of the fluctuations are connected by the relation

$$\alpha = -\eta \langle B' \cdot \nabla \times B' \rangle / \langle B \rangle^2, \qquad (7)$$

where η denotes the magnetic diffusivity. Here we have restricted ourselves to the isotropic case. Relations for the more general case in which v' corresponds to an anisotropic turbulence and α is a tensor are given in Rädler and Seehafer (1990).
Let us now consider a fluid volume surrounded by free space. Then, under the assumptions made above, it can be shown (cf. Rädler and Seehafer, 1990) that the energy stored in the mean magnetic field (which may occupy all space though currents are restricted to the fluid) can be prevented from decaying only if there is some subvolume in which

(a) both fluctuating and mean magnetic fields possess current helicities,

(b) $\langle B' \cdot \nabla \times B' \rangle$ and $\langle B \rangle \cdot \nabla \times \langle B \rangle$ have opposite signs,

(c) $|\langle B' \cdot \nabla \times B' \rangle| > |\langle B \rangle \cdot \nabla \times \langle B \rangle|$.

If we assume that the fluid is bounded by a perfectly conducting rigid wall and consider the magnetic energy in the fluid volume (istead of that in all space), then the existence of a subvolume in which the conditions (a)-(c) are satisfied proves necessary for the maintainance of this energy, too. This may be of importance for the solar atmosphere, since the photospheric boundary can to a certain degree be considered as a rigid wall for the upper atmosphere.

4. Conclusions from the Observed Hemisphere Dependence of the Current Helicity

The sign rule found for the current helicities of active regions together with the relation between current helicity and α-effect allows us to draw conclusions concerning the sign of the α coefficient.
In the traditional mean-field concept of the solar dynamo the mean field does not reflect the fields of individual active regions. Although these fields may contribute to the mean field, they are presumably mainly fluctuations. In this sense

it is $\langle \mathbf{B}' \cdot \nabla \times \mathbf{B}' \rangle$ which has been found to be negative in the northern and positive in the southern hemisphere. From Equation (7) we may then conclude that α is positive in the northern and negative in the southern hemisphere. This corresponds to the assumptions made in many traditional solar dynamo models. With these signs of α and an inward increasing angular velocity of the solar rotation the equatorward migration of strong magnetic field belts as indicated by the sunspots can be reproduced.

The interpretation of the magnetic fields of active regions as fluctuating fields is not compulsary, however. One may also argue that in active regions the field penetrating the deeper layers of the convection zone becomes visible, which is mainly the mean field. Then it would be $\langle \mathbf{B} \rangle \cdot \nabla \times \langle \mathbf{B} \rangle$ rather than $\langle \mathbf{B}' \cdot \nabla \times \mathbf{B}' \rangle$ which is negative in the northern and positive in the southern hemisphere. If, as shown for α^2-dynamos, the two helicities would again differ in sign, one arrived at signs of α opposite to those mentioned above. This reminds of some alternative dynamo models in which the α-effect is concentrated at the bottom of the convection zone, with just this distribution of the sign of α and an inward decreasing angular velocity.

Finally, also the possibility must be left open that the currents of active regions have nothing to do with the global dynamo. Then nevertheless an α-effect in the atmosphere seems possible. Taylor relaxation for example could work by means of an α-effect. In such a case the necessary helicity must be injected into the atmosphere from deeper layers.

References

Rädler, K.-H. and Seehafer, N.: 1990, in H. K. Moffatt and A. Tsinober (eds.), *Topological Fluid Mechanics*, Cambridge University Press, Cambridge, p.157.

Seehafer, N.: 1990, *Solar Phys.* 125, 219.

EVOLUTION OF FAST SAUSAGE MODE WAVE PACKETS IN CORONAL FLUX TUBES

P. M. Edwin [1], G. Mann [2], B. Roberts [1] and I. Zhelyazkov [3]

1) Department of Applied Mathematics, The University, St. Andrews KY16 9SS, U. K.

2) Zentralinstitut für Astrophysik der AdW, Observatorium für solare Radioastronomie, Tremsdorf, 15Ø1, G.D.R.

3) Faculty of Physics, Sofia University, 1126 Sofia, Bulgaria

Abstract: Flux tube waves can be generated in coronal loops due to the flare process. Wave packets of the fast sausage mode can appear for several seconds in the solar corona. The radio signature of these wave packets manifests in slowly drifting stripes of enhanced emission in dynamic frequency spectra during solar type-IV radio bursts.

The solar corona is a highly structured atmosphere dominated by magnetic forces. Closed magnetic field structures above active regions appar as curved dense loops in the coronal low beta plasma. High energetic particles produced during the flare process are trapped in such loops and act as a source of solar type-IV radio bursts. These flux tubes can support magnetohydrodynamic body waves. Since the disturbances accompanied with such body waves occupy the whole interior of the loop these waves can influence the radio radiation originated in the loop.

A lot of fine structures appear during solar type-IV radio bursts. Slowly drifting stripes of enhanced radio emission are a special type of them. Few examples are observed during the event on April 24, 1985 (Aurass et al., 1987). They show typical drift rates of -1MHz/s, instantaneous bandwidths of 1 MHz and durations between 4s up to 1Øs in dynamic radio spectra. Because of their slow drift these features distinguish from usual fiber bursts (Bernold, 1983). Adopting a coronal height scale of 1ØØ ØØØ km the drift rate and the instantaneous bandwidth indicate a velocity of 1ØØØ km/s and a spatial length of 1ØØØ km of the source of this fine structure, respectively.

Here, these emission stripes are interpreted as the radio signature of wave packets of the fast sausage mode travelling along a coronal loop.

The coronal loop is modelled by a infinitely extended magnetic cylinder with the radius a. The loop axis and the magnetic field are directed along the z-axis. In coronal flux tubes the internal magnetic field B_i has approximately the same amount as the external one B_e; but the internal density ϱ_i is greater than the external one ϱ_e. Thus, the Alfvén speed v_{Ai} within the tube is less than in its environment v_{Ae}.

In order to consider flux tube waves the linearized ideal magnetohydrodynamic equations supplemented by the boundary conditions, namely the continuity of the radial component of the velocity and the total pressure across the tube boundary, are employed. Furthermore, the gravitational force is neglected and the plasma beta is assumed to be zero. This provides the following dispersion relation for the fast sausage (symmetric) mode

$$\frac{J_1(n_i a)}{J_0(n_i a)} \frac{K_0(m_e a)}{K_1(m_e a)} = -\frac{n_i}{m_e} \qquad (1)$$

with $n_i = |k|(u^2 d-1)^{1/2}$, $m_e = |k|(1-u^2)^{1/2}$, $d = \varrho_i / \varrho_e$ and $u = \omega / k v_{Ae}$ (Wentzel, 1979; Wilson, 1980, Spruit, 1982; Edwin and Roberts, 1983). Here, ω and k denote the frequency and the wave number, respectively. J_n and K_n are the Bessel functions of order n (usual notation). The sausage mode can exist as a free one for $k > k_c = j_{0,1}(d-1)^{-1/2}/a$ ($j_{0,1}$, first zero of J_0) (Edwin and Roberts, 1983). In the wave number region $k \gtrsim k_c$ and $k \gg k_c$ this mode is strongly and weakly dispersive, respectively. In the limit of weak dispersion the dispersion relation (1) takes the approximative form

$$\omega = v_{Ai} k(1 + j_{1,1}^2 / 2(ka)^2) \qquad (2)$$

($j_{1,1}$, first zero of J_1).

A wave packet is a superposition of linear waves with different amplitudes, frequencies and wave numbers. Wave

packets are melting away due to dispersion. In the case of weak dispersion the decay time of such a wave packet becomes large. Therefore, the evolution of fast sausage mode wave packets is studied in the wave number range of weak dispersion. The evolution of the z-component of the magnetic field perturbation at the tube axis can be described by

$$B_z(z,t) = \int_{-\infty}^{+\infty} dk\, B_z(k)\, e^{i(kz-\omega(k)t)} \qquad (3)$$

Assuming an Gaussian shape of the initially generated perturbation

$$B_z(z,t=0) = B_{max}\, e^{-4z^2/L^2} \cdot e^{ik_0 z} \qquad (4)$$

with $k_0 \gg k_c$ and $k_0 L \gg 1$ the characteristic decay time is found to be

$$t_d = L^2/8v'_G \qquad (5)$$

with $v'_G = v_{Ai} j_{1,1}^2 / k^3 a^2$ as the group dispersion. Using the following parameters for typical coronal conditions: v_{Ai} = 1000 km/s, d = 4, k_0 = 0.01 km^{-1}, a = 1000 km, i.e. $k_0 a$ = 10 and L = 1000 km one obtains t_d = 8.5 s.

High energetic particles produced by the flare process are trapped in a coronal loop. Thus, a loss-cone particle distribution is established. It is unstable and can excite an enhanced whistler wave level, which is tranfromed into escaping electromagnetic waves by coalescence with Langmuir waves (Kuijpers, 1975). Since a wave packet of the fast sausage mode disturbes the magnetic field in the whole interior of the loop they can influence the whistler wave level within the wave packet owing to a variation of the local loss-cone angle. Thus, the radio radiation originated in the loop is modulated by this wave packet (Berney and Benz, 1978; Roberts et al., 1984; Mann et al., 1989).

Localized wave packets of the fast sausage mode can exist for several seconds in coronal flux tubes and can appear as slowly drifting stripes of enhanced radio emission in dynamic frequency spectra during solar type-IV radio bursts.

References

Aurass, H., Chernov, G. P., Karlicky, M., Kurths, J. and Mann, G.: 1987, Solar Phys. 112, 347

Berney, M. and Benz, A. O.: 1978, Astron. Astrophys. 65, 369

Bernold, T. E. X.: Thesis, Zürich

Edwin, P. M. and Roberts, B.: 1983, Solar Phys. 88, 239

Kuijpers, J.: 1975, Solar Phys. 44, 173

Mann, G., Baumgärtel, K., Chernov, G. P. and Karlicky, M.: 1989, Solar Phys. 120, 383

Roberts, B. Edwin, P., M. and Benz, A. O.: 1984, Astrophys. J. 279, 857

Spruit, H. C.: 1982, Solar Phys. 75, 3

Wentzel, D. G.: 1979, Astron. Astrophys. 76, 20

Wilson,P. R.: 1980, Astron. Astrophys. 87, 121

LINEAR STABILITY OF LINE-TIED CORONAL LOOPS

P. De Bruyne[1], M. Velli[2], and A. W. Hood[1]

[1] Department of Mathematical and Computational Sciences, St. Andrews University, Fife, KY16 9SS, Scotland (U. K.)

[2] Département de Recherche Spatiale, Observatoire de Paris, Section de Meudon, 92195, Meudon Principal Cedex, France

Abstract. The ideal linear MHD stability of line-tied 1-D coronal loops is investigated. It is shown that an extended Suydam criterion, obtained from a local analysis, provides a necessary condition for stability of the global kink mode.

1. Introduction

One of the objectives of magnetohydrodynamics (MHD) is to provide models for coronal structures such as loops, arcades and prominences. Since their observed lifetime is much longer than the typical dynamical time scale, they are often regarded as being in or near static mechanical and thermodynamical equilibrium. An appropriate model is then constructed by solving the corresponding magnetohydrostatic force and energy balance equations. Often, this is a complicated problem in itself (for an introduction to the subject see, for instance, Chapters 3 and 6 of Priest, 1982). It is, however, only half the story, for if small disturbances, which inevitably occur on a seething Sun, lead to a gradual departure of the equilibrium from its initial state then the model is unstable. Hence it is important to study the effect of small perturbations on an equilibrium. Mathematically, if such perturbations lower the potential energy of a conservative system (all dissipation mechanisms are assumed negligible on the ideal MHD time scale) then that system is linearly unstable and hence cannot exist *as such* in nature.

The change in potential energy due to a coronal disturbance, $\boldsymbol{\xi}$, can be written in the following physically illuminating way (Bateman, 1978) :

$$\delta W(\boldsymbol{\xi},\boldsymbol{\xi}) = \frac{1}{2}\int_{plasma} dV \left\{ \frac{1}{\mu}\left|\mathbf{B}_{\perp}^{1}\right|^{2} + \mu\left|\frac{1}{\mu}\mathbf{B}_{\parallel}^{1} - \frac{\boldsymbol{\xi}\cdot\nabla p}{B^{2}}\mathbf{B}\right|^{2} + \gamma p\left|\nabla\cdot\boldsymbol{\xi}\right|^{2} + \right.$$
$$\left. + \frac{\mathbf{j}\cdot\mathbf{B}}{B^{2}}\mathbf{B}\times\boldsymbol{\xi}\cdot\mathbf{B}^{1} - 2\boldsymbol{\xi}\cdot\nabla p\,\boldsymbol{\xi}\cdot\boldsymbol{\kappa}\right\}. \qquad (1.1)$$

The first three terms are positive and thus stabilising. They represent the effect of bending and compressing the field, causing Alfvén and magneto-acoustic waves to propagate. The last two terms are potentially destabilising. A decrease in the parallel current ($\mathbf{j}\cdot\mathbf{B}$) may lead to a *kink mode*, while the unfavourable interplay of pressure gradients (∇p) and field line curvature ($\boldsymbol{\kappa}$) can drive *interchange modes* (for a classification of instabilities see, for instance, Freidberg, 1982). Gravity is assumed to be unimportant here.

The kink mode is a global instability distorting the axis of the coronal loop into what resembles a helix. It might well be nonlinearly unstable and will then destroy the equilibrium.

Interchange modes, on the other hand, are very localised about a flux surface, producing ripples that follow the field lines. They are likely to be sensitive to hitherto neglected physical effects such as finite Larmor radius, resistivity and viscosity. Also, they might well saturate at an early stage, leaving the equilibrium relatively untouched. From this one could be drawn to the conclusion that an equilibrium need not be tested for stability to localised interchange modes.

The contrary was proved by Goedbloed and Sakanaka (1974) for an *infinite* 1-D cylinder. In that case the stability criterion for localised interchange modes is purely analytic, involving equilibrium profiles only, and is known as *Suydam's criterion* (Suydam, 1958). Goedbloed and Sakanaka (1974) showed that violation of Suydam's criterion implies instability of the global kink mode. It is the principal aim of this paper to demonstrate that this powerful result applies equally well, *mutatis mutandis*, to coronal loops.

2. Stability of Coronal Loops

Since the observed aspect ratio of coronal loops is large enough for toroidal effects to be neglected, they are usually modelled as straight circular plasma cylinders. In polar coordinates r, θ, z the equilibrium magnetic field and plasma pressure are then of the form

$$\mathbf{B} = (0, B_\theta(r), B_z(r)), \qquad p = p(r), \tag{2.1}$$

satisfying the magnetohydrostatic equation $\nabla p = \mathbf{j} \times \mathbf{B}$, where $\mu \mathbf{j} = \nabla \times \mathbf{B}$. A coronal loop has a *finite* length L, with both footpoints firmly anchored in the dense photosphere. Because coronal perturbations have to vanish there, i.e.,

$$\boldsymbol{\xi} = \mathbf{0} \qquad \text{at } z = \pm L/2, \tag{2.2}$$

this provides an effective stabilising mechanism. From a mathematical point of view, it also renders the stability analysis intrinsically two-dimensional. That is, writing $\boldsymbol{\xi}$ as

$$\boldsymbol{\xi}(\mathbf{r}, t) = \sum_m \sum_n \boldsymbol{\xi}(r) \exp\left[i\left(m\theta + \frac{2n\pi}{L} z - \omega t\right)\right], \tag{2.3}$$

where m, n, ω are the poloidal and axial mode number and the angular frequency (imaginary in case of an instability) respectively, the boundary condition (2.2) couples the different n, as opposed to the 1-D analysis of Newcomb (1960) for an infinite cylinder. Different instabilities can be characterised by their poloidal mode number : the $m = 0$ sausage mode, $m = 1$ kink mode, $m \geq 2$ flute modes, and $m \gg 1$ localised interchange modes.

To study the stability of high m-modes De Bruyne and Hood (1989a) constructed an *extended Suydam criterion*, incorporating the effect of line-tying. Like the original criterion, it is purely analytic and very easy to apply. The low m-modes need to be treated numerically. To this end Velli, Einaudi and Hood (1990a) developed a tractable procedure that involves the integration of a set of coupled ordinary differential equations. It was applied by, for instance, Velli, Einaudi and Hood (1990b) for a force-free field and De Bruyne, Velli and Hood (1990) for a non-force-free field.

Here both methods are used to investigate the stability of the equilibrium (see Anzer, 1968)

$$\begin{aligned} B_\theta = B_0 \bar{r} e^{-\bar{r}/2}, \qquad B_z = B_0 \bar{\lambda} [\sigma + (2 + 2\bar{r} - \bar{r}^2) e^{-\bar{r}}]^{1/2}, \\ \mu p = B_0^2 \frac{1 - \bar{\lambda}^2}{2} [\sigma + (2 + 2\bar{r} - \bar{r}^2) e^{-\bar{r}}], \end{aligned} \tag{2.4}$$

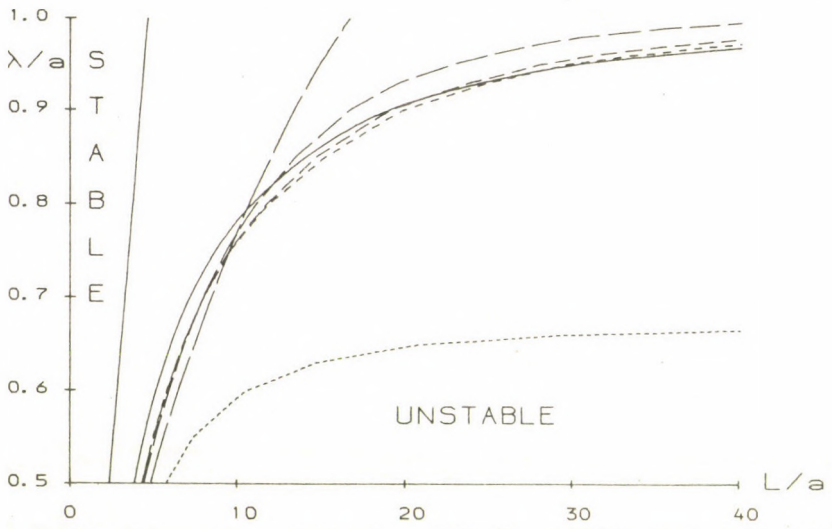

Fig. 1. Stability diagram for $\sigma = 0.15$ and $\gamma = 5/3$. The equilibrium is absolutely stable for parameter values to the left of the straight line. It is unstable for parameter values to the right of the curved lines; these are the marginal instability curves for the localised interchange mode (full curve) and the $m = 1, 2, 3, 4, 0$ modes (in order of decreasing dash length).

where $\bar{r} = r/a$ and $\bar{\lambda} = \lambda/a$. B_0 and a are the characteristic equilibrium magnetic field strength and length scale, respectively. λ governs the departure from a force-free state, with $\bar{\lambda} = 1$ implying a purely force-free loop, while σ accounts for a constant component in the axial field. Figure 1 shows the stability diagram, plotting $\bar{\lambda}$ versus the scaled loop length L/a. The instability curve for localised interchange modes (full curved line) intersects the instability curve for the $m = 1$ kink mode (broken line with longest dashes) at $\bar{\lambda} \approx 0.8$. It follows that for coronal values of $\bar{\lambda}$ — the corona is thought to be near force-free — a localised interchange instability implies a global $m = 1$ kink instability with an appreciable growth rate. This result is the counterpart of what Goedbloed and Sakanaka (1974) found for an infinite loop. Figure 2 depicts the radial eigenfunctions $\xi_r(\bar{r})$ at the midplane $z = 0$ of the force-free loop. As the poloidal mode number m increases the perturbations become more peaked about the radius predicted by the local analysis. Similar results were obtained for different equilibria.

3. Conclusions

It was shown that a local analysis, using the extended Suydam criterion of De Bruyne and Hood (1989a), yields a necessary condition for stability to a potentially fatal $m = 1$ kink mode in line-tied coronal loops. Moreover, it gives a good indication of the radius where the instability is driven. These results confer a new significance on the investigation of localised interchange modes. The method used hereto is readily extendible to 2-D equilibria including gravity (De Bruyne and Hood, 1989b).

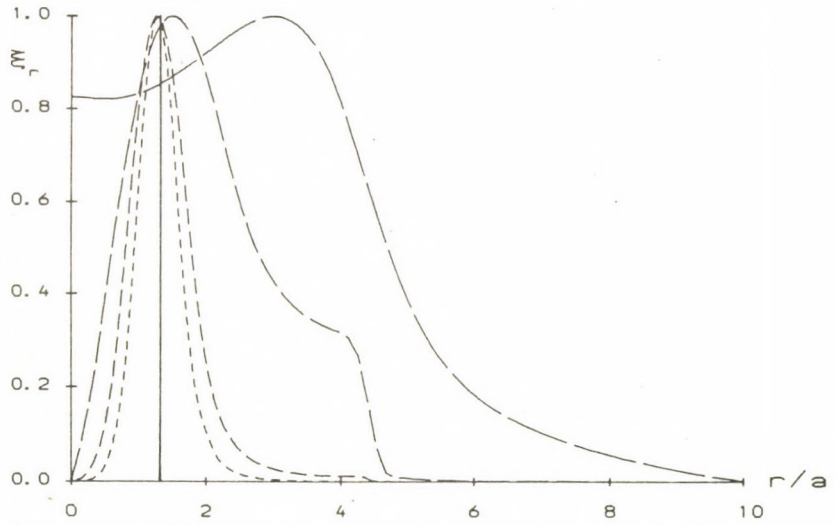

Fig. 2. Marginal radial eigenfunctions ξ_r versus $\bar{r}$ at the midplane $z = 0$ of the force-free loop. The broken lines are the eigenfunctions for the $m = 1, 2, 3, 4$ modes (in order of decreasing dash length). The solid line indicates the radius where the localised interchange mode is driven in case of a slight departure ($\bar{\lambda} = 0.99$) from the force-free state.

Acknowledgement. PDB aknowledges financial support from the University of St. Andrews.

References

Anzer, U.: 1968, *Solar Phys.* **3**, 298.
Bateman, G.: 1978, *MHD Instabilities*, MIT Press, Cambridge, Massachusetts.
De Bruyne, P. and Hood, A. W.: 1989a, *Solar Phys.* **119**, 87.
De Bruyne, P. and Hood, A. W.: 1989b, *Solar Phys.* **123**, 241.
De Bruyne, P., Velli, M., and Hood, A.W.: 1990, *Comp. Phys. Comm.* , in press.
Freidberg, J. P.: 1982, *Rev. Mod. Phys.* **54**, 801.
Goedbloed, J. P. and Sakanaka, P. H.: 1974, *Phys. Fluids* **17**, 908.
Newcomb, W. A.: 1960, *Ann. Phys.* **10**, 232.
Priest, E. R.: 1982, *Solar Magnetohydrodynamics*, D. Reidel Publ. Co., Dordrecht, Holland.
Suydam, B. R.: 1958, in *Proc. Second United Nations Internat. Conference on the Peaceful Uses of Atomic Energy*, United Nations, Geneva, **31**,157.
Velli, M., Einaudi, G., and Hood, A. W.: 1990a, *Astrophys. J.* **350**, 419.
Velli, M., Einaudi, G., and Hood, A. W.: 1990b, *Astrophys. J.* **350**, 428.

Properties of Magnetic Null Points
and
an Example of a Selfsimilar 3-D Magnetic fields

Klaus Galsgaard and Åke Nordlund
Copenhagen University Observatory
Øster Voldgade 3, 1350 Copenhagen K, Denmark

1. Introduction

Observations have shown that the horizontal distribution of the magnetic field in the solar photosphere has a nearly constant fractal dimension over more then three orders of magnitude in linear size (Title et. al. 1990, Title 1990). In the light of this, it is reasonable to investigate properties of fractal three dimensional magnetic fields, and try to assess what properties such fields possible may have in common with real, astrophysical magnetic fields. If a fractal magnetic field contains magnetic null points at all, their distribution is also fractal. Properties of magnetic null points are therefore likely to be important for an understanding of fractal three dimensional magnetic fields.

2. Single Null Points

In a small region around each point in space, the magnetic field may be represented by a linear expansion

$$\mathbf{B}_i(\mathbf{r}) = \sum_j \frac{\partial B_i}{\partial r_j} \delta r_j = \underline{\underline{\mathbf{G}}} \cdot \delta \mathbf{r} \tag{1}$$

where $\underline{\underline{\mathbf{G}}}$ is the magnetic field gradient matrix. Since $\nabla \cdot \mathbf{B} = 0$, the gradient matrix has a vanishing trace, and the sum of the eigenvalues is zero. A magnetic null point is, to first order, characterized by the eigenvalues of the gradient matrix. These are the roots of a third order polynomium, which allows only two, non-trivial, classes of null points: 1) all eigenvalues are real; 2) one real and two complex conjugate eigenvalues. For the null points with real eigenvalues, the field lines diverge out from an axis along the eigenvector belonging to the largest eigenvalue, onto a plane defined by the two eigenvectors belonging to the smallest eigenvalues. In the complex case, the field lines spiral out from an axis defined by the real eigenvector, onto a plane defined by the two complex conjugate eigenvectors.

3. Formalism

To generate reasonable complicated, "non-text-book", magnetic field, we represent $\mathbf{B}$ with a series of exponentials $e^{\mathbf{k}\cdot\mathbf{r}}$, with complex wavenumbers $\mathbf{k} = \mathbf{k}_{real} + i\mathbf{k}_{imag}$.

$$\mathbf{B}(\mathbf{r}) = \mathrm{Re}\left\{ \sum_i \sum_j f_i \mathbf{B}_j e^{g_i \mathbf{k}_j \cdot \mathbf{r}} \right\} \quad (3)$$

where j indexes a group of component with similar wave numbers $\mathbf{k}_j$, and i indexes several sets of these groups, scaled with wavenumber scaling factors g_i and amplitude scaling factors f_i. We generate the magnetic field from a scalar potential Φ and a vector potential $\mathbf{A}$

$$\mathbf{B} = \mathbf{B}_\Phi + \mathbf{B}_A = \nabla\Phi + \nabla \times \mathbf{A} \quad (2)$$

This formalism gives one constraint on each wavevector, in the scalar potential case. The generated magnetic field has to be divergence free, and this is only fulfilled if each wavevector have real and complex parts of equal length:

$$\mathbf{k}^2 = 0 \quad (4)$$

4. 3-D Example

By choosing series of terms of similar type with increasing wavenumbers and decreasing amplitudes, we produce magnetic fields that are selfsimilar over a given region of wavenumbers. Our example, a scalar potential magnetic fields, represent an unstressed, minimum energy fields, with no electric current. Still, this relative simple magnetic field, fig(1) (i=j=1,2), shows an amazing complexity on the scale of the smallest wavevector. By adding more terms (i > 2) with the the same relation between the wavevector and amplitude as the one shown, we get even more fine structure within a given length scale, fig(2). The deformation of such fields, for example by "photospheric footpoint motion", generate stressed fields with similar topologies. Such deformations are likely to lead to the formation of tangential discontinuities, or strongly localized gradients, as the stress is propagated through an initially complex topology. To understand the topological evolution of real magnetic fields, we have to learn the rules of the game, and here magnetic null points may play a crucial role.

References

Fukao, S., U. Masayuki and T. Takao.: 1975 *Rep. Ionos. Res. Jpn.* **29**, 133

Galsgaard, K. and Nordlund, Å.: In Preparation

Galsgaard, K. and Nordlund, Å.: In Preparation : Proceedings of the "Mechanisms of chromospheric and coronal Heating", Heidelberg, Germany, 5-8 June 1990

Green, J.M.: 1988 *J. Geophys. Res.* **93**, 8583

Seehafer, N.: 1986a *Astrophys. and Space Science* **122**, 247

Seehafer, N.: 1986b Proceedings of the Joint Varenna-Abstumani International School and Workshop on "Plasma Astrophysics" held in Sukhumi, USSR, 19-28 May 1986

Title, A.M. et. al.: 1990 IAU Symposium no. **138**, 49. "Solar Photosphere: Structure, Convection and Magnetic fields". Edited by J.O Stenflo

Title, A.M.: 1990 Private Communication.

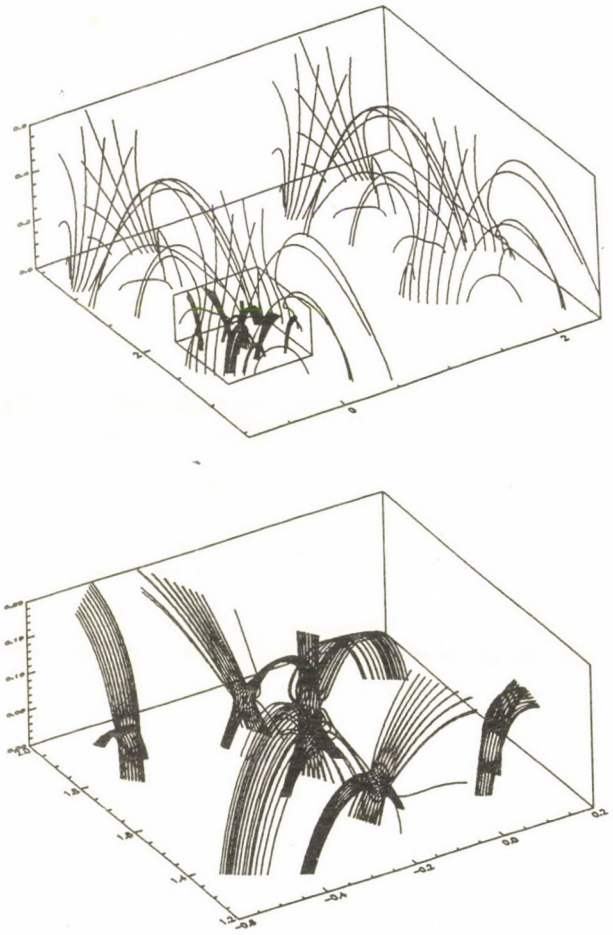

Figure 1. The potential fields shown on the plots above were generated with two components in each group of terms $\sum_j f_i \mathbf{B}_j e^{g_i \mathbf{k}_j \cdot \mathbf{r}}$, and with two groups $\sum_{i=1,2}$. The coefficients are

$$\mathbf{k}_1 = \{0, 5/2i, -5/2\}, \quad \Phi_1 = \quad 0.2e^{-real(0.05 g_i \mathbf{k}_z)}$$
$$\mathbf{k}_2 = \{4i, 3i, -5\}, \qquad \Phi_2 = -0.1e^{-real(0.05 g_i \mathbf{k}_z)}$$

and the scaling factors are $f_i = \{1, 0.1\}, g_i = \{1, 4\}$. The upper panel shows field line traces on the scale of the group of terms with i=1, with an inset box showing the scale of the second group of terms with i=2. The lower panel is a blow up of the inset from the upper panel, showing field lines on this size scale.

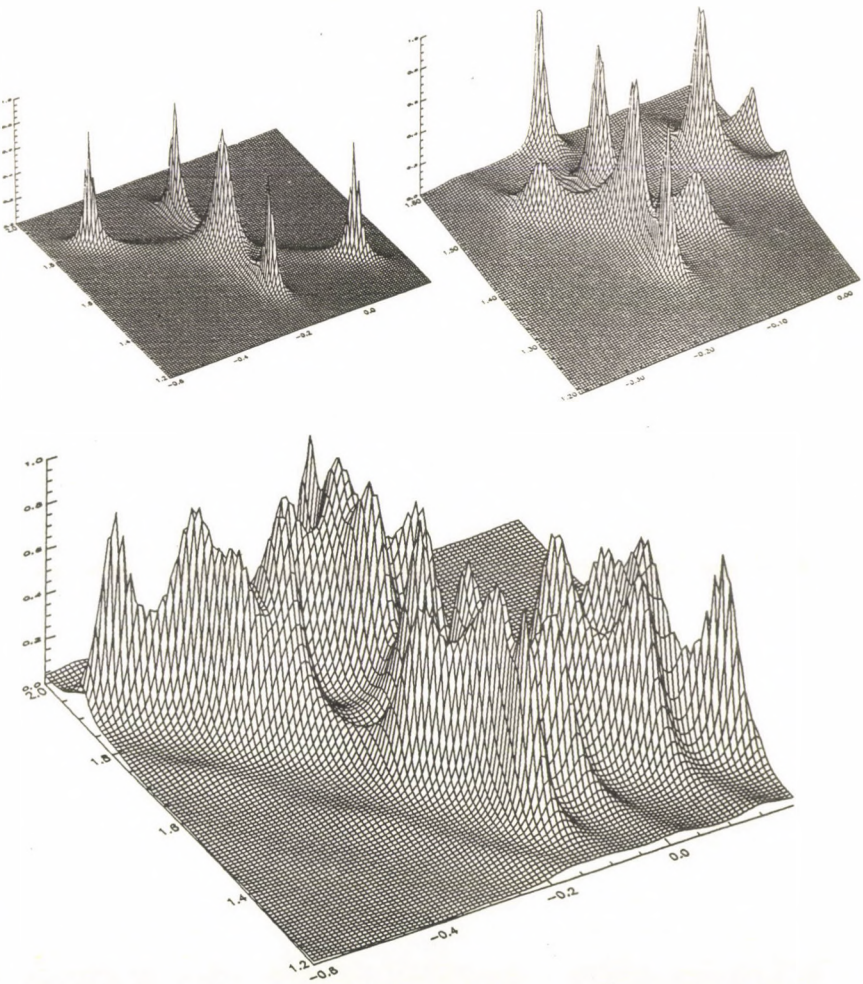

Figure 2. Surface plots provide an easy way to find positions of possible null points in a given z plane. We have chosen to plot $f(\mathbf{B}) = (B_{min}^2 + B_0^2)/(B^2 + B_0^2)$, where B_{min} is the smallest value encountered on the grid, and B_0 is the value of B a few mesh point from the minimum. The figures shows the same field as in fig(1), with z=0.05, the null point level. The upper left panel shows a surface plot of the potential field from fig(1b), with two groups, i=1,2. The upper right panel shows a blowup of the foremost null point in the upper left panel, with three groups, i=1,2,3, $f_3 = 0.01$, $g_3 = 16$. The lower panel shows the same area as the upper left, but with three groups.

FORMATION OF NETWORK BRIGHT POINTS BY GRANULE COMPRESSION

R. Muller, Th. Roudier, J. Vigneau
Pic du Midi Observatory, France
Z. Frank, R. Shine, T. Tarbell, A. Title
Lockheed Palo Alto Research Laboratory, USA
G. Simon
Air Force Geophysical Laboratory, Sunspot, USA

The Network Bright Points (NBPs) are subarcsecond features associated with magnetic flux tubes, brighter than the average photosphere (either in white light or in photospheric lines) ; they form the photospheric network.

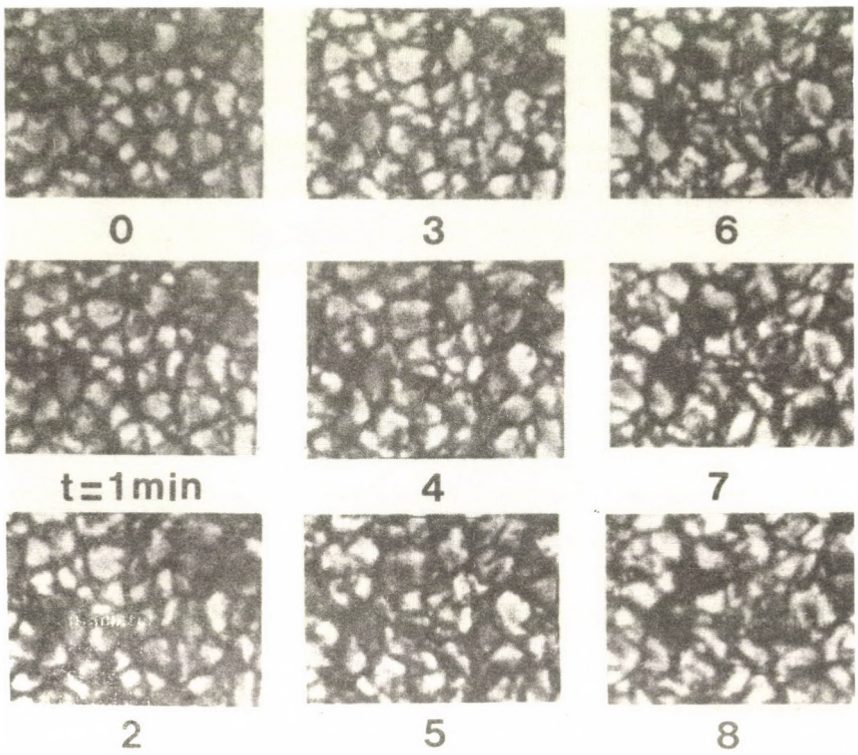

Figure 1 : Formation of a Network Bright Point in the center of the field of view (15" x 12").

Muller (1983) found that they appear in large intergranular spaces, at the junction of several granules, and have a mean lifetime of 18 minutes. A new 3-hour high resolutions movie of the quiet solar photosphere obtained at the Pic du Midi Observatory and processed with the Lockheed Palo Alto Research Laboratory movie processing (Franck et al., 1989) help us to see in more details the formation of NBPs and how they interact with the surrounding granules. A characteristic example of formation is shown in Figure 1 : an NBP appears inside a rather large space while the surrounding granules converge, giving the impression of compressing the Point. 5 minutes later, the Point is very bright and sharp although its size is very close to the diffraction limit of the instrument (a 50cm refractor at the wavelenth 5750 Å). At this moment the compressing granules form the characteristic "daisy-like" pattern described by Muller, Roudier and Hulot (1989), which is probably due to the back reaction of the magnetic field or to some strong downflow. Then, while the surrounding granules evolve, the NBP slowly fade away.

The magnetic flux associated to NBPs is believed to be stable and long-lived. Our observation suggests that the formation of an NBP corresponds to a concentration phase of a flux tube ordinarily less concentrated and not visible as a brightening ; an NBP can thus be considered as a brightening, or a flash. It will be important to know the field strength during the "ordinary" phase and the "concentration" phase : is it normaly relatively weak, not exceeding a few hundred gauss, and compressed to a kG field ; or is it normaly already as high as 1 to 2 kG as suggested by the fact that 90 % of the field is concentrated to a kG magnetic field (Stenflo, 1973) and increased to an even higher value for a short time ?

Acknowledgements

This work has been funded by the U.S. Air Force, Lockheed Independant Research and the Centre National de la Recherche Scientifique.

References

Muller, R. : 1983, Solar Phys. 85, 113.

Frank, Z., Muller, R., Roudier, Th., Vigneau, J., Shine, R., Tarbell, T., Title, A., Topka, K., and Simon, G. : 1989, Bull, Am. Astr. Soc. 21, 841.

Muller, R., Roudier, Th., and Hulot, J.C. : 1989, Solar Phys. 119, 229.

Stenflo, J.O. : 1973, Solar Phys. 32, 41.

NUMERICAL MODELS OF QUIESCENT NORMAL POLARITY PROMINENCES

R. A. S. Fiedler and A. W. Hood
Department of Mathematical and Computational Sciences, University of St. Andrews, KY16 9SS, U.K.

Abstract

Two dimensional numerical models of quiescent solar prominences with normal polarity are presented. These models provide an extension to the classical Kippenhahn-Schluter model in that the prominence is treated as having finite width and the external coronal field is matched smoothly. Using typical prominence and coronal values solutions to the Grad-Shafranov equation which provide the necessary support are found. Some extensions to the basic model are discussed.

1. Model and basic equations

We consider a two component model. The coronal plasma is assumed to be isothermal with a pressure scale height H_c. The prominence is also assumed to be isothermal but has a pressure scale height $H_p \ll H_c$. The magnetic induction **B** is expressed in term of the flux function $A(x,z)$:

$$\mathbf{B} = \left(-\frac{\partial A}{\partial z}, 0, \frac{\partial A}{\partial x}\right), \tag{1}$$

where A satisfies the well known Grad-Shafranov equation

$$\frac{\partial^2 A}{\partial x^2} + \frac{\partial^2 A}{\partial z^2} = -\mu\left(\frac{\partial p}{\partial A}\right). \tag{2}$$

The pressure is denoted by $p(A,z)$. The prominence material is assumed to lie completely within the region $-x_p < x < x_p$, $A > A_p$ where x_p and A_p are to be prescribed. At the footpoints of the coronal arcade ($z = 0$) the pressure is prescribed, whereas continuity of pressure is enforced along the field lines entering the prominence. Thus the overall pressure distribution is given by

$$p(A,z) = \begin{cases} p(A,0)\,\mathrm{e}^{-z/H_c}, & |x| > x_p \text{ or } A < A_p; \\ p(A,0)\,\mathrm{e}^{-z/H_c} - (z - z_p)/H_p, & |x| < x_p,\ A \geq A_p, \end{cases} \tag{3}$$

where $z_p(A)$ is the height at which the field line enters the prominence. Obviously there is a discontinuity in the pressure across $A = A_p$, $|x| < x_0$ thus creating a current sheet. Rather than solving (2) along this line we require the total pressure to be continuous across the current sheet *i.e.*

$$\left(\frac{(\partial A/\partial x)^2 + (\partial A/\partial z)^2}{2\mu} + p\right)_{\text{prom}} = \left(\frac{(\partial A/\partial x)^2 + (\partial A/\partial z)^2}{2\mu} + p\right)_{\text{cor}}. \tag{4}$$

As the base of the prominence must correspond to a field line (Anzer and Hood, 1990), it is useful to express (2) and (4) in terms of flux coordinates, *i.e.*, use A and v, where v is related to the distance along a field line, as independent coordinates and solve for x and z. The Grad-Shafranov equation takes the same form as equation (7) of Cally (1990). The pressure balance equation (4) is transformed similarly.

2.Results for a Particular Model

We assume all of the magnetic flux is concentrated into the region $x_0 < |x| < x_{max}$ at $z = 0$. The field line defined by $A = 0$ is set to be horizontal and the shape of the outermost field line defined by $A = A_{max}$ is also prescribed. Symmetry about $x = 0$ has been assumed in the models presented here but asymmetric arcades are easily handled. We employ finite differences and solve the resulting nonlinear equations using a Newton type line relaxation scheme.

For the model displayed we have taken the mean vertical magnetic field strength to be 5 G at the base of the corona and the gas pressure to be 0.005 Pa. All the magnetic flux at the base emerges from $H_c/2 \leq x \leq H_c$. The coronal pressure scale height is set to 6×10^4 km which corresponds to a temperature of 10^6 K whereas the prominence pressure scale height is taken as 200 km which is appropriate for an atmosphere with a temperature of about 6000 K. The prominence has a width of 3000 km and is taken to lie above 1/3 of the total magnetic flux, *i.e.* $A_p = A_{max}/3$.

In figure 1 we display the magnetic structure obtained. The short heavy lines about $x = 0$ correspond to

field lines passing through the prominence. It is easily seen that the field lines bend downward in an attempt to support the denser material of the central region.

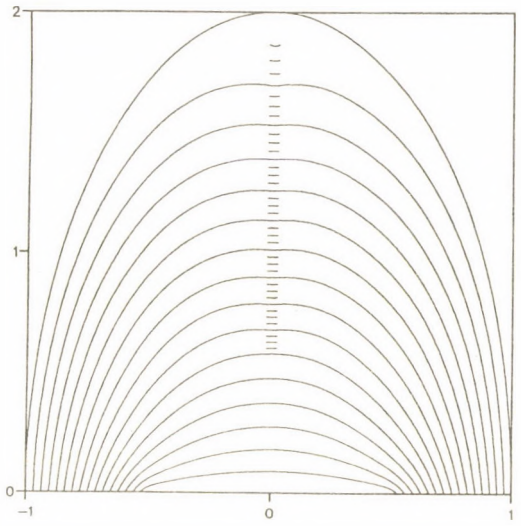

Fig 1.*Field line configuration for the model outlined above. The short heavy lines are field lines within the prominence.*

3. Extensions to the Basic Model

One extension to this model which is currently being investigated is the inclusion of a component of magnetic field in the y-direction. In fact, this extension is absolutely necessary since observations have shown that the magnetic field can make quite an acute angle with the prominence (Leroy, 1988). Most simply, this component could be specified *a priori* as a function of A and included into the Grad-Shafranov equation without any difficulty. It is more realistic, however, to specify a shearing of the footpoints of the arcade. This invoves the solving of an additional nonlinear integro-differential equation for this component (Cally, 1990) or, if we formulate the problem in terms of Euler potentials, an additional partial differential equation (Zwingmann, 1987). In the second case it has been shown that the use of flux coodinates simplifies the problem significantly (Fiedler and Hood, 1990).

We must also consider the stability of these models. The formulation of the problem in flux coordinates makes it quite feasible to apply the methods of De Bruyne and Hood (1990) to investigate the stability of the structure to ballooning modes since this just involves integrating a set of differential equations along the fieldlines. The inclusion of shear is expected to have a significant effect upon the stability of the structures.

References

Cally, P. S.: 1990,*J. Comput. Phys.* (in press).
De Bruyne, P. and Hood, A. W.: 1990,*Solar Phys.* **123**, 241.
Fiedler, R. A. S. and Hood, A. W.:1990 (in preparation).
Hood, A. W. and Anzer, U.:1990,*Solar Phys.* **126**, 117.
Leroy, J.L.:1988, in E.R. Priest (ed.), *Dynamics and Structure of Quiescent Solar Prominences,* Kluwer Academic Publishers, Dordecht, Holland, Ch 4.
Zwingmann, W.: 1987,*Solar Phys.* **111**, 309.

TESTING TOOLS OF TURBULENCE ON A CONNECTION MACHINE

H. SCHOLL
OBSERVATOIRE DE LA COTE D'AZUR
NICE, FRANCE

Abstract. The architecture of a Connection Machine, a massively parallel supercomputer, is briefly described. Measured duration rates for complex-complex FFT's and rates for the solution of the 2-D Navier-Stokes equation by a spectral method on a 16K Connection Machine in a Fortran environment are presented.

1 The architecture of a Connection Machine

A Connection Machine is a so-called Single Instruction Multiple Data machine. Thousands of simple processors each accompanied by a small memory of its own perform simultaneosly the same statement on different data. The memories of the processors can exchange information, they can "talk" to each other. The communication pattern is based on the topology of a Boolean N-cube or hypercube, a very economic way to minimize both the number of wires between the processors and the number of steps to route data among the processors. The availability of floating point accelerators working in parallel makes the Connection Machine an attractive supercomputer for "floating point calculations". The processors receive the instructions from a front-end computer where a user's code is executed. A Connection Machine can be considered as a sample of thousands of microcomputers connected by a particularly fast network. Each physical microcomputer can simulate some numbers of virtual microcomputers. This is transparent for a user. A master-computer sends the flow of instructions simultaneously to all microcomputers. The total memory of a Connection Machine is equal to the sum over all microcomputer's memories. At present, the largest Connection Machine with 65536 (64K) processors, has a total memory of 2048 Mbytes. The speed of a Connection Machine is mainly determined by the product of the number of microcomputers and of the speed of a single microcomputer. Speeds of the order of Gigflops can be obtained. The total memory of a Connection Machine is comparable to the one of other supercomputers.

2 Solution of MHD equations by a pseudo-spectral method on a Connection Machine.

We consider the MHD equations when the velocity field is driven by a prescribed solenoidal body force $\mathbf{f}(\mathbf{x},t)$, periodic in space and time:

$$\partial_t \mathbf{u} = \nabla \cdot (\mathbf{bb} - \mathbf{uu}) - \nabla p + \nu \nabla^2 \mathbf{u} + \mathbf{f} \quad (1)$$

$$\partial_t \mathbf{b} = \nabla \times (\mathbf{u} \times \mathbf{b}) + \eta \nabla^2 \mathbf{b} \quad (2)$$

$$\nabla \cdot \mathbf{u} = 0 \qquad \nabla \cdot \mathbf{b} = 0 \quad (3)$$

Usual notations are used.

In a first step, we solve for the 2-D Navier Stokes equations by a pseudo-spectral method based on Fast Fourier Transforms. Periodic boundary conditions are assumed. The general idea is to evaluate multiplications in the physical space and derivates in Fourier space. It is clear that the computing time depends mainly on the speed of the Fast Fourier Transform. A complex- complex FFT written at very low language level by the manufacturer of the Connection Machine, Thinking Machines Corporation, is available. In order to use this particularly fast complex-complex FFT, the 2-D Navier-Stokes equation is written in complex form. Then, two FFT's are necessary per time step. The fast FFT code provided by the company was implemented in a Fortran environment. The timing tests of the FFT were performed on the CM-2 of INRIA, Sophia Antipolis, France. This machine has 16K (16384) processors and a total of 512 Mbytes main memory. There are are 512 32-bit Weitek floating point accelerators. Each floating point accelerator performs 32 floating-point operations in parallel.

The following table shows averaged values for durations of FFT's. Theses values are derived by averaging over 100 forwards and inverse complex-complex FFT's.

Size	Duration	Rate
1024*1024	0.35 seconds	300 Mflops
128*128*128	0.92 seconds	240 Mflops

Solving the 2-D Navier-Stokes equation in complex form with a resolution of 1024*1024, a CPU time of 0.85 seconds was obtained for one time step on a 16K machine. As outlined above, two FFT's have to be computed during one time step which already needs 0.7 seconds according to the table above. Unfortunately, a complex-complex FFT can not be used efficiently at present for solving the 3-D Navier-Stokes equation; a fast real-real FFT is not yet available. On the other hand, the 2-D and 3-D MHD equations can be solved by a pseudo-spectral method using exclusively complex-complex FFT.

The massively parallel architecture of the Connection Machine looks promising for solving 2-D Navier-Stokes and 2-D/3-D A new version of the FFT subroutine, about 4 times faster than the old one, is expected to be provided in the near future.

PROMINENCE MODELS WITH LINE CURRENTS : STABILISATION BY FLUX CONSERVATION

U.Anzer[1] and J.L.Ballester[2]

1)Max-Planck-Institut für Astrophysik
D-8046 Garching,FRG
2)Departament de Fisica
Universitat de les Illes Balears
E-07071 Palma de Mallorca
Spain

Abstract

A model for prominence eruption based on a filament which consists of a line current has been proposed by Démoulin and Priest(1988).They assumed in their investigation that the current of the filament is constant during its eruption.Here we replace the line current by a filament of finite cross section .In this case one finds that for reasonable values of the filament radius this instability disappears when the assumption of constant current is replaced by the correct physical constraint of constant magnetic flux (Anzer and Ballester,1990)

Basic Equations

The prominence is represented by a current of strength I, located at $x = 0$,$z = h$,the prominence mass(per unit length) is denoted by λ. The equilibrium then is given by

$$F_m - \lambda g = 0$$

where F_m represent the magnetic forces.Outside the prominence one assumes a force-free magnetic field with

$$\vec{\nabla} \times \vec{B} = \alpha \vec{B}$$

and α = constant.
The field is described by a flux function A,for which we take the simple expression

$$A(x,z) = -\cos \pi x \, e^{-\gamma_1 z} - b \cos 3 \pi x \, e^{-\gamma_3 z}$$

where the normalisations $B_0 = 1$ and $L = 1$ have been introduced and b is a free parameter. In this investigation we shall concentrate on the simplest possible case which consists of a purely bipolar magnetic structure.The expression for the magnetic flux crossing the z-axis between the prominence and the photosphere is given by :

$$\phi = \int_0^{h-\varepsilon} B_x\,(0,z)\,dz$$

ε is the small (but finite !) radius of the prominence. The sign of the current determines the type of model : $I < 0$ gives N - polarity models, $I > 0$ such with I - polarity.

Stability Analysis

The equilibrium described in the previous section is unstable with respect to vertical displacements if

$$\frac{dF_m}{dh} > 0$$

is satisfied. If the flux ϕ is conserved during the displacement then I is no longer a constant. Its variation is obtained from

$$\frac{d\phi}{dh} = 0$$

Conclusions

Our analysis shows that 2-d models of prominences which are based on filaments with circular cross section in a strictly bipolar magnetic region are stable with respect to vertical displacements except for filament radius which are unrealistically small. This results holds for configurations with normal polarity as well as for those with inverse polarity and implies that such simple configurations cannot model prominence eruptions. These results clearly demonstrate the importance of including the effect of flux conservation in a dynamical situation. We found that the run-away instability described by Démoulin and Priest no lomger exists if the magnetic flux below a finite size filament is conserved. But we want to emphasize that these results only apply to the limited class of 2-d equilibria containing a cylindrical filament which are subjected to strictly 2-d perturbation. More realistic prominences could well be unstable.

References

Anzer, U and Ballester, J.L. : 1990, Astron. Astrophys. (In press)
Démoulin, P. and Priest, E.R. : 1988, Astron. Astrophys., 206, 336

MHD-STABILITY OF A QUIESCENT PROMINENCE EMBEDDED IN AN EXTERNAL VERTICAL MAGNETIC FIELD

J. Galindo Trejo
Instituto de Astronomía, UNAM, México

ABSTRACT. The plasma structure known as quiescent prominence is one of the most stable phenomena on the solar atmosphere. They are usually located above the neutral line which separates polarities of the vertical component of the bipolar magnetic field between two sunspot regions. MHD-theoretical studies consider quiescent prominence in mechanical equilibrium resulting from the balance of the Lorentz force, pressure gradients and the force of external gravity. Quiescent prominences oscillate in a stable state as a consequence of disturbances, which are excited by solar flares (Bashkirtsev and Mashnich, 1984; Wiehr *et al.*. 1984). These oscillations have a rather horizontal polarization (Kleczek and Kuperus, 1969). We have examined the linear MHD-Stability of a solar prominence described by the two-dimensional model of Osherovich (1989). This equilibrium model takes into account explicitly the influence of an external vertical magnetic field so that the prominence is on the boundary between two regions of opposite magnetic polarity. We analyse its stability against perturbations within ideal MHD by using a numerical method based on the Energy Principle of Bernstein *et al.* (1958). Due to the conservative character of ideal MHD and the two–dimensionality of the equilibrium, it is allowable to assume the most general three–dimensional complex perturbation displacement of the form:

$$\underline{\xi}(\underline{r},t) = \underline{\xi}(\underline{r})e^{i\omega t} = [\hat{\xi}_x(y,z)\underline{e}_x + \hat{\underline{\xi}}_\perp(y,z)]e^{i(kx+\omega t)} \qquad (1)$$

In our study specific cases of physical parameters observed in quiescent promi-

nences are considered. We have obtained mainly instability with the exception of some combinations of the parameter which describes the relative strength of the filament's internal magnetic field and a free parameter defining the relative width of the filament. Then the polarization of the stable oscillations and their periods are consistent with reported short-period oscillations in prominences.

We have examined briefly the stability properties of Osherovich's model in other parameter ranges which could be relevant for plasma structures in other stellar atmospheres. A striking feature is the generalized appearance of instability.

References

Bashkirtsev, V.S. and Mashnich, G.P.: 1984, *Solar Phys.*, **91**, 93.

Bernstein, I.B., Frieman, E.A., Kruskal, M.D. and Kulsrud, R.M.: 1958, *Proc. Roy. Soc. London*, **A244**, 17.

Kleczek, J. and Kuperus, M.: 1969, *Solar Phys.*, **6**, 72.

Osherovich, V.A.: 1989, *Astrophys. J.*, **336**, 1041.

Wiehr, E., Stellmacher, G. and Balthasar, H.: 1984, *Solar Phys.*, **94**, 285.

THE THERMAL STABILITY OF A PLANAR PLASMA IN THE PRESENCE OF A LINE-TIED AND SHEARED MAGNETIC FIELD

D. Hermans, A.W. Hood and L. Clifford

Dept. of Mathematical and Computational Sciences
University of St. Andrews
North Haugh, St. Andrews
KY16 9SS, Scotland

The thermal stability of a planar plasma is studied in order to understand the basic properties of this instability mechanism when non-uniformities of the plasma and line-tying of the magnetic field is taken into account. This investigation is motivated by the existence of condensations, e.g. prominences, in the solar corona. The instability is triggered by the optical thin radiation. The anisotropic heat conduction constitutes a stabilizing effect and is taken into account. Since the magnetic field lines are anchored in the dense photosphere, the effect of the 'line-tying ' has to be studied, as well as the non-uniformities in the plasma and the shear in the magnetic field.

The growth rates of the linear perturbations about a given basic state are studied both analytically and numerically. The static basic state consists of a plasma slab embedded in a unidirectional magnetic field. The plasma is isothermal, while the pressure, density and magnetic field strength can vary across the magnetic field. The equilibrium magnetic field is given by $\mathbf{B} = B_o \tanh(z)\,\mathbf{1}_x$, with $\mathbf{1}_x$ the unit vector along the magnetic field and z the coordinate across the magnetic field. Accordingly, the plasma pressure is given by $p(z) = (p_o/\beta_o)\,sech^2(z)$, with $\beta_o = 2\mu p_o/B_o^2$.

The different characteristic time scales serve as the basic parameters and are defined by

$$\tau_{\parallel} = \frac{L^2 p_o}{\kappa_{\parallel} T_o(\gamma-1)}, \qquad \tau_{\perp} = \frac{L^2 p_o}{\kappa_{\perp} T_o(\gamma-1)},$$

$$\tau_{rad} = \frac{p_o}{\mathcal{L}_o(\gamma-1)}, \qquad \tau_A = \frac{L}{v_A}.$$

$\kappa_{\parallel}$ and $\kappa_{\perp}$ are the thermal conductivity along and across the magnetic field respectively. $\mathcal{L}_o = \chi\rho_o^2 T_o^{\alpha} - H$ is the heat loss function (radiation minus heating), $v_A = B_o/\sqrt{\rho_o\mu}$ is the Alfvén velocity, and, L is the typical length scale along the magnetic field, i.e. the half length of the loop.

The linearized MHD equations are used to describe small perturbations about the given basic state. These equations are supplemented with the assumption that the temperature is fixed at the boundaries $x = \pm a$ and $z = \pm L$.

I. Analytic approach

We used τ_{rad}, L, B_o, T_o and ρ_o as units of time, length, magnetic field strength, temperature and density respectively. In first instance, we neglect the terms of order τ_A/τ_{rad} or higher and concentrate on the effect of the perpendicular thermal conductivity. For $\beta_o = 1$ and by choosing an appropiate scaling for the different perturbed quantities, we can reduce the linearized MHD equations to a single second order differential equation in θ:

$$\gamma\rho_o\sigma\theta = \frac{\tau_{rad}}{\tau_{\parallel}}\frac{\partial^2\theta}{\partial x^2} + \frac{\tau_{rad}}{\tau_{\perp}}\frac{\partial^2\theta}{\partial z^2} + (2-\alpha)\rho_o^2 T_o^{\alpha-1}. \qquad (1)$$

We look for solutions of the form $\theta(x,z) = \theta(z)\cos((m+1/2)\pi x)$ and use a WKB analysis to determine the growth rate of the thermal instability.The small parameter involved is $\varepsilon = \sqrt{\tau_{rad}/\tau_{\perp}}$. This procedure leads to analytic expressions for the growth rates in some simple models. Equation (1) can also be solved numerically. In Fig 1, the growth rates are plotted as a function of ε for the different values of n, which gives the number of nodes

in $\theta(z)$. Increasing the perpendicular thermal conductivity stabilizes the instability. The different approaches are in good agreement for $\varepsilon \ll 1$. For $\varepsilon \to 0$, which is the realistic limit for the solar corona, the growth rates for different n accumulate near the same value, so that the onset of the instability can trigger smaller spatial scales across the magnetic field.

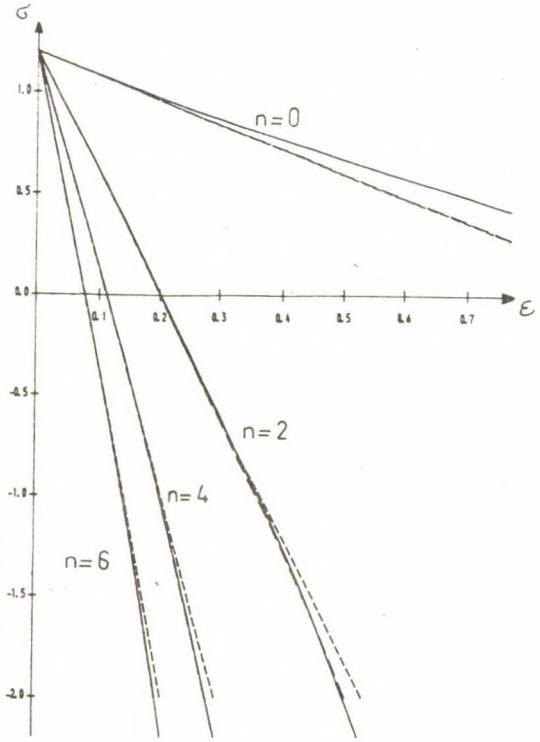

Figure 1: growth rates for different n as a function of ε. ———: numerical solution of Eq. (1), — — —: Bohr-Sommerfeld condition and - - - - - : analytic solution for $\varepsilon \to 0$ and $z \to 0$.

II. One-dimensional numerical approach

We used a finite element eigenvalue code applied on the complete set of compressible MHD linearized equations to be able to extend the study of the thermal instability for different ranges of the dimensionless parameters. For $\tau_A/\tau_{rad} \ll 1$, we found a good agreement with the analytic approximation. For larger values of ε, the exact nature of the boundary conditions at $z = \pm a$ becomes important. On the other hand, when $\varepsilon \to 0$, the eigenfunctions are localized around $z = 0$ and the boundary conditions at $z = \pm a$ have no significant effect on the instability.

Results have also been displayed for $\tau_A/\tau_{rad} = 10^{-2}$. In this case, the interaction of the thermal instabilities with the slow magneto-acoustic and Alfvénic part of the linear spectrum is studied. A parameter study of the growth rates is planned. Different pressure and magnetic field profiles will be studied and a fully 2-D numerical code is being developed to study the thermal stability of line-tied plasmas in sheared magnetic fields.

NBPs : CENTER TO LIMB VARIATION OF THE OBSERVED CONTRASTS

H. Auffret, R. Muller,
Pic du Midi Observatory, Bagneres F - 65 200

Network Bright Points (NBPs) are the smallest features (0.3") associated with kG magnetic fields in quiet regions. At the surface level, they are visible as tiny bright points embedded in the intergranular network. Due to the magnetic pressure, the inside of a flux tube is partly evacuated and we look deeper in it than at the same optical depth outside the tube. So that at the same optical depth, the temperature inside a NBP is higher than in the surrounding photosphere ; On the contrary, the temperature is lower at the same geometrical depth inside the tube than outside.

As sunspots, pores and knots appear darker than the photosphere, NBPs are seen brighter. This is due to the relative importance of convective heat inhibition from deep layers and radiative heat contribution from the walls of the tube.

In this poster, we present a complete Center to Limb Variation (CLV) of the contrast of NBPs. More than 1100 of the latter ones have been simultaneously detected on Ca II k pictures and white-light pictures. Observations were done on July 9th 1978 with the 50 cm refractor of Pic du Midi Observatory along the equator over very good seeing conditions. The performed resolution reaches 0.25". After digitizing and processing, 881 NBPs remain for analysis :

The contrast is defined as the excess of brightness according to the mean local intensity of the photosphere.

The CLV of the contrast is shown Fig. 1

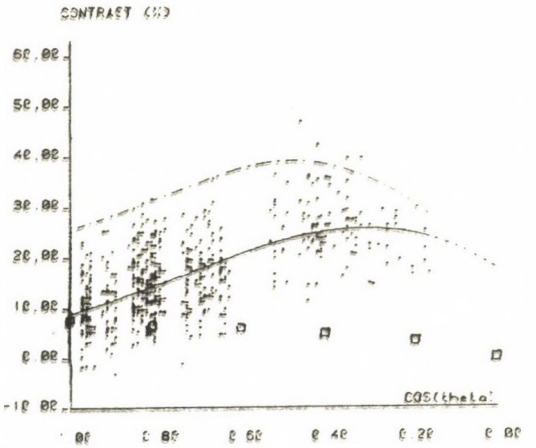

Fig. 1 : Center to Limb Variation of the contrast (solid line) and of the rms of the fluctuations of the granulation (squares)

It confirms the increase of the contrast from 8 % at the center of the solar disk to about 28 % at a position close to cos(theta)=0.3, where theta is the heliocentric angle. Towards the limb, the contrast drops. We think that previous discordant results, showing a constant increase of the contrast towards the limb, are explained by the use of a much lower resolution (> 0.8").

However, this result is to be considered with caution. The main reason for it is the disappearance of NBPs towards the limb as no more than 15 % of those at disk center remain visible near the limb. We have measured that the smallest and/or the faintest ones disappear at first so that the NBPs sample does not remain homogenous all along the equator, Fig. 2 :

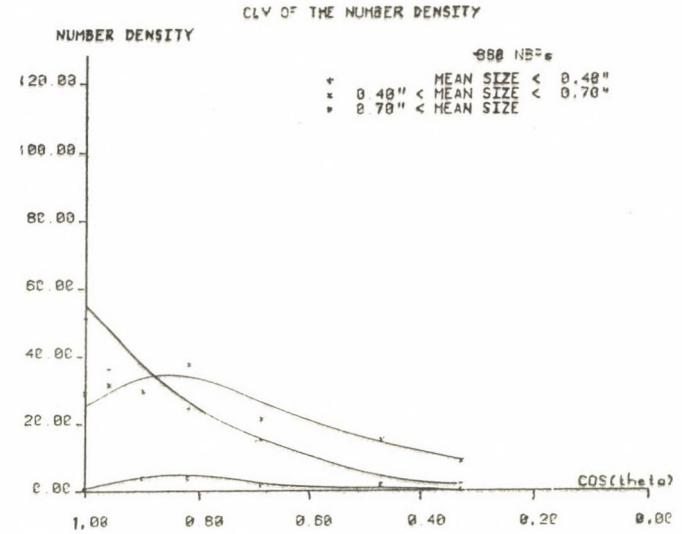

The main reason for the limb selection is probably a combined effect of foreshortenning and blurring. Geometrical effects have to be considered as well.

references :

Auffret,H. and Muller, R. : 1990, the whole of this work, to be published in Astronomy and Astrophysics.
Chapman,G.A. and Klabunde,D.P. :1982, Ap. J. 261 ,387
Muller,R. : 1985, Sol. Phys. 100, 237
Spruit,H.C. : 1981, in The Sun as a Star, NASA Sp-450, 385
Steiner,O. et al.: 1986, Astron. and Astrophys. 170,126

HEATING OF CORONAL ARCADES

C.D.C Steele and E.R. Priest, The University, St Andrews, Scotland.

The thermal structure of a coronal arcade can be found by considering it as an assembly of individual magnetic loops. This procedure is valid as the thermal conductivity parallel to the magnetic field is orders of magnitude greater than that perpendicular to the field. For the present work, the arcade considered is a cylindrical one with its axis on or below the photosphere. Thus, moving along a loop within the arcade, the cross-sectional area remains constant. Another assumption made is that the effects of gravity can be neglected (i.e. the pressure is constant along each loop).

An equation of thermal equilibrium can be solved along each loop. This equation is a balance between the conductivity along the loop, the radiative cooling (Hildner, 1974) and coronal heating which is assumed to be directly proportional to plasma density. It is assumed that the footpoints have temperatures of 2×10^4 K and that the summit temperature gradients are zero due to symmetry.

It can be shown (Hood and Anzer, 1988; Steele and Priest, 1990a) that several forms of loop are possible. **Hot Loops** exist with hot summits and cool footpoints; **cool loops** are at temperatures of less than 8×10^4 K along their whole lengths; **hot-cool loops** have cool summits and cool footpoints but hotter regions between. In addition **warm loops** exist; these are technically hot loops but they are cool along the majority of their lengths and their summits lie in the range 8×10^4 K to about 3×10^5 K. The nature of the temperature profile along the loop is determined by two non-dimensional constants, namely L^*p^* and h^*/p^* where L^*, h^* and p^* are proportional to the loop length, the pressure and the amount of coronal heating respectively.

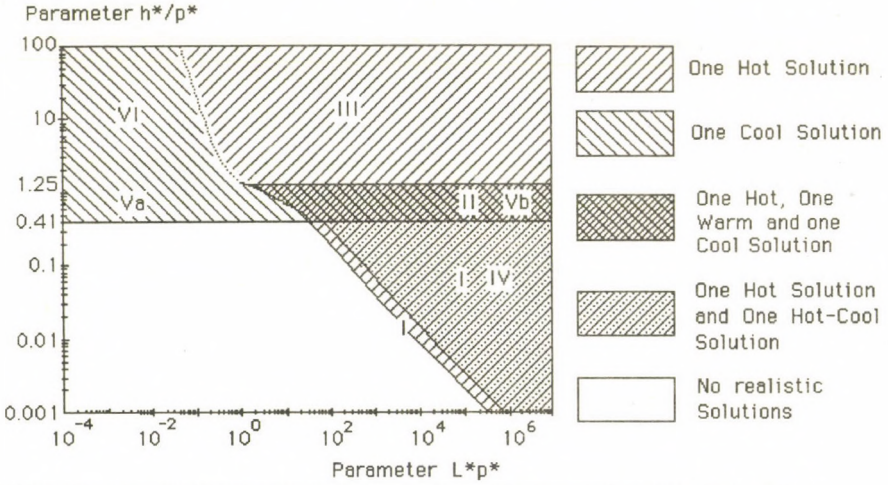

Figure 1 The areas of two-dimensional parameter space in which the various categories of solutions may exist

Figure 1 (Steele and Priest, 1990a) shows the areas of two-dimensional L^*p^*-h^*/p^* parameter space for which the various types of loops detailed above may exist. For the region in the lower left-hand corner, no equilibria at all may be

found (for non-negative footpoint temperature gradients) whereas for other areas of parameter space as many as three different equilibria may occur.

Moving from loop to loop within the arcade, as the loop length and possibly also the pressure and heating, change, the arcade can be represented by a contour in two-dimensional L^*p^*-h^*/p^* parameter space. The exact shape of this contour depends on the form of arcade modelled and the assumptions made.

An arcade is considered (Steele and Priest, 1990b) with its axis on the photosphere and a pressure enhancement close to the axis. Moving out from the axis, the loop length increases but the pressure decreases. If the ratio of axial pressure to external pressure is less than about 3.2 the parameter L^*p^* increases monotonically moving away from the axis; otherwise it decreases for an interval. If the coronal heating term is assumed to be constant (apart from its density dependence) then the parameter h^*/p^* increases on moving out from the axis. The contour may pass through several different areas of parameter space. Some arcades pass through the area where no equilibria area possible (close to the axis) while for others, moving outwards from the axis, new equilibria may appear or equilibria may cease to exist.

An alternative arcade (Steele and Priest, 1990c) is an isobaric one with its axis beneath the photosphere. If the heating is assumed to be constant, the parameter h^*/p^* is invariable for the arcade; the parameter L^*p^* increases monitonically moving out from the axis. In this case too the contour may pass through different areas of parameter space and Figure 2 shows how the possible summit temperatures vary as a function of summit height. Profile 1 has the greatest value of coronal heating. For profiles 2 and 3 for some ranges of summit height more than one summit temperature is possible.

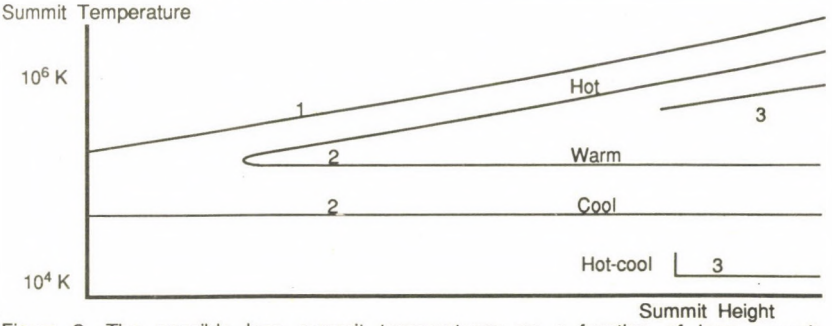

Figure 2. The possible loop summit temperatures as a function of loop summit height for the arcade of Steele and Priest (1990b)

An alternative is to assume that heating is proportional to the square of the magnetic field. Again the thermal structure may be found but unless shearing is carried out there is an upper limit to the size of the arcade

References

Hildner, E. :1974, *Solar Phys.*, **35**, 123
Hood, A.W. and Anzer, U. :1988, *Solar Phys.*, **115**, 61
Steele, C.D.C, and Priest, E.R. :1990a, *Solar Phys.*, **125**, 295
Steele, C.D.C, and Priest, E.R. :1990b, *Solar Phys.*, in press
Steele, C.D.C, and Priest, E.R. :1990c, *Solar Phys.*, submitted

SUPPORT OF A PROMINENCE BY A CONSTANT-CURRENT FORCE-FREE FIELD

C. Ridgway, T. Amari and E. R. Priest
Dept. of Mathematics, University of St. Andrews,
St. Andrews,Fife, Scotland, KY16 9SS.

Assumptions and equations

1) The prominence is represented by a current sheet lying along the z-axis between $z = z_1$ and $z = z_2$ containing mass and located in the coronal region $z > 0$.

2) The model is invariant in the x-direction and symmetrical about the vertical plane $y = 0$.

3) The coronal magnetic field, which may be written in terms of a scalar flux function $A(y,z)$ as $\mathbf{B} = [B_x(y,z), \partial A(y,z)/\partial z, -\partial A(y,z)/\partial y]$, is taken to be of constant-current, force-free type with $B_x(A) = \pm 2c\sqrt{A}$. The magnetohydrostatic equilibrium equation ($\mathbf{j} \times \mathbf{B} = \mathbf{0}$) then yields

$$\nabla^2 A + \frac{d}{dA}\left[\frac{B_x^2(A)}{2}\right] = 0 \qquad (1)$$

4) The field components B_x and B_y are continuous across the sheet but B_z reverses direction resulting in a surface current density $\mathbf{j}_\Sigma(z) = 2B(0^+,z)/\mu\, \mathbf{e}_x$.

5) For the prominence to be in equilibrium, the downward gravitational force must be balanced along the whole of the sheet by an upward Lorentz force so $B_y(0,z)\, B_z(0+,z) \geq 0$ for $z_1 \leq z \leq z_2$.

6) If this equilibrium is achieved the resulting prominence mass density per unit length is $m(z) = j_\Sigma\, B_y(0,z) / g$.

The boundary-value problem

We consider the problem (see Figure 1) in which we impose (from observational data perhaps) the normal field components along the photosphere

$$B_z(y,0) = -f_1(y) \qquad -\infty \leq y < \infty \qquad (2)$$

and across the prominence

$$B_y(0,z) = f_2(z) \qquad z_1 \leq z \leq z_2 \qquad (3)$$

while the symmetry of the system gives

$$B_z(0,z) = 0 \qquad 0 \leq z \leq z_1,\ z \geq z_2 \qquad (4)$$

Equations (1) to (4) may be reformulated as the following mixed boundary value problem for $A(y,z)$ in the first quadrant of the y-z plane.

$$\nabla^2 A + 2c^2 = 0 \qquad \text{for } y > 0,\ z > 0$$

$$\frac{\partial A}{\partial y}(0,z) = 0 \qquad 0 \leq z \leq z_1,\ z_2 \leq z < \infty$$

$$\frac{\partial A}{\partial z}(0,z) = f_2(z) \qquad z_1 \leq z \leq z_2$$

$$A(y,0) = f_1(y) \qquad 0 \leq y < \infty$$

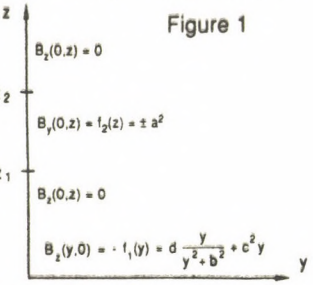

Figure 1

The solution may be obtained by transforming the problem into a mixed boundary value problem for $B = B_y - i\, B_z$ on the upper-half plane and may be written as

$$B(\eta,\bar{\eta}) = -ic^2\bar{\eta} + \frac{2}{\pi}\frac{(\eta^2+z_2^2)^{1/2}}{(\eta^2+z_1^2)^{1/2}}\left[I_1 - I_2 + \frac{\pi}{2}(\beta - i\alpha)\right]$$

where

$$I_1 = \int_0^{\infty} \frac{t\,h(t)\,(t^2+z_1^2)^{1/2}\,dt}{(t^2-\eta^2)\,(t^2+z_2^2)^{1/2}}, \qquad I_2 = \int_{z_1}^{z_2} \frac{t\,(f_2(t)+c^2t)\,(t^2-z_1^2)^{1/2}\,dt}{(t^2+\eta^2)\,(z_2^2-t^2)^{1/2}}$$

$$h(t) = f_1(t) + c^2t, \qquad \eta = y + iz$$

For a particular form of the field components (see Figure 1) examples of locally bounded normal and inverse configurations are illustrated (Figures 2a and 3a) in which the prominence sheet is in equilibrium everywhere along its vertical extent (Figures 2b and 3b). In particular note that for the first time we have been able to generate analytically a locally bounded, inverse type, equilibrium configuration with closed field lines above the prominence and an X-type neutral point below.

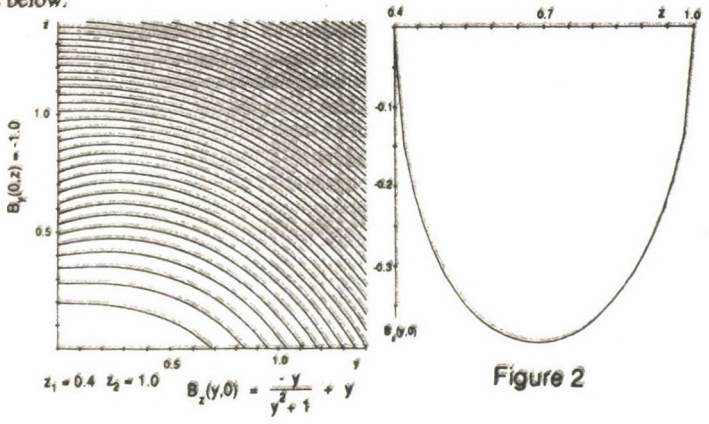

Figure 2

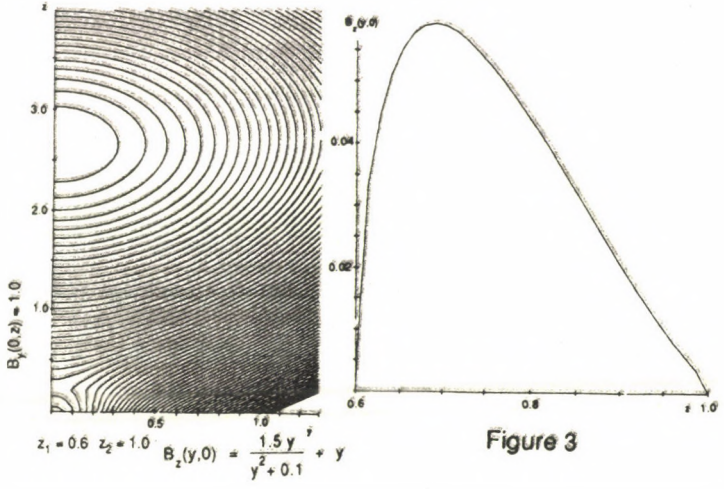

Figure 3

TWO-DIMENSIONAL MAGNETIC NEUTRAL POINTS

N R Strachan and E R Priest
Mathematics Institute, The University,
St Andrews, Fife KY16 9SS, Scotland

Neutral Points Studied

There are four main types of two-dimensional neutral point namely the X-point, Y-point, T-point and cusp-point. We proceed by writing the magnetic field in terms of the flux function, A, as

$$\mathbf{B} = \text{curl } A\mathbf{k} \tag{1}$$

in cylindrical polar co-ordinates.

The X-point is modelled most simply by

$$A = r^2(K-\cos 2\theta) \tag{2}$$

or more generally by

$$A = r^n(K-\cos 2\theta) \tag{3}$$

where $-1 \leq K \leq 1$.

A Y-point may be modelled by

$$A = r^n \cos(3\theta/2) \tag{4}$$

which has a currrent sheet at $\theta=\pi$.

A potential T-point may be constructed with a flux function

$$A = \begin{cases} -x & , \ x>0 \\ -xy & , \ x<0, \ y>0 \\ xy & , \ x<0, \ y<0 \end{cases} \tag{5}$$

This has current sheets along the y-axis and negative x-axis. It can be generalised by

$$A = \begin{cases} -r\cos\theta & , \ |\theta| < \pi/2 \\ |r^n \sin^m\theta \cos^M\theta| & , \ \pi/2<\theta<3\pi/2 \end{cases} \tag{6}$$

The cusp-point can be modelled by the flux function

$$A = \begin{cases} y^2-c^2x^4 & , \ x\geq 0 \\ y^2 & , \ x<0 \end{cases} \tag{7}$$

or more generally

$$A = \begin{cases} y^{2m}-c^{2m}x^{2n} & , \ x\geq 0 \\ y^{2m} & , \ x<0 \end{cases} \tag{8}$$

where $n>m$ and $m\geq 2$

The physical difference between Y-points , T-points and cusp points is as follows. A Y-point, has a magnetic field tends to zero from all three principal directions as one approaches it. A cusp point has a field that tends to zero more quickly from the direction arrowed and a T-point has a field that tends to zero more quickly along the two arrowed directions (see Figure 1). The above solutions have been generalised further by Strachan and Priest(1990, in preparation) to include sheets along the separatrices,

different curvature of the separatrices and more flux lobes.

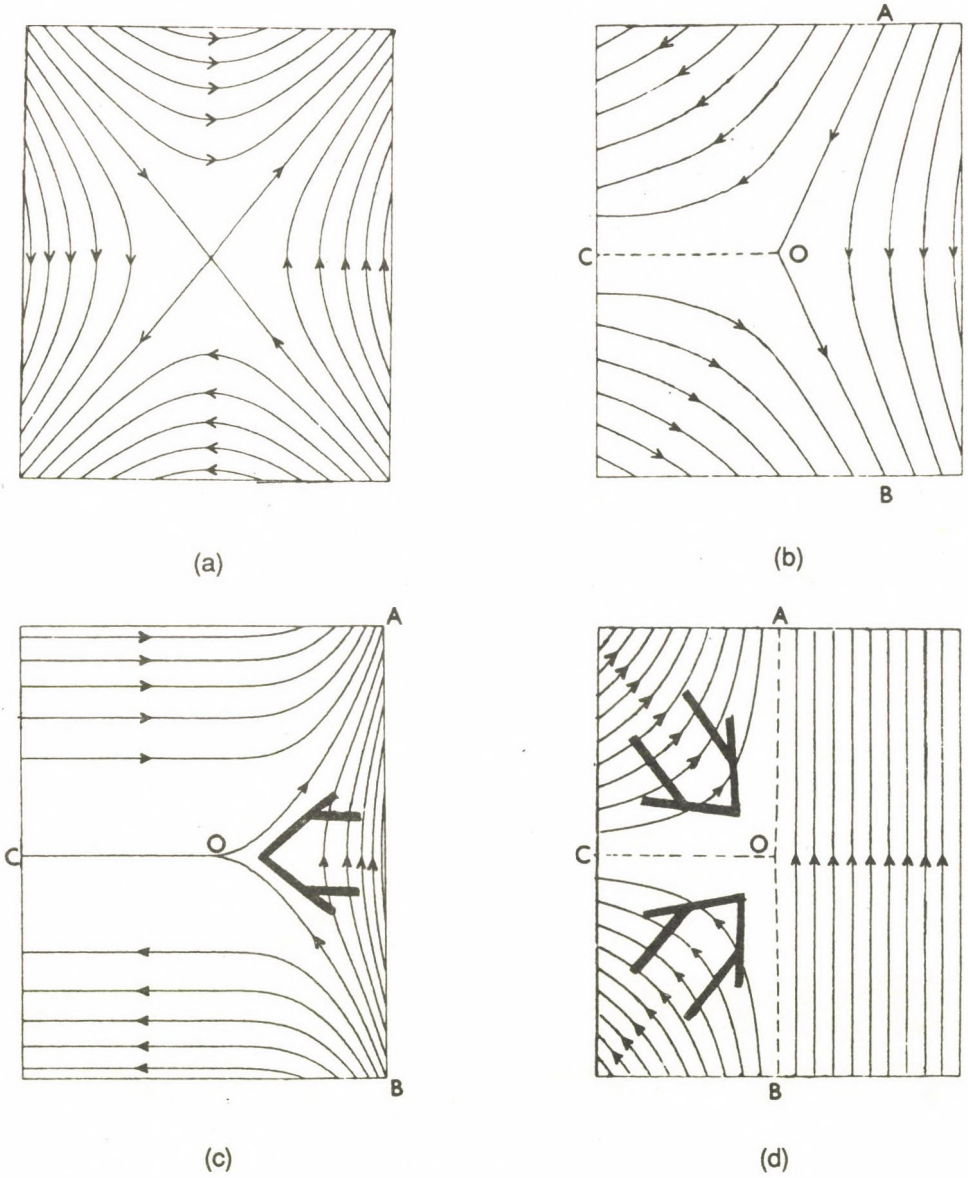

Figure 1. Magnetic field lines for the simple neutral points: (a) X-point, (b) Y-point, (c)cusp-point, (d) T-point. Heavy arrows indicate directions along which the field approaches zero quickest for the cusp- and T-points.

EFFECT OF AN EXTERNAL MAGNETIC FIELD ON PROMINENCE PROPERTIES

R. Oliver, J. L. Ballester
Departament de Fisica
Universitat de les Illes Balears
E-07071 Palma de Mallorca. Spain
and
E. R. Priest
Mathematical Sciences Department
University of St Andrews
St Andrews KY16 9SS. Scotland

Abstract

Using analytical approximations we study the effects of different external magnetic configurations on the half-width, mass and internal magnetic structure of a quiescent solar prominence, modelled as a thin vertical sheet of cool plasma. Firstly, we build up a zeroth-order model and analize the effects produced by a coronal potential field and a constant-α force-free field. This model allows us to obtain the half-width and mass of the prominence for different values of the external magnetic field strength, pressure and shear angle. Secondly, the effects of these external magnetic configurations on a two dimensional model proposed by Ballester and Priest (1987) are studied. The main features are a change of the half-width with height, an increase of the mass, a decrease of the magnetic field strength with height and a change in the shape of the magnetic field lines.

Zeroth-order model

We modify the classical one-dimensional model due to Kippenhahn and Schlüter (1957) by imposing coronal boundary conditions at a finite distance. We take as external magnetic configuration either a current-free (potential) arcade or a constant-α force-free arcade, assuming that the range of altitudes is much smaller than Λ_c and k^{-1}. The external magnetic field and pressure therefore will not vary with z, so that the edge between the prominence and the corona is vertical. Then, the matching of the two structures provides us with an analitical equation for the position of the boundary (w_0) in terms of the internal scale-height (Λ_p), the coronal pressure (p_0) and the external magnetic field strength (B_0).

Increasing B_0 both the half-width and mass of the prominence increase, while increasing p_0 only produces a decrease in the half-width. Moreover, the larger the shear of the coronal field, the smaller the half-width and supported mass of the sheet.

First-order effects

Now we perturb the one-dimensional zeroth-order model making it two dimensional, but considering as boundary conditions those

given by a two-dimensional coronal structure (potential or linear force-free). Assuming that $kz \ll 1$ and $z/\Lambda_c \ll 1$, imposing the equality of the magnetic field components and the gas pressure and linearising the equations, we obtain the shape of the new boundary.

There are two basic ways the width of prominence changes with height: in some cases the sheet broadens at the base with respect to its zeroth-order size and narrows as height increases, whereas in other cases the opposite behaviour is found. On the other hand, the internal magnetic field lines are not equally spaced as in the zeroth-order model: a solution in which the sheet narrows with height possesses field lines that bend more as height increases, and viceversa. In all the cases, the magnetic field is found to decrease with height.

The calculation of the perturbed supported mass always yields larger values than the zeroth-order ones. Furthermore, the greater the external magnetic field perturbation the larger the supported mass, as it is expected.

Conclusions

Taking analytical approximations we have studied the effects that two different external magnetic configurations (potential and linear force-free) produce on a prominence modelled as a thin vertical cool sheet of matter.

The main features appearing in the zeroth-order model are:
(1) an increase of the external field (B_0) or a decrease of the coronal pressure (p_0) produces an increase in the half-width of the prominence, and viceversa;
(2) for the linear force-free field the half-width of the prominence decreases as shear increases;
(3) an increase in the value of B_0 produces an increase of the mass of the prominence. However, in the force-free field case, the supported mass is lower than in the potential case, due to the effect of the shearing.

When first-order effects are taken into account, the main changes we obtain in comparison with the zeroth-order model are:
(1) the width of the prominence is either found to increase or to decrease with height.
(2) the prominence mass is always found to grow with the perturbation;
(3) the magnetic field strength inside the prominence always decreases with height.
(4) when the width of the prominence grows with height, the internal magnetic field lines flatten with height, and viceversa.

References

Ballester, J. L. and Priest, E. R.: 1987, Solar Phys., 109, 335
Kippenhahn, R. and Schlüter, A.: 1957, Z. Astrophys., 43, 36
Oliver, R., Ballester, J. L. and Priest, E. R.: 1990 (in preparation)

CHROMOSPHERIC STRUCTURE UNDER AN H-ALPHA FILAMENT

P. Heinzel[1], E.V. Kononovich[2], O.B. Smirnova[2]
[1]*Astronomical Institute, Ondrejov, Czechoslovakia*
[2]*Sternberg Astronomical Institute, Moscow, USSR*

We discuss the morfology and intensity structure of the chromosphere underlying the Hα filament located close to the solar limb.

Observations
Observations of the filament (16 – 19 September 1989) were carried out at wavelengths Hα, Hα $\pm$0.25A, Hα $\pm$0.5A, Hα $\pm$0.75A and Hα $\pm$1A (see the figures below). We used the OPTON coude-refractor (150 mm diameter) equipped with the OPTON tunable Hα filter (passband 0.25A). The instrument is located at High Altitude Observatory near Alma Ata (USSR) and operated by Moscow Sternberg Institute.

Structure of the Chromosphere
(i) At the line center and at Hα $\pm$0.25A, we observe typical bright rims along the centerward side of the filament body.
(ii) In the line wings, we already see the underlying chromospheric structure with absence of the dark network within a relatively bright 'channel' following the magnetic neutral line. This channel is visible even at Hα $\pm$1A.
(iii) However, from the microdensitometer scans (see plots below) we clearly see that the true intensity of this channel (rim) is quite comparable to that of bright structures *between the network elements* outside the filament. Note that some authors indicate small positive contrast of the rim *relative to a mean chromosphere*, including the network structure. The centerward boundary of the filament is presumably quite transparent in Hα wings so that this part of the channel which we see as a bright rim in the line core should not be significantly affected by the filament opacity.

Bright Rims
Bright rims, frequently observed along the centerward side of most filaments, are usually explained in terms of
a) MHD-brightening (reconnection ?) - Engvold (1988)
b) Chromospheric brightening due to an Hα irradiation by the overlying filament (back scattering) - Kostik and Orlova (1975), Zirin (1988).
However, from our observations it seems that this effect is more or less *an optical delusion* pertinent to low-resolution Hα pictures. The contrast of the rim is really higher as compared to a mean chromosphere, but it seems to be comparable to bright chromospheric areas between the network structures. Seemingly enhanced contrast is caused, in our case, by the lack of dark network elements under the filament (bright channel). Of

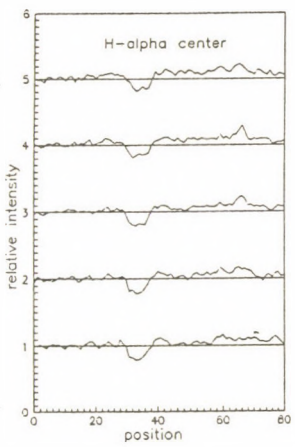

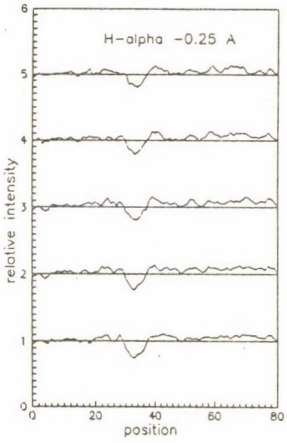

course, this contrast effect is most conspicuous near tle limb and practically absent at the disk center (which is actually observed).

Our idea is supported by the following few facts:

Using several higher-resolution Hα filtergrams, we were unable to identify the bright rims for the filamemts close to the limb; we only observed an absence of the dark network below the filament. Moreover, by examination of many CaIIK filtergrams we have found no rims visible in this line. This seems to contradict the hypothesis of MHD heating to which the K-line should be sensitive.

Conclusions

Irrespectively of the above results, it can not be excluded that some amount of back-scattered radiation is responsible for small enhancement of Hα (see numerical analysis of Kostik and Orlova, 1975). To check this quantitatively, we plan to use calibrated OPTON filtergrams, as well as spectral observations of the filaments in various chromospheric lines. Observations of the corresponding filament *on the limb* would help us to determine its opacity. Detailed non-LTE computations of the back-scattering effect (a prominence 'blanketing'), using five-level hydrogen atom and recent chromospheric models, are now in progress.

References

Engvold, O.: 1988, in *Dynamics and Structure of Quiescent Solar Prominences*, E.R. Priest (ed.), Kluwer, p.47.

Kostik, R.I. and Orlova, T.V.: 1975, Solar Phys. 45, 119.

Zirin, H.: 1986, *Astrophysics of the Sun*, Cambridge University Press.

IS DYNAMO LIKELY TO OPERATE IN THE BOUNDARY LAYER AT THE BOTTOM OF THE CONVECTION ZONE ?

G. Belvedere[1], M.R.E. Proctor[2] and G. Lanzafame[1]

[1] Istituto di Astronomia, Universitá di Catania, Italy
[2] Department of Applied Mathematics and Theoretical Physics, Cambridge, UK

ABSTRACT

Most recent helioseismological data suggest the location of dynamo action in the boundary layer between the radiative and convective zones. This is confirmed by some preliminary results of a non-linear dynamo model in a spherical shell (0.05 $R_\odot$ thick), with full time and latitude resolution.

INTRODUCTION

The impact of helioseismology on solar physics results also in a new challenge to dynamo theory, which is currently considered as the most plausible theoretical framework to understand both solar and stellar activity, even if several uncertainties do still exist.

The location of dynamo in the boundary (overshoot) layer between the convective zone and the radiative one is indirectly supported by the helioseismic results. Most recent helioseismological data (e.g. Harvey 1988) seem to agree as to the following scenario:

(i) the surface angular velocity $\omega(R_\odot,\vartheta)$ persists throughout the convection zone (1 $R_\odot$ -> 0.7 $R_\odot$): i.e. $(d\omega/dr) \approx 0$ or slightly > 0.

(ii) beneath the convection zone (0.7 $R_\odot$ -> 0.65 $R_\odot$), rigid rotation dominates with $\omega \approx 2.7\cdot10^{-6}$ rad s^{-1}, which is the surface value at latitude $\approx 37^\circ$. All this implies that the equatorial and polar rotation rates do converge to the intermediate value ω below the convection zone.

Let us see what the implications to solar dynamo are:

(i) radial shear driven dynamo, operating in the convection zone, might be unrealistic;

(ii) radial shear driven dynamo, operating in the boundary layer, is still supported by helioseismological data. The argument is the following (with reference to the northern hemisphere).

Since $\alpha < 0$ in the boundary layer (Yoshimura 1975; Glatzmayer 1985 a,b) and, interpolating the helioseismological results in the boundary layer itself, $\partial\omega/\partial r < 0$ at higher latitudes ($> 37^\circ$) and $\partial\omega/\partial r > 0$ at lower latitudes ($< 37^\circ$), we get poleward ($\alpha\cdot\partial\omega/\partial r>0$) and equatorward ($\alpha\cdot\partial\omega/\partial r<0$) migration respectively, in agreement with the observational evidence shown by different tracers of solar cycle (polar faculae and prominences on the one side, spots and faculae on the other side). Therefore, dynamo can still work and reproduce the observations if is located in the boundary layer.

THE MODEL

This has very recently been confirmed by results obtained in the context of a boundary layer (0.05 $R_\odot$ thin) nonlinear α-ω dynamo model with full time and latitude resolution.

The mean field dynamo equation for the time evolution of the magnetic field $\mathbf{B} = B(r,\vartheta)\Phi + \nabla\times(A(r,\vartheta)\Phi)$, where r, ϑ are spherical polar coordinates, Φ is the unit vector in the azimuthal direction, $B\Phi$ is the toroidal and $\mathbf{B}_p = \nabla \times A\Phi$ the poloidal part of $\mathbf{B}$, are:

$$\frac{\partial A}{\partial t} = \alpha F(r,\vartheta)\ B + \eta_T\left[\nabla^2 - \frac{1}{r^2 \sin^2\vartheta}\right] A \qquad (1)$$

$$\frac{\partial B}{\partial t} = r \sin\vartheta\ \mathbf{B}_p \cdot \nabla\left[\frac{U(r,\vartheta)}{r\sin\vartheta}\Phi\right] + \eta_T\left[\nabla^2 - \frac{1}{r^2\sin^2\vartheta}\right] B \qquad (2)$$

Here αF is the usual α-effect, with F representing its spatial structure and α its magnitude. The quantity η_T is a turbulent diffusivity.
The dynamical influence of the magnetic field enters the model through its effect on the differential rotation $U(r,\vartheta) = u_o + u$, where u_o is a prescribed velocity field and u is a perturbation driven by the mean Lorentz force and subject to viscous damping.

The simplest equation that encompasses these features is:

$$\frac{\partial u}{\partial t} = \frac{1}{\mu_o}\left[(\nabla\times\mathbf{B})\times\mathbf{B}\right]_\Phi + \rho\nu_T\left[\nabla^2 - \frac{1}{r^2\sin^2\vartheta}\right] u \qquad (3)$$

where ν_T is a turbulent viscosity.

The model equations have been solved in a spherical shell representing the boundary layer, with suitable boundary conditions. For full details about the method we address the reader to Belvedere, Pidatella and Proctor (1990) who worked out a similar model in the solar convection zone.

Assuming the differential rotation profile u_o in the boundary layer as given by interpolating the most recent helioseismological data, the results show the existence of periodic (dynamo wave-like) stable solutions with both equatorward and poleward migrating branches, as shown by the related butterfly diagram in the figure. These solutions are found for dynamo number $D = \alpha\omega_o d^3/\eta^2 \approx -1$, where d is the the thickness of the boundary layer.

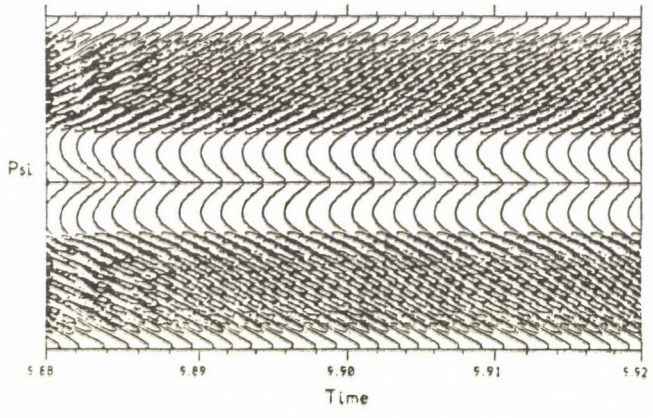

REFERENCES

Belvedere, G., Pidatella, R.M. and Proctor, M.R.E.:1990, Geophys. Astrophys. Fluid Dyn. **51**, 263.
Glatzmaier, G.A.:1985a, Geophys. Astrophys. Fluid. Dyn. **31**, 137.
Glatzmaier, G.A. :1985b, Astrophys. J. **291**, 300.
Harvey, J.W.:1988, in *Seismology of the Sun and Sun-like Stars*, E.J. Rolfe ed. ESA-SP **286**, 55.
Yoshimura, H.:1975, Astrophys. J. Suppl. **29**, 467.

DO CURRENT SHEETS NECESSARILY FORM IN 3D SHEARED MAGNETIC FORCE-FREE FIELDS ?

J.J. Aly

Service d'Astrophysique - CEN Saclay - F-91191 Gif-sur-Yvette Cedex

Summary : Consider a uniform vertical magnetic field extending between two horizontal plates and embedded in a perfectly conducting low-beta plasma, and deform that field by imposing some arbitrary slow velocity field to its footpoints on the plates. Then, at least during some finite interval of time, the field may relax quasi-statically at each instant to a smooth force-free equilibrium. In particular, no current sheet does form spontaneously. If the velocity field has some degree of topological complexity, however, the electric currents in the neighbourhood of some particular surfaces concentrate into layers of thickness decreasing to zero in time.

1. Introduction

An appealing process for heating the solar corona is the dissipation of thin current sheets (CS) which may form spontaneously when the coronal magnetic field evolves quasi-statically through a sequence of force-free states as a result of the motions imposed to its footpoints on the photosphere by the dense plasma below. It is generally well recognized that CS do appear indeed in complex topology configurations, being thus located along the "separatrix" surfaces. It has also been argued by Parker (e.g. /1/ and references therein) that CS may form in simple topology configurations too, i.e. in the absence of any separatrix. The aim of this Communication is to present some arguments which shed some new light onto Parker's statement.

2. Solution of Parker's problem for not too large times

Let us consider in the 3D domain $\{-h < z < h\}$, supposed to be filled of a perfectly conducting low-beta plasma, a uniform magnetic field $\underset{\sim}{B}_o = B_o \hat{z}$, and bring that field into an evolution by applying to its footpoints on the boundary planes some slow velocity field. If we assume this evolution to be quasi-static, the field $\underset{\sim}{B}$ passing through a sequence of force-free configurations, the Euler potentials $u(\underset{\sim}{r},t)$ and $v(\underset{\sim}{r},t)$ of $\underset{\sim}{B}$ [$\underset{\sim}{B} = B_o \nabla u \times \nabla v$] must satisfy at each time t the equations and boundary conditions /2/

$$\nabla \cdot [\nabla u \times (\nabla u \times \nabla v)] = \nabla \cdot [\nabla v \times (\nabla u \times \nabla v)] = 0 \ , \qquad (1)$$

$$(u,v)\ (x,y, \mp h\ ;\ t) = (U^{\mp}, V^{\mp})\ (x,y\ ;\ t) \ , \qquad (2)$$

where the functions $U^{\mp}$ and $V^{\mp}$ — determined by writing that their initial values (x and y, respectively) are conserved when following the motion of a footpoint — may be quite generally written in the form

$$(U^{\mp}, V^{\mp})\ (x,y\ ;\ t) = (x,y) + t\ (U_1^{\mp}, V_1^{\mp})\ (x,y\ ;\ t) \ . \qquad (3)$$

A solution of (1)-(2) may be written

$$(u,v)\ (\xi\ ;\ t) = (x,y) + t\ (u_1,\ v_1)\ (\xi\ ;\ t)\ , \qquad (4)$$

where u_1 and v_1 have to satisfy at each time t (just inject (3)-(4) into (1)-(2)^1)

$$L\ .\ \begin{pmatrix} u_1 \\ v_1 \end{pmatrix} = t \begin{pmatrix} M_1\ (u_1,\ v_1,\ t) \\ M_2\ (u_1,\ v_1,\ t) \end{pmatrix}\ , \qquad (5)$$

$$(u_1,v_1)\ (x,y,\ \overline{+}\ h\ ;\ t) = (U_1^{\overline{+}}\ ,\ V_1^{\overline{+}})\ (x,y\ ;\ t)\ ; \qquad (6)$$

the 2 × 2 matrix L in (5) is a second order differential linear operator and the M_i are second order differential nonlinear operators.

Owing to some peculiar properties of L, solving (5)-(6) presents some basic difficulties. However, we have found that it is possible to set up an iterative scheme for these equations, which converges for t not too large towards a smooth solution : no CS form in the fields produced by the braiding motions, even in the absence of any symmetry of the boundary velocity pattern.

3. Behaviour of the field for large times

Of course, the previous result leaves open the possibility that CS do develop when the stressing of the field becomes large enough. Actually, there is a quite simple argument showing that, even if no true CS (i.e. zero thickness singularities) does form, at least very thin current layer should be produced near some particular surfaces if the velocity field has some degree of topological complexity.

For definiteness, consider a boundary velocity field $\underset{\sim}{v}$ which vanishes on the upper plane, and is stationnary on the lower one, its streamlines being as shown on Figure 1a and thus admitting an eight-shaped separatrix L.

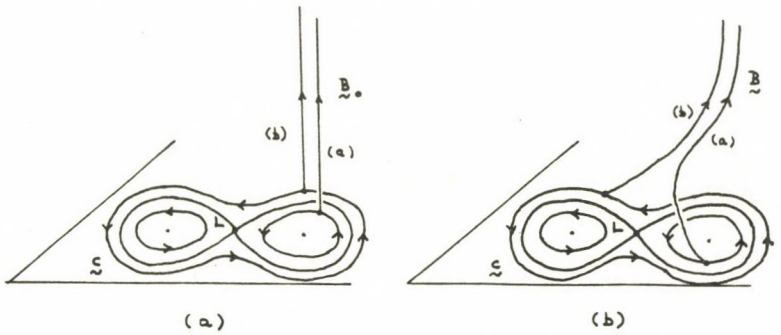

Figure 1 - (a) Initial configuration ; (b) Configuration at some large t.

Let S(t) be the surface in D formed by the field lines originating from that curve. Any footpoint on L will undergo only a finite displacement for $0 \leq t < \infty$, approaching asymptotically the X-point of $\underset{\sim}{c}$. On the contrary the footpoints of the lines (a) and (b) located on each side of S, will undergo infinite displacements ; on the other hand, albeit initially as close as we want from each other, they will be separated by finite distances during intervals of large times. Consequently, the shear of $\underset{\sim}{B}$ will grow faster in a neighbourhood of S than away from that surface, and electric currents concentrate indeed into a layer around S whose thickness (defined e.g. as the typical horizontal distance over which $\underset{\sim}{B}$ rotates by some fixed angle - $\pi/4$, say) must decrease in time.

4. Conclusion

For not too large deformations imposed to the field, Parker's problem admits a smooth solution, no CS do develop. For large deformations, CS formation cannot be excluded (although we feel that this process is not likely). In any case, when the shearing velocity on the boundary has some topological complexity, thin layers of current should appear and thus the situation one obtains should be physically equivalent to that one conjectured by Parker.

References

/1/ Parker, E.N., in "Topological Fluid Mechanics", ed. H.K. Moffat, University Press, Cambridge (1990).
/2/ Aly, J.J., Comp. Phys. Comm. 59, 13 (1990).

HOW MUCH ENERGY CAN BE STORED IN A STABLE FORCE-FREE MAGNETIC FIELD ?

J.J. Aly

Service d'Astrophysique - CEN Saclay - F-91191 Gif-sur-Yvette Cedex.

Summary : Let $\mathcal{R}$ be the set of all the finite energy force-free fields contained in the half-space $\{z > 0\}$ and having their normal component on the plane $\{z = 0\}$ equal to a given function q. Then : i) the energy of any field in $\mathcal{R}$ is not larger than the energy of the unique totally open field contained in that set ; ii) when q is characterized by a single length-scale, $\mathcal{R}$ contains fields which are linearly stable with respect to ideal MHD perturbations and have an energy of the order of the maximum allowed value.

1. Introduction

It is generally well admitted that solar flares are powered by the free energy of the coronal force-free magnetic field which has been stressed by the unceasing motions imposed to its footpoints by the dense photospheric plasma. The energy released in an eruptive site is then smaller than the maximum energy which can be stored in a stable way in its magnetic structure. In this Communication, we show that this maximum energy is necessarily smaller than the free energy of the open force-free field which is uniquely defined by the distribution of the magnetic flux at the basis of the considered active region, but that it may be of the same order.

2. A upper bound on the energy stored in a force-free magnetic field

Let us represent the corona by the half-space $D = \{z > 0\}$ and consider the set $\mathcal{R}$ of all the finite energy force-free fields in D whose normal component B_z on the "photosphere" $\partial D = \{z = 0\}$ is equal to a given function $q(x,y)$ (tending fast to zero at infinity and having zero flux through ∂D). As proved in /1/, the "energy" $C[\underset{\sim}{B}] = \int_D |\underset{\sim}{B}|^2 \, d\underset{\sim}{r}$ of any field $\underset{\sim}{B}$ in $\mathcal{R}$ is bounded from above, i.e. there is a number C_m (which of course depends only on q) such that

$$C_m = \sup C[\underset{\sim}{B}] < \infty . \qquad (1)$$

It was conjectured in /1/ that

$$C_m = C[\underset{\sim}{B}_{op}] , \qquad (2)$$

where $\underset{\sim}{B}_{op}$ is the unique totally open force-free field contained in $\mathcal{R}$ (actually, $\underset{\sim}{B}_{op}$ is potential everywhere in D but on a surface S accross which it reverses, S being thus a current sheet in mechanical equilibrium). Let us list the arguments which support (2) :

i) (2) may be checked by direct calculations to hold true when q is choosen to belong to a restricted class of boundary functions /1/.

ii) If the Fourier transform $\hat{q}(\underset{\sim}{k})$ of q vanishes for $k \leq K$, then one may construct in $\mathcal{R}$ a sequence $\{\underset{\sim}{B}_\alpha : 0 \leq |\alpha| \leq K\}$ of constant $-\alpha$ force-free fields, for which (2) is satisfied /2/.

iii) Suppose that C_m is reached for only one field $\underset{\sim}{B}^+$ belonging to $\mathcal{R}$ (i.e. $C[\underset{\sim}{B}^+] = C_m$). As C_m, $\underset{\sim}{B}^+$ must be unambiguously defined from the only boundary function q. But there are in $\mathcal{R}$ only two fields which have this property : the potential field $\underset{\sim}{B}_o$ (satisfying $\nabla \times \underset{\sim}{B}o = 0$ in D) and the open field $\underset{\sim}{B}_{op}$. As one has by a well known theorem $C[\underset{\sim}{B}_o] \leq C[\underset{\sim}{B}]$ for any $\underset{\sim}{B}$ in $\mathcal{R}$, $\underset{\sim}{B}^+ \neq \underset{\sim}{B}_o$, and we are left with the only possibility $\underset{\sim}{B}^+ = \underset{\sim}{B}_{op}$ /2/.

iv) From any $\underset{\sim}{B}$ in $\mathcal{R}$, we can construct time-sequences of fields $\underset{\sim}{B}(t)$ of $\mathcal{R}$ ($t \geq 0$, $\underset{\sim}{B}(o) = \underset{\sim}{B}$) which represent quasi-static evolutions driven by footpoints motions on ∂D keeping q invariant (D is supposed to be filled up with a perfectly conducting plasma). It is intuitively quite clear that, if $\underset{\sim}{B}$ admits a bundle of lines connecting the regions of ∂D of positive and negative polarities, respectively, one can choose boundary motions which twist more T and thus increase the energy of $\underset{\sim}{B}$; on the contrary, moving only the footpoints of the open lines - if any - does not change the configuration. Let us now assume that C_m is reached for some field $\underset{\sim}{B}^+$ of $\mathcal{R}$. As $\underset{\sim}{B}^+$ has the maximal energy, it results at once from the previous argument that all its lines must be open. But open lines cannot carry along electric currents, as this would imply an infinite energy. Therefore, $\underset{\sim}{B}^+$ has to coincide with $\underset{\sim}{B}_{op}$ indeed. This argument is given a formalized presentation in /2/.

v) Let us start from $\underset{\sim}{B}$ in $\mathcal{R}$ and apply on ∂D a stationnary velocity field preserving q and moving all the footpoints. Assuming that the field in D (containing a perfectly conducting plasma) evolves through a sequence of force-free configurations $\{\underset{\sim}{B}(t)\}$ ($\underset{\sim}{B}(t)$ belonging to $\mathcal{R}$), it may be shown that $\underset{\sim}{B}(t) \rightarrow \underset{\sim}{B}_{op}$ when $t \rightarrow \infty$ /3/. As the asymptotic field corresponds to an infinite shearing or twisting of $\underset{\sim}{B}$, it must have a larger energy : $C[\underset{\sim}{B}] \leq C[\underset{\sim}{B}_{op}]$ for any $\underset{\sim}{B}$, and then (2) holds indeed. It is also worth noticing that the asymptotic field $\underset{\sim}{B}_{op}$ has an infinite relative helicity /2/, and thus is also the state of maximal helicity in $\mathcal{R}$ - as it must be by the asymptotic result above.

We feel that the last two arguments constitute a convincing "physical" proof of our conjecture. (To construct a complete mathematical proof, several gaps should be filled ; in particular, one would need to have a formal proof of existence of the sequence $\{\underset{\sim}{B}(t)\}$, which can be currently asserted only on the basis of physical arguments).

3. Construction of a stable field with an energy of the order of C_m

The next natural question to address is the following one : is it possible to store in a stable way an energy of the order of C_m in a field of $\mathcal{R}$. We can prove that this is the case indeed, at least if q is characterized by a single length-scale ℓ. Our arguments may be sketched as follows :

i) We first construct a family of fields in $\mathcal{R}$ by imposing the supplementary condition : $\alpha = |\alpha|_m h$ on ∂D^+, where α is the usual force-free function ($\alpha = \hat{B}.\nabla \times \hat{B}$), $h(x,y)$ is a given function varying on a length-scale ℓ and such that $\sup_{\partial D} |h| = 1$, and $|\alpha|_m \geq 0$ is a parameter. Such a family (parametrized by $|\alpha|_m$) may be shown to exist if and only if $|\alpha|_m \ell \lesssim 1$ /1,4,5/.

ii) From rigorous estimates derived in /4/, the free energy stored in one of the fields is of the order of : $(|\alpha|_m \ell)^2 C[\underset{\sim}{B}_o]$.

iii) A field of the family is linearly stable with respect to ideal MHD perturbations (this results from rigorous criteria established in /6/, which imply if $|\alpha|_m \ell \lesssim 1$).

Thus we can conclude that there must be indeed a field in $\mathfrak{B}$, corresponding to $|\alpha|_m \ell \simeq 1$, which is stable and has a free energy of the order of $C[\underset{\sim}{B}_o]$ - i.e. of the order of the maximal possible free energy, as in general $C[\underset{\sim}{B}_{op}] - C[\underset{\sim}{B}_o] \simeq C[\underset{\sim}{B}_o]$ /1/.

4. Conclusion

The general results reported in this Communication have some interesting consequences for our understanding of solar flares. They show in particular that : i) it is possible to store in a stable way an energy large enough to power even the big flares ; ii) the coronal field cannot effect a spontaneous transition to an open configuration, as assumed in many models. The scenario that we have suggested earlier /3/ on the basis of a 2D model is perfectly compatible with these constraints. In that scenario, the coronal field undergoes two phases of quasi-static evolution : i) a storage phase, during which it stably accumulates a free energy of the order of the maximal possible value ; ii) a metastable phase during which it expands towards the open field up to a time at which a finite amplitude perturbation (generated e.g. by new flux emergence or a nearby flare) induces a fast transition by reconnection to a state of lower energy.

References

/1/ Aly, J.J. : Ap. J. 283, 349 (1984).
/2/ Aly, J.J. : Ap. J. (submitted).
/3/ Aly, J.J. : Comp. Phys. Comm. 59, 13 (1990).
/4/ Aly, J.J. : Astron. Ap. 203, 183 (1988).
/5/ Aly, J.J. : in preparation.
/6/ Aly, J.J. : Phys. Fluids B (in press).

SESSION 4

May 22, Tuesday (p.m.)

PARTICLE ACCELERATION AND NON-THERMAL EMISSIONS

Chairman: A. O. BENZ
Institut für Astronomie, Eidgenössische Technische Hochschule
Zürich

Invited reviews:

G. TROTTET
Observations of Non-Thermal Particles

L. VLAHOS
Particle Acceleration and Propagation in Flares

These two review talks are jointly summarized in the Extended Abstract published here:

G. TROTTET and L. VLAHOS
Energetic Particles in Solar Flares: Observations, Modeling and Acceleration Processes

and 7 (oral and poster) contributions

ENERGETIC PARTICLES IN SOLAR FLARES: OBSERVATIONS, MODELING AND ACCELERATION PROCESSES

(Extended Abstract)

Gerard Trottet [1] and Loukas Vlahos [2]

1. Observatoire de Paris-Meudon, DASOP and CNRS-URA 324, 5 Place J.Jansen, 92195 Meudon Principal Cedex, France.
2. Department of Physics, University of Thessaloniki, 54006 Thessaloniki, Greece.

I. Introduction

Charged particles with energies much higher than the thermal energy of the flare plasma are usually called "*Energetic Particles or High Energy Particles or Non-thermal particles*". The energetic particles are responsible for a variety of solar bursts in several wavelengths and are detected in space. A successful flare model should in principal explain the origin, the evolution and radiation signatures produced by these particles. Observations from all wavelengths have produce over the years an enormous but fragmented data bank. Only a small part of the existing observations can be fitted in the existing theoretical modelling.

Modelling of energetic particle evolution has evolve over the years and it is today a major tool for solar flare physics. We outline briefly the main techniques and the conclusions reached so far, and use all the informations selected so far from the observations and modelling to restrict the existing theories on particle acceleration. This circle is incomplete if does not close back to the observations and re-defines new observational projects for the feature.

Many reviews have been devoted to particle acceleration and transport on and from the Sun in the past 4-5 years. Nevertheless most of them have focused on the impulsive phase of flares. In this review we present a global approach which discusses the different phases of solar flares and phenomena associated with long lasting particle acceleration even in the absence of an optical flare. The main reason is to underline the complexity of the driver and of the magnetic topology which influence the way the flare energy is released and distributed.

An extended and complete article will be published elsewhere. Here we summarise the approach we have taken and the main conclusions and remarks that can be drawn from the observations, modelling and theory on particle acceleration.

II. Observational diagnostics of Energetic Particles

The most direct diagnostics (model independent) of energetic particles interacting with the solar atmosphere or escaping from the sun are radio bursts, Hard X-ray and Gamma-ray emissions and direct particle detection in the interplanetary space. In the following we discuss these observations for the different phases of solar flares. Based on the hard X-ray time profiles of well developed bursts, such as the March 30,1969 event (Frost and Dennis, 1971) we identify five different phases (a) *pre-impulsive phase* corresponding to phenomena occurring before the detection of Hard X-ray emission; (b) *the pre-flare phase* some tens of seconds where a weak Hard X-ray emission is detected (e.g. Benz et al. 1983); (c) *the flash phase* which corresponds to the sharp increases of the Hard X-ray emission. The duration of this phase is a few minutes and the ensemble of the pre-flash and flash phases are generally referred as *the impulsive phase*; (d) *the Hard X-ray extended or gradual phase* which may last for tens of minutes and which is visible up to hundreds of Kev photons; (e) finally what we usually refer as *post gradual phase* corresponds to long lasting acceleration (hours) which follows the Hard X-ray extended phase (stationary type IV) or which occurs without associated optical flares (noise storms). In both cases no Hard X-ray emission is detected.

Of course these deferent phases are not observed in all flares and most of the flares ($\approx 90\%$) show the impulsive phase only. Nevertheless it is instructive to examine, the main characteristics of the different phases. The major points are summarised bellow:

- Radio emission due to energetic electrons occurring several minutes before the impulsive phase have been reported for a few flares (Gergely and Kundu, 1981; Benz et al., 1983). This indicates that particle acceleration may occur before the impulsive phase but there is a lack of systematic study of pre-impulsive radio bursts.

- Acceleration becomes stronger during the pre-flash phase. Such a phase is not systematically detected in the Hard X-ray domain (Benz et al.,1983). Hard X-ray detectors with better sensitivity are needed to determine if pre-flash Hard X-ray emission is common to all flares and a systematic study of the radio emission during this phase should be done. For the largest events the starting time of the Hard X-ray emission increases with energy (Klein et al.,1987) and the amount of energy released is comparable with that released during moderate flash phases (Vilmer et al., 1987).

- The flash phase corresponds to the bulk of electron and ion acceleration and is usually triggered when one or several magnetic structures are involved in addition to those observed during the pre-flash phase (e.g. Raoult et al.,1985; Machado et al.,1988; Willson et al., 1990).

- Electrons up to relativistic energies and ions up to hundreds of $Mev/nucl$ are accelerated simultaneously during the flash phase on time scales of seconds (see Chupp, 1984; Yoshimori, 1989 for reviews). Generally Hard X-ray and Gamma-ray line emission peak simultaneously but for some events the latter occurs a few seconds to a few tens of seconds later than the former (see Yoshimori, 1989) This has been taken by several

authors (e.g. Bai, 1982) as an indication for two step acceleration process. On the other hand it has been shown that such delays may be due to propagation effects (e.g. Vilmer et al., 1982; Hulot et al., 1989).

• Millisecond spikes in both the Hard X-ray and radio domain are observed in about 10% of the impulsive events (e.g. Kipilinger et al., 1983; Benz, 1985; Stahli and Magun, 1986; Gudel and Benz, 1990). This is usually taken as an evidence of fragmentation of the energy release (e.g. Benz,1986).

• Various observations suggest that during the impulsive phase the site of acceleration is located in the corona at densities ranging from a few $10^9 cm^{-3}$ to a few $10^{10} cm^{-3}$. The main arguments for this are : (a) the similarity between the time profiles of Hard X-ray and Radio spike events, the latter being observed between 600 MHz and 3 GHz (Benz and Kane, 1986); (b) the systematic behaviour of the frequency drifts of type III like radio bursts which indicates that at frequencies lower than 800 MHz ($n_e < 2 \cdot 10^9 cm^{-3}$) electron beams propagate outwardly (Benz and Zlobec, 1978; Elgaroy, 1980; Aschwanden and Benz, 1986) while at frequencies larger than 3 MHz ($n_e > 2.8 \cdot 10^{10} cm^{-3}$) they propagate towards the photosphere (Stahli and Benz, 1987).

• Gradual phase acceleration involves a rather complex magnetic structure, large corona volumes and continual energy release (see Trottet, 1986 for a review). Due to the lack of a systematic study of the radio emission during this phase there is no clear evidence of the fragmentation of the energy release and how this phase is triggered is not understood. Contrary to the impulsive phase most of the accelerated ions escape from the solar atmosphere (Cliver et al., 1989). This suggests that the impulsive and gradual phases either correspond to different acceleration processes or to different physical conditions at the acceleration site. Moreover both phases do not seem to have any strong correlation; the presence and characteristics of the one does not influence the other. Indeed, (a) most impulsive bursts are not followed by a gradual bursts; (b) gradual bursts have been observed without preceding impulsive bursts (Tsuneta et al., 1984; Ohki et al.,1983; Kai et al.,1983; Kai et al., 1986).

• Contrary to the common believe that large scale coronal shock waves (associated with type II radio emission), driven by the impulsive phase, accelerate the particles needed to produce the gradual Hard X-ray bursts (e.g. Frost and Dennis, 1971; Hudson et al., 1982) and interplanetary particle events (e.g. Evenson et al., 1985; Reames, 1988) there is strong evidence that these shocks play little or no role in the production of high energy particles. Indeed: (a) some impulsive Hard X-ray events which are associated with type II bursts occur without gradual phase and interplanetary particles (Klein et al., 1988); (b) despite their widely separated locations dm and metric radio emission and Hard X-ray emission have similar starting times and durations independently of the occurrence of a type II burst (Klein et al.,1983; Trottet, 1986); gradual Hard X-ray and microwave bursts sometimes occur without type II or several tens of minutes after a type II (Kai et al.,1986).

• Long lasting acceleration (hours) of electrons occurring after the gradual phase or in the absence of optical flares are respectively associated with radio stationary type

IV and noise storms. These radio emissions have similar properties, they both consist of continuum emission and short narrow band type I bursts. Type I bursts may be considered as local and micro acceleration of electrons but the continuum is not the result of the accumulation of the observed discrete energy releases (Elgaroy,1977). Even if long lasting production of non thermal electrons is not yet understood there are some indications that they are triggered in a similar way as the impulsive phase (Kerdraon et al., 1983). Indeed as in the case of the flash phase the noise storm emission is initiated when a new magnetic structure appears but the time evolution and energy content of both kinds of phenomena are different.

III. Modelling of Energetic Particles

Most solar flare models assume a localised energy release region. Energetic particles accelerated in this region are transported away in different parts of the solar atmosphere. Transport of energetic particles inside complex magnetic topologies is by itself an active research topic. We usually start with an arbitrary injection function $S_0(\mathbf{r}, \mathbf{v}, t)$ and follow the evolution of the injected particles as they propagate away from the acceleration region using a transport equation. The evolution of the velocity distribution that describes the energetic particles in space and time depends on several external parameters such as (a) the magnetic topology, (b) the ambient density profile $n_e(\mathbf{r}, t)$, (c) the ambient temperature profile $T_e(\mathbf{r}, t)$ and the charge composition of the solar atmosphere. All existing transport models use two basic magnetic topologies (i) magnetic trap, (ii) open field lines. Energetic particles loose energy and scattered either by waves (external or self-exited) or by Coulomb collisions. It is almost impossible to follow the evolution of the distribution of the energetic particles in space and time taken into account simultaneously the influence of waves and Coulomb collisions. The two effects have widely separated time and space scales.

The transport equations used over the years for the evolution of the energetic particles are:

- **Monte Carlo** was used to describe the space and time evolution of the distribution function in homogeneous or inhomogeneous magnetic topologies (Bai,1982; Hua et al., 1989; Miller and Ramaty, 1989).
- The **Continuity** equation was used extensively the last ten years to describe the evolution of the velocity distribution in space and time in closed and open magnetic topologies (Vilmer et al.,1986; Hulot et al.,1989).
- The **Fokker-Planck** equation was used also in the same type of problems recently but the comparison with observations is still incomplete (Lu and Petrosian, 1988; Lu and Petrosian, 1989).
- Finally, the **Quasilinear** equation was used to describe mainly the evolution of electron beams in open field lines (Takakura and Shibahashi, 1976; Hamilton and Petrosian, 1987; Moghaddam-Taaheri and Goertz, 1990).

All the above equations are approximations of the Vlassov equation (Krall and Trivelpiece, 1973). It is instructive to derive the transport equations quoted above from the Vlassov equation and point out the different approximations made and the limitations in each one but this is beyond the scope of this extended abstract and it will be presented elsewhere. The references quoted above are not a complete list of the authors that have contributed in this field but we believe that the interested reader can trace all remaining references by starting with the articles quoted above.

It is well known that the observed radiation is the end product of the form of the injection function and its evolution in time and space from the acceleration region to the part of the atmosphere that the energetic particles will radiate. The main goal of the above mentioned transport models is to separate the important characteristics of the injection function from those added by propagation in the observed emission. The main results reached so far are:

• Most transport models use an injection function of the form $S = N(E)\Phi(\mu)R(t)$, where E is the energy and μ the cosine of the pitch angle. The standard form for $N(E) \approx E^{-\delta}$, where $2 < \delta < 4$ and Φ isotropic. Variations on the standard model have also been used e.g. Delta function energy injection or anisotropic distributions.

• The time evolution of the injection function has a gaussian profile

$$R(t) \approx exp(\frac{(t - t_j)^2}{\tau^2}),$$

where t_j and τ are important free parameters for the model and play essential role on the acceleration mechanisms since they define the injection time in several energies (t_j) and the acceleration time (τ). The comparison with the observations in several frequencies just started in most transport models and numbers for these parameters are not available yet.

We can then conclude that after more than two decades of modelling of the transport of energetic particles in solar flares the restrictions posed on the acceleration mechanisms are relatively weak. Basically an acceleration mechanism is relevant for solar flares only when it satisfies three criteria (1) Accelerates the total number of particles needed to produce all the radiated emission, (2) The acceleration time is comparable with the observations, (3) The energy release process is related to the acceleration mechanism.

IV. Mechanisms for the acceleration of the Energetic Particles

Several acceleration mechanisms have been proposed for solar flares (e.g. Electric Field, Stochastic acceleration, Shock waves, Multiple shock waves or Multiple Double Layers). We review briefly the conclusions reached so far:

• **Electric fields** are known to be present in reconnecting magnetic topologies. The strength, the spatial and temporal characteristics of the Electric field are not known.

Although direct electric fields are the easiest and fastest way to accelerate particles it is almost certain that are not the dominant acceleration process in solar flares. Idealised neutral sheet models proposed recently by Holman et al (1989) are highly questionable since their stability and formation are not well understood. In summary, isolated electric fields fail to satisfy the criteria for particle acceleration in solar flares.

• **Stochastic** acceleration by MHD or electrostatic turbulence with given amplitude and spectrum satisfy most of the criteria presented in the previous section. The only difficulty is the relation of the waves to the energy release region (Melrose,1974; Melrose, 1983; Ramaty and Murphy, 1987).

• Large scale **turbulent shock waves** have almost the same advantages and disadvantages with stochastic acceleration, but as we already mention in section II there is no obvious connection between type II bursts and energetic particles in solar flares (Decker,1989; Elisson and Ramaty,1987; Decker and Vlahos,1986).

• We can overcome many of the difficulties mentioned above if we abandon the idea of a *single* electric field, *single* energy release, *single* loop etc. Following recent developments in the stability of active region magnetic field lines (Parker, 1988; Moffat,1987; Low and Wolfson,1988), Vlahos (1989) and Anastasiades and Vlahos (1990) proposed that bipolar fields above the surface of the sun are filled with small scale reconnection events which end up in **multiple explosions**. Multiple explosions or highly turbulent flows will form a large number of discontinuities moving randomly in space. Anastasiadis and Vlahos (1990) study the acceleration of particles in such an environment and proved that this model successfully meets all the requirements for a solar flare acceleration mechanism, (1) accelerates the required number of particles, (2) it is a fast acceleration process, (3) it is well connected to the global energy release process.

V. Discussion

In this review we have proposed a number of points that should be taken in to account in feature studies on Energetic Particles in solar flares.

(1) The **fragmentation and fillamentation** of the energy release should be taken into account in feature models.

(2) Acceleration and energy release starts before the impulsive phase and last much longer and it is event present without an optical flare.

(3) Single Loops or Shock waves or Double Layers should give their position to multiple fibbers, multiple shocks, multiple Double Layers and statistical approaches.

(4) Noise storms and Radio Continuum is the "**flaring**" of the upper corona.

(5) Emerging of new magnetic flux both in the upper and low corona is the way the impulsive phase is triggered. Thousands or Millions of small scale reconnection events are active before and after the flash phase, it is the emerging new magnetic flux that increased the number and the strength of these explosive events as well as it organises them in space ant time.

We will return and expand our arguments in all these points in a feature article.

REFERENCES

Anastasiadis,T., and Vlahos, L.:1990, Astron. Astrophys., in press.
Aschwaden,M., Benz,A.O.:1986, Astrn. Astrophys., **158**,102.
Bai,T.:1982, Astrophys.J., **259**,341.
Bai,T.:1982, in Gamma Ray Transients and related Astrophysical Phenomena, eds.,R.E. Lingenfelter, H.S. Hudson, D.M. Worall, A.I.P., New York, p.135.
Benz,A.O.: 1985, Solar Phys., **96**,357.
Benz,A.O.: 1986, Solar Phys., **104**,99.
Benz,A.O. and Kane, S.R.: 1986, **104**,179.
Benz,A.O., Barrow, C.H., Dennis,B.R., Pick, M., Raoult, A. and Simnet, G.: 1983,Solar Phys., **83**, 267.
Benz,A.O. and Zlobec, P.:1978, Astron. Astrophs., **63**,137.
Chupp,E.L.:1984, Ann. Rev. Astron. Astrophys., **22**,359.
Cliver,E.W., Forrest,D.J., Cane,H.V., Reames, D.V., McGuire,R.E., von Rosenvinge, T.T., Kane, S.R., MacDowall, R.J.: 1989,Astrophys. J., **343**,953.
Decker,R.B. and Vlahos,L.:1986, Astrophys.J.,**306**,710.
Decker,R.D.:1988, Space Sc. Reviews, **48**,195.
Elgaroy, O.: 1977, Solar Noise Storms, International Series in Natural Philoshophy, ed. Ter Haar, Vol. 90 (New York).
Elgaroy,O.: 1980, Astron. Astrophys., **82**, 308.
Ellison,D.C. and Ramaty,R.:1885, Astrophys. J.,**298**, 400.
Evenson,P.,Hoverstadt,P.,Meyer,P.,Moses,D.: 1985, Proc. 19th Int. Cosmic Ray Conf., San Diego, **4**, 74.
Frost, K.J. and Dennis, B.R.:1971, Astrophys. J., (Lett.),**241**,L113.
Gergely, T. and Kundu, M.R.:1981, Solar Phys., **71**, 65.
Gudel, M. and Benz, A.O.:1990, Astron. Astrophys., **231**, 20.
Hamilton,R.J. and Petrosian,V.:1987, Astrophys. J., **321**, 721.
Holman,G.D., Kundu,M.R., Kane, S.R.:Astrophys. J., **345**,1050.
Hua,X.-M.,Ramaty,R., and Lingenfelter, R.E.:1989, Astropyhs.J., **341**,516.
Hulot,E., Vilmer,N., Trottet, G.: 1989, Astron. Astrophys., **213**,383.
Hudson,H.S., Lin,R.T., Stewart, R.T.:1982, Solar Phys., **75**,245.
Kai,K., Nakajima,H., Kosugi,T.,Kane,S.R.:1983, Solar Phys., **86**,231.
Kai,K., Nakajima,H.,Kosugi,T., Stewart, R.T., Nelson, G.J., Kane,S.R.: 1986, Solar Phys., **105**,383.
Kerdraon, A., Pick, M., Trottet,G., Sawer,C., Illing,R., Wagner,W., House,L.,:1983, Astrophys. J., (Lett.),**265**,L19.
Kipilinger, A.L., Dennis, B.R., Emslie,A.G., Frost,K.J.,Orwiq,L.E.: 1983, Astrophys. J., **271**,376.

Klein,K.-L., Anderson,K.,Pick,M.,Trottet,G.,Vilmer,N.,Kane,S.R.: 1983, Solar Phys., **84**,295.
Klein,K.-L.,Pick,M.,Magun,A.,Dennis,B.R.:1987, Solar Phys.,**111**, 225.
Klein,K.-L., Trottet,G.,Benz,A.O.,Kane,S.R.:1988, ESA SP-285 I,57.
Krall,N.A. and Trivelpiece,A.W.:1973, Principles of Plasma Physics, McGraw-Hill, New York.
Low,B.C. and Wolfson, R.:1988, Astrophys.J.,**324**,574.
Lu,E.T. and Petrosian,V.:1988, Astrophys. J., **327**,405.
Lu,E.T. and Petrosian.V.:1989, Astrophys.J.,**338**,1122.
Machado,M.E.,Moore,R.L.,Hernandez,A.M.,Rovira,M.G.,Haygard,M.J., Smith,J.B.:1988, Astrophys.J.,**236**,425.
Melrose,D.B.:1974, Solar Phys.,**37**,353.
Melrose,D.B.:1983,Solar Phys.,**89**,149.
Moffat, H.K.:1987, in Advances in Turbulence, ed. G.Comte-Bellot and J.Matieu, Sprinder-Verlag, p.240.
Miller,J.A. and Ramaty,R.:1989,Astrophys.J.,**344**,973.
Moghaddam-Taaheri,E. and Goertz, C.K.:1990, Astrophys. J.,**352**,361.
Ohki,K.,Takakura,T.,Tsuneta,S., Nitta,N.:1983, Solar Phys.,**86**,301.
Parker,E.N.:1988,Astrophys. J.,**330**, 474.
Ramaty,R. and Murphy,J.:1987, Space Sc. Reviews, **45**, 213.
Raoult,A.,Pick,M.,Dennis,B.R.,Kane,S.R.:1985,Astrophys.J.,**299**,1027.
Reames,D.V.:1988,Astrophys. J.,(Lett.),**330**,L71.
Stahli,M. and Benz,A.O.: 1987, Astron. Astrophys., **175**,221.
Stahli,M. and Magun,A.:1986, Solar Phys., **104**,117.
Takakura,T. and Shibahashi,H.:1976, Solar Phys., **46**,323.
Trottet,G.:1986, Solar Phys.,**104**,145.
Tsuneta,S.,Takakura,T.,Nitta,N., Ohki,K.,Makishima, K., Murakami, T., Oda,M., Ogawara,Y., Kondo,I.:1984, Astrophys. J.,**280**,887.
Vilmer,N., Trottet,G., MacKinnon,A.L.:1986, Astron. Astrophys.,**156**,64.
Vilmer,N., MacKinnon,A., Klein,K.-l.,Trottet,G.:1987, Proc. 20th Int. Cosmic Ray Conf. Moscow, SH 2.1-2.
Vilmer,N.,Kane, S.R.,Trottet, G.:1982, Astron. Astrophys.,**108**,306.
Vlahos, L.:1989, Solar Phys.,**121**,431.
Wilson,R.F.,Klein,K.-L.,Kerdraon,A., Lang,K.R.,Trottet,G.:1990, Astrophys.J., **357**,662.
Yoshimori,M.:1989,Space Sc. Reviews, **51**,85

EVOLUTION OF ENERGY SPECTRA IN SOLAR FLARE X-RAY BURSTS.

According to the data from VENERA-13 and VENERA-14 Spacecraft.

S.V.Bogovalov, Yu.D. Kotov Moscow Engineering Physics Institute, 115409 Kashirskoe Shoes 31, Moscow, USSR.
V.G.Kurt, E.V.Yurovitskaya Moscow State University, Institute of Nuclear Physics, 119899, Leniniskie Gory, Moscow, USSR
V.M.Zenchenko Space Research Institute, Academy of Sciences, 117810, Profsoyusnaya 84/32, Moscow, USSR.

1.INTRODUCTION. Solar flare X-ray spectra and their evolution provide data for diagnostics of subrelativistic electrons behavior. Experiments performed with germanium detector aboard the balloons by Lin and Schwartz (1987) and with a CsJ(NaJ) scintillator aboard the SMM and HINOTORY satellites have shown that the slope of the hard X-ray spectra from solar flares are most probably a "piece wise" power form which may considerably vary during the flare. It should be taken into account that thoughts results are very important, their number still not enough to make proper conclusions. In order to verify the validity of that idea, it is important to determine the spectrum form for many X-ray bursts.

2.OBSERVATION. This report presents the results of the spectral analysis of 88 impulsive X-ray solar flares recorded with the French-Soviet experiment SIGNE-2M on board the VENERA-13 and VENERA-14 Spacecraft. Hard X-ray emission was recorded in five wide energy windows covering the energy interval from55keV up to 760keV.Time resolution for spectral data was 0,5s. Unfortunately we could not measure more then 128 spectra per flare. The fitting was made with two trial spectral shapes:a power law $A*E^{-\gamma}$ and exponential function,corresponding to the spectrum of hot optically thin plasma $A/E*\exp^{E/Eo}$. In order to get sufficient statistics in energy range ≅125-300keV,the accumulation time for each spectrum was getting longer till the number of counts exceed 30. Since energy channels were only five we could examine spectral shape by two parameters.

The main results of our spectra recovery in impulsive X-ray solar flares are presented below.

3.RESULTS. 1.Observation of fast spectral variability of the emission. Figure 1 presents the time behavior of the spectra during 1981 November 12, 18:12 UT hard X-ray flare. The flare was recorded by both instruments, on board VENERA-13, and VENERA-14 Spacecraft. We show fitting with a isothermal shape. The top panel shows how the total number of photons varies with time from the beginning of the burst T_o. Adjacent time bins were accumulated together if required for proper statistical accuracy. The middle part of Figure 1 gives the χ^2values and the number of degrees of freedom $N=N_k-2$, where N_k is the number of energy channels. The χ^2 value is shown by a solid line (left scale). The N value is presented by dashed line with a scale shown on the right.The bottom part demonstrates $E_o$value with confidence intervals 3σ.

A peculiarity of the flare is the fast spectral variability found in the both Spacecraft"s data set. The arrow in the bottom

panel marks the moment when value E_o jumps almost twice. This jump occurs during 0,5s interval, and is above the statistical fluctuations. This jump is seen simultaneously on both data set.

2. The analyses of a large number of flares revealed an essential typical feature. As a rule, in the vicinity of the major peaks the spectrum cannot be described by any of the trial function. This result is close to Lin and Schwartz (1987) conclusion that the spectrum near the peak can be describe by power law with a break at 60-80 keV. (in that aspect 1981 November 12, 18:12 UT flare is not a typical case-χ^2 near the peak is small).

3. Usually the hardness of the X-ray emission of solar flare is characterized by the spectral index $\langle\gamma\rangle$, or by effective temperature $\langle E_o \rangle$ accumulated over the entire lifetime of the flare. Sometimes the hardness of the X-ray emission is characterized by the spectral index γ_{max} or (E_{omax}) near the time of major peak. In this respect two questions arise: a) how strong does $\langle\gamma\rangle$ or $\langle E_o \rangle$ differs from γ_{max} or E_{omax} in every event? b) what are values $\langle\gamma\rangle$ or $\langle E_o \rangle$ change from flare to flare? Figure 3 compares the spectrum index $\langle\gamma\rangle$ averaged out over the flare, with its value γ_{max}. Obviously in most cases spectral slope during one flare varies within value 0,5-0,7, whereas flare-to-flare variability of the spectral in dice $\langle\gamma\rangle$ is from 2,4 to 6. Consequently we make just as well use of spectral indices $\langle\gamma\rangle$ or γ_{max} ($\langle E_o \rangle$ or E_{omax}) to describe the flare spectrum for some purposes.

4. Our results confirm well known correlation of spectral hardness with peak intensity of the X_rays in solar flares. (See Figure 3. Discussed trend is obvious but the points scattering is high enough. The same positive correlation of spectral hardness and-X-ray intensity keeps during each impulsive flare. Usually the hard X-ray flare consists of a series of impulsive bursts. Passing by every impulsive burst we can see that spectral slope modify in such a way: soft- hard-soft.

REFERENCES. Bai T. 1986 Ap. *308*, 912.
Chambon G., Hurley K., et al. 1979, Space Sci. Instr. *5*, 73.
Lin R.P., Schwartz R.A., Ap.J., 1987, *312*, 462.
Smith D.F., Orwig L.E. Ap.J. 1988, *327*, 466.
Yoshimory et al., J. Phys.Soc.Japan, 1985, 442.

FIGURE CAPTIONS.

Fig.1. Parameters for exponential fit (photon number, χ^2, E_o) vs time for both data sets for the 1981 November 12, 18:12 UT, measured by VENERA-13,14.

Fig.2 Example of impulsive event, showing relationship between hard X-ray intensity and the E_o value for the isothermal fit.

Fig.3. Scatter plot of γ_{max} (for peak X-ray count rate at energies above 55keV) vs $\langle\gamma\rangle$.

Fig.4. Scatter plot of γ_{max} vs peak rate of the X-ray bursts at energies above 55keV.

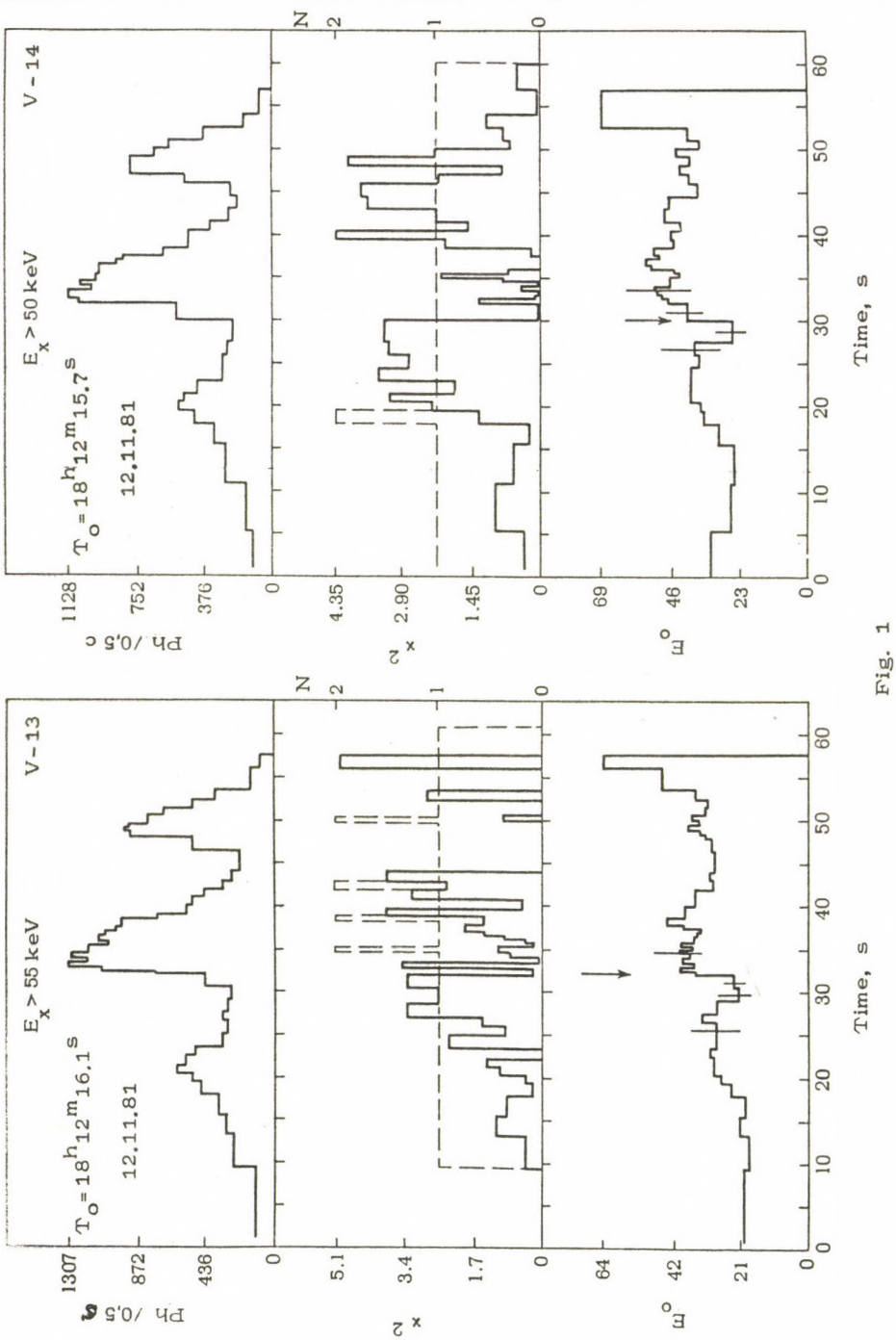
V-14
$E_x > 50$ keV
$T_o = 18^h 12^m 15.7^s$
12.11.81
Ph /0,5 s
1128
752
376
0
N
2
1
0
χ^2
4.35
2.90
1.45
0
ω°
69
46
23
0
0
10
20
30
40
50
60
Time, s
V-13
$E_x > 55$ keV
$T_o = 18^h 12^m 16.1^s$
12.11.81
Ph /0,5 s
1307
872
436
0
N
2
1
0
χ^2
5.1
3.4
1.7
0
ω°
64
42
21
0
0
10
20
30
40
50
60
Time, s

Fig. 1

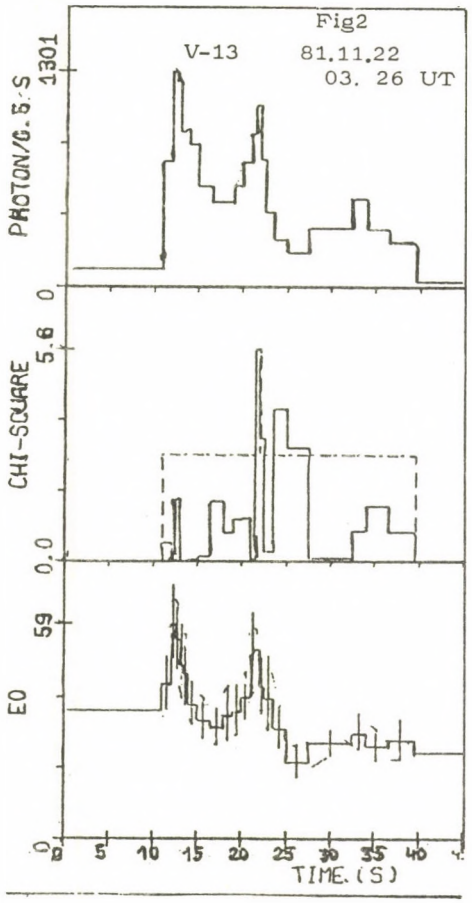
Fig2
V-13 81.11.22
03. 26 UT
PHOTON/C.S.S
1301
CHI-SQUARE
5.8
0.0
EO
59
0
5
10
15
20
25
30
35
40
TIME.(S)

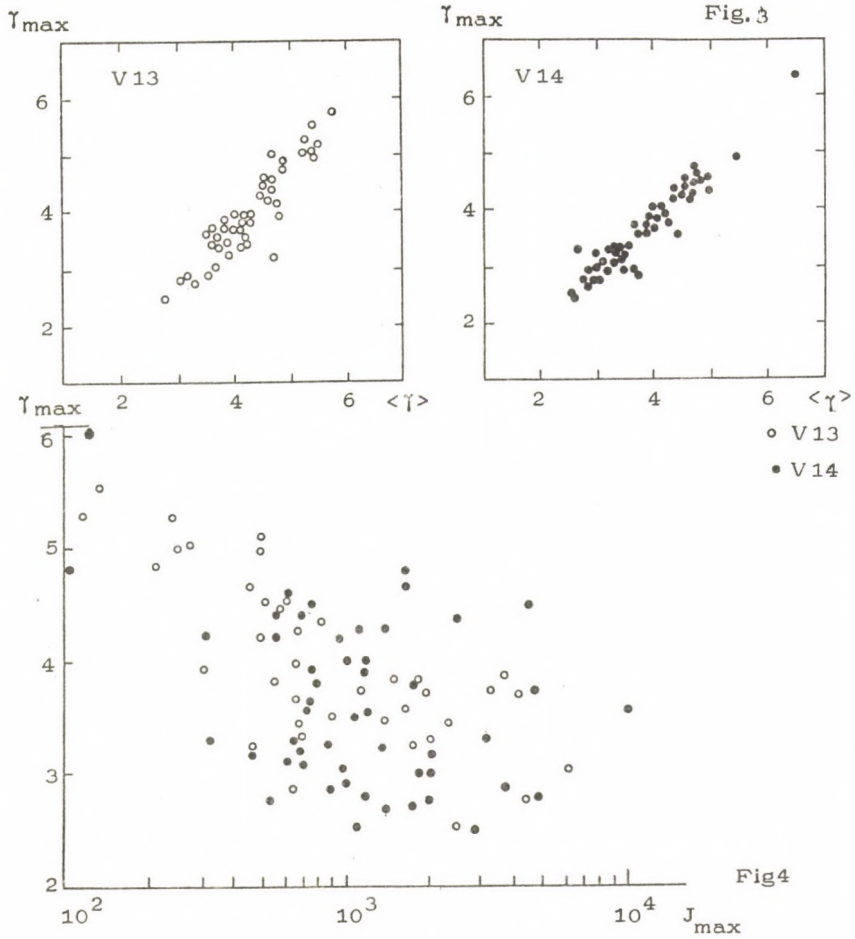
Fig. 3
γmax
V13
V14
<γ>
V13
V14
Fig4
10^2
10^3
10^4
Jmax

The Attractor Dimension of Solar Decimetric Radio Pulsations

J. Kurths[1], A.O.Benz[2], M.J. Aschwanden[3]

[1] Zentralinstitut für Astrophysik, AdW
DDR-1501 Tremsdorf

[2] Institut für Astronomie, ETH
CH-8092 Zürich

[3] NASA Goddard Space Flight Center
Code 602.6, Greenbelt, MD 20771, U. S. A.

Abstract

We have analyzed the temporal characteristics of decimetric pulsations and related radio emissions during solar flares. Since the flux variations in general are not periodic, we make use of the statistical methods recently developed for non-linear, dynamic systems. The quantitative characterization of 20 pulsation events gives good evidence that they typically have their origin in deterministic chaos corresponding to motion on a strange attractor of low dimensionality. The correlation dimension in general turned out to be a useful way to quantify the regularity and hidden order of the irregular or quasi-periodic pulsations. To judge the reliability of its estimate even from rather small data samples, we have studied an optimum choice of the algorithmic parameters as well as experimented with known models.

The correlation dimension has generally been found to be in the range 2.5 – 3.5. A metric periodic oscillation and an extraordinarily regular event of 'sudden reductions' have yielded a dimension of 2, and modulations on two type IV continua exhibited dimension around 4. These findings suggest that the source of pulsating emissions in the simplest case can be described by the orbit of a point in a three dimensional phase space. In more complicated events, coinciding in general with more powerful energy release, four up to eight free parameters characterize the source.

Observations

Broadband pulsating continua are one of the most frequently observed and often the strongest decimetric radio emissions during solar flares (Güdel and Benz, 1988). They have the following characteristics (Aschwanden, 1987):

- The pulsations cover a broad range $\Delta\nu$ of frequencies, typically $\Delta\nu/\nu = 0.5$.

- The single elements have similar maximum and minimum frequencies, but varying amplitudes.
- Their typical separation in time is one second.

Various degrees of regularity of the pulses have been found ranging from rigorously periodic to low-dimensional chaotic behavior. The purpose of the present paper is to study whether chaos is a typical state of decimetric pulsations. Therefore we have analyzed twenty well observed events.

Fourier Analysis

Applying the method of maximum entropy the resulting power spectra calculated from the pulsations may be classified into three groups:

A) exponential decay
B) power law ($f^{-\gamma}$)
C) broad spectral peaks

In no case narrow spectral peaks (indicating rigorous periodicity) were observed.
A gliding spectral analysis shows the temporal evolution within an event. In this way qualitative changes could be revealed for the April 3, 1980, and May 16, 1981 events (Kurths and Karlicky, 1989).

The Fourier analysis points out that the analyzed pulsations are not periodic. The method does not allow to decide whether the processes have a complex deterministic behaviour or are noise-like, stochastic structures.

Dimension of Attractors

The behaviour of dynamic systems can be quantitatively studied by various parameters, such as **dimensions, Lyapunov exponents,** or **Kolmogorov entropy**. They take the role of the Fourier modes in the theory of linear system and characterize the attractor, the limit set of trajectories of the system in phase space. Loosely speaking, the dimension indicates the number of independent variables which characterize the motion of the system on the attractor. Surprisingly the dimension of complicated sets, called **strange attractors,** can be a fractal number, which reveals irregular (chaotic), but deterministic behaviour. A stochastic process, on the other hand, has generally no finite dimension.

Phase Space Reconstruction

To determine the dimension from one-dimensional observed time profiles, the attractor in the m-dimensional phase space has to be reconstructed. The method of time delay replaces the measured value x_t at time t with a vector (Takens, 1981, Kurths and Herzel, 1987)

$$\mathbf{x}_t = (x_t, x_{t+\tau}, \ldots x_{t+(m-1)\tau}). \tag{1}$$

The time delay τ and the embedding dimension m have to suitably chosen.

Correlation Dimension

From a local density function $n_i(x)$ defined by

$$n_i(r) = \sum_j \theta(r - |\mathbf{x}_i - \mathbf{x}_j|), \tag{2}$$

(θ = Heaviside function), the correlation dimension D_2

$$C(r) := \frac{1}{N} \sum_{i=1}^{N} n_i(r) \sim r^{D_2} \tag{3}$$

can be calculated (Grassberger and Procaccia, 1983). The study of power-law scaling in eqs.(3) is simplified in logarithmic presentation of the derivative of the correlation sum $C(r), d\log C(r)/d\log r$ — called local slope. Applying this procedure to finite data sets we are faced with typical problems:

- *Determination of delay time. τ. As a rule of thumb the maximum shift $T_w = (m-1)\tau$ should be (T_c = correlation time):*

$$T_c < T_w < 3T_c \tag{4}$$

- *Minimum length of data set. From experiments with known dynamical systems we have found that 500–1000 data points may be enough to decide whether a low - dimensional attractor exists.*

c) *Influence of noise. With increasing noise the width of the interesting scaling region is reduced. In extreme cases one may have to smooth the data.*

Results

1. We have found a low-dimensional attractor in the majority of pulsation events. The correlation sum $C(r)$ according to eq.(3) shows a power-law scaling over a broad range. The estimated dimensions are in the range from 2 to 5. The majority is compatible with $\bar{D} = 3.0 \pm 0.5$.
2. There is generally no relation between the shape of the Fourier spectrum (type or value of γ) and the attractor dimension.
3. The correlation between hard X-ray count rate and correlation dimension of the radio pulsations is not significant.

Main Conclusion

The found correlation dimensions of decimetric pulsations indicate that their emission process is not stochastic.The observed time series can be described by a deterministic, chaotic motion in phase space. The dimensions suggest that the source has, in principle, three up to six free parameters (in more irregular cases one or two more).

References

Aschwanden, M.J.: 1987, *Solar Phys.* **111**, 113.
Grassberger, P. and Procaccia, I.: 1983, *Phys.Rev.Lett* **50**, 346.
Güdel, M. and Benz, A.O.: 1988, *Astron.Astrophys.Suppl.Ser.* **75**, 243.
Kurths, J. and Herzel, H.: 1987, *Physica* D **25**, 165.
Kurths, J. and Karlicky, M.: 1989, *Solar Phys.* **119**, 399.
Takens, F.: 1981, *Dynamical Systems and Turbulence, Lecture Notes in Mathematics*, Vol **898**, Springer-Verlag, Berlin.

Table 1 : Structural parameters of the investigated decimetric radio pulsations.

date	start [UT]	duration [s]	frequency [MHz]	hard X-ray fluence counts/s	satellite	Fourier spectrum type	T_c[s]	γ	correlation dimension $\bar{D}_z$	
80/3/29	09.11.43	124	616	0	ISEE-3	A	4.8	–	2.6±0.4	
	09.43.15	110	616	242	ISEE-3	A	0.9	–	4.1±0.5	
	14.42.52	112	901	31	ISEE-3	B	4.0	1.9	2.3±0.2	
	14.45.23	54	901	31	ISEE-3	C	0.6	–	incr.with m	
	14.45.23	54	616	31	ISEE-3	A	0.7	–	incr.with m	
	14.46.33	130	901	73	ISEE-3	B	0.8	1.7	3.4±0.5	
	14.46.33	130	616	73	ISEE-3	B	3.7	1.6	3.0±0.2	
	14.46.33	130	349	73	ISEE-3	A	4.5	–	2.5±0.2	
80/3/30	15.27.00	90	901	27	ISEE-3	B	3.6	1.7	no plateau	
	15.27.00	90	616	27	ISEE-3	A	4.7	–	3.2±0.2	
	16.19.09	200	616	17	ISEE-3	B	3.1	1.8	3.9±0.5	
80/4/3	07.17.35	30	234	150	SMM		1.5	–	2.0±0.2	1)
	07.18.10	80	234	540	SMM	A	2.1	1.9	2.6±0.3	1)
80/4/15	05.47.56	180	336	234	SMM	A	5.	–	2.4±0.3	
80/5/1	16.22.10	76	907	444	SMM	C	1.	–	3.0±0.4	
80/8/31	09.24.06	200	313	335	SMM	A	1.	–	3.2±0.5	
81/2/4	10.53.28	36	463	0	ISEE-3	C	0.6	–	incr.with m	
81/5/16	08.52.00	240	296	1700	Prognoz8	B	0.9	3.5	4.2±0.6	
	08.56.35	75	296	1700	Prognoz8	B	0.6	3.	4.6±0.8	
	08.57.50	150	296	1700	Prognoz8	A	0.6	–	incr.with m	
82/6/3	12.04.20	40	778	30	SMM	C	1.5	–	3.5±0.2	2)
83/6/13	12.23.48	82	914	–	–	C	1.2	–	3.2±0.5	3)
	12.23.48	82	719	–	–	C	3.6	–	no plateau	3)
83/8/2	16.20.02	33	610	0	SMM	A	0.5	–	4.8±0.8	4)
	16.20.49	7	770	0	SMM	B	0.07	2.8	3.5±0.3	5)

1) from Kurths and Karlicky (1989), sudden reductions.
2) from Kurths and Herzel (1986)
3) sampling time reduced to $\Delta t = 0.2$ s
4) $\Delta t = 0.025$ s
5) sampling time of initially 0.002 s reduced to $0.006 - 0.01$ s.

PULSATIONS DURING A TYPE IV BURST OBSERVED AT TRIESTE AND THE VLA

P. Zlobec *), M. Messerotti *), G. A. Dulk **) and T. Kucera **)

*) Trieste Astronomical Observatory, Italy
**) Department of Astrophysical, Planetary and Atmospheric Sciences - University of Colorado, Boulder, USA

On November 14, 1988 we made simultaneous, 327/330 MHz observations of a type IV burst at the VLA and the Trieste Astronomical Observatory, obtaining high spatial resolution with the VLA and high time resolution at Trieste.

The type IV burst started at 14^h35^m UT, lasted about an hour, and exhibited pronounced pulsations for 24 minutes. The average pulsation period was 12.5 seconds with a range from about 11 to 14 seconds. The figure 1 shows the variation of the pulsation frequency during the time interval from 15^h6^m, to 15^h30^m; the Fourier analysis was computed with subintervals two minutes long. The range of periods is rather long compared to those normally reported for solar pulsations. The pulsations were totally left-hand circularly polarized and arose from a source about 1′ in size located about 4′ from the flare site.

The observed characteristics favor a model involving fundamental plasma radiation from a source, probably in a magnetic loop, with propagating MHD waves. The magnetic field strength in the pulsating source, derived from the model and the observed source parameters, is about 75 G, corresponding to a gyromagnetic frequency of 210 MHz. With a plasma frequency of 330

MHz, the ratio of plasma to gyro frequency is 1.6, and with a temperature of 10^7 K in the flaring flux tube, the derived plasma beta is about 0.08, indicating the dominance of the magnetic field.

The complete version of this paper will appear in Solar Physics.

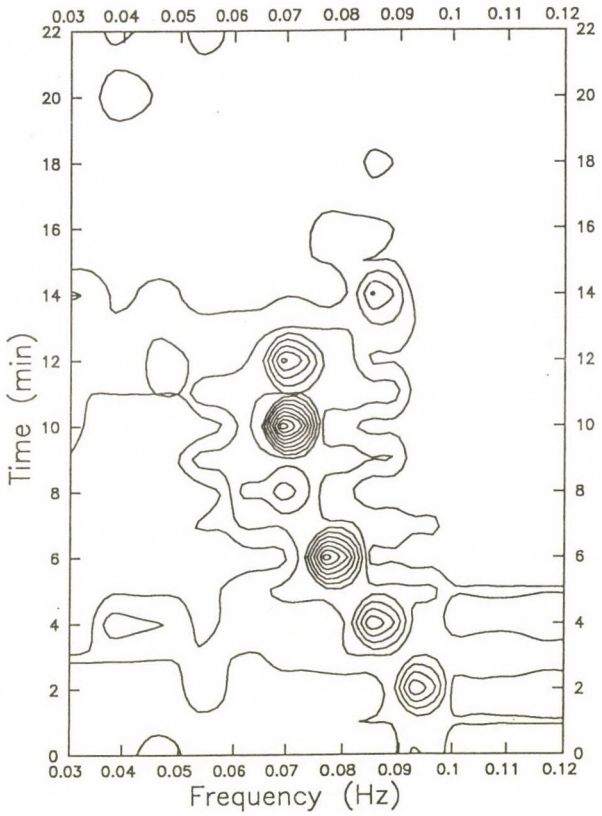

Figure 1. Time evolution of the pulsation amplitude and frequency at 237 MHz. The dominant line is so weak in the last 6 minutes that it does not appear on the contour plot.

NEGATIVE FLARES ON THE SUN

L. van Driel-Gesztelyi[1,2] , J.C. Brown[3], J.C. Hénoux[4],
J. Aboudarham[4], G.H.J. van den Oord[3,4], O. Gerlei[1] and F. Fárník[5]

[1] Heliophysical Observatory of the Hungarian Academy of Sciences, P.O. Box 30, H-4010 Debrecen, Hungary
[2] Sterrenkundig Instituut, Postbus 80.000, NL-3508 TA Utrecht, The Netherlands
[3] Department of Physics and Astronomy, University of Glasgow, Glasgow G 12 8 QQ, Scotland
[4] Observatoire de Paris DASOP, 92195 Meudon Principal Cedex, France
[5] Astronomical Institute, 251 65 Ondřejov, Czechoslovakia

Introduction

In two former articles (Hénoux *et al.* 1990; Aboudarham *et al.* 1990) we published calculations to predict that an analog event of stellar negative preflares can also exist on the Sun. We showed that under certain conditions at the beginning of a solar white-light flare (WLF) event an electron beam can cause a transient darkening before the WLF emission starts. We named this event as "black light flare" (BLF) as a counterpoint of the subsequent WLF.

We pointed out that at the very beginning of the bombardment if the beam is intense and impulsive enough, it has two effects: (i) it enhances the hydrogen recombination emission in the upper atmosphere (ii) it increases the H^- population in the lower atmosphere. The increase of H^- causes an enhanced absorption which results in a transient decrease of the white-light emission (negative flare or BLF). The event lasts ($\approx$20 sec) until the heating of the atmosphere turns the absorption into emission and the WLF starts.

Here we propose optimal conditions for possible observation of solar negative flares and present an observation, which may be the first identified observation of such events.

Conditions for BLF observations

The most common location of WLFs is in the penumbrae of big δ-spots, frequently near umbral/penumbral boundaries. To find BLFs we have to look for dark spots in the penumbrae, or transient enhancements of umbral areas in the vicinity of the flare centre. We expect that BLFs will appear as diffuse dark patches for about 20 seconds preceding WLFs with intense and impulsive hard X-ray bursts, at the same place as the forthcoming bright patches. Their contrast depends on the position of the flare on the solar disc and on the wavelength band of the observation (Hénoux *et al*, 1990; Aboudarham *et al*, 1990). The ideal diagnostic would be to observe at several different wavelengths in the same time between 365-570 nm and above 820 nm with a sampling time not longer than 10 seconds.

Observation of a BLF

The WLF event of 26 July 1981 (2B, X3.5) occurred in Hale region 17760 in a big δ-spot, where opposite polarity umbrae of different ages, embedded in a common penumbra, compressed and sheared the magnetic fields (Gesztelyi *et al.* 1986).

At Debrecen Heliophysical Observatory two full-disc white-light photoheliograms were taken before the WLF maximum, (Fig. 1) at the beginning of and during the impulsive phase of the hard X-ray burst (Gesztelyi *et al.* 1986) The second photoheliogram (taken at 13:51:03 UT, see Fig. 1) shows already a weak WL emission at the border of the umbral-penumbral border of the big (S polarity) umbra *a*, and an even weaker emission at the edge of opposite (N) polarity umbra *b*: this was the beginning stage of the WLF. The first photoheliogram, which was taken unfortunately under worse seeing conditions at 13:49:31 UT (Fig. 1), shows no sign of WLF yet, but on the contrary: umbrae *a* and *b* seem to be elongated towards the places of the forthcoming

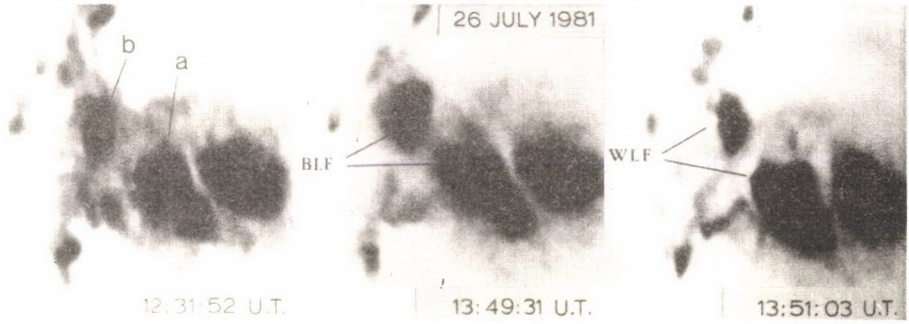

Figure 1: Photographs of the δ spot in Hale region 17760 taken respectively 80 and 1.5 minutes before, and at the start of, the WLF on 26 July 1981. Umbrae *a* and *b* had opposite polarities and at these two umbrae the WLF patches appeared. At 13:49:31 UT, at the beginning of the hard X-ray burst (Gesztelyi *et al.* 1986), 1.5 minutes before the WLF observation dark patches can be seen where the WLF patches appeared later - these may be an example of a BLF.

WLF patches. If we compare their form and area with an observation taken 80 minutes earlier at 12:31:52 UT (Fig. 1), we find that spots *a* and *b* were definitely bigger at 13:49:31 UT than they were 80 minutes before or 1.5 minutes later. Umbrae can not change their area so much so quickly, therefore this can be only an arbitrary area growth, an effect of earth atmospheric seeing or an effect of the solar atmosphere. Our argument in favour of the solar effect is that although the bad seeing changed the shape of umbrae the probability is low that it created elongations (darkenings) by chance precisely at the places of both future WLF patches. We suspect therefore that these darkenings are patches of a genuine BLF, but even if it is not so, it certainly illustrates the kind of manifestation which can be expected.

Acknowledgement

One of us (L. v.D.-G.) would like to thank The Royal Society of Edinburgh and The UK SERC for financial support during her visit in Glasgow.

References

Aboudarham, J. and Hénoux, J.C., Brown, J.C., van den Oord, G.H.J., van Driel-Gesztelyi, L., and Gerlei, O.: 1990, *Solar Phys.* in press

Gesztelyi, L., Karlicky, M., Fárník, F., Gerlei, O., and Valniček, B.: 1986, in D.F. Neidig (ed.) *The Lower Atmosphere of Solar Flares*, NSO/Sacremento Peak (Sunspot, NM), p. 163.

Hénoux, J.C., Aboudarham, J., Brown, J.C., van den Oord, G.H.J., van Driel-Gesztelyi, L., and Gerlei, O.: 1990, *Astron. Astrophys.*, in press

A FOKKER–PLANCK DESCRIPTION OF THE TRAPPING AND PRECIPITATION OF FAST ELECTRONS IN FLARES

K.G. McClements

Rutherford Appleton Laboratory,
Chilton, Didcot, Oxfordshire,
OX11 0QX, England, U.K.

Abstract

We investigate numerically the dynamics of energetic electrons in a flaring coronal loop with a converging magnetic field. The precipitation rate F_p and the ratio of chromospheric to coronal hard X–ray emission R are obtained for a wide range of parameters. If the electrons are injected isotropically into a high density loop, F_p is much less than the injected flux and $R << 1$ (in accordance with observations). Our results may help to explain the apparent non–existence of large Doppler shifts in soft X–ray emission lines.

1. Introduction

There are good observational and theoretical reasons for believing that nonthermal electrons may be trapped in the flaring solar corona by a magnetic mirror configuration. Results from HXIS and Hinotori seem to indicate that X–rays in the 14–38keV range are predominantly coronal in origin (MacKinnon *et al.*, 1985). Less direct evidence for trapping lies in the observed time evolution of soft X–ray line spectra. Hydrodynamic simulations of flaring loops, with zero pitch angle electrons injected into a uniform magnetic field, consistently predict a large blueshift of the CaXIX resonance line. McClements and Alexander (1989) have shown that blueshifts of the predicted magnitude do not occur. From the theoretical point of view, magnetic trapping is attractive because it helps to overcome the electrodynamic problems associated with a large beamed flux of electrons. EUV observations indicate small flare areas, which in turn implies electron beam fluxes which are so high that the resulting return current Ohmic losses would stop the beam before it could produce all the hard X–rays which are observed in large events. One solution to this paradox is that the magnetic field converges towards the chromosphere, so that the loop cross–section area is greater at the loop apex than at the footpoints.

2. The Model

Consider a symmetrical, semi–circular loop, threaded by a magnetic field of the form $B(x, y, z) = B_0 e^{z/\ell}$, where z is the distance along the loop axis from the apex. Considering only the effects of Coulomb collisions and magnetic field convergence, the steady–state electron distribution f then satisfies the following Fokker–Planck equation:

$$\mu v \frac{\partial f}{\partial z} = \alpha n \left(\frac{\partial}{\partial v} \left(\frac{f}{v^2} \right) + \frac{1}{v^3} \frac{\partial}{\partial \mu} \left[(1 - \mu^2) \frac{\partial f}{\partial \mu} \right] \right) + \frac{1}{2\ell} v (1 - \mu^2) \frac{\partial f}{\partial \mu}, \quad (1)$$

where n is the plasma density and α is (approximately) constant. v and μ denote the electron speed and pitch angle cosine. The effectiveness of trapping will clearly depend on the angular distribution of electrons at $z = 0$: in the absence of collisions, only those electrons outside the loss cone will be confined in the corona. Highly anisotropic distributions are generally unstable to plasma wave generation, which tend to isotropize the electrons on a collisionless timescale. With this in mind, we assume that the electrons initially have an isotropic distribution. In such cases, $f(\mu)$ remains sufficiently close to isotropy throughout the loop that plasma instabilities are unlikely to be excited, and therefore the Fokker–Planck description is valid. Coulomb collisions therefore represent the only energy loss mechanism. If most of the electrons are confined to the corona, it follows that the decay time t_X of a hard X–ray burst cannot be less than the collision time t_c in that region. HXRBS observations show that $t_X \gtrsim 1$s in typical events: the coronal density required to give $t_c = 1$s in the case of a 30keV electron is about $3 \times 10^{10} \mathrm{cm}^{-3}$. Given that most of the X–ray emission observed by HXRBS is produced by electrons with energies of around 30keV, it follows that coronal densities

of this order are required if the trap model is to explain hard X-ray variations as short as 1s. All our numerical results were obtained with $n = 3 \times 10^{10}\text{cm}^{-3}$. The loop length L was taken to be 10^9cm.

3. Results

Numerical computations show that the electron pitch angle distribution becomes less isotropic as z approaches L, but remains very broad: the e-folding width is always greater than about 60°. It thus appears that the Fokker-Planck model is self-consistent (insofar as wave-particle interactions can be neglected) provided the electrons are injected isotropically. One is thus encouraged to look for approximate isotropic solutions of Eq. (1). Putting $\mu = 1$ on the left hand side, and taking $f(0, v, \mu) = f_0 v^{-\delta}$, one obtains

$$f(z, v, \mu) = f_0 v^2 v_c^{-(\delta+2)}, \tag{2}$$

where $v_c = (v^4 + 4\alpha n z)^{1/4}$. This expression agrees closely with the numerical results except in the limit $\ell \to \infty$, $\mu << 1$.

The precipitating flux of electrons with $v \geq v_0$ is given by

$$F_p = A_f \int_0^1 \mu d\mu \int_{v_0}^{\infty} v f(L, v, \mu) dv, \tag{3}$$

where A_f is the area of the loop footpoint. We compute F_p as a function of the loss cone angle at the loop apex, θ_0. In every case, $F_p << F_i$, even when the magnetic field is uniform. This is due to a combination of collisional degradation and geometric effects. The precipitation rate in the absence of collisions is given by

$$\frac{F_p}{F_i} = \frac{1}{2} \sin^2 \theta_0. \tag{4}$$

We find numerically that F_p/F_i is almost exactly proportional to $\sin^2\theta_0$, the constant of proportionality depending on the extent to which collisions degrade the distribution function. We can obtain an upper limit for F_p by noting that $f(z, v, \mu)$ is given approximately by Eq. (2). The resulting analytical expression is accurate provided the electron mean free path is greater than L. The precipitating flux per unit area has only a weak dependence on loss cone angle, but (depending on the coronal column depth) may be less than 10% of the injected flux per unit area. Such a reduction would have serious consequences for chromospheric evaporation, and in particular could explain the apparent non-existence of large Doppler shifts in the CaXIX resonance line.

To compute the X-ray emission from trapped and precipitating electrons, we assume that the coronal plus the chromospheric parts of the loop constitute a thick target. The total X-ray intensity I_t can then be calculated analytically, while the footpoint intensity I_{fp} can be obtained numerically from the precipitating flux. The ratio $R = I_{fp}/(I_t - I_{fp})$ was computed numerically as a function of loss cone angle, for the same parameters as those used to obtain the precipitation rate. F_p and R have a qualitatively similar dependence on θ_0. An analytical expression for I_{fp}, based on the assumption of isotropic f, may be derived, which again agrees closely with the results obtained numerically.

The main conclusion to be drawn from this work is that the flux of electrons precipitating from a flaring loop can be significantly less than the injected flux due to *either* a strongly converging field *or* a high coronal column density. By invoking the latter, one is able to argue that hard X-ray emission is predominantly coronal in origin (in accordance with observations), and also that the collision time in the corona is sufficiently short that the rapid fluctuations in hard X-ray light curves can be accounted for.

The numerical and analytical results described above have been published elsewhere (McClements, 1990).

References

MacKinnon, A.L., Brown, J.C., Hayward, J.: 1985, *Solar Phys.* 99, 231
McClements, K.G.: 1990, *Astron. Astrophys.* (in press)
McClements, K.G., Alexander, D.: 1989, *Solar Phys.* **123**, 161

DYNAMIC FEATURES OF A SLOWLY EVOLVING SOLAR PROTON FLARE

B. Rompolt, Astronomical Institute of the Wroclaw University
S. Urpo, S. Pohjolainen, Metsähovi Radio Research Station of the Helsinki University of Technology
H. Auraß, A. Krüger, Central Institute for Astrophysics, Potsdam-Babelsberg

Abstract
We present a study of optical and radio observations of a limb flare on 10 May 1981. The evolution of the flare volume and related dynamical processes provide interesting information about a characteristic example of a class of big slowly evolving flare events.
Remarkable features are the occurrence of a strong microwave burst accompanied by hard and soft X-ray LDE emissions, the presence of a coronal mm-wave source (CMMS), the development of an isolated spray blob, and the excitation of an H-alpha prominence probably by a Moreton-wave. The time profiles of the radio emission, the missing evidence of high-speed shock waves, and the absence of type II radio bursts indicate the unusual existence of efficient particle acceleration without strong impulsive or explosive phases.

1. Introduction

As it is well known, the standard radio signatures of strong proton flares consist of
(A) a strong impulsive (or "explosive") microwave burst ($S_v \geq$ 500 sfu, $t_d \geq$ 5 min at about 10 GHz),
(B) a sudden onset of metre wave burst components (Type III/V, flare continuum, type II/IV).
Feature (A) indicates the existence of accelerated particles confined in solar loop structures magnetically connected with the centre(s) of primary flare-energy release. Feature (B) traces the propagation of accelerated particles and released energy outward through the corona.
While most of the solar proton events hitherto recorded are quite in accordance with the above radio picture, a few flare events seem to deviate from the standard form thus challenging new ways of interpretation and promising deeper insight into the physics of solar particle events.
Exception from the standard picture involve:
* the occurrence of proton events without apparent association of impulsive solar flare events at all;
* the occurrence of prolonged proton events in the interplanetary space probably associated with long-living coronal post-flare arches visible in mm- and X-ray emissions;
* slowly evolving proton flares.

The present study reconsiders a prominent event of the last kind, viz. the big limb flare on May 10, 1981.

2. Observations

The observational data comprise:
- 8mm-wave maps of the Sun,
- single-frequency time profiles of the radio burst at cm- and m-waves,
- choronographic observations in H alpha.

(cf. also Urpo et al. (1983).

3. Development of the proton flare

The flare shows the following phases of development:

(1) Gradual pre-burst phase at microwaves (11:30-12:07 UT) and pre-flare loops in H alpha developing in a loop system.

(2) Slow rising phase in microwaves (12:07-12:22 UT), dissolution of the flare-loop system.

(3) Steeper rising phase (12:22-112:32 UT) displayed in microwaves, widely invisible in H alpha.

(4) Maximum phase of the microwave burst (12:32-12:40 UT) coinciding with deep flare-loop formation at another site and plasma blob (jet) ejection in H alpha.

(5) Microwave-burst decline (12:40-1258 UT), confinement of the H-alpha flare-loop system.

(6) Secondary narrow-band microwave maximum coinciding with post-flare loop formation in H alpha (12:58-12:20 UT).

(7) Microwave post-burst increase (13:20->16:00 UT), observation of a coronal mm-wave off-limb source (CMMS), elevation of post-flare loops, and filament eruption in H alpha (13:46-14:00 UT).

4. Microwave burst spectra

The microwave spectra exhibit two puzzling features (cf. Stähli et al., 1989). There is

- no detectable frequency variation of the spectral maximum during all burst stages, and
- a remarkable steep low-frequency spectrum during the burst maximum (slope = 7.0).

6. Summary and Conclusions

* The slow evolution of the event is consistent with a large source volume and an extended sequence of sites of elementary energy release.
* The constancy of the frequency region of the spectral maximum at microwaves is in favour of an averaging effect over an extended source region.
* Shock-wave induced particle acceleration cannot be directly proved (absence of type II bursts, shortcoming of other m-wave burst components may be due to centre-limb variation of radiation).
* An anticorrelation of H alpha and microwave radiation at the time of the burst maximum may be due to an increase of ionization at chromospheric levels during that time.
* There is indicated the action of a Moreton wave leading to filament activation.
* While softly declining microwave can be easily explained by inhomogeneous source structures (cf. Böhme et al., 1977), the only plausible explanation for the spectrum declining steeply towards low frequencies in our case may be the Razin-effect.

References

Böhme, A., Fürstenberg, F., Hildebrandt, J., Saal, O., Krüger, A., Hoyng, P., Stevens, G.A.: 1977, Solar Phys. 53, 139.

Stähli, M,. Gary, D.E., Hurford, G.J.: 1989, Solar Phys. 120, 351.

Urpo, S., Teräsranta, H., Rompolt, B., Garczynska, I.: 1983, URSI XI Radiotieteen päivät, Otaniemi 1983.

SOLAR FLARE 5.11.82 (08:33 UT): DYNAMICS OF THE PROCESS ACCORDING TO COMBINED OBSERVATIONS IN RADIO AND X-RAY RANGES.

V.G. Kurt. Institute of Nuclear Physics, Moscow State University, 119899, Moscow, Leninskie Gory, USSR
O.A. Sheiner. Radio- physical Research Institute, 603600, Gorky, USSR

It will be interesting to note that the occurrence of impulsive high-energy X-ray solar flares with a time delay $\delta\tau \geq 0{,}5$s of high energy photon with respect to photon energy 30-50 keV is infrequent. We registered only two such events during 15 months of the observation of X-ray bursts by spectrometer SIGNE-2M (Chambon G., et al., 1979) during VENERA-13 and VENERA-14 mission. (see Bogovalov S.V., et al., 1989).

OBSERVATION. The SB importance flare (HR 17969, S10, W11) with time delay we are considering occurred at about 08:33 UT on 5 November, 1981. The microwave burst emission was recorded by the RT-22 KRAO with mapping scale size 4,5'6' by a sweeping spectrograph in frequency range 8-12 GHz. Spectral data were obtained with 1s time resolution and 100 MHz frequency resolution. (Panfilov X.D. et al., 1981) The X-ray intensity was recorded in 5 energy channels from 57keV up to 800 keV with a 0,5s time resolution.

Figure 1-5 show the main experimental results:

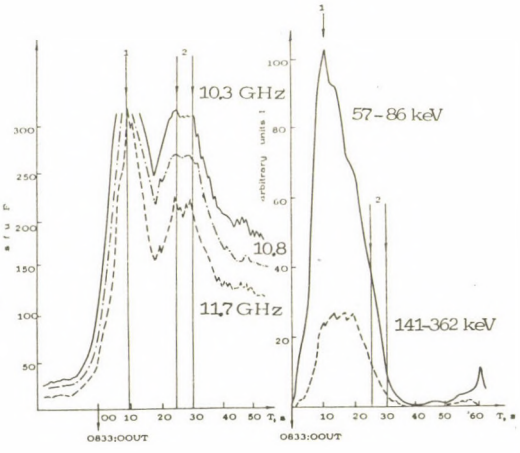

Fig.1 Shows microwave flux as a function on time for the flare 1981 November 5, about 08:33UT. Observation are at 10,8-11,4 GHz, and at 4-11, 8GHz (on the left). Right part shows SINGE-2M counting rate in the energy ranges 57-78keV, 125-350keV, as a function of time during the flare.

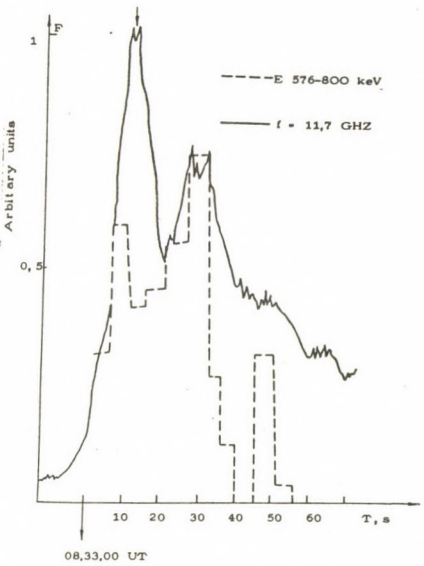

Fig.2 The same as Fig.1 for microwave flux at 11,4HGz in comparison with Ex> 500 keV photon counting rate. The scale in arbitrary units is linear.

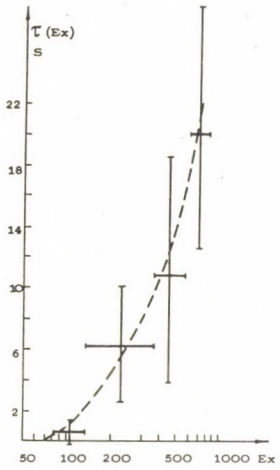

Fig.3 Time delays of the maxima in the five channels of SIGNE-2M as a function on energies. The curve calculated for plasma density $\cong 2*10^{11}$ cm^{-3} and $\delta\tau \sim E^{3/2}$.

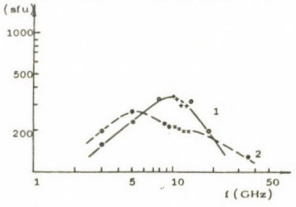

Fig.4 Microwave spectra compiled from SGD (o,o), and RT-22 data (x); at the time of the first feature (about 08:33:10UT) (o,x) at the time of the second feature (08:33:25UT) (o,x) (o,x).

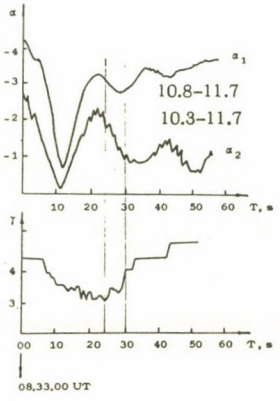

Fig.5 Curves of the spectral indices α1 and α2 as a function on time for two frequencies intervals 10,8-11,4 GHz and 10,3-11,8 GHz respectively, and γ for power-law X-ray energies.

Let $\gamma(t)$, $\delta(t)$ and $\alpha(t)$ denote the spectral indices of the hard X-ray photon flux, the source distribution of energetic electrons and the optically thin part of the microwave spectrum, respectively.

INTERPRETATION. We find the most reasonable explanation of this event in the trap+precipitation model. The hard X-rays are due to thick-target emission from non-thermal populations of electrons. The fast electrons have an energy spectrum which is approximately a single power dependence between a few ten keV and 700keV with $\delta \cong \gamma+1 \cong 4{,}2-4{,}7$.

The first microwave peak and the X-ray peak for photon energies of about 57-300keV were emitted by electrons streaming down the legs of a magnetic loop. The energy spectrum of electrons δ is compatible with the microwave spectral index. The high energy electrons are trapped for 10to 15s. The trap density was $n_i \cong (1-4)*10^{11} cm^{-3}$. We estimated the total number N_o of electrons above energy E_o>100 keV up to 300 keV in the microwave source for first *feature* $N_o=10^{31}$ and magnetic field value B≅500G.

The second micro- wave peak grew as the number of trapped high energy electrons increased. Tests proved by Kai,(1986) demonstrated that F_μ is larger for trap model than for the precipitation model by an order of magnitude of two to three. This way we can explain why the microwave flux in the first and second peaks have practically the same value while the number of electrons differs by 300 to 500 times. Moreover the shapes of the frequency microwave spectra in both peaks $\alpha 1=1$, $\alpha 2=0{,}45$ are consistent with the slopes of the curves for nonrelativistic and relativities power-law electron distributions obtained by Ginzburg and Syrovatskii(1965) .If there is some preferential trapping of the high energy (microwave-producing) electrons in the upper part of the magnetic loop, the B value will decrease. According to this we see a shift in the position of the maximum frequency of the second peak.

Also note that as far as we know from SGD, a type V burst was observed at 08:33-08:36 UT. Therefore, the existence of some number of trapped electrons in the upper chromosphere and the corona seems plausible.

REFERENCES BogovalovS.V etal.,Cosmicheskie. Issledovania, 1989, 27, 907.
Chambon G., et al., Space Si. Instr.,1979,5,73.
Kai K, Sol Phys., 1986, 104, 235.
Panfilov X.D., et al., Bulletin of Invention, 1981,No11, Author certificate No 81567 (USSR).

SESSION 5

May 24, Thursday (a.m.)

SPECTROSCOPY OF THE UPPER ATMOSPHERE

Chairman: Ph. LEMAIRE
Institut d'Astrophysique Spatiale - CNRS, Univ. de Paris
Verrières le Buisson

Invited reviews:

J. SYLWESTER
X-ray Spectroscopy of the Upper Solar Atmosphere

H. E. MASON
UV and EUV Spectroscopy of the Upper Solar Atmosphere

and 10 (oral and poster) contributions

X-RAY SPECTROSCOPY OF THE UPPER SOLAR ATMOSPHERE

J. Sylwester
Space Research Centre, Polish Academy of Sciences, Wrocław

1. INTRODUCTION

The aim of this review is to comment on selected problems which, in my opinion, constitute important set in the field. Especially, I would like to stress these observational evidences which link up with the fine filament source structure.

The solar soft X-ray (SXR) spectroscopy has been a subject of intensive research during past two decades covered by now in the numerous reviews [1,6-12,14-19,21,22,25-27,29,30].

I would restrict my review to the soft X-ray wavelength interval 1-25 Å. A multitude of prominent features from excited stages of many abundant ions of N, O, Ne, Na, Mg, Al, Si (K-shell transitions), Ar, Ca, Fe and Ni (K- and L-shell transitions) are contained in this band. All these features are detected in emission above the continuum. This region of the spectrum is most easily accessible to measurements by using the Bragg crystal spectrometers of various types, in which a dispersive element consists of the flat (bent) crystal of preselected spacing. A description of the properties of crystals used in the soft X-ray astrophysical spectroscopy may be found in [3], while the basic theory of X-ray diffraction is explained in [4]. A list of important recent space experiments has been prepared by Doschek [8]. Much of this review will deal with interpretation of the spectra obtained by P78-1, SMM and Hinotori experiments. The spectrometers placed aboard these spacecrafts were scanning devices, therefore on the SXR spectra the intensity at each wavelength has been recorded in slightly different time. The exception was the XRP-BCS spectrometer incorporating the bent crystal architecture which allowed the whole spectrum to be recorded at the same instant. What seems to be a deficiency of the spectrometers mentioned is that they had the entire solar disk within the field of view. As a consequence no absolute wavelength calibration was possible, except the XRP-FCS equipped with 13"x13" collimator.

2. X-RAY SOURCES IN THE SOLAR CORONA

Spatial resolution of recent imaging instruments makes possible (to some extent) to observe individual structures in the corona. Most of the structures observed in white light could be disassembled into separate loops or arches of diameter down to 1000-2000 km and lengths from several thousand to several hundred thousand km. The shape of the structures is evidently imposed by the configuration of the magnetic field in the corona. Extension of imaging to UV and SXR produced evidences (SKYLAB and earlier rocket experiments) of a similar appearance of a corona in bands most directly related to the characteristic coronal temperatures $T \geq 1$ MK. Therefore, the outstanding aspect of the coronal sources is their inhomogeneity. In "classical" coronal structures like bright

points, active regions and flares the emission is organized in the loop like volumes (loops). The elementary loop has its footpoints anchored in the lower temperature regions of opposite magnetic polarity. These bright structures have higher emission because of the increased, relative to the ambient volumes, density of the confined plasma. This is caused by increased energy deposition within these volumes. The plasma is kept inside the loop by action of the sufficiently strong magnetic pressure. Structures related to the "open" field lines (lines going sufficiently far from the Sun to be regarded as open) are weak in SXR emission (coronal holes). Structures related to magnetic field lines emerging from active regions, where the lines are densly packed, assemble the apparent bright coronal active region atmosphere. Loops may connect opposite polarities in different active regions; sometimes they cross the equator. Recent (normal incidence) NIXT images[64] obtained with superior resolution in the Fe XVI line at 63.5 Å (T ~ 2-3 MK) show structures down to perpendicular scale of about 0.75 arc sec (500 km) with indications that *self-similar* fine structure persists down to much smaller scales. The loop structures generally terminate in the penumbra of the spots. It is observed on the high resolution SXR images of the corona that the cross-section of the individual loop does not vary substantially throughout its length. Some loops appear to be slightly wider at the apex relative to the footpoint, but generally not more than a factor of 3. UV images of flare loops analyzed in[56] show for most of the loops no pronounced variation in the loop widths along their lengths. However, the finite resolution of the observations may account partly for the effect of no or small variation of the cross section. The reason for slow divergence of the field lines could be the presence of field parallel currents inside the loop. This regions of stronger (overpotential) field are most probably surrounded by volumes with a relatively weaker fields (no currents) which may correspond to the diffuse SXR component in active regions[14]. However (see H. Mason review[16]) Mg X ion line analysis indicate for filamentary structure even in these diffuse regions. Rather slow divergence of loops, implies corresponding slow decrease of the magnetic field strength along the length of the loop, slower than resulting from point or line dipole potential field approximations.

The implicit assumptions behind the elementary loop idea are that the magnetic field is everywhere well-ordered, and the physical conditions inside the loop are *uniform across* (but could vary *along* the length), with a sharp outer boundary . This means that the energy deposition is uniform in the plane across the loop. The assumption of cross-B uniformity has been challenged recently by interpretation of the BCS flare spectra[100,101].

In relation with dominant role of the magnetic field in the corona, the local physical conditions may substantially differ on perpendicular scales, of the order of the gyro-radius of dominant plasma constituents: protons, and alpha particles. These scales are in most coronal situations smaller than few

meters.
We are still learning about the mechanism which heats-up the corona i.e. the whole ensemble of individual loop entities. Spectroscopical hard, SXR, EUV and radio data provide the most important information on the possible energy deposition processes. Most of the present ideas on coronal heating[23] draw on magnetic energy to heat the plasma. It appears that the energy deposited in the corona (i.e. particular set of individual loop structures) comes, from dissipation of the overpotential part of the energy stored in the actual non-potential configuration of the local magnetic field, with some role played possibly by MHD waves[14] for long lasting (more than half of a day) structures. Parker[23] advocates the idea that *the X-ray corona is essentially a cloud of nanoflares*.

2.1 STEADY STATE IDEALIZED PICTURE
What would be expected if the inhomogeneous corona is in steady state and the rate of volumetric heating e_H is inhomogeneously distributed through the corona? Since each magnetic field line could be associated with an "independent coronal atmosphere" (if one neglects for simplicity cross-field transport processes), the structure of the atmosphere along the field line can be described by the solution corresponding to steady state scaling laws. Two types of structures are expected for close field line topology, corresponding to the so called hot (classical RTV-Rosner,Tucker and Vaiana[85]) and cool (AN-Antiochos and Noci[34]) solutions. In the hot solutions, the pressure along the loop is approximately constant, the temperature structure determined by conduction, and the transition region extremely sharp. Maximum temperature is above ~1.5 MK. In cool solutions, all gradients (pressure, temperature, density) are defined by gravity, the transition region is extended, maximum temperature is less than the temperature at which the radiative loss function (RLF) reaches maximum (T_{maxRLF}) . Flows should be common in cool loops[76] as being easily induced by even minor asymmetries in heating. The maximum temperature is located (in most of the simple cases) at the apex in both types of solutions. Scaling laws predict[14,34] the forms of dependence of essential physical parameters of static loop atmosphere on the maximum rate of energy release e_H shown in Table I. Since the UV and SXR volumetric emission rate is proportional to the emission measure ε ($d\varepsilon = N_e^2 dV$), the total coronal emission would be roughly proportional to $\int_V e_H dV$. (where V is the volume of the heated plasma). The SXR arises from plasma being at $T > 1.5$MK, therefore hot solutions are of greater interest for interpretation of this radiation.
It follows from Table I that the temperature and the density of the plasma in the loop increases together with increasing the rate of energy deposition - the conclusion confirmed by

observations[44,34]. The rate of energy deposition in steady state structures may reach 0.1 erg/cm^{3}s and the thermal energy density tens of ergs/cm^3.

Table I
Scaling of physical parameters in steady state loops

	Hot (RTV)	Cool (AN)
T_{top}	$\sim e_H^{2/7} L^{4/7}$	$T_{top} < T_{maxRLF}$
N_{top}	$\sim e_H^{4/7} L^{1/7}$	$\sim e_H^{1/2} \left[P_r(T_{top})\right]^{-1}$
SXR volumetric emission rate	$\sim e_H^{8/7} L^{2/7}$	$\sim e_H \left[P_r(T_{top})\right]^{-2}$

Here L is semilength of the structure, T_{top} and N_{top} are temperature and density at the apex, P_r represents the radiative loss function.

2.2 TRANSIENT IDEALIZED PICTURE

The most intense and violent SXR sources are solar flares in which the local rate of energy deposition may reach tens of ergs/cm^{3}s and the plasma energy density hundreds to thousands of ergs/cm^3. In flares, a large amount of energy (up to 10^{31-32} ergs) is released in small volumes in the corona in time scales short (~100-1000s) compared to relaxation time to steady state. During flares, imbalance exists (for an atmosphere along the field line) between the total input energy and the integrated radiative losses forcing other forms of plasma energy to be activated, i.e.: turbulent and directed plasma motions, particle acceleration, waves. Turbulence may cause substantial increase of the transport rates across the magnetic field lines (diminishing them along field lines) and may allow for physical linking in cross-B direction[68]. Beams of accelerated particles generated in flare may influence transport along the field lines. During initial flare phases, (over)exposure of the transition region (TR) plasma to the increased energy deposition along the related field line causes the TR plasma to evaporate rapidly, filling the corresponding structure with matter thus increasing (local) density by orders of magnitude.

3. TASKS OF THE SXR SPECTROSCOPY

Three general tasks emerge in context of the soft X-ray spectroscopy of the solar corona:

a) Identification of the observed spectral features
b) Identification of the atomic processes responsible for their presence
c) Reproduction of the observed spectra, based on (*a* & *b*) and the appropriate *physical model* of the source.

Most of the problems related with task *a* and *b* have been solved to the level accomplishing the accuracy of the measurements. I

refer the reader to a number of review papers[2,10,11,12,21,27,28] and to papers on recent new line identification in the following ranges: 1.85–1.89 Å[71] 1.89–1.92 Å[82], 3.12–3.24 Å[88], 5.7–19.6 Å[83], 7.8–10 Å[58] and 10–200 Å[56]. With inclusion of the processes leading to formation of the doubly excited states, the understanding of the spectral shape in vicinity of the strong resonance lines has been possible. Numerous satellite lines[11] have been identified both in solar and laboratory[2] plasma and the ionization temperature scale became better adjusted with the electron one. The accuracy of calculations of the transition rates corresponding to resonance and so called dielectronic satellite lines is by now adequate to explain SXR spectra of the laboratory plasma to within few percent[13,39,5]. Therefore, satellite to resonance line intensity ratio temperature diagnostics is well sounded on both theoretical and experimental side. However, there is less confidence in the accuracy of the ionization balance calculations. Especially, the exact values of ionization/recombination rates are to be concerned about (Chapter 4.3). The temperature dependence of line[79] and continuum[80] emissivities have been recalculated and tabulated based on the best selection of atomic data.
What concerns task c, the reproduction of the observed spectra depends on how realistic is the physical model of the source. Variety of possible physical circumstances concerning the source plasma have been suggested. I have listed some of them:

a) Plasma composition (uniform, non-uniform, steady or time dependent),
b) Local or non-local approximation for transport and excitation processes,
c) Maxwellian or non-Maxwellian velocity distribution,
d) Equilibrium or non-equilibrium ionization state,
e) Optically thin or thick source,
f) Dynamic state of source plasma,
g) Electron vs ion velocity distribution,
h) Izothermal or multi-temperature structure of the source.

The most natural choice of assumptions concerning the physical conditions prevailing in the source is the following simplest one: locally Maxwellian, isothermal plasma of uniform composition in ionization equilibrium, optically thin in SXR. Some of the authors address models using different set of assumptions. I would like to mention shortly these attempts.

3.1 NON-LOCAL EFFECTS

Classical plasma kinetic and transport theory gives an appropriate description of most of the loop atmosphere. Exceptions arise when transition regions (TR), separating volumes of different temperature exist (chromosphere-corona TR for example). The results of the numerical simulations and laboratory observations discussed in [25,93,81] show , that the "classical" conductivity tends to overestimate the actual heat flux in upper transition region boundary layers by factors 2-10. Furthermore, the local electron distribution is not fully determined by local conditions, particularly in the tail of the

distribution. Two difficulties are pointed out[25]: first, that the local conductive flux and its divergence, cannot be derived from local measurements of the temperature gradient alone, but instead depend on the temperature profile as a whole. Second, that the enhanced energy tails can significantly affect ionization balance in the transition region. For further discussion of this problem and the transport perpendicular to magnetic field see[25]. Peres, Rosner and Serio[81] warn that *naive* (local approximation) *loop atmospheres may be substantially incorrect*. Karpen et al.[69], based on results of non-local hydrodynamic modeling of flaring loop predict that the blue-shifted component is less intense and less Doppler-shifted than its classical counterpart. The 'classical' two-component line structure predicted during the early impulsive phase does-not exhibit the splitting at any time during the flare in the non-local approach (as observed in most cases). Siarkowski et al.[92] considered the role of an increased amount (1%) of high energy tail electrons present in a lower temperature region (due to leaking from the neighboring higher temperature region) on the intensity of lines in the Mg XI 'triplet' band. They found that this small admixture of non-thermal electrons (marginally non-thermal model, MNTM) leads to a considerable increase of the collisional excitation processes in the resonance, intercombination, forbidden and innershell-excitation lines, without increasing the dielectronic satellite line intensity. MNTM could be useful in interpreting spectra for which innershell excitation lines are more intense than expected.

Jakimiec et al.[67] discuss the reverse situation, i.e. possible effects of leaking of the high energy tail electron distribution (caused by a small size of the high temperature region, comparable or less than the corresponding free path distance). Leaked electrons do not contribute to the high temperature line radiation because of no appropriate ions present but contribute to the continuum flux. This effect may account for at least part of the line-to-continuum ratio depletion (in Ca or Fe spectra) during the initial flare phase[61]. Presence of non-isotropic electron distribution could cause the SXR line radiation to be polarized. Detailed discussion of polarization effects on particular line intensities is given in[117].

3.2 OPACITY EFFECTS

Intensities of resonance lines for the most abundant elements could be modified from their optically thin value by the effect of scattering in the source[95]. The effect depends on the shape of the emitting volume being non-spherical and the optical thickness being not negligible (say > 0.1). The underlying assumption is that radiation in the direction of the longest dimension of the plasma (along the field line) suffers more scattering (i.e. resonance absorption) than radiation in other directions so that its intensity in that direction is reduced. However, when it is re-emitted in some other direction it escapes more readily giving some enhancement of the

intensity in this direction. For instance, in the Mg XII doublet at 8.421 Å[76,78], the more intense of two components should show this effect more strongly than the weaker so the intensity ratio can differ measurably from value $\cong 0.5$ predicted by theory[74,75]. Wide distribution of this ratio values (0.3-0.7) has been observed both for the INTERCOSMOS-7 and XRP-FCS spectra. These measurements can be explained based on the resonance scattering hypothesis. There are earlier rocket observations of the G-ratio for oxygen reported in[31] which also point towards the importance of the opacity effects in interpretation of the strong resonance transitions. Therefore, it seems substantial when interpreting line emission in resonance transitions of abundant elements to check whether optically thin assumption is adequate in the context of the investigated problem.

4. NARROW - BAND SPECTRAL ANALYSIS

It is clear by now, that virtually no SXR region is free from line emission; especially heavy blending occurs close to strong resonance lines. This implies that the preferred procedure to interpret measured spectral profiles is by means of spectral synthesis, where the flux measured in a particular wavelength bin is calculated based on the appropriate source model. Detailed knowledge of the sensitivity and instrumental response of the spectrometer $I(\lambda-\lambda_o)$ (windows due to first and higher order Bragg reflections) constitute substantial factor in calculations of the synthetic spectrum:

$$f(\lambda_j)=\int_{1}^{25\ \text{Å}} \left[\int f(\lambda_i,T,T_{ion})\varphi(T)dT\right] I(\lambda_j-\lambda_i)d\lambda_j \quad . \qquad (1)$$

Here $f(\lambda_i,T,T_{ion})$ is the expected level of the line and continuum emission at λ_i wavelength, including influence from all lines present, and the overlapping spectra from different sources (if uncollimated instrument).
Expected count rates in bins $f(\lambda_j)$ are therefore a complicated function of the model source ($\varphi(T)$, for instance). Problems with overlapping the line profiles from sources distributed on the solar disc in direction of the dispersion have received recently some attention. Zhitnik et al.[117] treated this as an inverse problem using multiplicative deconvolution algorithm. Results of the procedure applied to deconvolve the spectra measured by Vertical-9 and -11 are encouraging.
Most of recent SXR spectral data have been obtained in the narrow spectral intervals covering bands of 1-2 Å width in vicinity of strong spectral features. This was caused mostly by reasons of engineering or operational nature. This character of spectral measurements allowed for a special simplified analytical treatment when interpreting line intensities (narrow-band approach, NBA). When synthesizing the spectrum in narrow wavelength interval, where lines are present with similar dependencies of emissivity on temperature, it was found

that in most cases it is reasonable, for the spectroscopic purposes, to apply the isothermal approximation. Within the NBA approach, after fitting the synthetic spectrum, it is possible to decompose fluxes of lines forming the blends, into individual line components which afterwards may be used for further interpretation. Below I shall discuss few applications of the NBA concept.

4.1 PLASMA DYNAMICS IN FLARES

High resolution spectra in vicinity of strong resonance transitions of Fe XXV, XXVI, Ca XIX, XX and Mg XI, XII ions revealed presence of increased blue wing emission and increased width of lines during the rise phase of most flares. This rise phase spectra have been successfully fitted within NBA approximation, by incorporating two component model with stationary and moving plasma in the source[4]. A single component fits were found unsatisfactory for most of initial phase disk flare spectra[60]. Although the actual distribution of velocities in the flare plasma might involve more than two components, or be in fact a continuous distribution of velocities, even the two component approximation has more than enough free parameters to make the fit unique. The observations of anisotropic bulk motions of high temperature plasma (T > 2 MK) have been done before but with much lower sensitivity[70]. The single loop evaporation picture is usually applied in interpretation of the blue-shifted component and the observed rate of rise of the emission measure[4]. Different points of view are also advocated.

Gabriel et al.[62] pointed that model with evaporating region located deeper, in a well in the surrounding transition region, may explain the observed center to limb variation of the velocity and relative intensity of blue-shifted component (due to occultation) for limb flares. Such a model fits data the best if the blue-shifted plasma component has a pronounced filamentary structure. Antonucci[4] argues that blue-shifts are correlated with the impulsive hard X-ray emission which may indicate that their presence is a consequence of the ongoing energy release. Combined interpretation of intensities of Ca and Fe lines allowed to estimate the temperature of blue-shifted component[60]. Surprisingly, this temperature agrees with the temperature of the stationary component, with indications that it could be even higher. This may suggest that flare energy release is located somewhere low in the loop. Doschek et al.[59], based on spectral synthesis of Ca XIX and Fe XXV bands, performed similar analysis of the long-lasting flare and found that the blue-shifted component was several MK cooler than the stationary one, and was present for at least 28 min. from the onset of the event (the blue-shifted emission was not of "impulsive" character for this flare). Interpretation of the time variations of derived emission measure values for stationary and blue-shifted components leaves no room in this case for a single loop interpretation. It was suggested that some of the plasma responsible for blue-shifted component leaves the flare region (being related

to open field line magnetic structures) or that some of the flaring loops cool fast. This flare seems to be a good example of the event in which multiple loop structures are activated in a sequence. Each of the loop has its blue-shift phase delayed relative to the predecessing one. Accordingly, the overall observed history of the blue-shifted component characteristics arise from superposition of contributions from individual flaring loops, some of them cooling possibly faster than the other. This picture of time dependent activation of heating in consecutive flaring loops get support from observations of blue-shifted component in lines formed in cooler plasma. Zarro and Lemen[116] presented FCS observations of entirely blue-shifted Mg XI (T ~ 6 MK) resonance line profiles during *decay* of flare. The authors incorporate conductive-evaporative cooling, single loop model to interpret the observations, but within such model it is possible to explain only a short period (5 min) during the early decay. Multiple loop model could provide easier interpretation of these observations.
The increased line widths observed during early phases of flares are usually attributed to presence of significant turbulence. The observed widths are increased also in preflare period of some flares, big enough that their spectra could be measured well before onset of the hard X-ray impulsive phase. This observations have important consequences for interpretation of the energy release mechanisms[66,67,41,1]. Fludra et al.[60] based on their elaborated method of two-component spectral fitting, found evidences for presence of turbulence late in the flare decay and for continuous upflow during gradual phase. They pointed that correlation of these two types of motions is present for flares with intensive plasma upflows. Increased (above the thermal) widths of lines are also observed[86] in non-flaring active regions, at locations above the neutral line.

4.2 ELECTRON DENSITY

The determination of electron density in the corona from density sensitive line ratios is another example of NBA approach. A detailed review of different diagnostics has been given recently by Mason[15]. In SXR range , the density sensitive ratios are available for plasma temperatures of T ≤ 6 MK. P78-1 spectra analyzed by McKenzie[77] revealed the variation of R ratio (forbidden/intercombination line intensity) in He-like oxygen ion (T ~ 2 MK). If interpreted by theory[12], these variations reflect the increase of density from 0.5 to 2.0 10^{11} cm^{-3} during the flare rise phase. Electron density measurements (SMM-FCS) have been also derived from the ratio R of the helium like Ne IX ion (T ~ 3-4 MK) by Bhatia et al.[38] in the two-temperature approximation. Density of 1 10^{12} cm^{-3} has been obtained at the peak of the flare with subsequent decrease by order of magnitude 20 min later. From interpretation of R ratio for Mg XI ion Zarro et al.[116] found densities up to 5 10^{12} cm^{-3} early in the flare with subsequent decrease by order of magnitude to the end of flare. The same ratio was analyzed in[44] for active region spectra measured by

INTERCOSMOS-16 and a trend to increase the density with increasing the average plasma temperature has been found. An interesting way to interpret R ratios close to the low density limit on the (R-G) diagram has been suggested. McKenzie[77] found that in 10% of measurements (P78-1) for active regions the R ratio measured in O VII was below the low density limit pointing to densities 4-8 10^{9} cm^{-3} or below at the temperature 2 MK. Rather high densities determined spectroscopically for active regions and for the low-temperature component in flares require very small volumes occupied by a plasma with observed emission measure. This conclusions are in agreement with the concept of highly filamentary structure of the corona. Zarro et al.[110] values for density and emission measure lead to effective cross-dimension of emitting structure of the order of 100-1000 km. This implies very small instrumental filling factors, of the order of 10^{-5}-10^{-2}. We are still short of spectroscopic measurements of the source plasma density in the temperature range above 10 MK.

4.3 IONIZATION EQUILIBRIUM

Many observational evidences indicate for unsatisfactory state of present ionization equilibrium calculations. Before pointing these evidences, let me summarize the role of possible non-equilibrium effects expected to play a role during the early rise phase of flares when the flare plasma is being heated to T > 10 MK. The ionization temperature as measured by the fractional population of the highly ionized ions may lag behind the electron temperature in this phase, due to finite time required to ionize ions. That is, at the particular electron temperature, the ion fractional populations are characteristic of a temperature lower than in ionization equilibrium. If the density is high enough, there would be no perceptible differences in ionization and electron temperatures over time scales greater than seconds. However, for sufficiently low densities, large differences may exist. The equilibration time (the longest for Fe ions) is quite short (<10 s) for reasonable flare electron densities and temperatures as pointed out in[52]. No strong conclusion has been reached on presence of transient conditions in flares, based on analysis of the collected spectra. However, as many people expect, the increase in the spectrometer sensitivities by an order of magnitude relative to SMM-BCS or Hinotori would allow to see transient effects in flare iron spectra[52].

If ionization equilibrium is assumed, then the distribution of fractional ion populations at given temperature (often called ionization balance) may be derived. There are now several sources of ionization and recombination rates allowing the ionization balance calculations. These are given in[84,90,55,37,20]. These different calculations lead to significantly different spectra. Figure 2 in[71] provides an illustration of the differences that result from the choice of ionization balance. The analysis of the calcium and iron spectra from P78-1 and SMM[54] have shown that present

calculations of ionization equilibrium cannot reproduce accurately the temperature variation of the Ca/Fe resonance line ratio. Doyle and Raymond[55] proposed ionization balance calculations with ionization rate coefficients smaller than adopted by other authors. With these smaller ionization rates, for a given electron temperature iron and calcium are not as highly ionized as in the Arnaud and Rothenflug[37] for instance. Antonucci et al.[35,36], published semiempirical ionization balances corrected to fit measurements of highly ionized calcium and iron ion fractions. Doyle and Raymond[55] and Antonucci et al.[35,36] balances agree better with Doschek at al.[54] results, and with results of analysis of the line to continuum ratio[105,67,107]. Therefore, it appears that the ionization balance calculations with ionization/recombination rate ratio decreased by factor ~ 2 better describe the temperature dependence of fractional He-like ion abundances. What concerns the interpretation of the H/He like line ratios for iron, Tanaka[109], derived temperature trend that could be fitted if the ionization/recombination rate ratio is increased (relative to this used in[37]) by factor of about three.
Presence of above mentioned discrepancies may indicate a real problem in this part of atomic physics which provides ionization/recombination rates.

5. DIFFERENTIAL EMISSION MEASURE

Isothermal approach usually fails, when used to fit spectra containing lines formed in significantly different temperature ranges. This most probably indicates that the structure of the source is of a multitemperature nature. One of the important goals of the spectral analysis is determination of the temperature distribution of differential emission measure (DEM) in the source. DEM distribution fully determines the output SXR spectrum for a plasma of a given composition and defines the total radiative energy losses in the source in EUV and SXR range.
The unknown, always positive DEM distribution $\varphi(T)$ may be derived based on measured fluxes $\mathcal{F}_i$ (in selected bins, lines, bands etc.) by solving the following system of integral equations:

$$\mathcal{F}_i = \int_0^\infty f_i(T)\ \varphi(T)\ dT; \quad (i = 1,2..k). \qquad (2)$$

The temperature dependence of the kernel emission function $f_i(T)$ is known from atomic theory.

Procedures used for deconvolution of Eq. (2) have been critically discussed in[102]. Since that time several new deconvolution techniques have been tested and applied to various data bases. Fludra and Sylwester[59] compared three methods of DEM analysis, namely: conjugate gradients (CG), maximum entropy (ME) and modified Withbroe[114] iterative technique (WS)[102]. It turns out that WS method gives acceptable solutions when the unknown DEM distribution is

likely to be continuous in broad (several MK) temperature intervals. The ME method, though time consuming is recommended when no additional a priori information about $\varphi(T)$ is available. Modified CG method is effective in deriving regularized solutions. Tests have been performed to what extent different procedures for deriving DEM are pointing towards similar solutions. Cross-comparison presented in[59] is illustrative and indicates that in spite of inherent non-uniqueness in the problem of $\varphi(T)$ determination[48,49], all compared methods provide similar results. In the process of deconvolution it is possible to "resolve" structures in the DEM distribution of the characteristic width slightly less than the width of the emission function peaking at a corresponding temperature. Different approach to inversion of the set of input Eqs. (2) was made by Siarkowski[92]. He applied the nonlinear least square method (NLS) and compared the results of inversion with the corresponding WS output. The NLS method appears to be better in recovering discontinuous types of $\varphi(T)$ distributions and may be directly applied to estimate the plasma electron density, if density sensitive lines are included in the input data set. Lemen et al.[73], have used parametric approach suggested in[45]. They expressed DEM as $\varphi(T) = \alpha \exp(\omega T)$; (with ω being the polynomial function of temperature) and derived set of a_j values in the process of best-fitting. Solutions are in agreement with corresponding results obtained by WS method. In conclusion, it appears that recent methods of DEM deconvolution, if used with the same input data and formulated to satisfy the *a priori* general condition that $\varphi(T) \geq 0$, provide similar solutions. This paves the way to the physical interpretation of the DEM distribution calculations based on measured inputs. Despite some ambiguity in the precise shape of the calculated DEM distribution, the total emission measure i.e.

$$\varepsilon = \int \varphi(T)\, dT \quad ; \tag{3}$$

as well as higher moments of DEM distribution (representing for instance the plasma thermal energy content), can be computed to within a few percent.

It turned out from SMM-XRP data analysis that the two component DEM model fits observations the best for flares[33,97,115,42]. Both components (T ~ 4-7 MK and T ~ 10-25 MK) preserve their identity during flare evolution which may indicate that they are related to physically separate regions (separate loops with different pressures?). If reconfirmed generally, presence of individual components in DEM distribution could be a result of different modes of energy dissipation (with characteristic rates of energy dissipation differing by two orders of magnitude). The two component character of DEM flare distribution has been reconfirmed by independent technique of Bornman[42], which make use of the time dependence of measured fluxes $\mathcal{F}_i$, together with measured fluxes itself. In this way, it was possible to overcome some problems related to the instrument calibration or elemental abundances uncertainties,

which may bias the results of DEM analysis. It should be noted however, that in spite the apparent success of two temperature DEM approximation in explaining the selected set of SXR line intensities, this approximation is to simple to account for some of the measurements. Spectra obtained by Hinotori[108,109] suggest that for some flares, a superhot component is present during flare maximum with characteristic temperature ~ 40 MK. Presence of this component (or a corresponding non-thermal counterpart in the electron distribution) is necessary to account for the observed intensities of Fe XXVI/XXV Lyα complex at 1.78–1.80 Å.
The observed shape of the DEM distribution for flares and active regions[40,14] can not be explained in a single loop approximation neither with varying cross section geometry, nor with transient flaring conditions. As pointed out by Antiochos and Noci[34], combination of loops corresponding to both hot and cool solutions is sufficient to explain the observations qualitatively and predict the observed ratio of the SXR to EUV emission measures for these structures. Presence of a system of individually flaring loops or loops with temperature gradient across them[100,101] seems necessary to explain observed flare DEM distributions.

6. COMPOSITION OF THE CORONAL PLASMA

A revival of interest in solar abundance determinations has recently taken place because of new sources of information, such as solar flare γ-ray emission[24], in situ composition measurements of solar wind[03,40] and solar energetic particles[43]. Interpretation of all these new data indicate for presence of systematic differences in composition between the photosphere and corona. The most prominent feature is an enrichment of elements with a low first ionization potential (FIP $\leq$ 10 eV) relative to high FIP elements in solar wind and solar energetic particles by a factor of about four.
The SXR spectra of coronal structures contain emission lines of numerous elements like N, O, Na, Mg, Al, Si, S, Ar, Ca, Fe, Ni seen above the continuum, but no one of the experiments yet performed, was particularly designed for studies of the composition. Therefore the analysis of relative/absolute abundances from SXR spectra is limited to few cases of suitable ratios. The line ratio technique used in abundance studies is the most independent on the temperature structure of the source, when the emission functions of lines (belonging to different elements) have as similar as possible temperature dependence. In that case: $\mathcal{F}_{El_1}/\mathcal{F}_{El_2} = A_{El_1}/A_{El_2}\ f_1(T)/f_2(T)$, and the measured ratio of line intensities is related directly to the corresponding ratio of relative element abundances if $f_1(T)/f_2(T) \cong$ const.. When the line to continuum ratio is considered, then $\mathcal{F}_{El_1}/\mathcal{F}_{cont} = A_{El}\ f_1(T)/f_{cont}(\lambda,T)$. If the continuum emission is measured at such wavelength that $f_1(T)/f_{cont}(\lambda,T) \cong$ const, then the measured ratio is

proportional to the absolute (i.e.. relative to hydrogen) abundance of element, since the SXR continuum emission is nearly independent on the composition of elements heavier than He.

Veck and Parkinson[111], based on analysis of SXR line to continuum emission of flare spectra observed by the OSO-8 spectrometer suggested the idea that the differences between photosphere and flare plasma composition depend on FIP. Antonucci et. al.[36] and Doschek et al.[51] based on different line ratio analysis of BCS and P78-1 spectra argued that the enhancement of abundance for flare plasma is less for argon than for calcium, leading to an argon/calcium ratio smaller for flares than for the 'quiet sun'. Analysis of SKYLAB UV NRL spectroheliograms by Widing and Feldman[113], indicate changes of the neon/magnesium abundance ratio from a value of 2.2 in the prominence to 0.64 in the active region, while the magnesium to silicon ratio does not vary. Sylwester et al.[103,105,106,107] and Lemen et al.[72] investigated the flare to flare variability of the Ca XIX resonance to near-by continuum intensity ratio and found substantial differences in Ca abundance between flares (by factor up to four). Flare abundances are greater than photospheric ones and the active region dependence is suggested. The method of line to continuum ratio analysis seems to be the most promising for future SXR abundance studies.

Possible explanation of low/high FIP element differentiation and differentiation of abundances between the structures in the corona might be the ion-atom separation across magnetic field. In this mechanism, initially neutral particles are driven across the magnetic field undergoing ionization at different times and places depending on the type of the particle. Such a mechanism has been modeled in[112]. Results of modeling show that the mechanism could efficiently reproduce the FIP dependent fractionation, provided that there are structures in the atmosphere with length scales across the magnetic field of the order of 10 km.

Observed differences of the abundance between structures in the corona influence many spectroscopic problems. A few examples are: the calculations of a DEM distributions, diagnostics of electron density using lines from different elements, the calculations of the radiative loss function (RLF).The effect of coronal elemental abundances on the shape of the (RLF) has been investigated by Cook et al.[47]. They found that the use of coronal set of abundances instead of the photospheric one may substantially change the shape of the RLF, causing the peak to move from 2 10^5 K to temperature nearer to 1 MK. This may cause that the cool loop solution could be possible for temperatures greater than 2 10^5 K.

7. SUMMARY AND FUTURE PROBLEMS

Direct imaging, and discussed spectroscopic results provide arguments that solar corona consists of self similar loop-like structures (filaments) with cross-dimensions down probably to tens of km. This prompt conclusion, if confirmed by results of

dedicated researches, would have important consequences regarding the problem of coronal heating. Idea of filamentary corona has strong influence on the methodology of spectroscopy research and analysis, and probably will accelerate development of new observational and analytical techniques.
A major unsolved problem of SXR and UV spectroscopy is the nature of coronal structures which undergo subsequent flaring. We do not know physical conditions prevailing in loop structures which subsequently are sources of the SXR emission. Recent SXR spectroscopical experiments have suffered from either poor time and/or spatial resolution or low sensitivity. All present SXR spectra of the coronal structures have been obtained with spatial resolution insufficient to separate individual elementary constituents of the coronal atmosphere. Therefore, values of the spectroscopically derived physical characteristics should be considered as averages. A possibility of improved measurements of ionization state of plasma, its motions, composition, temperature structure, morphology (with resolution of the order of 1500 km over broad range of temperatures), etc. will come soon (1991) with the launch of Japanese Solar-A mission carrying aboard, among other instruments, the Bragg Crystal Spectrometer (BRCS) and the Grazing Incidence SRT Telescope. BRCS will have comparable spectral resolution to the best spectrometers flown, but will have approximately an order of magnitude higher sensitivity. Such sensitivity will make possible studies earlier in the rise phase of flares, which is crucial to resolve many 'hot' problems discussed in this review.
The use of the continuum level measurements appears to be the important tool in SXR spectroscopic diagnostics, as a basis for line intensity interpretation. Studies of line to continuum ratio may help in understanding the fractional ion equilibrium balance, non-equilibrium effects, plasma composition, role of non-local effects etc.
The discussion of the SXR spectroscopic results alone may leave the reader with somewhat limited view, therefore for a better perspective I strongly recommend Helen Mason's review[16] on the XUV aspect of the solar spectroscopy.

ACKNOWLEDGEMENTS
The author would like to thank dr. Barbara Sylwester for reading the manuscript and helpful discussion. This work has been performed within the Polish CPBP 01.20 program of Space Research. Prof. J.L. Culhane, Director of the Mullard Space Science Laboratory is acknowledged for making possible visit of the author to MSSL which helped in preparation of the review.

REVIEW ARTICLES AND BOOKS

[1] Antonucci, E: 1989, *Solar Flare Spectral Diagnosis: Present and Future*, Solar Phys., **121**, 31
[2] Boiko, V.A., A.Ya. Faenov, S.A. Pikuz: 1978, *X-ray Spectroscopy of Multiply Charged Ions from Laser Plasmas*, J. Quant. Spectrosc. Radiat. Transfer, **19**, 11

(3) Burek, A.: 1975, *Crystals for Astronomical X-ray Spectroscopy*, Space Sci. Instr., Vol. 2, 53
(4) Compton, A.H and S.K. Allison: 1935, *X-Rays in Theory and Experiment*, van Nostrand, New York
(5) Dolder, K: 1988, *The Study of Collisions Between Charged Particles by Crossed Beam Techniques in Astrophysical & Laboratory Spectroscopy*, ed.R. Brown and J. Lang, The Scottish Universities Summer School in Physics, 367
(6) Doschek, G.A.: 1972, *The Solar Flare Plasma, Observations and Interpretation*, Space Sci. Rev., **13**, 765
(7) Doschek, G.A.: 1975, *X-ray and EUV Spectra of Solar Flares and Laboratory Plasmas in Solar Gamma-, X-, and EUV Radiation*, ed. S. Kane, IAU, 165
(8) Doschek, G.A.: 1985, *Diagnostics of Solar and Astrophysical Plasmas Dependent on Autoionization Phenomena*, 1985, *in Autoionization*, ed. A. Temkin, Chapter 6, 171
(9) Doschek, G.A.: 1988, *Introduction to Solar Spectroscopy in Astrophysical & Laboratory Spectroscopy*, ed.R. Brown and J. Lang, The Scottish Universities Summer School in Physics, 237
(10) Doschek, G.A.: 1988, *The Solar X-ray Spectrum in Astrophysical & Laboratory Spectroscopy*, ed.R. Brown and J. Lang, The Scottish Universities Summer School in Physics, 279
(11) Dubau, J., and S. Volonte: 1980, *Dielectronic Recombination and its Applications in Astronomy*, Rep. Prog. Phys., **43**, 199
(12) Gabriel A.H., and C. Jordan: 1972, in *Case Studies in Atomic Collision Physics*, ed E.W. McDaniel and M.R.C. McDowell, North-Holland, p. 209
(13) Gianella, R.: 1988, *High Resolution X-ray Spectroscopy at Jet*, Journal de Physique, Colloque C1, Supplement au n°3, Tome **49**, c1-283
(14) Jakimiec, J.: 1987, *Investigation of the Coronal Part of Solar Active Regions from X-ray Observations*, in *The Sun*, ed. L. Hejna, M.Sobotka, Proceedings of the 10th European Regional Astronomy Meeting of the IAU, 219
(15) Mason, H.E.:1988, *Spectroscopic Techniques for Determining Electron Densities in the Solar Atmosphere*, 1988 Journal de physique, Colloque C1, Supplement au no 3, Tome **49**, Mars 1988, C1-13
(16) Mason, H.E.:1990, EUV *Spectroscopy of the Upper Solar Atmosphere, this issue.*
(17) Mewe, R.: 1984, *Hot Optically Thin Plasmas in Astrophysics*, Physica Scripta, Vol. T7, 5
(18) Mewe, R. : 1989, *Ionization of Hot Plasmas*, in *Physical Processes in Hot Cosmic Plasmas*, Kluwer Acad. Publ., Dorderecht, *in press*
(19) Mewe, R.: 1988, *Ionization Balance in Low-density Plasmas, Steady-State and Transient Case* in *Astrophysical & Laboratory Spectroscopy*, ed. R. Brown and J. Lang, The Scottish Universities Summer School in Physics, 129

[20] Mewe, R.: 1988, *Ionization Rate Coefficients in Astrophysical & Laboratory Spectroscopy*, ed.R. Brown and J. Lang, The Scottish Universities Summer School in Physics, 141
[21] Mewe, R.: 1988, *Satellite Lines as a Diagnostic in Astrophysical & Laboratory Spectroscopy*, ed.R. Brown and J. Lang, The Scottish Universities Summer School in Physics, 167
[22] Noci, G.: 1971, *Atomic Processes in the Solar Corona*, in *Physics of the Solar Corona*, ed. C.J. Marcis, 13
[23] Parker, E.N.: 1990, *Solar and Stellar Coronae*, Adv. Space Res., Vol **10**, No **9**, (9)17
[24] Ramaty, R., and J. Murphy: 1987, *Nuclear Processes and Accelerated Particles in Solar Flares*, Space Sci. Rev., **45**, 213
[25] Rosner, R., A.B.C. Low, T.E. Holzer: *Physical Processes in the Solar Corona*, 1986, in *Physics of the Sun*, ed. P.E. Sturrock Chapter 11, Vol. **II**, 135
[26] Sylwester, J.: 1988, *Coronal Loops - X-Ray Diagnostics*, Adv. Space Res., Vol. **8**, No **11**. (11)55
[27] Walker Jr., A.B.C.: 1976, *Spectroscopic Analysis of Solar and Cosmic X-ray Spectra*, Space Sci. Instr., Vol. **2**, 9
[28] Vainstein, L.A. and U.I. Safronova: 1978, *Wavelengths and Transition Probabilities of Satellite to Resonance Lines of H- and He-like Ions*, Atomic and Nucl. Data Tables, **21**, 49
[29] Zirin, H.: 1988, Chapter **8**, in *Astrophysics of the Sun*, Cambridge University Press
[30] Zirker, J.B.: 1987, *Spectroscopy of the Solar Corona*, in *Spectroscopy of the Astrophysical Plasmas*, ed. A. Dalgarno and D. Layzer, Cambridge Astrophysics Series, Cambridge Univ. Press, Chapter **6**, 165

ARTICLES

[31] Acton, L.W., and R.C. Catura: 1976, Phil. Trans. R. Soc. Lond. A. **281**, 383
[32] Acton, L.W.: 1978, Astrophys. J., **225**, 1069
[33] Akita, K.: 1982, *Proceedings of Hinotori Symposium on Solar Flares*, Institute of Space and Astronautical Science Publication, Tokyo, 58
[34] Antiochos, S.K., G. Noci: 1986, Astrophys. J., **301**, 440
[35] Antonucci, E., M.A. Dodero, A.H. Gabriel, K. Tanaka, J. Dubau: 1987a: Astron. Astrophys., **180**, 263
[36] Antonucci, E., D. Marocchi, A.H. Gabriel, G.A. Doschek, 1987b, Astron. Astrophys., **188**, 159
[37] Arnaud, M., R. Rothenflug: 1985, Astron. Astrophys. Suppl., **60**, 425
[38] Bhatia, A.K., B.C. Fawcett, J.R. Lemen, H.E. Mason, K.J.H. Phillips: Mon. Not. R. astr. Soc., **240**, 421
[39] Bitter, M., K.W. Hill, N.R. Sauthoff, P.C. Efthimion, E. Meservay, W. Roney S. von Goeler, R. Horton, M. Goldman, W. Stodiek: 1979, Physical Rev. Lett., **43**, No 2, 129
[40] Bochsler, P.: 1987, Physica Scripta, Vol **T18**, 55
[41] Bornman, P.L.: 1987, Astrophys. J., **313**, 449

(42) Bornman, P.L., and K.T. Strong: 1988, Astrophys. J., **333**, 1014
(43) Breneman, H.H., E.C. Stone: 1985, Astrophys. J. Lett., **299**, L57
(44) Bromboszcz, G., M. Siarkowski, J. Sylwester, V.V. Korneev,S.L. Mandelstam, S.N. Oparin, A.M. Urnov, I.A. Zhitnik: 1983, Solar Phys., **83**, 243
(45) Bruner, M.E., W.A. Brown, A. Fludra, J.R. Lemen, H.E. Mason, R.W.P. McWhirter: 1990, *in preparation*,
(46) Bruner,M.E, and R.W.P. McWhirter: 1988, Astrophys. J., **326**, 1002.
(47) Cook, J.W., C.-C. Cheng, V.L. Jacobs, S.K. Antiochos: 1989, Astrophys. J., **338**, 1176
(48) Craig, I.J.D. and J.C. Brown: 1976a, Nature, **264**, 341
(49) Craig, I.J.D. and J.C. Brown: 1976b, Astron. Astrophys., **49**, 239
(50) Doschek G.A., and R.D. Cowan: 1984, Astrophys. J. Suppl. Ser., **56**, 67
(51) Doschek, G.A., U. Feldman, J.F. Seely: 1985, Mon. Not. R. astr. Soc., **217**, 317
(52) Doschek, G.A. and K. Tanaka: 1987, Astrophys. J., **323**, 799
(53) Doschek, G.A., U. Feldman, J.F. Seely: 1989, Astrophys. J., **345**, 1079
(54) Doschek, G.A., A.Fludra, R.D.Bentley, K.J.H. Phillips, T. Watanabe: 1990, Astrophys. J., *in press*
(55) Doyle, J.G., and J.C. Raymond: 1981, Mon. Not. R. astr. Soc., **196**, 907
(56) Doyle, J.G., K.G. Widing: 1989, Armagh Observatory preprint, *to appear* in Astrophys. J.
(57) Dunn, J., R. Barnsley, K.D. Evans, N.J. Peacock: 1988, Journal de Physique, Colloque C1, Supplement au n°3, Tome **49**, c1-91
(58) Fawcett B.C., C. Jordan, J.R. Lemen, K.J.H. Phillips: 1987, Mon. Not. R. astr. Soc., **225**, 1013
(59) Fludra, A., J. Sylwester: 1986, Solar Phys., **105**, 323
(60) Fludra, A., J.R. Lemen, J. Jakimiec, R.D. Bentley, J. Sylwester: Astrophys. J., **344**, 991
(61) Fludra, A., R.D. Bentley, J.L. Culhane, J.Jakimiec, J.R. Lemen, J. Sylwester, S.T. Moorthy: 1990, *this issue*.
(62) Gabriel, A.H., F. Miller, N. Lizambert: 1988, Journal de Physique, Colloque C1, Supplement au n°3, Tome **49**, c1-325
(63) Geiss, J.: 1985, *ESA Workshop on Future Missions in Solar, Heliospheric & Space Plasma Physics*, ESA **SP-235**, 37
(64) Golub, L., M. Herant, K. Kalata, I. Lovas, G. Nystrom, F. Pardo, E. Spiller, J. Wilczynski: 1990, Nature, **344**, 842
(65) Jacobs, V.L., J. Davis, J.E., Rogerson, M. Blaha, J. Jain, M. Davis: 1980, Astrophys. J., **239**, 1119
(66) Jakimiec, J., A.Fludra, J.R. Lemen, R., B.R. Dennis, J. Sylwester: 1986, Adv. Space Res., Vol. **6**, No. **6**, (11)231
(67) Jakimiec, J., P.Preś, A.Fludra, R.D. Bentley, J.R. Lemen, R. Mewe, J. Schrijver, J. Sylwester: 1988, Adv. Space Res., Vol. **8**, (11)231
(68) Jakimiec, J.: 1990, Adv. Space Res., Vol **10**, No **9**, (9)109

(69)Karpen, J.T., C-C. Cheng, G.A. Doschek, C.R. De Vore: 1989, Astrophys. J., **338**, 1184
(70)Korneev, V.V., I.A.Zhitnik, S.L. Mandelstam, A.M. Urnov: 1980, Solar Phys., **68**, 391
(71)Lemen J.R., K.J.H. Phillips, R.D. Cowan, J. Hata, I.P. Grant: 1984, Astron. Astrophys., **135**, 313
(72)Lemen, J.R., J.Sylwester R.D. Bentley: 1986, Adv. Space Res., Vol 6, No 6., 245
(73)Lemen, J.R., R. Mewe, C.J. Schrijver, A. Fludra: 1989, Astrophys. J., **241**, 474
(74)Ljepojevic, N.N., R.J. Hutcheon, R.W.P. McWhirter: 1984, J.Phys. B., At. Molec. Phys., **17**, 3057
(75)Ljepojevic, N.N., R.W.P. McWhirter, S. Volonte: 1985, J.Phys. B., At. Molec. Phys., **18**, 3285
(76)McClymont, A.N.: 1989, Astrophys. J. Lett., **347**, L47
(77)McKenzie D.L., R.M. Broussard, P.B. Landecker, H.W. Rugge, R.M. Young, G.A. Doschek, U. Feldman: 1980, Astrophys. J. Lett., **238**, L43
(78)McWhirter, R.W.P., P.J. MacNeice: 1987, Sol. Phys., **107**, 323
(79)Mewe, R., E.H.B.M. Gronenschild, G.H.J. van den Oord: 1985, Astron. Astrophys. Suppl., 62, 197
(80)Mewe, R., J.R. Lemen, G.H.J. van den Oord: 1986, Astron. Astrophys. Suppl., 65, 511
(81)Peres, G, R. Rosner, S.Serio: 1987, Il Nuovo Cimento, **99B**, No. 1, 29
(82)Phillips, K.J.H., J.R. Lemen, R.D. Cowan, G.A. Doschek, J.W. Leibacher: 1983, Astrophys. J., **265**, 1120
(83)Phillips, K.J.H., J.W.Leibacher, C.J. Wolfson, J.H. Parkinson, B.C. Fawcett, B.J. Kent, H.E. Mason, L.W. Acton, J.L.Culhane, A.H. Gabriel: 1982, Astrophys. J., 256, 774
(84)Raymond, J.C., D.P. Cox, B.W. Smith: 1976, Astrophys. J., 204, 290
(85)Rosner, R., W.M. Tucker and G.S. Vaiana: 1978, Astrophys. J., 220, 643
(86)Saba, J.R.L., and K.T. Strong: 1986, Adv. Space Res., Vol 6, No 6, 37
(87)Schrijver, C.J., J.R. Lemen and R.Mewe: 1989, Astrophys. J., **341**, 484
(88)Seely, J.F., G.A. Doschek: 1989, Astrophys. J., **338**, 567
(89)Shull, J.M., and M. Van Steenberg: 1982a, Astrophys. J. Suppl., **48**, 95
(90)Shull, J.M., and M. Van Steenberg: 1982b, Astrophys. J. Suppl., **49**, 351
(91)Siarkowski, M., J. Sylwester, G. Bromboszcz, V.V. Korneev, S.L. Mandelstam, S.N. Oparin, A.M. Urnov, I.A. Zhitnik: 1982, Solar Phys., **81**, 63
(92)Siarkowski, M.: 1983, Solar Phys., **84**, 131
(93)Smith, D.F.: 1986, Astrophys. J., **302**, 836
(94)Summers, H.P., R.W.P. McWhirter: 1979, J. Phys. B, **12**, 2387
(95)B. Sylwester: 1974, Acta Astronomica, **24**, 299
(96)B. Sylwester: 1979, Thesis, Wroclaw University

(97) B. Sylwester, J.Sylwester, J. Jakimiec, R. Mewe, R.D. Bentley: 1983, Publ. of Debrecen Heliophys. Obs., **5**, 85
(98) B. Sylwester, P. Faucher, J. Jakimiec, V.V. Krutov, V.V. Korneev, R.W.P. McWhirter, J. Sylwester, M. Tomczak, S. Volonte, I.A. Zhitnik: 1986, Solar Phys., **103**, 67
(99) B. Sylwester, J. Sylwester, J.Jakimiec, A. Fludra, R.D. Bentley, J. Schrijver: 1986, *Contributions of the Astronomical Observatory Skalnate Pleso, Proceedings of the 12th Regional Consultation on Solar Physics*, Smolenice, **XV**, 145
(100) B. Sylwester, J. Sylwester, R.D. Bentley, A.Fludra: 1990a, Solar Phys., **126**, 177
(101) B. Sylwester, J. Sylwester, J. Jakimiec, S. Serio, F. Reale, A. Fludra, R.D. Bentley: 1990b, *this issue*
(102) Sylwester, J., J. Schrijver, R. Mewe: 1980, Solar Phys., **67**, 285
(103) Sylwester, J., J.R. Lemen, R. Mewe: 1984, Nature, **310**, 665
(104) Sylwester, J., J. Jakimiec, A. Fludra, J.R. Lemen: 1986, *Contributions of the Astronomical Observatory Skalnate Pleso, Proceedings of the 12th Regional Consultation on Solar Phys.*, Smolenice, **XV**, 153
(105) Sylwester, J: 1987, Artificial Satellites, Space Phys., No 7, Vol 22, 17
(106) Sylwester, J., M-C. Zolcinski-Couet, R.D. Bentley, J.R. Lemen: 1988, Journal de physique, Colloque C1, Supplement au no 3, Tome **49**, C1-189
(107) Sylwester J. et al.: 1990, *in preparation*
(108) Tanaka, K., N. Nitta, K. Akita, T. Watanabe: 1983, Solar Phys., **86**, 91
(109) Tanaka, K: 1986, Publ. Astron. Soc. Japan, **38**, 225
(110) Underwood, J.H., S.K. Antiochos and J.F. Vesecky: 1981, in *Solar Phenomena in Stars and Stellar Systems*, ed. R.M. Bonnet and A.K. Dupree, Dordrecht: Reidel, 227
(111) Veck, N.J. and J.H. Parkinson: 1981, Mon. Not. R. astr. Soc., **190**, 287
(112) von Steiger, R., and J. Geiss: 1990, Physical Institute, Bern University Preprint, *to be published* in Astron. Astrophys.
(113) Widing, K.G. and U. Feldman: 1989, Astrophys. J., **344**, 1046
(114) Withbroe, G.L.: 1975, Solar Phys., **45**, 301
(115) Wu, S.T., C. de Jager, B.R. Dennis and many other: 1986, in *Energetic Phenomena on the Sun*, NASA Conference Publication **2439**, 5-24
(116) Zarro, D.M., G.L. Slater, S.L. Freeland: 1988, Astrophys. J. Lett., **333**, L99
(117) Zhitnik, I.A., V.V. Korneev, V.V. Krutov, S.N. Oparin, A.M. Urnov: 1987, Trudy FIAN - Proceedings of the P.N. Lebedev Physical Institute, Moscow, vol **179**, 39 (in Russian)

UV AND EUV SPECTROSCOPY OF THE UPPER SOLAR ATMOSPHERE

Helen E. Mason

Department of Applied Mathematics and
Theoretical Physics,
Silver Street,
Cambridge CB3 9EW,
G.B.

ABSTRACT

The UV and EUV wavelength regions are rich in emission lines from the transition region and the corona. Spectroscopic diagnostic techniques have been used extensively to determine the physical conditions in the solar atmosphere for such diverse phenomena as coronal holes, active regions, surges, flares. Such knowledge is fundamental to a definition of the dominant physical processes. In this paper, we review diagnostic techniques which have been used in the analyses of space observations (eg Skylab, SMM, HRTS, CHASE). We look to future projects such as the CDS and SUMER instruments on SOHO which cover the UV and EUV wavelength regions and will provide a wealth of observations with excellent spatial, spectral and temporal resolution.

1. INTRODUCTION

The main question which will be addressed in this paper is 'What can we learn about the small scale structure and dynamics of the solar atmosphere from the UV and EUV emission line spectra?' We shall concentrate on the wavelength region to be covered by the Coronal Diagnostic Spectrometer (CDS) and Solar Ultraviolet and Emitted Radiation (SUMER) on SOHO, that is 160-1600Å. These instruments will investigate heating mechanisms for the solar corona and acceleration mechanisms for the solar wind. The spectroscopic diagnostic techniques which will be used involve line profiles, shifts and broadenings, emission measure analyses and line pair ratios to give electron temperature and density. Figure 1 illustrates the distribution of spectral lines as a function of temperatures and wavelength. The strongest coronal lines fall at the shorter wavelength region, with a sequence of lines from iron ions Fe IX - Fe XVI below 400Å. The CDS instrument will cover these lines using a normal incidence spectrometer (stigmatic slit) (310-380Å , 518-635Å) and a grazing incidence (astigmatic slit) (166-225Å , 252-322Å , 394-479Å , 680-788Å). The CDS instrument should achieve a 2" spatial resolution, a spectral resolution of $\lambda/\delta\lambda = 10^4$ and a temporal resolution of 1s in the strongest lines. The transition region and chromospheric lines fall predominantly at longer wavelengths and will be covered by the SUMER instrument, 500-800Å in second order, 800-1600Å in first order, with a band width of 20Å and 40Å respectively. The spatial resolution will be down to 1.2-1.5", the spectral resolution will be $\lambda/\delta\lambda$ = 1.9-4 x 10^4 and the temporal resolution of 1s. SUMER should be able to detect velocities

down to 1-3 km/s. In this paper, we shall look back over studies of existing datasets in this wavelength region (see table I) and review what has been learnt about the solar atmosphere in relation to the main questions which CDS and SUMER will address. In the first section, we look at spectral line widths and shifts in relation to proposed heating mechanisms and the origin of the solar wind. Next we look at spectroscopic diagnostics for determining the physical parameters of the atmosphere, paying particular attention to possible inhomogenieties in the emitting regions. Finally we look at the evidence for abundance variations in the solar atmosphere and consider the consequences of such anomalies.

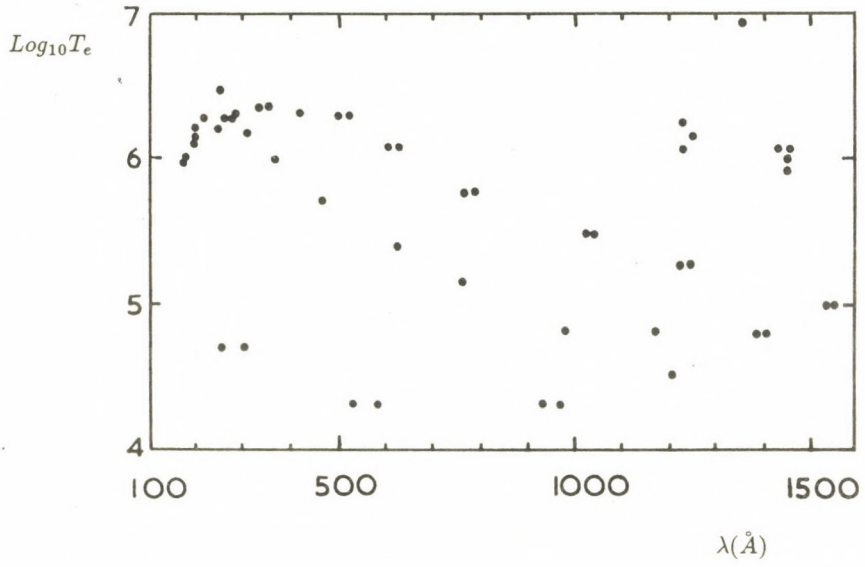

Figure 1 Distribution of strong emission lines as a function of T_e and wavelength, in the range covered by the SOHO CDS and SUMER instruments. The coronal lines between 1200-1500Å are included on this plot but they are very weak. The FeXXI line at 1354Å is also shown.

2. SPECTRAL LINE PROFILES

Various heating mechanisms have been proposed for the solar atmosphere. The energy required to heat the corona is around 10^7 ergs cm^{-2} s^{-1} (6×10^{29} ergs s^{-1}). Acoustic waves could possibly be the heating source for the chromosphere but the energy flux does not seem to be sufficient for the transition region and corona (Anderson and Athay, 1989). Alfvén waves are difficult to dissipate in the corona (Cheng *et al*, 1979a, Parker, 1987) although methods such as resonant cavities (Davila, 1987) have

Table I **UV instruments referred to in the text**

Satellite	Experiment	$\lambda\lambda$ range (Å)	Spectral Res. (Å)(best)	Spatial Res. (arc sec)^2
OSO-7	GSFC Spectroheliograph	190-300	0.42	20 x 60
Skylab ATM	NRL S082A UV slitless spectroheliograph	170-630	0.1	2 x 2
	NRL S082B Slit spectrograph	1170-3000	0.06	2 x 60
	HCO S0555 UV spectrometer	280-1350	1.6	5 x 5
SMM	UVSP UV spectrometer and polarimeter	1150-3600	0.05	3 x 3
Spacelab 2 rocket flights	HRTS High resolution telescope and spectrometer	1170-1700	0.05	1 x 1
rockets	LASP EUV coronal spectrometer	605-635 1210-1270	0.003	20 x 60
Spacelab 2	CHASE Coronal Helium abundance Spacelab expt.	150-1344	0.7	15 x 15
SOHO	CDS Coronal diagnostic spectrometer	165-800	0.02	2 x 2
SOHO	SUMER Solar UV measurements of emitted radiation	500-1600	0.02	1 x 1

been proposed. Alfvén waves could however provide significant energy flux into the solar wind. Different types of magneto-acoustic waves have also been considered. An alternative to wave heating proposed by Parker (1987, 1988) is that of small scale reconnection or nanoflares. These could be connected with hard X-ray spikes or EUV explosive events, but the energy released in both types of events is two orders of magnitude too small to provide the heating mechanism for the corona. Parker therefore proposed that swarms of nano-flares occur through the reconnection of flux bundles in bipolar fields and that the X-ray corona is thus created by the energy dissipation at many tangential discontinuities caused by random continuous motions of the footpoints of the field.

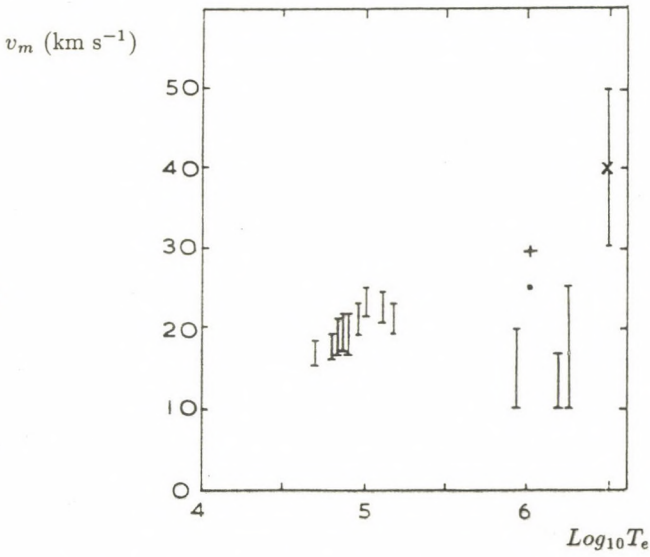

Figure 2 Nonthermal broadening as a function of temperature. The transition region values around 10^5K are from Doschek (1987b); the coronal values around 10^6K (full lines) are from Cheng et al (1979a), the (+) is from Feldman and Behring (1974), the Mg X value (•) is from Hassler et al (1990); the Mg XI value (x) is from Saba and Strong (1989).

The various heating mechanisms can be investigated by studying the UV spectral lines. Line widths from the transition region lines seen with the NRL S082B instrument on Skylab show an increase in random mass motions with temperature (Mariska *et al*, 1978, Doschek, 1987b). The non-thermal velocity rises from around 16 km s^{-1} at 5 x 10^4 K to around 24 km s^{-1} at 2 x 10^5 K (figure 2). This increase could be fitted by either a constant acoustic or a constant Alfvén wave flux of 1.3 x 10^6 erg cm^{-2} s^{-1}. Several weak coronal lines were observed in the wavelength region 1000-1500Å with S082B (Sandlin *et al*, 1977, Feldman and Doschek, 1977). However these coronal

lines, observed off the limb (0"-30") in active and quiet regions, had a low non-thermal velocity broadening of around 15 km s^{-1} (figure 2) (Doschek and Feldman, 1977, Cheng *et al*, 1979a, Mariska, 1986). These results are supported by more recent work on the same lines from SMM UVSP observations (Mason *et al*, 1990). It is interesting to note that the intensity of the Si VIII (1446Å , 8 x 10^5 K) line is almost the same in the quiet Sun and coronal hole regions, whereas the Fe XI (1467Å , 1.2 x 10^6 K) line disappears in the coronal hole region (Doschek and Feldman, 1977). The widths obtained from strong allowed coronal lines in the UV (eg Feldman and Behring, 1974, Hassler *et al*, 1990) give a higher non-thermal broadenings of around 25 km s^{-1} (figure 2). The X-ray line of Mg XI has been carefully studied with SMM XRP and an even larger value of 40 km s^{-1} has been obtained (Saba and Strong, 1989, Saba, 1990). The reason for the difference between these forbidden and allowed spectral line widths is not obvious. It is important to establish a value for the nonthermal broadening of coronal lines in different regions, since this places severe restrictions on the flux of energy flux carried by waves into the corona (Parker, 1987, 1988). McClements *et al* (1990) have suggested that a study be made with SUMER of limb to disk spectral line widths with high spatial resolution in order to differentiate between different types of wave motion.

The line profiles of the transition region lines such as CIV (1550Å) are complex and have been studied with high spectral and spatial resolution with the HRTS instrument (Breuckner *et al*, 1986, Breuckner, 1990, Dere, 1988, 1989). Several different types of dynamic events have been identified, including jets and explosive events (Dere *et al*, 1989a). Transient events in the transition region lines were also studied with the SMM-UVSP instrument. Porter *et al* (1984) studied transient brightening in Si IV and O IV lines and Porter *et al* (1987) found that the rapid intensity fluctuations in CIV emission seemed to be spatially located near the neutral lines of small bipolar region. They suggest a possible association with microflare events. The HRTS observations do not seem to show any obvious correlation between explosive events and X-ray brightenings. The explosive events are not clustered at the boundaries of super-granules, but could however be associated with emerging flux (Dere, 1990). The highest temperature line in the 1000 - 2000Å wavelength region is Fe XXI 1354Å (10^7 K). This has been studied with the S082B instrument (Cheng *et al*, 1979b) and also with SMM-UVSP (Mason *et al*, 1986). It would be interesting to study the relationship between transitient emission from Fe XXI and transition region ions.

Mass motions in the solar atmosphere have also been studied with UV emission lines. There is substantial evidence (Rottman *et al*, 1981, 1982, Orrall *et al*, 1983) for outflows of 12 km s^{-1} in Mg X (625Å) and 7 km s^{-1} in O V (629Å) over a coronal hole. The HRTS CIV results (Dere *et al*, 1989b, Dere, 1990) also show outflow velocities of 10 km s^{-1} in a coronal hole, which are well correlated with high magnetic field regions. The problem of mass flux into the solar wind (Withbroe, 1988, 1989) will be studied with the SOHO instruments.

3. SPECTRAL LINE INTENSITIES

The HCO S0555 instrument observed line emission from a wide temperature range. Rasters from Ly α, C III, O VI, Ne VII, Mg X, Fe XV clearly show the changing nature of the solar atmosphere with temperature on the disk and the limb. Coronal loops are most clearly defined in the Ne VII ($T_e = 5 \times 10^5$ K) emission and many excellent images in this and othes lines were obtained with the NRL S082A instrument which had a spatial resolution for well defined bright structures of down to 1-2". Recent images in the X-ray wavelength region obtained with NIXT (Martins *et al*, 1989, Golub *et al*, 1990) show well defined structures at coronal temperatures (FeXVI, 2×10^6 K, Mg X , 10^6 K) down to a spatial resolution of around 0.75".

In this section, we discuss two main diagnostic techniques which are used to study the transition region and coronal emission. The first is the determination of electron density from line intensity ratios, the second is the determination of the distribution of material as a function of temperature. Several reviews on spectroscopic diagnostics are available covering different solar features, ranging over coronal holes, quiet Sun, active regions, surges, sunspots and solar flares (Doschek, 1985, 1987a, Dere and Mason, 1981, Gabriel and Mason, 1982, Mason, 1988, 1990a, 1990b). Below, we briefly outline the methods used and illustrate them with a couple of examples.

The line emissivity (per unit volume, per unit time) for an optically thin spectral line is given by

$$\varepsilon(\lambda_{ij}) = N_j A_{ji} \frac{hc}{\lambda_{ij}} \tag{1}$$

where A_{ji} is the spontaneous transition probability and N_j is the number density of the upper level j

$$N_j = \frac{N_j(X^{+m})}{N(X^{+m})} \frac{N(X^{+m})}{N(X)} \frac{N(X)}{N(H)} \frac{N(H)}{N_e} N_e \tag{2}$$

Here, $N(X^{+m})/N(X)$ is the ionisation ratio of the ion X^{+m} relative to the total number density of element X (primarily a function of electron temperature for low electron densities); $N(X)/N(H)$ is the element abundance; $N(H)/N_e$ is the Hydrogen abundance (0.8); N_e is the electron number density; $N_j(X^{+m})/N(X^{+m})$ is the population of level j relative to the total number density of the ion X^{+m} and is determined by solving the statistical equilibrium equations for the ion. In coronal equilibrium, the upper level is excited by electron collisions from the ground level and decays by a radiative transition to the ground level. Thus

$$N_i N_e C_{ij} = N_j A_{ji} \tag{3}$$

where C_{ij} is the electron collision rate coefficient. For allowed transitions, the radiative decay rate is very large and the bulk of the population of the ion remains in the ground

level so one can assume that $N_i(X^{+m})/N(X^{+m}) = 1$. Thus one obtains that the line intensity, which is the integration of the line emissivity over the emitting volume, is

$$I(\lambda_{ij}) = \int_V G(T_e) N_e^2 dV \tag{4}$$

where $G(T_e)$ can be calculated from the ionisation ratio, element abundance and atomic parameters. Equation (4) can be written in the form

$$I(\lambda_{ij}) = \int_{T_e} G(T_e)\phi(T_e) dT_e \tag{5}$$

Here $\phi(T_e)dT_e$ gives the distribution of material as a function of temperature. The electron density can be estimated assuming that the spectral line is emitted over a homogeneous volume measured from images in that line.

3.1 ELECTRON DENSITY DIAGNOSTICS

Above we have considered a simple two level system. However, if the radiative transition probability is small, other mechanisms can de-excite the upper level. For example, for forbidden or intersystem transitions, the electron de-excitation rate may become larger than the radiative decay rate as the electron density is increased. Eventually, for high enough densities, the upper and lower levels may be in statistical equilibrium. A level which has a significant population relative to the ground level is called a metastable level. Other levels in the ion can be excited from these metastable levels. The intensities of spectral lines connected with metastable levels has a different functional dependence on N_e than equation (4). Thus if we compare ratios of different types of spectral lines from the same ion or temperature region, we can determine an average value for the electron density which is independent of the shape or size of the emitting volume.

This diagnostic technique has been applied to coronal emission from the quiet Sun, active regions and flares (Feldman *et al*, 1978, Dere *et al*, 1979, Mason *et al*, 1984, Doyle *et al*, 1985, Brown *et al*, 1986, Bhatia *et al*, 1989). We note that some useful coronal lines from the sequence of iron ions occur in the UV range to be covered by CDS. Limb spectra of these lines were studied with the GSFC spectroheliograph on the OSO 7 satellite (Kastner *et al*, 1974, 1976, Kastner and Mason, 1978). A review of electron density diagnostics for the corona together with a discussion of diagnostic lines which will be used by the SOHO CDS and SUMER instruments is given in Mason (1990b).

Many diagnostic lines have also been developed for the transition region spectra, references are given in Dere and Mason (1981), Doschek (1985, 1987b), Mason (1988). For example the lines around 1400Å from O IV have been studied extensively. The intensity ratio between different lines from O IV can be used to derive a density, or the ratio of an O IV line to a Si IV line. Dere *et al* (1982) derived values for the pressure in

a quiet limb region (10^{15} cm^{-3}K), sunspot and plage ($10^{15} - 10^{16.5}$ cm^{-3}K) from the O IV line ratios, indicating filamentary structure. Hayes and Shine (1987) carried out a detailed study of the O IV lines using SMM UVSP observations and found that the transition region shows continual small scale activity possibly from dense structures embedded in a background transition region. The nature of the transition region has been investigated further with HRTS observations. Dere *et al* (1987) find an electron pressure from O IV which indicates a path length for the CIV transition region features of less than 10 km, which contrasts starkly with the extent of the features along the slit (about 2400 km)! The conclusion is that the transition region emission is produced by subresolution filamentary structures which sparsely fill the volume.

Recent work (Orrall and Rottman, 1986, Orrall *et al*, 1990) indicates that there could also be significant irregularities in the corona due to small scale density fluctuations. They compare intensities from the Mg X emission (proportional to N_e^2) and K-corona emission (proportional to N_e) above the limb. They conclude that their observations are explained by structures which are more than 40 times denser than the background but occupy less than 20% of the volume. The possibility of inhomogeneous structures in the corona is discussed further in Mason (1990b), together with a more extensive survey of diagnostic line ratios for the corona and corresponding atomic physics calculations. New atomic calculations for Mg X (Burgess *et al*, 1989) and other coronal ions (Burgess *et al*, 1990, Fawcett and Mason, 1989, 1990) have recently been carried out. Work is also in progress on assessing and storing atomic parameters for input into solar analyses programs (Burgess *et al*, 1988).

Inhomogeneous structures in the emitting volume may affect the diagnostic line ratio techniques. This problem was discussed by Doschek (1984) and further work has recently been carried out by Almleaky *et al*, 1989, 1990) who considered both inhomogeneous thermal and non-thermal plasmas. Other non-equilibrium processes may also be important in the transition region and corona. For example, non-Maxwellian velocity distributions can effect the spectral line ratios as demonstrated by Keenan *et al* (1989) for Si III. Detailed studies have recently been carried out of non-Maxwellian velocity distributions for the transition region (Ljepejovic and Burgess, 1990) and solar flares (Ljepejovic and MacNeice, 1988, Ljepejovic, 1990) and their effect on heat conduction in the solar atmosphere (Ljepejovic and MacNiece, 1989). One must also consider the effects of flows, for examples through the transition region (Raymond and Dupree, 1978, Mariska, 1986) or in loop structures (Noci *et al*, 1989, Spadaro *et al*, 1990, Spadaro, 1990).

3.2 EMISSION MEASURE ANALYSES

Equation 5 can be used to derive the distribution of material as a function of electron temperature for different solar features. New observations from CHASE (170-1330 Å) cover a wide temperature range from chromospheric lines to coronal lines. A detailed study of the CHASE observations for quiet Sun regions has been carried out by Lang *et al* (1990) and a differential emission measure curve has been derived.

This powerful technique for probing the solar atmosphere must be carefully handled to ensure solutions which are both mathematically valid and physically meaningful (Monsignori- Fossi, 1990). Important aspects of the problem are the peak temperature which determines boundary conditions for energy transfer processes, and the steep gradient at lower temperatures which is difficult to explain (Antiochos and Noci, 1986).

3.3 ABUNDANCE ANOMALIES

There now seems to be substantial evidence that the element abundance in the upper solar atmosphere is in variance with that of the photosphere. This evidence comes from three main sources, the solar wind fluxes and solar energetic particles (Schmid *et al* , 1988), and the UV observations. Excellent reviews are given by Meyer (1985, 1990). It seems that elements with low first ionization potentials (FIPs) are overabundant relative to those with higher FIPs. Widing and Feldman (1989) looked at the Ne/Mg ratio for several different solar features and found that the ratio was smallest for open field regions and was close to the local galactic value for an impulsive flare. Recent work by Doschek and Bhatia (1990) indicates that the Ar/Fe abundance is significantly lower in the transition region than the local galactic value. Such abundance variations are extremely important. To explain them is a challenge in itself. In addition there are consequences for the radiative power loss curves (Cook *et al*, 1989) which could affect the energy transfer mechanisms.

4. CONCLUSION

The deeper we look into the solar atmosphere, the more complex it seems to be! The high spatial resolution observations in the UV and X-ray wavelength region show an intricate structure of emission. The transition region would seem to be composed of unresolved filamentary structures protruding into the corona. There are indications that the coronal emission is also inhomogeneous. Plasma motions are prevalent in the transition region and corona giving rise to spectral line broadening and shifts. These could be produced by wave motions and plasma flows along loops or into the solar wind. The evidence for abundance differences between the photosphere and the upper atmosphere is now substantial and has a relationship to the value of the first ionisation potential for the element. This could arise in the region of formation of the transition region and corona. Any abundance anomalies have important repercussions in the analyses of solar spectra.

The SOHO mission to be launched in 1995 will focus directly on these problems. In particular the SUMER and CDS instruments will obtain observations of the chromosphere, transition region and corona with high spatial, spectral and temporal resolution. Other instruments will study the atmosphere further out towards the solar wind. The next decade of solar physics promises to provide some exciting new observations in the UV and X-ray wavelength regions, not only with SOHO but also with other projects such as SOLARA, OSL and various rocket borne instruments. Shall we ever fully probe the secrets of the Sun?

How did the Sun get in her place
with her round and shiny happy face?
Who cast the shadows, high and low?
I do not know, I do not know!

REFERENCES

Almleaky, Y.M., Brown, J.C. and Sweet, P.A.: 1989, *Astron. Astrophys.*, **224**, 328.
Almleaky, Y.M., Brown, J.C., Dwivedi, B.N. and Sweet, P.A.: 1990, *preprint.*
Anderson, L.S. and Athay, R.G.: 1989, *Astrophys. J.*, **336**, 1089.
Antiochos, S.K. and Noci, G.: 1986, *Astrophys. J.*, **301**, 440.
Bhatia, A.K., Fawcett, B.C., Lemen, J.R., Mason, H.E. and Phillips, K.J.H.: 1989, *Mon. Not. R. astr. Soc.*, **240**, 421.
Brown, W.A., Mason, H.E., Brunner, M.E. and Acton, L.W: 1986, *Astrophys. J.*, **301**, 981.
Breuckner, G.E.: 1990. *Advan. Space Res.*, in press
Brueckner, G.E., Bartoe, J.-D.F., Cook, J.W., Dere, K.P. and Socker, D.G.: 1986, *Advan. Space Res.*, **6**, 263.
Burgess, A., Mason, H.E. and Tully, J.A.: 1988, *J. de Physique*, **49**, C1-107.
Burgess, A., Mason, H.E. and Tully, J.A.: 1989, *Astron. Astroph.*, **217**, 319.
Burgess, A., Mason, H.E. and Tully, J.A.: 1990, *preprint*
Cheng, C.-C., Doschek, G.A. and Feldman, U.: 1979a, *Astrophys. J.*, **227**, 1037.
Cheng, C.C., Feldman, U and Doschek, G.A.: 1979b, *Astrophys. J.*, **233**, 736.
Cook, J.W., Cheng, C.-C., Jacobs, V.L. and Antiochos, S.K.: 1989, *Astrophys. J.*, **338**, 1176.
Davila, J.M.:1987, *Astrophys. J.*, **317**, 514.
Dere, K.P.: 1988, *J. de Physique Coll.*, **49**, C1-3.
Dere, K.P.: 1989, *Astrophys. J.*, **340**, 599
Dere, K.P.: 1990, *E. G. S. meeting*
Dere, K.P., Bartoe, J.-D.F. and Breuckner, G.E.: 1982, *Astrophys. J.*, **259**, 366.
Dere, K.P., Bartoe, J.-D.F. and Breuckner, G.E.: 1989a, *Sol. Phys.*, **123**, 41.
Dere, K.P., Bartoe, J.-D.F., Breuckner, G.E., Cook, J.W. and Socker, D.G.: 1987, *Sol. Phys.*, **114**, 223.
Dere, K.P., Bartoe, J.-D.F., Brueckner, G.E. and Recely, F.: 1989b, *Astrophys. J.*, **345**, L95.
Dere, K.P. and Mason, H.E.: 1981, *Active Regions*, ed. F. Orrall, Colorado Univ. Press, **Ch. 6**, p129.
Dere, K.P., Mason, H.E., Widing, K.G. and Bhatia, A.K.: 1979, *Astrophys. J. Suppl.*, **40**, 341.
Doschek, G.A.: 1984, *Astrophys. J.*, **279**, 446.
Doschek, G.A.: 1985, *Autoionization*, ed. A. Tempkin, Plenum Publ. Co., **Ch. 6**, p171.
Doschek, G.A.: 1987a, *Sol. Phys.*, **114**, 223.
Doschek, G.A.: 1987b, *Theoretical Problems in High Resolution Solar Physics*, eds. G. Athay and D.S. Spicer, NASA conf. publ. **2483**, p37.

Doschek, G.A. and Bhatia, A.K.: 1990, *Astrophys. J.*, in press.
Doschek, G.A. and Feldman, U.: 1977, *Astrophys. J.*, **212**, L143.
Doyle, J.G., Mason, H.E. and Vernazza, J.E.: 1985 *Astron. Astrophys.*, **150**, 69.
Fawcett, B.C. and Mason, H.E.: 1989, *Atomic and Nucl. Data Tables*, **43**, 245.
Fawcett, B.C. and Mason, H.E.: 1990, *Atomic and Nucl. Data Tables*, in press.
Feldman, U. and Behring, W.E.: 1974, *Astrophys. J. Lett.*, **189**, L45.
Feldman, U. and Doschek, G.A.: 1977, *J. Opt. Soc. Am.*, **67**, 726.
Feldman, U. Doschek, G.A., Mariska, J.T., Bhatia, A.K. and Mason, H.E.: 1978, *Astrophys. J.*, **226**, 1129.
Gabriel, A.H. and Mason, H.E.: 1982, *Applied Atomic Collision Physics, Vol. I*, eds. H.S.W. Massey, B. Benderson and E.W. McDaniel, Academic Press, **Ch. 12**, p345.
Golub, L., Herant, M., Kalata, K., Lovas, I., Nystrom, G., Parado, F., Spiller, E. and Wilczynski, J.: 1990, *Nature*, **344**.
Hassler, D.M., Rottman, G.J., Shoub, E.C. and Holzer, J.E.: 1990, *Astrophys. J.*, **348**, L77.
Hayes, M. and Shine, R.A.: 1987, *Astrophys. J.*, **312**, 943.
Kastner, S.O., Rothe, E.D. and Neupert, W.M.: 1974, *Astron. Astrophys.*, **37**, 339.
Kastner, S.O., Rothe, E.D. and Neupert, W.M.: 1976, *Astron. Astrophys.*, **53**, 203.
Kastner, S.O. and Mason, H.E.: 1978, *Astron. Astrophys.*, **67**, 119.
Keenan, F.P., Cook, J.W., Dufton, P.L. and Kingston, A.E.: 1989, *Astrophys. J.*, **340**, 1135.
Lang, J., Mason, H.E. and McWhirter, R.W.P.: 1990, *Sol. Phys.*, in press.
Ljepojevic, N.N.: 1990, *J. Q. S. R. T.*, **44**, 203.
Ljepojevic, N.N. and Burgess, A.: 1990, *Proc. R. Soc. Lond.*, A**428**, 71.
Ljepojevic, N.N. and MacNeice, P.: 1988, *Sol. Phys.*, **117**, 123.
Ljepojevic, N.N. and MacNeice, P.: 1989, *Phys. Rev.*, A**40**, 981.
Mariska, J.T.: 1986, *Ann. Rev. Astron. Astrophys.*, **24**, 23.
Mariska, J.T., Feldman, U. and Doschek, G.A.: 1978, *Astrophys. J.*, **226**, 698.
Martins, P.C.H., Golub, L. and Herant, M.: 1989, *Workshop on Plasma Phenomena in the Solar Atmosphere*, Cargese.
Mason, H.E.: 1988, *J. de Physique*, **49**, C1-13.
Mason, H.E.: 1990a, *I.A.U. Coll. no. 115*, in press.
Mason, H.E.: 1990b, *Advan. Space Res.*, in press.
Mason, H.E., Bhatia, A.K., Kastner, S.O., Neupert, W.M. and Swartz, M.: 1984, *Sol. Phys.*, **92**, 199.
Mason, H.E., Shine, R.A., Gurman, J.B. and Harrison, R.A.: 1986, *Astrophys. J.*, **309**, 435.
Mason, H.E., Shine, R.A. and Gurman, J.B.: 1990, in preparation.
McClements, K.G., Harrison, R.A. and Alexander, D.: 1990, *Sol. Phys.*, submitted.
Meyer, J.P.: 1985, *Astrophys. J. Suppl. Ser.*, **57**, 173.
Meyer, J.P.: 1990, *Advan. Space Res.*, in press.
Monsignori-Fossi, B.: 1990, *Advan. Space Res.*, in press.
Noci, G., Spadaro, D., Zappala, R.A. and Antiochos, S.K.: 1989, *Astrophys. J.*, **338**, 1131.

Orrall, F.Q. and Rottman, G.T.: 1986, *Coronal and Prominence Plasmas*, ed. A.A. Poland, NASA conf. publ. **2442**, p395.
Orrall, F.Q., Rottman, G.J., Fischer, R.R. and Munro, R.H.: 1990, *Astrophys. J.*, **349**, 656.
Orrall, F.Q., Rottman, G.J. and Klimchuk, J.A.: 1983, *Astrophys. J.*, **226**, L65
Parker, E.N.: 1987, *Cambridge Cool Stars Workshop*, Springer and Verlag, p341.
Parker, E.N.: 1988, *Astrophys. J.*, **330**, 474.
Porter, J.G., Toomre, J. and Gebbie, K.B.:1984, *Astrophys. J.*, **283**, 879.
Porter, J.G., Moore, R.L., Reichmann, E.J., Engvold, O. and Harvey, K.L.: 1987, *Astrophys. J.*, **323**, 380.
Raymond, J.C. and Dupree, A.K.: 1978, *Astrophys. J.*, **222**, 379.
Rottman, G.J., Orrall, F.Q. and Klimchuk, J.A.: 1981, *Astrophys. J.*, **247**, L135.
Rottman, G.J., Orrall, F.Q. and Klimchuk, J.A.: 1982, *Astrophys. J.*, **260**, 326.
Saba, J.L.R.: 1990, *Advan. Sp. Res.*, in press.
Saba, J.L.R. and Strong, K.T.: 1989, *Proc. of 2nd Workshop on Thermal and Non-thermal processes in Solar Flares*, **RAL-89-102**.
Sandlin, G.D., Breuckner, G.E. and Tousey, R.: 1977, *Astrophys. J.*, **214**, 898.
Schmid, J., Bochsler, P. and Geiss, J.: 1988, *Astrophys. J.*, **329**, 956.
Spadaro, D.: 1990, *Advan. Space Res.*, in press.
Spadaro, D. Noci, G., Zappala, R.A. and Antiochos, S.K.: 1990, *Astrophys. J.*, **355**, 342.
Withbroe, G.L.: 1988, *Astrophys. J.*, **325**, 442.
Withbroe, G.L.: 1989, *Astrophys. J.*, **337**, L49.
Widing, K.G. and Feldman, U.: 1989, *Astrophys. J.*, **344**, 1046.

OBSERVED LINE PROFILES AND MASS FLUXES IN THE TRANSITION REGION ABOVE SUNSPOTS

P. Maltby, P. Brekke, N. Brynildsen, O. Kjeldseth-Moe
Institute of Theoretical Astrophysics, University of Oslo

and

J.-D.F. Bartoe and G. E. Brüeckner
E. O. Hulburt Center for Space Research,
US Naval Research Laboratory, Washington DC

ABSTRACT

Spectrograms obtained with the High Resolution Telescope and Spectrograph (HRTS), both on rockets and on Spacelab 2, show strong mass flows through the transition zone that are particularly prominent above sunspot regions. Most characteristic for the flow associated with sunspots are regions with supersonic downflows, but upward flowing gas is also observed with generally smaller velocities. The flow pattern changes from one day to the next and even within a time span of minutes, but the general character is maintained and appears always to be present.

Another characteristic property of the flow is the presence of several distinctly different flow speeds within the one arc second resolution element. Multiple flow speeds are also observed in areas with upflows except at some locations inside the sunspot, where only a single velocity component is seen.

An apparent lack of balance between up- and downflowing massfluxes is found. Generally the net massflux appears to be directed downward. Possible reasons for this result are briefly discussed in terms of observability and line emission area filling factor.

I. INTRODUCTION

The intriguing gas flows observed in sunspots show that sunspots are not in magnetohydrostatic equilibrium. At photospheric heights the flow is observed to be subsonic, nearly horizontal, and directed out of the sunspot. At chromospheric heights the flow is directed in the opposite direction, i. e. towards the center of the sunspot. This inverse flow has a larger horizontal extent and appears to follow superpenumbral filaments; for a review, see Sivaraman (1984). The flow in the transition region above sunspots reach downflow velocities close to 200 km/s in some regions (Brueckner 1981; Brekke *et al.* 1987). Both subsonic and supersonic flows are found to occur within the same spatial resolution element (Kjeldseth-Moe *et al.* 1988). In some cases the flows are even oppositely directed. In this paper the emphasis is on the spatial distribution of line-of-sight velocities, mass fluxes and the corresponding time dependences.

II. OBSERVATIONS AND DATA REDUCTION

The observations were obtained with the HRTS instrument (Bartoe and Brueckner 1975) as a part of the Spacelab 2 mission from July 29 to August 6, 1985 (Bartoe *et al.*

1986; Brueckner *et al.* 1986). The sunspot in active region NOAA AR 4682 was observed on seven occasions over a period of 5 days. The present investigation is based on previous results including full frame spectra (1196 - 1680 Å) and quantitative measurements of short frame spectra (14 Å width) centered on the CIV resonance lines. The measurements are from observing programs with raster scans. On August 3, 1985 the same area (60" x 50") was studied three times with time intervals of 13 and 5 min. Twenty two hours later on August 4, 1985 a larger area (100" x 60") including the same sunspot area was observed with one raster scan.

During microphotometry the spectra have been oversampled to maintain the spectral and best angular resolutions of 0.05 Å and 1". Noise has been removed with Fourier filtering. The wavelength scale is obtained from measured positions of selected lines from neutral and singly ionized atoms and all measured velocities in the CIV 1548 line are relative to the low chromosphere. The relative intensity calibration has been obtained by a detailed comparison of spectrograms of the same region on the Sun, taken closely together in time, but with different exposure times. The absolute intensities are determined with the quiet solar spectrum as the source. A detailed description of the procedures is given by Brekke *et al.* (1987).

Each observed line profile is fitted with up to 3, in a few cases 4, symmetrical Gaussian line components with intensities and line shifts determined by a least-squares method (Bevington 1969). The line components have the very same width for a given profile, but the actual value is determined by the fit and may alter from one line profile to another.

III. OBSERVED LINE PROFILES

Generally the line profiles show complicated shapes indicating asymmetries or "flags". The line component width is often larger than the thermal width; on the average 0.11 Å compared to 0.06 Å. Figure 1 shows examples of observed line profiles that are fitted with 1, 2 and 3 Gaussian line components.

In the sunspot area and immediate vicinity more than half of the line profiles consist of more than one line component, except for the August 3, 02:16 UT observations where 62 per cent of the profiles could be fitted with a single Gaussian. On August 3 the observed fraction of profiles showing 2 components ranges from 0.13 to 0.19, whereas the fraction with 3 components ranges from 0.25 to 0.38. The corresponding values for the August 4 observations are 0.31 and 0.29. The observations contain an emerging magnetic flux area showing strong line broadening (Brueckner *et al.* 1988), but these data are not included here.

a) Spatial Distribution of Velocities

Figure 2 shows the blueshift (left) and redshift (right) for the line component in each profile showing the largest line shift. Since the heliocentric aspect angle of the sunspot is small, $\cos\theta = 0.95$ and 0.94, the blueshift/redshift will be referred to as upflow/downflow. The upflow is most pronounced in the central parts of the sunspot. Regions with strong downflows are observed at and close to the eastern rim of the sunspot on August 3. Two regions with strong downflow occur on August 4, one close to the centre and one inside as well as outside the western part of the sunspot. Apparently the strongest downflows

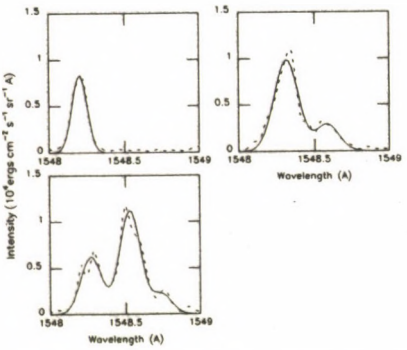

Fig. 1. Observed line profiles fitted with Gaussian line components.

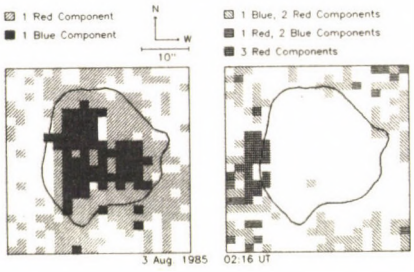

Fig. 3. Spatial distribution of line-of-sight velocities.

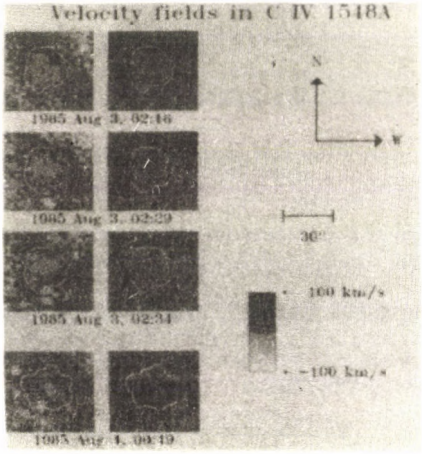

Fig. 2. Blueshift (left) and redshift (right). Line component with largest shift is shown.

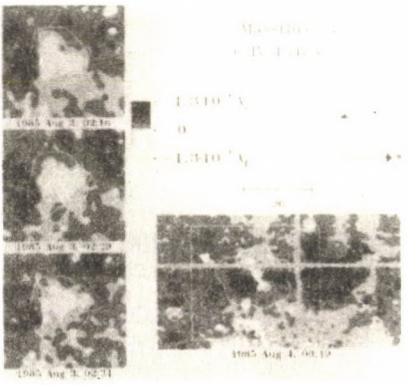

Fig. 4. Massflux as function of spatial position.

are concentrated to relatively small regions and their position in the sunspot region alters from one day to the next.

The spatial distribution of line-of-sight velocities depend on the line component in question. In order to study this more closely, the spatial distribution for line profiles containing 1, 2, and 3 line components were considered separately. Figure 3 (left) gives the spatial distribution on August 3, 02:16 UT for line profiles that may be represented with a single Gaussian. Outside the sunspot nearly all single Gaussian line profiles show downflow. Line profiles that require 2 line components are in most cases found outside the sunspot. The 2 components may both be redshifted, alternatively redshifted plus blueshifted. Only in a few isolated cases are 2 blueshifted components observed.

Figure 3 (right) gives the spatial distribution on August 3 for line profiles requiring 3 line components. These line profiles occur outside or at the eastern rim of the sunspot. The strong downflows at the rim of the sunspot originate from line profiles consisting of 3 redshifted components. Further away from the sunspot 2 of the 3 components are redshifted, 2 blueshifted components are also observed.

In the central part of the sunspot the extent of the upflow area is smaller on August 4 than on August 3, 1985. Other regions, both inside and outside the sunspot also show marked changes from one day to the next. The three sequences observed during a time span of 18 minutes on August 3 give the same overall results, but show significant differences, even within 5 min.

b) Multiple Flow Speeds

The distribution of measured velocities for line components that belong to profiles with 3 components have been studied in detail for the August 4 data. The distribution of velocities for the strongest of the 3 line components shows a maximum around 15 km/s. The middle intensity line component shows two maxima, whereas the weakest line component shows maxima around - 45, 50 and 100 km/s. This suggests that there may be preferred values of the velocities. A line profile with 3 redshifted components will have a tendency to show flow speeds of 15, 40 and 100 km/s. Simulations with different relative component intensities suggest that the observed maxima are real. It is difficult to draw conclusions from observations of a single line. However, the present study confirms the finding of multiple flow speeds in another sunspot, using several transition zone lines (Brekke *et al.* 1987; Brekke, Kjeldseth-Moe, and Brueckner 1989).

IV. PARTICLE DENSITIES AND MASS FLUXES

With the full spectral coverage of the HRTS instrument a series of density sensitive lines have been studied earlier (Kjeldseth-Moe *et al.* 1984). The intensity ratio between the NIV 1486 line and the CIV 1548 line was used to find the electron pressure and to study the relation between the total integrated intensity, I_{tot}, of the CIV 1548 line and the electron pressure, resulting in the following relation (in cgs units): $P_e = 0.035 I_{tot}^{\frac{1}{2}}$. The corresponding mass flux may be expressed as $\Phi = 4.24 \times 10^{-15} I_{tot}^{\frac{1}{2}} v A_f$, where A_f is the area filling factor of the emission. Dere *et al.* (1987) found $A_f \leq 0.01$. The mass upflow, downflow and net massflow averaged over the 60"× 50" region, but excluding the emerging

flux region, are 0.88, 2.66 and 1.78 $\times 10^{-9} gcm^{-2}s^{-1}$ on August 3 for $A_f = 0.01$. For August 4 the corresponding numbers are 0.75, 3.06 and 2.31 $\times 10^{-9} gcm^{-2}s^{-1}$. Evidently, more mass appears to be moving down than up.

Figure 4 illustrates the mass flux as function of spatial position. The area with upward directed mass flux in the central part of the sunspot is quite extended on August 3. After 22 hours the extent of this upflow region has decreased considerably and a strong mass flux directed downward occurs in two regions, one on the eastern side, close to the center of the sunspot and one positioned in the western part of the sunspot. If the positions of these strong downward mass fluxes are compared with white light images, one observes that an umbral lightbridge coincides in position with the downflow on the eastern side, close to the centre of the sunspot. The strong mass downflow region observed on the eastern penumbral rim on August 3 has disappeared on August 4. The observations suggest that strong downflows may coincide in position with an umbral lightbridge, but may also occur without its presence.

A closer comparison of the three rasters observed on August 3 is interesting. The downflowing region that is elongated in the north-south direction and situated along the eastern penumbra rim changes shape and becomes circular during a time span of 18 min. Changes are also seen in the downflow region in the north-western part of the image; significant changes are even present during a time span of 5 min.

V. DISCUSSION

In this study it is emphasized that the line profiles observed in the sunspot region are rather complicated, often showing 2 or 3 line components with different line-of-sight velocities. Material flow is regarded as the most probable origin for the line shifts (e.g. Kjeldseth-Moe *et al.* 1988). The observed multiple flow speeds within the spatial resolution element suggest the presence of a fine scale spatial structure with preferred velocity values.

The net mass flux for the whole sunspot area is observed to be directed downward. This conclusion rests on two assumptions, i.e. that the observabilities of upflows and downflows are equal and that the line emission area filling factor is independent of flow speed and direction. Three possible sources for differences in observability may be pointed out, i.e. a compression shock, a variation in ionization balance and a systematic difference in temperature between upflow and downflow. If a compression shock occurs the observed line profile may contain information about the same flow twice (Maltby 1989). The characteristic times for ionization and recombination are functions of the flow speed. For downflows, the contribution to the CIV line may extend over a larger range in temperature than in the case with upflow (e.g. Hansteen 1989). One possible origin for a difference in observability is an upflow that starts with a temperature that is consistently too low to give strong line emission. If the gas is heated as it moves along the flux tube, the downflow may occur at a higher temperature with correspondingly high line emission.

This research was supported by the Norwegian Research Council for Science and the Humanities and by NASA grants.

References

Bartoe, J.-D.F., and Brueckner, G.E. 1975, *J. Opt. Soc. Am.*, **65**, 13.

Bartoe, J.-D.F., Brueckner, G.E., Cook, J.W., Dere, K.P., Morrison, M.D., Prinz, D.K., Socker, D.G., and VanHoosier, M.E. 1986 in *Proc. AIAA 24th Aerospace Sci. Meeting*, Reno, Nevada.

Bevington, P.R. 1969, *Data Reduction and Error Analysis for the Physical Sciences* (New York: McGraw-Hill).

Brekke, P., Kjeldseth-Moe, O., Bartoe, J.-D.F., and Brueckner, G.E. 1987, in *Proc. 8th ESA Symposium on European Rocket and Balloon Programmes and Related Research* (ESA-SP-270), p. 341.

Brekke, P., Kjeldseth-Moe, O., and Brueckner, G.E. 1989, in *XI European Regional Meeting IAU* (La Laguna, Tenerife), in press.

Brueckner, G.E. 1981, in *Solar Active Region*, ed. F.Q. Orrall (Boulder: Colorado Associated University Press), p. 113.

Brueckner, G.E., Bartoe, J.-D.F. Cook, J.W., Dere, K.P., and Socker, D.G. 1986, *Advances in Space Research*, Vol. **6**, *Solar and Stellar Activity*, ed. F. Praderi and H.S. Hudson (Oxford: Pergamon), 263.

Brueckner, G.E., Bartoe, J.-D.F., Cook, J.W., Dere, K.P., Socker, D., Kurokawa, H., and McCabe, M. 1988, *Ap. J.*, **335**, 986.

Dere, K.P., Bartoe, J.-D.F., Brueckner, G.E., Cook, J.W., Socker, D.G. 1987, *Solar Phys.*, **114**, 223.

Hansteen, V. 1989, in *Proc. MINI-Workshop on Flux Tubes in the Solar Atmosphere*, eds. E. Leer and P. Maltby (Oslo: Institute of Theoretical Astrophysics), p. 35.

Kjeldseth-Moe, O., Andreassen, Ø., Maltby, P., Bartoe, J.-D.F., Brueckner, G.E., and Nicolas, K.R. 1984, *Adv. Space Res.* **4**, No. 8, 63.

Kjeldseth-Moe, O., Brynildsen, N., Brekke, P., Engvold, O., Maltby, P., Bartoe, J.-D.F., Brueckner, G.E., Cook, J.W., Dere, K.P., and Socker, D.G. 1988, *Ap. J.*, **334**, 1066.

Maltby, P. 1989, in *Proc. MINI-Workshop on Flux Tubes in the Solar Atmosphere*, eds. E. Leer and P. Maltby (Oslo: Institute of Theoretical Astrophysics), p. 3.

Sivaraman, K.R. 1984, *Kodaikanal Obs. Bull.*, **4**, 11.

HIGH RESOLUTION SPECTROGRAPHY IN ULTRAVIOLET

B.Schmieder *, W.T.Thompson **, W.M.Neupert *, R.J.Thomas ***, K.P.Dere ****.**

* Observatoire de Paris, Section de Meudon, F-92195 Meudon Principal Cedex, France

** Applied Research Corporation, 8201 Corporate Drive, Landover, MD 20785, USA

*** NASA Goddard Space Flight Center, Code 680, Greenbelt, MD 20771, USA

**** E.O.Hulburt Center for Space Research, U.S.Naval Research Laboratory, Washington DC 20375-5000,USA

Introduction

We point out some of the advantages of coordinated observations with ground-based and space instrumentation by means of examples of two such programs supported by the Meudon solar observatory. In the first example, results obtained during the rocket flight of the Solar Extreme-ultraviolet Rocket Telescope and Spectrograph (SERTS) for a preflaring region are presented. In the second part, we point out the complementarity of observations with the High Resolution Telescope and Spectrograph (HRTS) which permits the detection of dynamical structures in hot plasma surrounding cool structures such as prominences and sunspots seen in visible light.

SERTS Rocket on May 5, 1989

Coordinated observations (Table 1) have been obtained with an extreme ultraviolet (240 Å - 450 Å) imaging Spectrograph (SERTS-3) described in Neupert *et al.* (1989). Two spectroheliograms (5' x 8') with a spatial resolution between 5" to 10" and quasi-stigmatic slit spectra were obtained simultaneously over 3 different areas on the south-west side of the Sun. We focus our interest on the AR 5464 (S18, W53) observed in spectroheliogram mode between 17:46:42-17:48:41 UT and in slit spectrum mode between 17:48:51-17:52:58 UT. Using Meudon spectroheliograms (K_{1V} - Hα) and a Big Bear magnetogram, good coalignment was obtained since numerous Hα features were identifiable on the Fe XVI and Mg IX spectroheliograms from SERTS (Figure 1 a,b,c).

More than 90 lines were recorded on the quasi-stigmatic EUV spectra covering the temperature range from 50 000 K (He II) to 3 million K (Ni XVIII). Solar features observed included several active region loops, a large sunspot, an active region filament, and a site that flared just minutes later. Over the 5' length of the spectrograph entrance slit, there was no evidence of explosive events. An analysis of the relative intensity of 20 lines (Table 2) measured in different sections along the slit (Figure 1 a) and compared with the quiet sun intensity leads to the following preliminary remarks:

The relative intensity in the preflaring region is significantly higher than in the AR at observed temperatures below 6. 10^5 K (Figure 1 d). This may be evidence for a build up in density at these temperatures just prior to flare onset.

Over the large sunspot, line emission is more intense than in the quiet sun at observed temperatures below 5. 10^5 K and again above 2. 10^6 K, but we find a relative lack of emission around 10^6 K.

Table 1: List of observations available.

Location	Instrument	Observations (Wavelengths)
Rocket	SERTS	Spectroheliograms (Mg IX and Fe XVI ..), Spectra between 240 Å - 450 Å
Meudon	Spectroheliograph	K_{IV}- Hα
	MSDP spectrograph	Hα profiles
SMM	UVSP	Spectroheliograms: continuum wavelength with O V line
Big Bear	Magnetograph	Photospheric line

Table 2: List of the lines used for SERTS-3 analysis in Figure 1 d.

Ion	λ(Å)	log T	Ion	λ(Å)	log T
He II	256.32	4.7	Fe XII	364.47	6.2
Ne V	416.22	5.5	Fe XIII	359.64	6.2
Ne VI	401.94	5.6	Fe XIV	264.78	6.3
Mg VI	349.16	5.7	Fe XIV	334.18	6.3
Mg VII	434.94	5.8	Fe XIV	353.83	6.3
Mg VIII	436.75	5.9	Fe XV	284.16	6.3
Mg IX	368.07	6.0	Fe XV	417.26	6.3
Si X	356.03	6.1	Fe XVI	335.40	6.4
Fe X	345.73	6.1	Fe XVI	360.76	6.4
Fe XI	352.67	6.1	Ni XVIII	291.99	6.5

HRTS on Spacelab 2, August 1985

1. Prominence

Ultraviolet spectra of a prominence were obtained by the NRL High Resolution Telescope and Spectrograph (HRTS) on August 5, 1985, during the Spacelab 2 mission (Figure 2 a). Hα and Ca K spectroheliograms were also obtained at the Meudon observatory (Figure 2 b,c). These show a large prominence consisting of several loop

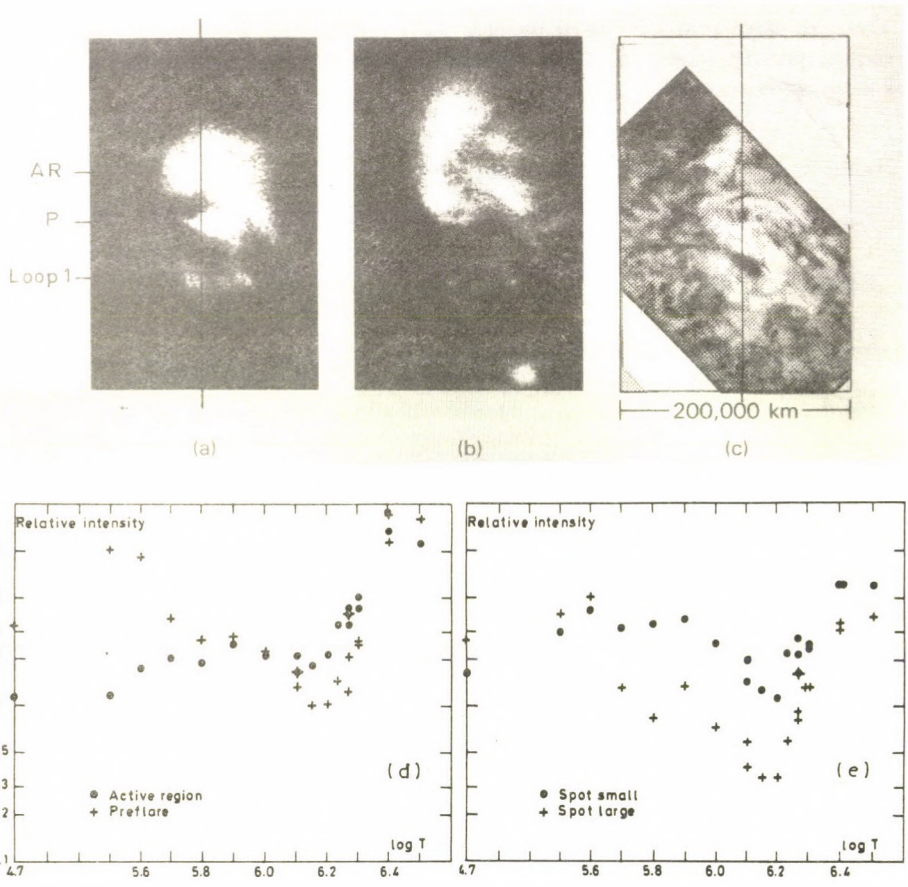

Figure 1 SERTS spectroheliograms in (a) Mg IX and (b) Fe XVI lines, MSDP observations in (c) Hα observed on May 5, 1989, at 17:50 UT. The vertical line indicates the position of the slit of the SERTS spectrograph. The region is quite active; a large flare occurred at 12:27 UT at the location of loop 1 [visible in (a) and (b) maps] which could be a remnant of this flare. In the bright region (preflare P), an enhancement of UV emission will occur 10 minutes later (UVSP data). Between loop 1 and P, a lack of emission corresponds to a large sunspot (S). The loop arcade in the top part of the map (active region AR) overlays bright Hα faculae. Between AR and P regions, the slit crosses the penumbra of a small sunspot. On the left side of the (b) map, a bright loop is visible in Mg IX that is not seen in Fe XVI or in Hα.
(d) and (e) Relative Intensity versus Temperature of EUV emission from the preflaring region (P), the active region (AR) and the large sunspot (S) compared with that from the quiet sun.

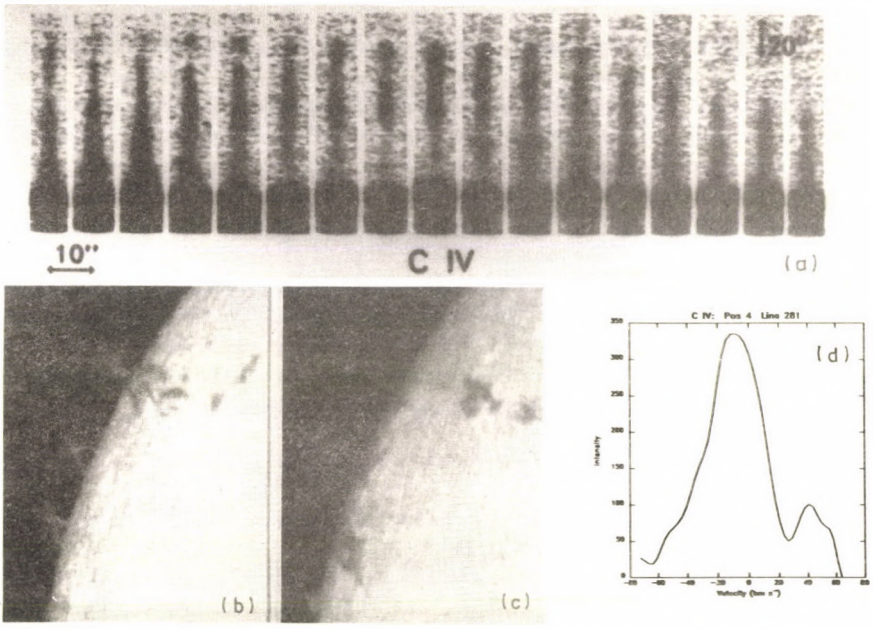

Figure 2 (a) HRTS spectra through a quiescent prominence in C IV lines on May 5, 1985. (b) Hα prominence observed at Meudon on May 5, and (c) on May 6. The C IV arch corresponds to the southern loop seen in Hα. (d) Profiles of C IV lines at the footpoints of the prominence.

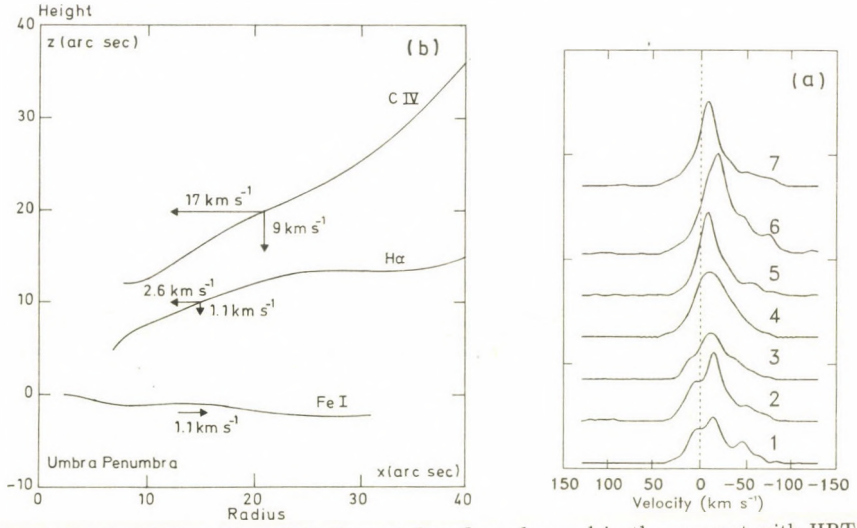

Figure 3 (a) C IV profiles of the largest downflow observed in the sunspot with HRTS during 20 min on May 2 1985. (b) Sketch of the flows 3 levels in the atmosphere in a sunspot.

structures that gradually disappeared over the next 3-4 days. The HRTS spectrograph slit was placed parallel to the solar radius and rastered in 10" increments. Spectra were recorded at 17 raster positions so that one complete loop of the prominence was spanned. At altitude in the prominence, the lines are all quite narrow. Most probable nonthermal velocities of only 3 to 8 km s^{-1} are derived from the line profiles. Most profiles show little evidence of net Doppler shifts higher than 3 km s^{-1}. Near-absolute velocities have been obtained by referencing the spectra to lines of Si I and Fe II observed on the disk. In one of the loop footpoints, Doppler shifts of 25 km s^{-1} are evident in the cooler lines. The strong C IV lines also show small regions with Doppler shifts of 50 km s^{-1} at several positions in the prominence (Figure 2 d). Comparing C IV and Hα images over 2 days we deduce that these large velocities are relative to an arch of the prominence situated in a plane perpendicular to the disk plane and containing the line of sight, and could be interpreted as horizontal flows along the arch.

2. Sunspot

A sunspot in AR 4682 was observed during several days with HRTS. These high resolution UV spectra evidenced high downflows (K-Moe *et al.* 1988). We have carefully analyzed sunspot profiles in Hα obtained during revolution 56 lasting 15 minutes on May 2, 1985, and they do not exhibit large flows. There are some, although not many, 50 km s^{-1} flows in Hα that could be called high speed sunspot flows (Figure 3 a). Thus, we have been able to study the Evershed effect over 3 levels in the atmosphere using Doppler shifts measured in photospheric, Hα, and C IV lines. Under the assumption of axial symmetry in the sunspot, the Evershed flows have been derived, and a sketch of the flows in and around the sunspot is presented in Figure 3 b. Note that the Evershed effect is reversed in the transition region and in the chromosphere (Dere *et al.* 1990).

Conclusion

These results show great promise for future coordinated observations involving rocket flights, the SOHO spectrographs (SUMER and CDS), and the MSDP spectrographs at Meudon, Pic du Midi, and the Canary Islands (VTT telescope).

Acknowledgments

We are grateful to Dr. Martres and Dr. Zirin for providing chromospheric and photospheric observations of AR 5464, to Dr. W. Henze for UVSP data, and to Dr. Alissandrakis for velocity vector computations in sunspots.

References

Dere K.P., Schmieder B., Alissandrakis C.E.: 1990, Astron. and Astrophys. **233**, 207
Kjeldseth-Moe *et al.* : 1988, Astrophys. Journal,**334**, 1066.
Neupert W.M., Epstein G.L., Thomas R.J.: 1989, BAAS,**21**,1027.

STUDY OF NON-UNIFORM HEATING IN SOLAR FLARES

B. Sylwester and J. Sylwester
Space Research Center of Polish Academy of Sciences, Wroclaw, Poland
J. Jakimiec
Astronomical Observatory, Wroclaw, Poland
S. Serio and F. Reale
Astronomical Observatory, Palermo, Italy
R.D. Bentley and A. Fludra
Mullard Space Science Laboratory, Dorking, Surrey, England

Abstract. We have analyzed the ratios of the temperatures derived from Fe and Ca spectra (T_{Fe}/T_{Ca}) for the rising phase of 11 solar flares. In order to interpret the measurements, we postulate the existence of non-uniformity of heating across the flare loop during the analyzed phase. Corresponding hydrodynamic models have been calculated and the obtained results are compared with the observational data for selected flares.

Introduction. In our earlier paper[1] (hereafter P. I.) we have analyzed ratios of temperatures T_{Fe}/T_{Ca}, obtained from Fe and Ca spectra during the quasi-steady-state (QSS) phase for 13 solar flares observed by Bent Crystal Spectrometer (BCS) on the Solar Maximum Mission (SMM). It turned out that the observed values of the ratio cannot be explained by the model consisting of a single, uniformly heated loop, with a constant or variable cross-sectional area. We have suggested that this problem may be solved by introducing some distribution of the rate of energy release in the direction perpendicular to the loop axis. Distribution of heating across the loop causes temperature gradient(s) across the loop. Let us notice that the ratio of temperatures obtained from Fe and Ca lines (T_{Fe}/T_{Ca}) reflects the proportion of hotter and cooler plasma in a flare.
In P. I. we have introduced the parameter α defining the temperature distribution across the loop at its top according to:

$$T_r = T_m\left[1 - \left(\frac{r}{R}\right)^{\alpha}\right] \qquad (1)$$

Here T_r is the temperature at the distance r from the loop axis, T_m is the temperature at the loop centre and R is the radius of the loop.
In the present analysis we apply the same approach to the analysis of rising phase of solar flares. First we consider the evolution of this ratio in the uniform heating approximation.

Uniform heating across the loop. We use the hydrodynamical models of loop of semi-length $2x10^9$ cm and constant cross section, with T_m = 21 MK . The models have been calculated using the Palermo-Harvard code[2]. The heating (release of energy) in these models was switched on and off abruptly and lasted for Δt = 50, 180, 300, 600 s. Based on the commonly known procedure[1,2,3] the electron temperatures of the plasma were calculated from the intensity ratios of j and w lines of Fe XXIV/XXV ions (T_{Fe}) and k and w lines of Ca XVIII/XIX (T_{Ca}). The results are presented in Fig. 1. It is seen that after the

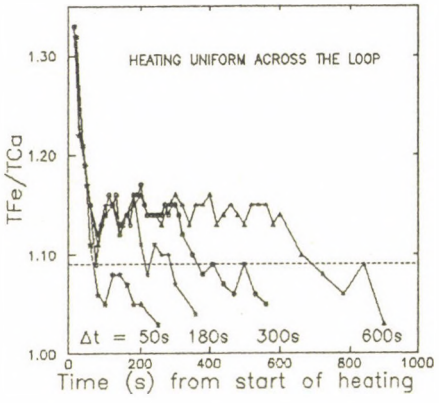

Fig. 1. Time variations of T_{Fe}/T_{Ca} ratio calculated for HD flare models with the heating *uniform* across the loop and for various duration of the heating (Δt = 50, 180, 300, 600 s).

start of heating, during first 50 s, the characteristic sudden decrease of T_{Fe}/T_{Ca} ratio from the value of ~ 1.3 is observed. During the period between 50 s and the termination of the heating the mean level of T_{Fe}/T_{Ca} ratio is constant and amounts to 1.14 ± 0.02. (For Δt = 50 s the heating is terminated before the ratio became constant). After termination of the heating, another, slower decrease of T_{Fe}/T_{Ca} ratio is observed with the rate similar for all cases. The dashed line in Fig. 1. represents the value of the ratio for steady-state loops (1.09). It is seen that when the heating is terminated, the analyzed ratio decreases, and at the end, the hot plasma confined in the loop tends to be isothermal ($T_{Fe}/T_{Ca} \Rightarrow 1$).

The common feature of the uniformly heated models is that T_{Fe}/T_{Ca} ratio always decreases or is constant at 1.14 level. We didn't get the rise of T_{Fe}/T_{Ca} ratio in any considered case .

Observations. We have selected 11 intense flares from BCS/SMM observations with relatively long rise phase and regular light curve. We have estimated the iron and calcium temperatures from the intensity ratios of j to w lines of Fe and k to w of Ca, which were taken from the best fitting of the observed and theoretical spectra[4]. T_{Fe}/T_{Ca} behaviour has been investigated for chosen flares. First, we have noticed that the measured T_{Fe}/T_{Ca} values in the most cases are in the range of 1.2 - 1.4 for the period immediately after the moment when the spectra begin to be strong enough to be recorded by the BCS. Second, for 6 flares systematic rise of this ratio during some period is seen. One example of such behaviour is presented in Fig. 7 of P. I. Other two cases are presented in Fig. 2. The dashed vertical lines show the period immediately after the maximum of flare heating (decrease of the temperature). It is seen that

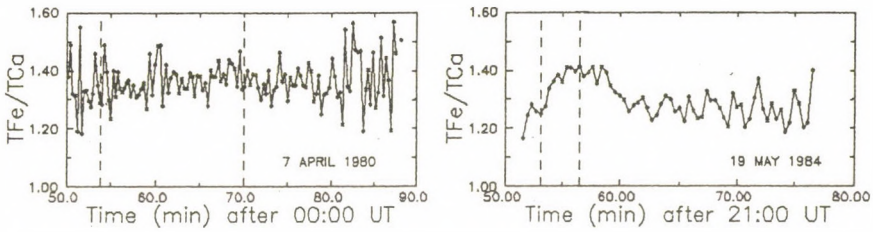

Fig. 2. Examples of observed variation of T_{Fe}/T_{Ca} ratio obtained from the SMM-BCS data.

after the maximum of flare heating, T_{Fe}/T_{Ca} ratio increases what is not expected for uniformly heated loop models (cf. Fig. 1.). For other flares the behaviour of T_{Fe}/T_{Ca} ratio also reveals that the model of uniformly heated loop cannot satisfactory explain the observations during rise phase.

Non-uniform heating across the loop. In order to interpret the observed T_{Fe}/T_{Ca} values we propose, as in P. I., to adopt a hypothesis of non-uniform distribution of the heating across the loop. Our calculations are based on the grid of hydrodynamical models obtained with Palermo-Harvard code for loop of semilength 2×10^9 cm and constant cross-section, uniformly heated across (180 s duration, abrupt start and termination of the heating). The grid consisted of models calculated for 6 values of heating rate (from e_H = 1 to 10 ergs $cm^{-3}s^{-1}$ with the step of $\Delta(\log e_H) = 0.2$). Using this grid we have composed the new family of models with a heating function

changing across the loop, $e_H(r)$. This means that the temperature at the top changes across the loop also, $T_m(r)$, and the dependence has been taken according to Eq. (1). We have calculated time sequences of such models for various values of the parameter α (assuming α = const. within each such sequence). The behaviour of the T_{Fe}/T_{Ca} ratio as obtained from such models is presented in Fig. 3. for chosen values of α = 0.2, 0.5, 2.0. The case with the uniform heating is also presented for the comparison. The dashed vertical line represents the time when the heating is terminated. The most characteristic features of Fig. 3 are: (1) presence of T_{Fe}/T_{Ca} values higher than for the corresponding "uniform" model, (2) the increase of T_{Fe}/T_{Ca} ratio after termination of the heating for some values of α (see Fig. 3). The fluctuations of T_{Fe}/T_{Ca} ratio are related with the rough approximation of the temperatute variation across the loop.

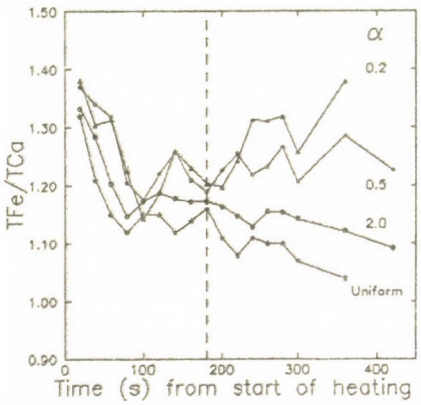

Fig. 3. Calculated variation of T_{Fe}/T_{Ca} ratio for the case of *non-uniform* heating across the loop. Values of parameter α - characterize constant in time shape of the temperature variation across the loop.

Conclusions. The models with non-uniform (across the loop) heating better represent the observational data. We attempt to interpret the time behaviour of T_{Fe}/T_{Ca} ratio by comparing the observed rate of changes with model results. For the most of analyzed flares the comparison suggests $0 < \alpha < 1$ (which means that the proportion of the amount of hotter to cooler plasma is rather low). In particular for the cases presented in Fig. 2, α is 0.7 and 0.3 respectively. For one flare only (2 May 1984, 19:15 UT) we have obtained $\alpha > 1$ which suggests more uniform

distribution of temperature across the loop at its top.
For more precise analysis it will be useful to extend the considerations for temperature ratios derived from lines which form at lower temperatures.

This work has been performed within the Polish CPBP 01.20 Program of Space Research.

References.

1. Sylwester, B., Sylwester, J., Bentley, R.D., and Fludra, A.: 1990, Solar Phys. **126**, 177.
2. Pallavicini, R., Peres, G., Serio, S., Vaiana, G., Acton, L., Leibacher,J., and Rosner, R.: 1983, Astrophys. J. **270**, 270.
3. Doschek, G.A., Boris, J.P., Cheng, C.-C., Mariska, J.T., and Oran, E.S.: 1982, Astrophys. J. **258**, 373.
4. Fludra, A.: 1987, Ph.D. thesis, Wroclaw University.

THE FORMATION OF THE MG I 12-MICRON EMISSION LINES

Mats Carlsson[1], Robert J. Rutten[2] and Natalya G. Shchukina[3]

[1] *Institute of Theoretical Astrophysics, Oslo, Norway*
[2] *Sterrekundig Instituut, Utrecht, The Netherlands*
[3] *Main Astronomical Observatory, Kiev, USSR*

The Mg I 12 μm lines

The emission features near 12 μm measured by Brault and Noyes (1983) and identified as Mg I Rydberg lines by Chang and Noyes (1983) supply sensitive diagnostics of solar magnetic fields (Deming *et al.* 1988)—but in order to use them their nature and sphere of formation should be known. Sofar it isn't clear whether they are chromospheric or photospheric, optically thick or thin, LTE or NLTE. We briefly discuss these issues here, using the observational facts that: (*i*)—the lines are in the infrared; (*ii*)—the lines consist of narrow central emission spikes and broad absorption wings; (*iii*)—both cores and wings limb-brighten in absolute intensity while the continuum darkens.

LTE or NLTE

LTE formation requires deep formation since the Saha–Boltzmann opacity is much too low higher up in the solar atmosphere. LTE formation also requires the presence of a minimum in the run of temperature with height to explain the profile shape. These points led Zirin and Bopp (1989) to postulate from their adoption of LTE that the chromosphere sits much deeper than anyone has ever thought, discarding all other evidence for the location of the temperature minimum, and to disclaim the existence of kilogauss flux concentrations in the photosphere as well.

However, the absorption dips map the temperature minimum if LTE holds, so that the lines should display similar intensity minima from center to limb, at increasing separation from line center. This is in obvious conflict with the observed wing brightening which shows immediately that, for LTE opacities, a frequency-dependent total source function is required, thus a NLTE S^l. Zirin and Bopp conclude that "the 12 μm lines can tell us quite a bit if we stare at them long enough" but a mere glance suffices to disprove any LTE scenario—including Zirin and Bopp's.

Chromospheric formation

Formation in the chromosphere requires large NLTE line opacity, appreciably exceeding Saha–Boltzmann populations. This can't be done in deeper layers where collisions are frequent because the infrared photon energies involved in Rydberg *bb* and *bf* transitions are much smaller than the kinetic energies of the ambient particles: only at large height can any NLTE process maintain appreciable departures against collisional thermalization. Such a process (*e.g.* charge exchange) must then produce enormous Rydberg-level overpopulations to produce sufficient opacity. The emission peak would then have to arise from a hot chromospheric layer which is optically thin at line center conform the limb brightening, whereas the extended absorption wings would then not come from the same layer but arise differently, far deeper. Such a split is unlikely because the wings limb-brighten similarly to the peaks.

Photospheric formation

The alternative is to have near–LTE line opacities but an NLTE line source function, *i.e.* divergence between the upper and lower level population departures. Lemke and Holweger (1987) have shown that small (5%) departure divergence suffices to produce satisfactory source function departure if it occurs deep enough in the photosphere. By ad-hoc postulation of such departure divergence they were able to fit the observations, both peaks and wings, including the limb brightening.

There are three reasons why such small divergence suffices. First, as pointed out by Lemke and Holweger, the sensitivity of the source function to population departure divergence increases towards the infrared with the importance of induced photo-deexcitation. Second, as pointed out by Goldberg (1983), the profile of the line extinction coefficient becomes more spiked towards the infrared. Third, the outward decreasing slope of temperature against height translates in the infrared (where the Planck function temperature sensitivity is small) into a flat infrared line source function for small NLTE departure, producing extended shallow absorption wings as observed.

However, Lemke and Holweger were unable to explain how such photospheric population divergence might arise. Their ad-hoc divergence remains far below the domain of population inversion (this wasn't grasped by Zirin and Bopp who erroneously equate population divergence with "laser action"), but it exceeds what infrared photon processes can typically produce.

Collisional NLTE: departure diffusion

We are currently modeling the solar Mg I spectrum including large numbers of Rydberg levels and lines using Carlsson's (1986) implementation of the method of Scharmer and Carlsson (1985) for a standard plane-parallel radiative-equilibrium model atmosphere without chromosphere.

Our preliminary results confirm the ad-hoc model of Lemke and Holweger and identify the NLTE mechanism. The emission is not due to selective properties of specific levels or to fortuitous pumping coincidences but is a natural consequence of the replenishing of NLTE population losses in a minority species from the population reservoir in the next higher ionization stage. We find that the driving population deficits are due to photon losses in lines with 6–7 eV excitation energy while stronger lines, ultraviolet overionization from low levels, ultraviolet autoionization resonances of higher levels and dielectronic recombination into Rydberg levels are less important. The replenishing from the Mg II reservoir occurs primarily through *collisional departure diffusion* along a close-stepped ladder of high-lying Rydberg states. Paradoxically, the high-n Mg I lines therefore display NLTE formation due to their domination by collisional processes.

References

Brault, J. and Noyes, R.: 1983, *Astrophys. J.* **269**, L61
Carlsson, M.: 1986, *A Computer Program for Solving Multi-Level Non-LTE Radiative Transfer Problems in Moving or Static Atmospheres*, Report No. 33, Uppsala Astronomical Observatory
Chang, E. S. and Noyes, R. W.: 1983, *Astrophys. J.* **275**, L11
Deming, D., Boyle, R. J., Jennings, D. E., and Wiedemann, G.: 1988, *Astrophys. J.* **333**, 978
Goldberg, L.: 1983, in P. B. Byrne and M. Rodonò (Eds.), *Activity in Red Dwarf Stars*, IAU Colloquium 71, Reidel, Dordrecht, p. 327
Lemke, M. and Holweger, H.: 1987, *Astron. Astrophys.* **173**, 375
Scharmer, G. B. and Carlsson, M.: 1985, *J. Comput. Phys.* **59**, 56
Zirin, H. and Bopp, B.: 1989, *Astrophys. J.* **340**, 571

HIGH RESOLUTION SOLAR PHYSICS FROM THE SPACE STATION WITH INTERFEROMETRIC TECHNIQUES : THE SOLAR ULTRAVIOLET NETWORK (SUN) — INSTRUMENT & OBJECTIVES

L. Damé[1,2], L. Acton[3], M. Bruner[3], P. Connes[2], T. Cornwell[4], B. Foing[5], J. Heyvaerts[6], R. Jalin[1], P. Lemaire[7], M. Martic[7], B. Moreau[1], R. Muller[8], T. Roca Cortés[9], J. Riehl[1], R. Rutten[10], A.M. Title[3], J.-C. Vial[7], H. Visser[11], G. Weigelt[12]

[1] ONERA, BP n° 72, 92322 Châtillon Cedex, France,
[2] Service d'Aéronomie, BP n° 3, 91371 Verrières-le-Buisson Cedex, France,
[3] Lockheed Palo Alto Research Laboratory, Palo Alto, CA 94304, USA,
[4] National Radio Astronomy Observatory, Socorro, NM 87801, USA,
[5] Space Science Department, ESTEC, Postbus 299, 2200 AG Noordwijk, The Netherlands,
[6] DAEC, Observatoire de Meudon, 92195 Meudon Principal Cedex, France,
[7] Institut d'Astrophysique Spatiale, B.P. n° 10, Verrières-le-Buisson 91371 Cedex, France,
[8] Observatoire du Pic-du-Midi, 85200 Bagnères de Bigorre, France,
[9] Instituto Astrofisica de Canarias, La Laguna, 38071 Tenerife, Spain,
[10] Sterrekundig Instituut, Postbus 80 000, NL-3508 TA Utrecht, The Netherlands,
[11] TNO-TPD Institute of Applied Physics, Postbus 155, 2600 AD Delft, The Netherlands,
[12] Max Planck Institut für Radioastronomie, D-5300 Bonn 1, FRG.

ABSTRACT

The Solar Ultraviolet Network (SUN) instrument is based on an interferometric concept capable of observations with a spatial resolution better than 0.013" (10 km) on the Sun, in the UV and visible wavelengths ranges. Following Stabilized Interferometry principles it consists in 4 telescopes of 20 cm diameter aligned non-redundantly on a 2 m baseline. Despite its size (2.1 x 1.0 x 0.7 m), and its intrinsic complexity, SUN would be perfectly suited for use on the Space Station, when implemented on a pointing platform of performances comparable with the Instrument Pointing System (flown on Spacelab2). The remarkable capabilities of the SUN instrument, resulting from its "compact" non-redundant configuration of telescopes, allow high resolution imaging on a 4 x 4 arcsec^2 field ; the dynamic on the reconstructed images is superior to 100 for phase stabilities $\geq \lambda/10$ and photon flux as low as 1000 ph/s/pixel. Observations can be carried on the solar disk (granulation, flares and micro-flares, prominences and filaments), or above the limb (coronal loops studies, spicules, etc...). The SUN instrument is part of the Solar Interferometric Mission for Ultrahigh Resolution Imaging and Spectroscopy (SIMURIS) which was proposed to ESA in the frame work of the Next Medium Size Mission (M2) in November 1989[1], and accepted for an Assessment Study in February 1990.

1. RATIONALE FOR HIGH RESOLUTION ON THE SUN

The Solar Ultraviolet Network is the first proposed interferometric experiment in Space at visible and ultraviolet wavelengths aimed at reconnaissance of solar features at angular scales much below 0.1 arcsec. Considerable evidence suggests that all scales of the Sun' structures, as well as other interesting astrophysical objects, are coupled to small-scale processes associated with intermittent magnetic fields and turbulent stresses. With a spatial resolution as high as 10 km (0.01 arcsec) on the solar surface, and a spectral resolution of 0.1-1 Å in the UV, the SUN investigation presents a unique possibility of observations at the ultimate resolution where the very fine structure of the magnetic field initiate the unstable energy processes responsible for the chromospheric and coronal heating.

Though the ultimate temperature gradient scale across a coronal loop might in principle be 25 cm (ion gyroradius), it will probably be smeared out by plasma micro-instabilities (such as drift

waves), and the relevant minimum observable scale is more realistically of the order of 1-10 km (≈ the photon mean free path in the chromosphere).

A breakthrough in high spatial resolution observations should allow to understand in finer physical details processes like magnetic heating in coronal loops (temperature profiles, time dependance, spatial localization of heating processes), but also, by access to visible wavelengths, the coupling between turbulent convective eddies and magnetic fields in the photosphere. The scientific objectives of SUN are fourfold : physics of coronal loops, plasma heating processes and thermal inputs of flares and microflares, fine magnetic field structures, and dynamics of the granulation ; they will be addressed through high resolution images, in the UV and in the visible, of coronal loops, flare kernels, internal flux tube structure and granules.

2. INSTRUMENT

The SUN experiment is intended for ultrahigh resolution imaging and spectroscopy of the Solar Atmosphere from the ultraviolet wavelength range (the C III line at 1175 Å) to the visible (where a 60 mÅ spectral resolution Fabry Perot allows direct magnetic field measurements of photospheric lines) and near infrared wavelengths (9000 Å). It consists in a 2 m long linear array of 4 telescopes. The telescopes, 20 cm in diameter, are non-redundantly spaced with inter-distances 1d-3d-2d, with d = 30 cm. The essential of the experiment has been described in a previous paper[2]. Specific to the SUN concept are : a diasporameter for the remote pointing stabilization on the solar limb (even during rotation of the array), the use of stabilization on a remote solar field in the visible (using white light fringe tracking from Differential Synchronous Reference Interferometers), and a detection system consisting in a Double Grating Spectrometer allowing adjustable narrow band filtergrams of the fringe pattern directly addressable by Radio Astronomy reconstruction methods for imaging on extended field of views. The SUN concept in which the telescope diameter is not negligible compared to the baseline, allows an exceptional spatial frequency coverage, suitable for direct imaging (high resolution imaging in one direction) and optimized for *high resolution imaging of an extended object* when complemented by a rotation of the array. The Modulation Transfer Function is "full", i.e. without any hole, a choice which allows excellent image reconstruction.

SUN is a fully stabilized instrument, using the Solar integrated white light to achieve *co-phasing* of the telescopes, a technique developed initially for Stellar Interferometry[3], and which has now been proven in Laboratory[4]. It has therefore the unique capability of very high sensitivity, since very long integration times can be afforded (several minutes) on weak structures, UV or visible. SUN can integrate as long as the structure itself does not evolve, or as long as the internal instrumental alignment holds. SUN can also follow fast events with instantaneous snap-shot imaging across any structure. This is particularly interesting for coronal loops since the radial profile of a loop will reflects the radial behavior of the length-averaged heating rate : an invaluable information for the heating process localization and its time dependance[5].

The SUN instrument is currently being studied by ESA in the frame work of the Assessment Study of SIMURIS, and should proceed in 1991 for a Phase A in the context of the Space Station Attached Payloads, for a possible launch before the end of the century.

REFERENCES

1. L. Damé et al. : *A Solar Interferometric Mission for Ultrahigh Resolution Imaging and Spectroscopy (SIMURIS)*, in answer to ESA D/Sci/RMB/val/3080 for the "Next Medium Size Mission — M2" (1989)
2. L. Damé et al. : *SOLAR ULTRAVIOLET NETWORK (SUN) : An Interferometric Investigation of the Fundamental Solar Astrophysical Scales*, in New Technologies for Astronomy, Proc. SPIE **1130**, 126 (1989)
3. L. Damé et al., *ASSI : An Optimized Fringe Tracking Stellar Interferometer*, in Active Telescopes Systems, Proc. SPIE **1114**, 225 (1989)
4. L. Damé et al. : *Laboratory Experiments on Fringe pattern Acquisition and Stabilization*, in Amplitude and Intensity Spatial Interferometry, Proc. SPIE **1237** (1990)
5. J. Heyvaerts, *About the Interest of Solar Interferometric Observations*, in Optical Interferometry in Space, Ed. N. Longdon and V. Davis, ESA SP **273**, 11 (1987)

HANLE EFFET WITH PARTIAL FREQUENCY REDISTRIBUTION

M. Faurobert-Scholl
Observatoire de la Côte d'Azur, BP 139 06003 Nice Cedex. France

Abstract: The coherent scattering of an anisotropic radiation field by atoms gives rise to a linear polarization of spectral lines, the so-called Resonance Polarization. In presence of weak magnetic fields the resonance polarization is decreased and the polarization plane is rotated, this effect, known as the Hanle effect, allows the determination of weak magnetic fields, in solar prominences for example.

Here I investigate the Hanle effect on optically thick lines formed by multiple scattering of photons. In particular the importance of the correlation between the frequencies of the absorbed and reemitted photons at each scattering event (partial frequency redistribution) is outlined.

1 Introduction

Landi degl'Innocenti *et al.*[5] have shown the interest of the analysis of the Hanle effect on the linear polarization of optically thick spectral lines for the determination of weak magnetic fields in solar prominences. It is well known that partial frequency redistribution effects play an important role in the formation of strong resonance lines, in particular they induce a resonance polarization in the wings which does not exist for subordinate lines formed with complete frequency redistribution[2, 3].

The vectorial transfer equation for the polarized line radiation in presence of weak magnetic fields has been derived in the most general form by Landi degl'Innocenti[4]. For lines formed with complete frequency redistribution it has been cast into an integral form and solved by Bommier *et al.*[1]. This integral method does not apply to lines formed with partial frequency redistribution. I have developed two numerical methods for solving directly the polarized transfer equation in a one-dimensional medium. The first one is a generalization of the well known Feautrier method, the other one relies on a Fourier expansion of the radiation field with respect to the azimuthal direction. Both methods apply to lines formed with complete or partial frequency redistribution. The polarization diagrams obtained with various depth-independent magnetic fields are shown for lines formed in isothermal semi-infinite atmospheres, with complete or partial frequency redistribution.

2 Polarization diagrams

The model used is a one-dimensional semi-infinite atmosphere with uniform temperature and magnetic field. The collisional destruction probability of photons, denoted by ε, and the ratio β of the continuum to line opacity are depth independent with $\varepsilon = 10^{-4}$ and $\beta = 10^{-7}$ which are typical values for strong lines in the solar chromosphere. The magnetic field colatitude is $\theta_B = 45^0$. The relevant quantity to measure the Hanle effect is the ratio $\gamma = 2\pi\nu_L g/A$ where ν_L is the Larmor frequency of an electron in the magnetic field, g is the Landé factor of the upper level of the transition and A its inverse life-time. Figure 1a,b shows the polarization diagrams $(Q/I, U/I)$ for 3 values of γ and a line of sight with $\theta = 75^0$. The close curves are described when the difference of the azimuthal angles $\chi - \chi_B$ rotates from 0 to 360^0. The complete frequency redistribution results (dotted curves) are compared to partial frequency redistribution results (full curves) at line center (Figure 1a) and at one Doppler width from line center (Figure 1b).

Figure 1

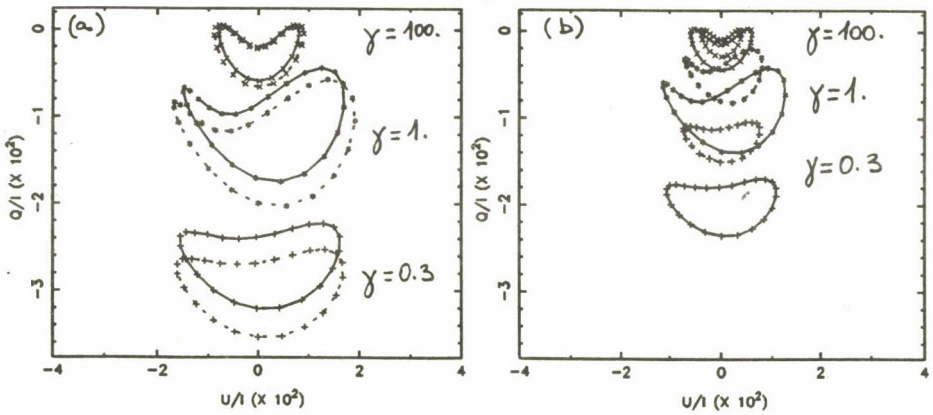

References

[1] Bommier, V., Landi Degl'Innocenti, E., Sahal-Bréchot, S.: 1989, *Atelier Transfert*, eds. H. Frisch and N. Mein, Publications of Paris Observatory.

[2] Faurobert, M.:1987, *Astron. Astrophys.* **178**, 269.

[3] Faurobert, M.:1988, *Astron. Astrophys.* **194**, 268.

[4] Landi Degl'Innocenti, E.: 1985, *Solar Physics* **102**, 1.

[5] Landi Degl'Innocenti, E., Bommier, V., Sahal-bréchot, S.: 1987, *Astron. Astrophys.* **186**, 335.

THE DECAY PHASE OF THREE LARGE SOLAR FLARES

A. Fludra[1], R.D. Bentley[1], J.L. Culhane[1], J. Jakimiec[2], J.R. Lemen[3], J. Sylwester[4], and S.T. Moorthy[1]

[1] Mullard Space Science Laboratory, University College London, UK. [2] Astronomical Institute, Wrocław University, Poland. [3] Lockheed Palo Alto Research Laboratory, Palo Alto, U.S.A. [4] Space Research Centre, Wrocław, Poland.

High resolution X-ray spectra of Ca XVIII - Ca XIX lines around 3.165 – 3.231 Å have been recorded by the Bent Crystal Spectrometer (BCS) on the Solar Maximum Mission during the decay phase of three large solar flares. The sites of these flares were observed for several consecutive satellite orbits (Table 1). This allows us: 1) to follow the cooling of the flare plasma and post flare region, 2) to analyse line broadening in the post flare region, and 3) to test whether the ratio of the Ca XIX resonance line to nearby continuum, as a function of temperature, changes within several hours of observation. Theoretical spectra have been fitted to the observed spectra (Fludra *et al.*, 1989) to obtain average electron temperatures, emission measures and line widths. To obtain a sufficient number of counts during later orbits, spectra had to be integrated for intervals between 5 and 15 minutes. This allowed us to extend the analysis to temperatures as low as $7.5 - 8 \times 10^6 K$ and to emission measures around 10^{48} cm^{-3}.

1. The density-temperature diagrams (Jakimiec *et al.*, 1986) have been constructed to analyse the cooling of the three flares, using data from all available orbits. All three flares have two typical phases: significant decrease of heating rate (the temperature decreases while the emission measure is nearly constant) and evolution parallel to the line representing the scaling law for static loops (Jakimiec *et al.*, 1986). In addition, later orbits of all three flares show behaviour which has been rarely seen in other BCS data: the emission measure decreases while temperature is constant or increases (Figure 1), which indicates that part of X-ray emission comes from different loops which may have greater length and/or smaller volume.

2. Spectra analysed by Fludra *et al.* (1989) had line widths greater than the thermal width during the 10 – 20 minutes of the decay phase. In the three flares lines are also broader than the thermal width. The line broadening is the smallest at the time of maximum emission measure and it is usually greater during later orbits (Figure 2). This excess line broadening could arise as a result of plasma motions or a spatial extent of the source in the East-West direction on the Sun, which corresponded to the dispersion axis of the spectrometer. An upper estimate of the source size in the E-W direction (from the FCS images in Si XIII line) for the flare of 5 May 1984 is 0.3, 0.6 and 1 arc minute for each subsequent orbit, respectively. The line widths, after correcting for this size, still have an excess over the thermal width equivalent to a turbulent velocity of about 40 km/s. Similarly, the E-W size of the intensity distribution of the 21 May 1980 flare can account only for 10 – 20% of the excess width.

3. We calculate the line-to-continuum ratio as a function of temperature separately for each orbit and use the method of Lemen *et al.* (1986) and Sylwester *et al.* (1990) to determine the variation of the Ca abundance after the maximum of each flare on a time scale of several hours. For the flares of 21 May 1980 and 25 April 1984 the abundance is constant during 2 and 5.5 hours of observation, respectively. During the flare of 5 May 1984 the Ca abundance decreased from 7.6×10^{-6} to 4.6×10^{-6}

over three hours (Table 1). However, such changes in the line-to-continuum ratio have been given an explanation different to that of abundance variation by Jakimiec *et al.* (1988), who point out that the volume of plasma which produces continuum emission may be larger than that which produces line emission.

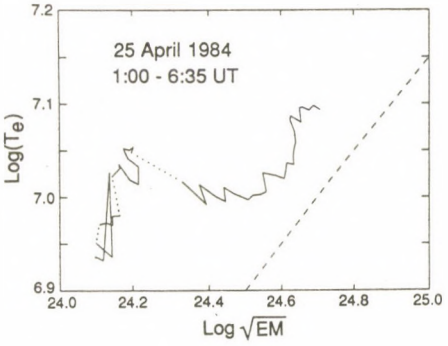

date, class, coordinates	time UT	A_{Ca}	δA (10^{-6})
21 May 80	21:05 – 21:30	5.9	0.5
X1.4	22:24 – 22:54	5.6	0.8
S14 W15			
25 Apr 84	1:00 – 1:50	5.0	0.5
X13	2:35 – 3:25	5.1	0.5
S11 E42	4:10 – 5:00	5.1	0.5
	5:45 – 6:35	5.7	0.6
5 May 84	18:25 – 18:37	7.9	0.6
M7.5	19:15 – 20:08	6.2	0.9
S11 W90	20:48 – 21:22	4.6	0.7

Fig. 1. Temperature as a function of emission measure during the four SMM orbits after the maximum of the flare of 25 April 1984. Time runs from the upper-right part of the diagram. Dotted lines show the satellite nights. The dashed line shows the inclination resulting from the scaling law for static coronal loops.

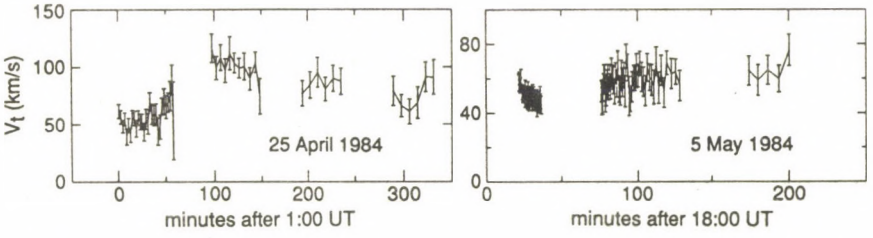

Fig. 2. The excess line width over the thermal width, expressed as a turbulent velocity, v_t. Alternatively, this excess could be produced by the source having a spatial extent equal to $0.03 \times v_t$ arc minutes in the E-W direction.

Fludra, A., Lemen, J.R, Jakimiec, J., Bentley, R.D. and Sylwester, J. 1989, *Ap. J.*, **344,** 991.

Jakimiec, J., *et al.* 1986, *in "Solar Maximum Analysis"*, eds. Obridko, V.V., and Stepanov, V.E., VNU Science Press, Utrecht, p.91.

Jakimiec, J., *et al.* 1988, *Adv. Space Res.*, **8, No. 11,** 231.

Lemen, J.R., Sylwester, J., Bentley, R.D. 1986, *Adv. Space Res.*, **6, No. 6,** 245.

Sylwester, J. *et al.* 1990, (in preparation).

High resolution UV Solar spectroscopy: wavelength accuracy

P. Lemaire
IAS - CNRS, Université de Paris XI
BP 10, 91371 Verrières le Buisson Cedex (France)

Abstract
The solar atmosphere is in a dynamic state. In high resolution spectroscopy the line of sight velocity is determined by the Doppler shift of the line. To establish an accurate budget of mass motions in the upper atmosphere there is a need to reference the lines profiles to an absolute wavelength scale. The use of solar lines and calibration source lines is discussed and some methods are developped that may be applied in the high resolution UV spectrometer (SUMER) in the ESA/NASA SOHO mission.

Introduction

The energy balance in the solar atmosphere can be expressed by the equation (Gabriel,1976)

$$\mathrm{Div}\,(F_{rad} + F_{cond} + F_g + F_{kin} + F_{enth} + F_{wave}) = Q$$

where the terms relate to the flux densities of radiative, conductive, gravitational, kinetic, enthalpy and wave energy; all other unspecified heating sources are represented by Q.

In the static case, the three first terms are predominant, whilst, when the plasma starts moving,e.g. in the chromosphere and corona, the last three terms as well as Q become important. F_g , F_{kin} and F_{enth} flux terms are proportional to the mass flux and thus to the velocity. The most prominent mode of F_{wave} , the Alfvén waves, can be expressed as

$$F_{wave} = N_p\, m_p\, \delta v^2\, (v_a + 3/2\, v_p)$$

and, also, is related to measurable velocity through v_p (v_a may be difficult to directly be measured).

In the photosphere, the amplitude of the velocity field is lower than 1 km s^{-1} . As the temperature rises and the density decreases in the chromosphere the amplitude of the velocity fields increases up to about 5 km s^{-1} on the chromospheric plateau (6000 - 7000°K). The strong discontinuity given by the transition zone induces a jump in velocities that may vary between few km s^{-1} and 20-30 km s^{-1} in the average with some peculiar area (explosive events) where the velocity may reach 400 km s^{-1} (Brueckner and Bartoe, 1983).

The determination of the line of sight velocity is deduced from the wavelength shift through the formula $\delta v/c = \delta\lambda/\lambda$. Thus high accuracy determination of the wavelength shift from its absolute wavelength rest is required. In the ultraviolet domain the relation between wavelength and velocity accuracies is given in figure 1.

Absolute wavelength measurement

From Kaufman and Edlen (1974) compilation, uncertainties in the absolute wavelengths measured in the laboratory between 500 and 2000 Å are: 0.0002 Å for Ne I, 0.0005 Å for Ar I and N I, 0.0007 Å for O I, 0.001 Å for Cl I, S I and Si I, and 0.0015 Å for C I. The best accuracy is provided by lines of neutral species.

Transfer to Solar lines in the 500-1600 Å wavelength range

The application is done for the SUMER (Solar Ultraviolet Measurement of Emitted Radiation - Wilhelm et al, 1988) instrumentation on the ESA/NASA SOHO satellite. In the SUMER instrumentation slits and wavelengths are selected using mechanisms that do not provide 0.001 Å movement accuracy. Nevetheless the 20 to 40 Å stigmatic bandpass with 0.02

to 0.04 Å spectral resolution along the slit (up to 300 arcseconds with 1 arcsec pixel size) is collected simultaneously by the bidimensional detector. Each 20 to 40 Å bandpass provides enough solar lines of neutral species to set a wavelength scale for accurate wavelength measurement of transition lines and low coronal lines.

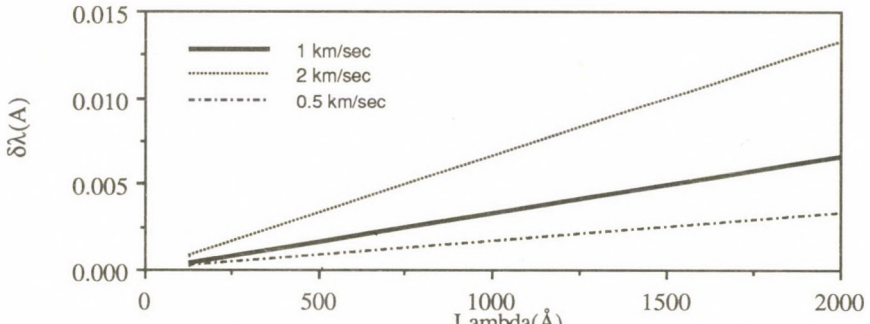

Wavelength shift related to Doppler shift

The solar lines of neutral species are issued from low chromosphere and as such are perturbed by either chromospheric oscillations (Deubner et al, 1990) or erratic mass motions (Dere et al, 1984). The chromospheric oscillations can be cancelled out by integrating over one or several periods; the residual velocity can be smaller than 0.5 km s^{-1} . The residual errors produced by erratic mass motions that appear in discrete (few arcseconds) locations can be minimized by integrating along the slit that covers several supergranular cells.

The accuracy of the absolute wavelength determination using solar lines is thus few 0.001 Å, i.e. about 1 km s^{-1} or 0.1 pixel.

The use of a calibration source , such as the Pt-Ne hollow cathode implemented in the I.U.E. (International Ultraviolet Explorer - NASA/ESA) satellite provides 0.003 Å absolute wavelength determination (Reader et al., 1986). The comparison of the wavelength accuracy given by the lines of the lamp, without taking into account the difficulties of implementation and operation of such a source, with the capabilities provided by the solar spectrum, in real time, shows that the lamp does not give a real gain in accuracy.

In conclusion, the solar spectrum , in the wavelength ranges where there are lines of some neutral species, gives by itself an accurate wavelength scale.

References

Dere, K.P. ,Bartoe, J.-D.F. ,and Brueckner, G.E.,"High resolution telescope and spectrograph observations of the quiet solar chromosphere and transition zone", Astrophys. J. **281**,870 (1984)

Deubner,F.-L. ,and Fleck,B. ,"Dynamics of the solar atmosphere. III. Cell-network distinctions of chromospheric oscillations", Astron. Astrophys. **228**, 506 (1990)

Gabriel, A.H., 1976,in 'The energy balance and hydrodynamics of the solar chromosphere and corona', R.M. Bonnet and P. Delache eds, Nice (1976), pp 375

Reader, J. and Acquista, N.,(1986) "Spectrum of Westinghouse Platinum - Neon Hollow Cathode Lamp", National Bureau of Standards, Gaithesburg, MD.

Wilhelm, K., Axford, W.I., Curdt, W., Gabriel, A.H., Grewing, M., Huber, M.C.E., Jordan,S.D., Lemaire, P., Marsch, E., Poland, A.I., Richter, A.K., Thomas, R.J., Timothy, J.G., and Vial, J.C.,(1989), SOLAR ULTRAVIOLET MEASUREMENT OF EMITTED RADIATION - SUMER, in The SOHO Mission -Scientific and Technical Aspects of the Instruments, ESA SP-1104, pp 31-37

CORONAL METER WAVELENGTH OBSERVATIONS DURING SOLAR MINIMUM: LOCATION OF DENSE STREAMERS

D. RIGAUD, P. LANTOS, Observatoire de Paris-Meudon, France
C.E. ALISSANDRAKIS, National University of Athens, Greece

The Nançay Radioheliograph has provided daily two-dimensional radio maps of the quiet corona at 164 MHZ during a period of very low solar activity in may-july 1986. The instrument and the method of Earth-rotation aperture synthesis are described in Alissandrakis, Lantos and Nicolaidis (1985). Figure 1 shows an example of radio map obtained on 27 may 1986. Isophotes are brigthness temperature levels with intervals of 25 000 °K. The lowest isophote corresponds to 100 000 °K. During solar minimum, most of the sources are due to thermal emission. The radio emission being mainly sensitive to electron density, the sources localize the denser regions of the corona.

As the radioastronomy observes the corona on the disk, it provides better resolution in longitude than limb observations (coronal lines or K-corona) and allows easier identification with chromospheric structures. Figure 2a shows the comparison of the location of the radio sources with the corresponding Meudon synoptic map deduced from chromospheric Hα and KI observations.

Fig 1: Solar map on 27 may 1986 at 164MHz

For the active longitudes (on the right of the synoptic map), the radio sources are close to active regions and to the filaments. Note that the largest active region has no meter wavelengths thermal counterpart because its density is higher than 3.5 10(8) cm-3 which is the plasma density at 164 MHz.

For quiet longitudes, there is no relationship between radio sources and filaments or small faculae. On the other hand, figure 2b, where the radio source locations are compared with the coronal sheet observed in K-corona (Sime et al.,1987), indicates a good agreement between localized radio emissions and the equatorial streamer belt. Thus radio observations at meter wavelengths provide a new tool, with better longitudinal resolution, to refine our knowledge of this region which is suspected to be at the origin of slow solar winds.

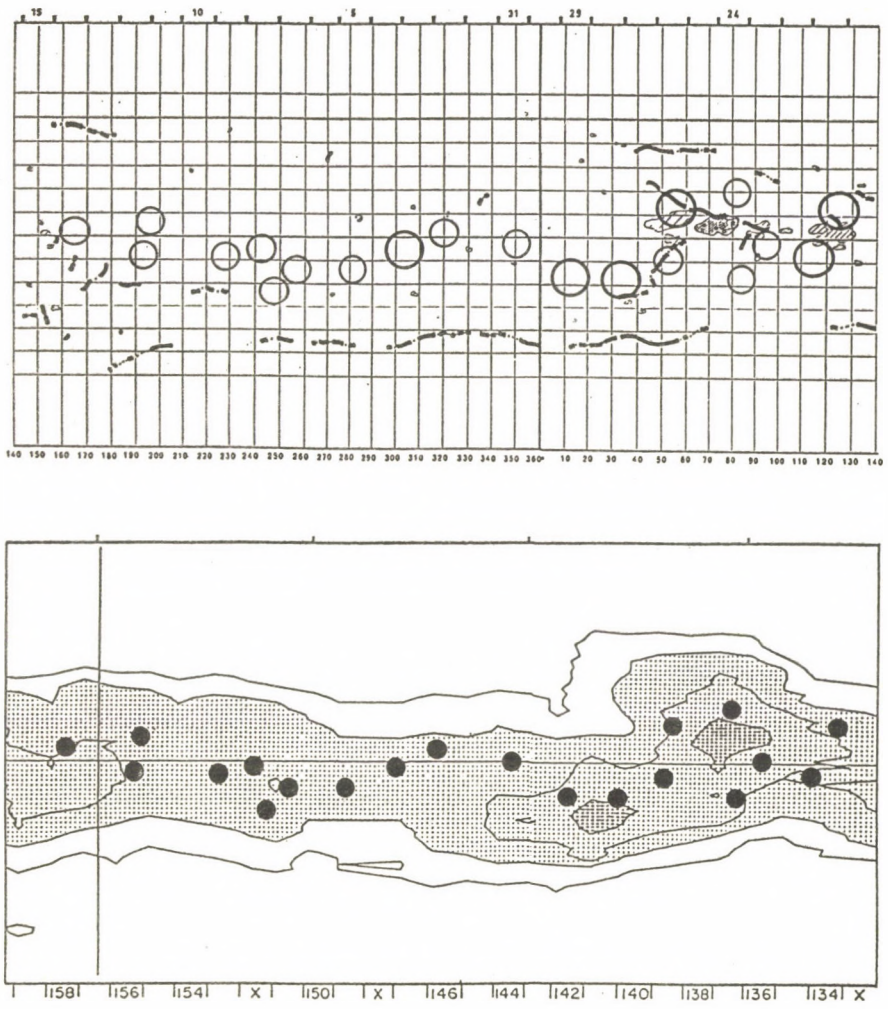

Figure 2: Comparison of the radio emission locations with:
a) chromospheric synoptic map
b) K-corona synoptic map.

References:

Alissandrakis C.E., Lantos P., Nicolaïdis E., Solar Physics, 97, 267, 1985
Sime D.G., Garcia C.,Yasukawa E., Lundin E., Rock K., NCAR Technical Note 280, 1987

Hα DIAGNOSTICS OF 16 MAY 1981 FLARE LOOPS

P. Heinzel, Astronomical Institute, Ondrejov, Czechoslovakia
P. Mein and B. Schmieder, Observatoire de Meudon, France

MSDP observations (Meudon) of 16 May 1981 post-flare loops are used to derive the hydrogen plasma parameters in flare loops. We compare two recently developed methods: a differential cloud model - DCM and a probabilistic transfer technique - PTT.

The plasma parameters near the loop tops (H=35000 km) , as derived from DCM (see Schmieder et al., 1988) are : w=0.8 A, τ=0.44, V=32 km s^{-1}, S=0.18 Ic. Here w is the Doppler width, τ is the line-center optical thickness of the loop, V represents the line-of-sight velocity and S is the line source function in units of the undisturbed continuum intensity Ic . Next we used these empirically derived parameters for non-LTE modelling, but instead of solving the full non-LTE problem for hydrogen loops (as in Heinzel and Karlicky, 1987), we used an efficient and extremely fast method, based on a probabilistic approach to Hα line transfer (five-level atom,Lyman transitions in detailed radiative balance). This PTT works quite well even on small PC's and gives approximate estimates of all important plasma parameters: T (kinetic temperature), vturb, D (loop thickness), electron density n_e, pressure P, S, τ and level populations. The results are consistent with detailed non-LTE solutions of Heinzel and Karlicky (1987). In this way, we got a fit to MSDP Hα profiles as shown in Fig. 1 (crosses indicate the observed profile, intensity in units of Ic). The corresponding plasma parameters, obtained with PTT are: T=10000 K, vturb=34 km s^{-1}, D=1700 km, P=0.17 dyn cm^{-1} and $n_e=3\times10^{10}$ cm^{-3}. For V=32 km s^{-1}, this solution leads to τ=0.45 and S=0.16Ic, the results quite comparable with those obtained with DCM. The macroscopic velocity is treated as in Heinzel (1987).

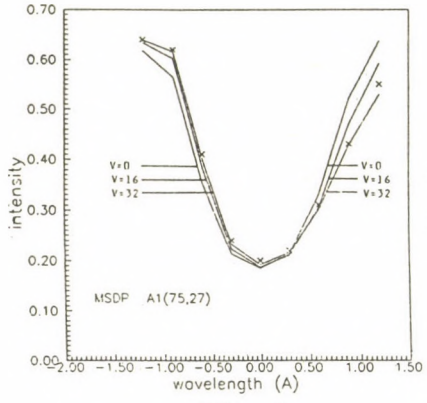

Fig. 1

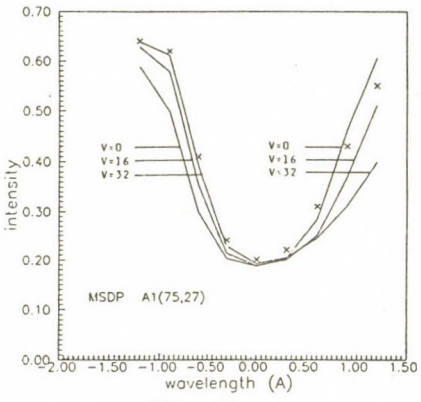

Fig. 2

To test the sensitivity of PTT to pressure variations, we increased the electron density to 5×10^{10} cm^{-3}. The resulting pressure is P=0.37 dyn cm^{-2} and the theoretical line profiles are displayed in Fig. 2. For V=32 km s^{-1} we see an evident discrepancy with MSDP profile . Therefore, it seems that Hα line profiles of post-flare loops as observed on the disc are rather sensitive indicators of the plasma pressure and electron density. Both thermal and microturbulent broadening was assumed to be gaussian, so that T=10000 K and v_{turb}=34 km s^{-1} lead to w=0.8 A as derived empirically from DCM.

The electron density derived in this paper is lower than 10^{11} – 10^{12} cm^{-3}, and thus the loop should appear in absorption against the disc, according to results of Svestka et al.(1986) and Heinzel and Karlicky (1987). However, in the present case, the background radiation passing through an optically-thin loop structure (τ=0.45) is somewhat enhanced due to corresponding flare activity and, moreover, v_{turb} is rather high – both these facts cause that the line-center contrast is almost equal to zero. The source function S=0.16 I_c can hardly be enhanced by increasing the electron density and simultaneously keeping a good fit in Fig. 1. However, certain enhancement could be reached by including the Doppler brightening effect for Hα line, as demonstrated by Heinzel and Rompolt (1987).Moreover, some additional source-function enhancement may also be caused by an irradiation of the loop structure from surrounding flare ribbons.Both these effects will result in a lowering of n_e , so that our value 3×10^{10} cm^{-3} seems to be an upper limit for the electron density (providing that the temperature is about 10^4 K).

The results of this paper are two-fold: first, we have determined some basic plasma parameters of post-flare loops which are necessary for further MHD and energy-balance considerations, and second, we have demonstrated the consistency of two different diagnostics techniques which we call DCM and PTT. Both methods can efficiently be used to get 2D maps of physical conditions within cool Hα structures of intermediate optical thickness, using the data from MSDP or other imaging spectrographs.

References

Heinzel, P.: 1987, *Proc. 10th IAU European Regional Meeting, eds. L.Hejna and M.Sobotka*, p. 199.

Heinzel, P. and Karlicky, M.: 1987, *Solar Phys.* 110, 343.

Heinzel, P. and Rompolt, B.: 1987, *Solar Phys.* 110, 171.

Schmieder, B., Mein, P., Forbes, T.G. and Malherbe, J.M.: 1988, *Adv. Space. Res.* 8 (11), 45.

Svestka, Z., Fontenla, J.M., Machado, M.E., Martin, S.F., Neidig, D.F. and Poletto, G.: 1987, *Solar Phys.* 108, 237.

SESSION 6

May 24, Thursday (p.m.)

WAVES IN ACTIVE REGIONS

Chairman: J. STAUDE

Zentralinstitut fur Astrophysik der Akad.d.Wiss.
Sonnenobservatorium Einsteinturm

Potsdam

Invited reviews:

F. KNEER

Waves in Active Regions: Observations

Y. D. ZHUGZHDA

Waves in Sunspots and Active Regions: Theory
(Only an Extended Abstract published here.)

and 6 (oral and poster) contributions

WAVES IN ACTIVE REGIONS: OBSERVATIONS

F. Kneer
Universitäts-Sternwarte
Geismarlandstr. 11
D-3400 Göttingen, Fed. Rep. Germany

Abstract. This review deals with oscillations in prominences, with the 5 min p modes in active regions, and with waves in sunspots. The oscillation periods in prominences range from 100 s to longer than 1 h. The oscillation periods vary with time, from one place to another within one prominence, and from one prominence to another. A picture of damped oscillations as reactions to magnetic field rearrangements seems plausible. The 5 min oscillations are reduced, by a factor 2 in velocity amplitude, in active regions compared to quiet regions. This rules out a substantial contribution of the p modes to chromospheric and coronal heating by dissipation of shock waves in the 5 min period range. Small-scale fluxtubes take part in the 5 min oscillations with about the same velocity amplitude as their surroundings. High speed motions, periodic or non-periodic, which would be able to explain large "macro"-velocities postulated from the interpretation of FTS data of Stokes V profiles are not seen in high resolution observations.

Sunspot umbrae have strongly reduced oscillations in the 5 min band (factor 3 in velocity) at the photospheric level, where other oscillations with low amplitudes and periods of 2-15 min are present. The umbral chromosphere oscillates predominantly periods of 2 - 3 min, in the vertical direction. Waves in the transition zone are highly correlated with chromospheric waves. The energy flux in the chromospheric oscillations is $2\ 10^{3}$ erg cm $^{-2}$ s $^{-1}$ (not counting the contribution of magnetic field fluctuations), which falls short of the chromospheric radiative losses by three orders of magnitude. A small magnetic field fluctuation of less than 1 % could supply enough energy. The nature of the resonators for the selection of periods within a narrow range is still under debate, and so is the excitation mechanism. Penumbral oscillations occur preferentially in simply structured penumbrae. Observations indicate that they are pressure waves along the magnetic field with periods of 200 - 300s, excited at the umbra-penumbra border.

1. INTRODUCTION

The last extensive review, to my knowledge, on the observational aspects of waves in active regions dates back to 1981, when Moore summarized the knowledge on sunspot dynamics. Moore and Rabin (1985) touch the subject of oscillations in sunspots, but only in a limited manner. Since much work has been addressed in the past decade to the behaviour of waves in active phenomena on the Sun, both observationally and theoretically, it is worth to collect the understanding at the present state of the art. It is natural that this collection of observational results presented below is biased due to mainly two causes: Firstly, my own knowledge will always be limited and prejudice creeps in through the selection of the literature at hand and easily accessible. Secondly, the work done in this field is much more numerous than could fit into a limited time and space of presentation. Thus, this review is not intended to be complete but to serve as an overview (from my standpoint) and as a guide to the observational base of the problems of waves in active regions.

In my opinion, there are two reasons to deal with waves. Firstly, waves provide a means to transport energy over large distances and to deposit it by dissipation processes. They may thus be responsible for the heating of stellar chromospheres and coronae. Secondly, waves are appealing for themselves. They represent space-time structures produced from an unordered state, and it is obvious that one wishes to understand the mechanisms leading to coherent behaviour of matter. In solar active regions, in addition to gravity and pressure, the magnetic field **B** (magnetic flux density) is involved which substantially increases the complexity of wave motions. Yet, the theoretical aspects will be treated in the review by Zhugzhda (1990, these proceedings) following the present one and it is unnecessary to expand on theory here.

The expression "active regions" embraces broad areas of research into solar physics. Below, I shall deal shortly with oscillations of prominences and with the 5 min p modes observed in small-scale magnetic fluxtubes and in active regions as outlined by brightenings in CaII K filtergrams, but not necessarily containing sunspots. (These two topics were only touched in the discussions following the oral presentation of this session. A few more words are appropriate here, at least in order to give references to work done in this field.) The largest part of this contribution is devoted to waves in sunspots, i. e. in sunspot umbrae and penumbrae.

2. WAVES IN PROMINENCES

Special conferences on prominences have taken place during the past few years. Their proceedings (Ballester and Priest, 1988, Ruzhdjak and Tandberg-Hanssen, 1990) deal more deeply with the phenomenon than is possible here. The following picture arises from the observations of Wiehr et al. (1984), Balthasar et al. (1986, 1988), Tsubaki and Takeuchi (1986), and Tsubaki et al. (1987, 1988): Prominences oscillate in velocity with amplitudes of 1-3 km s^{-1}. Intensity changes do occur, but uncorrelated with the velocity, with different periods and at different places. There is no preferred period, different prominences oscillate differently, different periods occur simultaneously in one and the same prominence at different positions or at the same position at different times. The periods range from about 100s to more than 1 h. The above authors do not find waves propagating within prominences. Also, from observations by Malherbe et al. (1987) from filaments on the disc, radial oscillations are not seen. Schmieder et al. (1990) point out the relevance of the behaviour of the fine structure within prominences. A relation to waves in the photosphere with periods of 3-5 min is doubtful because these periods are not dominant in prominences and, if they occur, can be coherent over 20.000 km (Tsubaki and Takeuchi, 1986).

The overall impression is that prominences, and their finestructures, react with damped oscillations upon changes in the configuration. If the magnetic field is the restoring force the frequency of the oscillation can be estimated to (Kleczek and Kuperus, 1969)

$$\omega^2 \approx \frac{V}{M} \frac{B^2}{4\pi L^2} ,$$

with B = magnetic flux density, L = characteristic length of magnetic field, M = mass, and V = volume of (part of) the prominence. The period is then

$$P \approx 2\pi L / v_a ,$$

with v_a = Alfvén velocity. Depending on the involved magnetic field, mass, and volume, a wide range of periods can occur.

3. MAGNETIC FLUXTUBES, ACTIVE REGIONS

3.1. Small-scale Magnetic Elements

Observations of the motions within small scale magnetic structures were obtained as early as 1978 by Giovanelli et al. who used the position of the zero crossing of the Stokes V profile as a velocity indicator. The spatial resolution was limited by a pinhole of about 3 x 3 arcsec^2. The outcome of these observations was that the magnetic elements perform the same oscillations as their surroundings with amplitudes of 0.3 - 0.8 km s^{-1}. Up to date, this result is not contradicted by observations with higher spatial resolution (e.g. Wiehr, 1988). Fleck and Deubner (1990) show that the phase of oscillation within the fluxtubes may strongly vary within a few arcsec.

It is worth mentioning that the high speed motions of 2 - 5 km s^{-1} required for the interpretation of Stokes V profiles obtained in low spatial and low temporal Fourier transform spectrometer observations (Solanki, 1986, Zayer et al., 1989) have so far not been identified in high resolution observations, neither as oscillatory motions nor as non-periodic flows. This demonstrates the strong need for observations of small-scale magnetic fluxtubes, and bundles of fluxtubes, with the highest available spatial and temporal resolution in order to alleviate our lack of understanding the physical processes in the structured, magnetized solar plassma and to avoid speculation.

3.2. Active Regions

The observation of p mode absorption by sunspots and their surroundings (Abdelatif et al., 1986, Braun et al., 1987, 1988) deserves a more extended treatment than is possible here. In short, Braun et al. demonstrate that a subphotospheric layer of 7 - 10 Mm thickness and of about 40 Mm in diameter, i.e. being much larger than the sunspot itself and covering the active region, is responsible for the absorption. Such observations give valuable information on the interaction of magnetic structures and acoustic waves. (See e. g. Ryutov and Ryutova, 1976, Abdelatif and Thomas, 1987, Hollweg, 1988, and Bogdan, 1989, to mention only very little of the theoretical work done in this field.)

Investigations of the 5 min p modes in active regions not containing larger sunspots and of the effects of activity on the oscillating line profiles have been carried out by Bonet et al. (1988) and Alamanni et al. (1990). In these low spatial resolution observations the power in the p modes is strongly reduced (by a factor 4) in active regions and, as can be concluded from the behaviour of the line bisectors, does not increase as strongly, if at all, with height in the atmosphere as in quiet regions. It is thus unlikely that the p modes contribute significantly to chromospheric or coronal heating by dissipation of their energy after shock formation in high layers. If the p modes are involved in heating their energy must be delivered to the active regions in subphotospheric layers. The power spectra of the 5 min oscillation of low resolution

in wavenumber show fewer frequency peaks in active regions than in the quiet Sun. Presumably, this is due to the limitation of the data sets, and the conjecture that active regions "select" modes is not confirmed by high resolution observations by Tarbell et al. (1988), who could resolve the modal structure in the k - ω - plane.

4. SUNSPOTS: UMBRA, PENUMBRA

4.1. Oscillations of the Magnetic Field in Umbrae

Does the magnetic field in sunspot umbrae oscillate, and, if it does, what are the periods and the amplitudes? As we shall see below, the answer to these questions is relevant for the identification of umbral oscillatory modes and for the energy transport to the chromosphere and corona above umbrae. Mogilevskii et al. (1973) find fluctuations with periods P = 125 - 225 s. Gurman and House (1981) observe oscillations of B with periods between 200 s and 400 s, but no significant oscillation in the transverse component $B_{\perp}$. Moore (1981) quotes Gurman's and House's measurement with $\delta B / B \approx 10$ %, which is quite a lot (see below). Bachmann (1983) states that periodic field fluctuations are not detectable in his measurements. He ascribes the fluctuating signal to variable seeing conditions. Also, for the transition zone (TZ) between chromosphere and corona, no magnetic field oscillations are found with the UVSP instrument onboard the SMM satellite (Henze et al., 1984).

4.2. Umbra: Photospheric Oscillations

The velocity amplitudes of the umbral photospheric oscillations are very low, $v \leq 100$ m s^{-1}, which is at the limit of photographic noise. To investigate the occurrence of wave periods, Soltau and Wiehr (1984) measured the Doppler shift of the nonsplit Fe I 7090 Å line in several sunspots in long time sequences (up to 8 h). A power analysis with a moving window of 1 h gives the stability of the various oscillations. The result is demonstrated in Figure 1 (after Soltau and Wiehr, 1984).

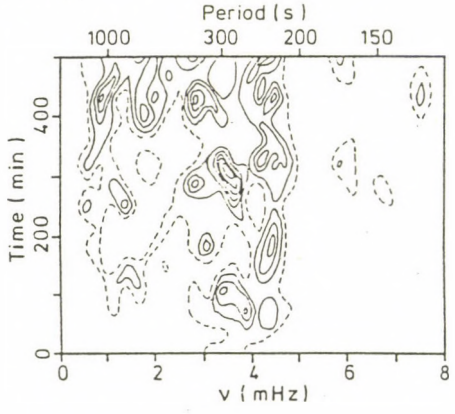

Fig. 1: Contourplot of power from velocity measurements in the photosphere of a sunspot umbra showing the changes of oscillatory frequency with time. After Soltau and Wiehr (1984).

The authors ascribe the oscillations near P = 1000 s to changes of the umbral structure, e. g. umbral dots, with this timescale. The varying power at P = 240 s is due to the internal period of the hour drive which moves periodically the image of varying umbral structure across the pinhole of the measuring setup. Although the strongest power stems from the oscillations with periods near 5 min it is still much lower than the 5 min power in the quiet photosphere, usually by a factor 10 after Balthasar et al. (1987).

4.3. Chromosphere, Umbral Flashes

In continuation of early investigations, and detections of chromospheric oscillations and umbral flashes, by e. g. Beckers and Tallant (1969), Wittmann (1969), and Giovanelli (1972), substantial observational efforts have been undertaken during the past decade to clarify the nature of the chromospheric waves (e. g. Kneer et al., 1981, Lites et al, 1982, Turova et al., 1983, von Uexküll et al., 1983, Mattig et al., 1984, Lites, 1984, 1986a, b). The spectral features mostly used to investigate the chromosphere are the lines Fe I 5434 Å (whose center is formed in the lower chromosphere), Na D_1 and D_2, Hα, Ca II H and K, and the IR lines, and He I 10830 Å.

The main results may be summarised as follows. The periods of the chromospheric oscillations range from 120 s to 190 s, the 5 min oscillation is almost absent.

Figure 2 shows typical power spectra of velocity measurements in Hα and the photospheric Fe I 6303 Å line (after Thomas et al., 1984). Note that the power from the Fe I line has been multiplied by a factor 10 in Figure 2. The motions are vertical, parallel to the magnetic field, and the amplitudes range from $v \approx 0.5$ km s^{-1} in the Na D lines to $v \approx 3$ km s^{-1} in Hα.

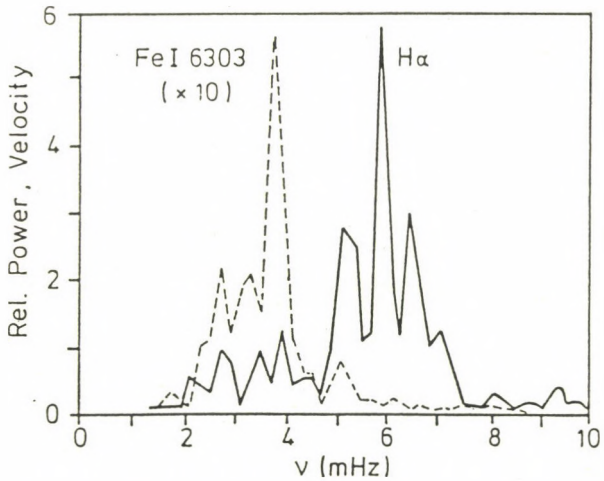

Fig. 2: Velocity power spectra of Hα and Fe I line in umbra. After Thomas et al. (1984).

Lites (1986a) finds on the one hand that oscillations with different frequencies, modes, may occur simultaneously at the same places in umbrae. The mode frequencies drift in time on timescales of 30 min or even split. On the other hand, the modes occur in patches in sunspot chromospheres as would be expected from oscillations with non-zero horizontal wavenumber. The patches have sizes of 3 - 5 arcsec and their location changes with frequency. It is not known whether different parts of umbrae (in different patches) oscillate coherently.

Umbral Flashes are best seen in K line filtergrams. They are especially high amplitude oscillations with strong intensity increases in the K line emission core, possibly resulting from the superposition of several modes with matching phase. The impression is that they occur everywhere in an umbra from time to time. Figure 3 shows a typical time sequence of profiles of the K line core (a) and of the 8542 Å line (b) at one position in a sunspot umbra (from Kneer et al., 1981).

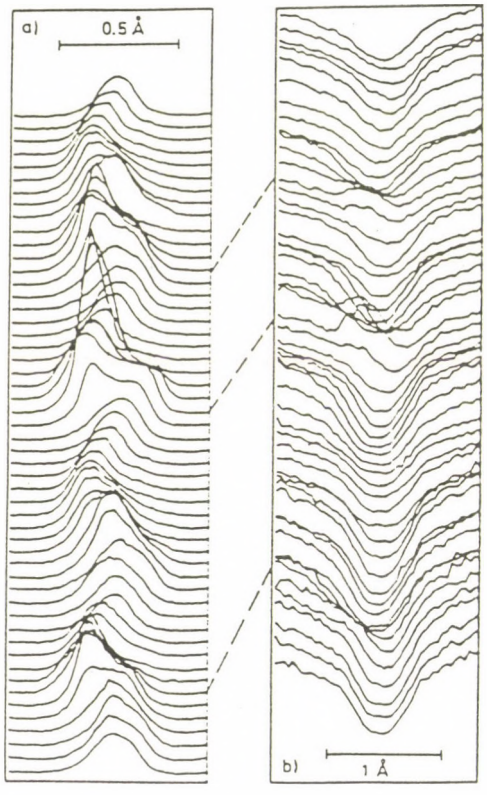

Fig. 3: Time sequence (duration 13 min from bottom to top) of CaII K (a) and 8542 Å (b) line cores at one position in a sunspot umbra. From Kneer et al. (1981)

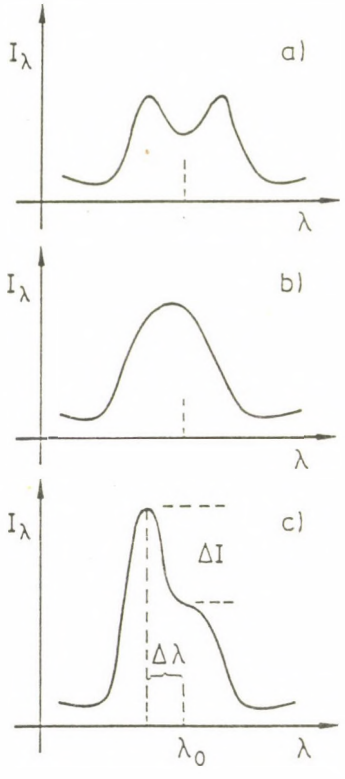

Fig. 4: Schematic profiles of K line emission core. a) from atmospheric modeling, b) averaged observed profile, c) during flash phase.

During the flash phase, the integrated core intensity in the K line increases by a factor 2 - 4 above average, and the IR line tends to have a blue-shifted emission core.

4.4. Radiative Transfer, Interpretation of Ca II Lines

The ratio of the oscillatorstrengths of the K and H lines is 2. The intensity ratio of the emission cores in sunspots is $I_K/I_H \approx 1.2$ and the intensity fluctuations in these lines are highly correlated (Kneer et al., 1981, Turova et al. 1983). From this follows that the emissions of H and K come from optically thick chromospheres (Kneer and Mattig, 1978). Modeling of the K line in thick chromospheres gives selfreversed emisson cores as depicted schematically in Figure 4a, while the observed profiles show mostly nonreversed emission (Figure 4b). There is, to arrive theoretically at pure emission cores, need for substantial macro-velocities $v_{macro} = 3 - 5$ km s^{-1}, which have not (yet) been observed. The essential point to make here is that it is not straightforward to derive from the wavelength shift $\Delta\lambda$ of the K emission a velocity or from the intensity fluctuation ΔI a pressure- or temperature fluctuation, $\Delta\lambda \neq \alpha v$, $\Delta I \neq \beta \Delta T$ (Figure 4c). Line transfer calculations in dynamic atmospheres are needed. They have not yet been performed. To measure velocities one should use then only pure aborption lines.

4.5. Energy Flux in Umbral Waves

The radiative energy losses from an umbral chromosphere are typically (including losses in Lyα) $F_{rad} = 1...2\ 10^6$ erg cm^{-2} s^{-1}. The question is whether this energy can be supplied by the oscillations described above. Supposing small amplitude waves in an infinitely conducting medium the energy flux by waves is (e. g. Bray and Loughhead, 1974)

$$F_{wave} = \delta p\ v + \frac{1}{4\pi}\ \delta B \times (v \times B_o) ,$$

where δp and δB denote pressure and magnetic field fluctuations, respectively. The first term of the rhs above has the average vertical component (e. g. Mein and Schmieder, 1981)

$$F_{z,1} = p(z)\ \frac{k_z}{\omega}\ v^2/2 ,$$

with vertical wavenumber k_z, frequency ω, and velocity amplitude v. From phase differences of oscillations at two heights one can determine k_z as

$$k_z = (\varphi_{z2} - \varphi_{z1}) / (z_2 - z_1) .$$

With the measurements of velocity amplitudes and phases in the Na D_1 and D_2 lines and with the model calculations in Kneer et al. (1981) and von Uexküll et al. (1983) one obtains

$$F_{z,1} \approx 2\ 10^3 \text{ erg } cm^{-2} s^{-1},$$

that is , this part of energy transport is completely negligible for the sunspot chromospheric energy budget. The energy supply from the fluctuations of the Poynting vector is difficult to estimate. Let us assume

$$F_{z,2} \approx \frac{1}{4\pi} B^2 v \frac{\delta B}{B}$$

and B = 2000 gauss, B/B = 0.01, and v = 50 m s $^{-1}$. This would yield

$$F_{z,2} \approx 2\,10^7 \text{ erg cm}^{-2}\text{ s}^{-1},$$

i.e. by far enough for the needs. However, the angles between velocity, magnetic field, and its fluctuations must be taken into account for a better estimate, and, in addition, transverse magnetic field oscillations are strongly reflected downward due to the increase of the Alfvén velocity with height (Thomas, 1978). In conclusion, the problem of heating processes of umbral chromospheres is by far not settled.

4.6. Transition Zone (TZ)

Much information on waves in the TZ above sunspots has been gained withe the UVSP instrument onboard SMM. Gurman et al. (1983) find in TZ lines velocity oscillations of similar amplitudes and periods as in the chromosphere and intensity and velocity correlations compatible with acoustic waves propagating upward. The energy flux in these waves is estimated as F ≈ 2 10^3 erg cm $^{-2}$ s $^{-1}$, which is the same value as obtained above for the acoustic waves in the chromosphere. Figure 5, after Thomas et al. (1987), shows a particularly good observational achievement, simultaneous velocity measurements from the same area on the Sun with the UVSP imstrument and from ground. The good coherence of the oscillations in the TZ and in the chromosphere is clearly seen.

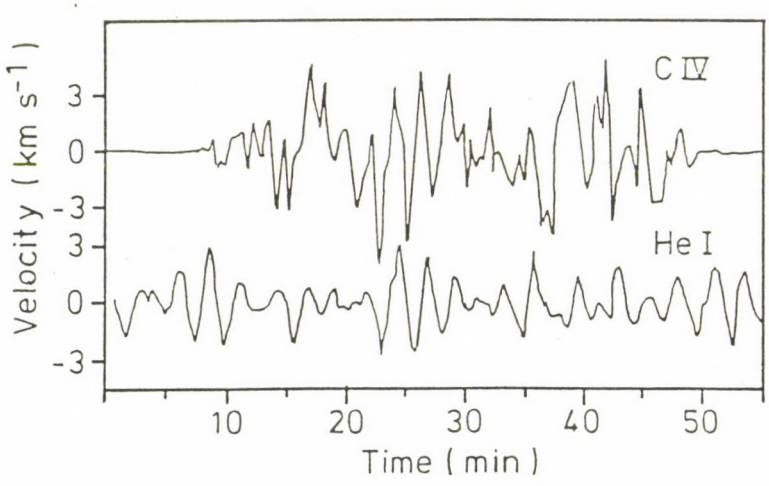

Fig. 5: Simultaneous space and ground-based observation of velocities in the C IV 1548 Å and He I 10830 Å lines. After Thomas et al. (1987).

4. 7. Photosphere-Chromosphere Connection

How are the chromospheric waves related to the photospheric waves? Abdelatif et al. (1986) find in the dark parts of some sunspots velocity oscillations in the umbral photospheric line Ti I 6304 Å at the same frequency as for the chromospheric oscillations (Figure 6a, arrow). The energy density in the photospheric oscillation is 5 times higher than in the chromospheric oscillation, supporting the model of a "photospheric resonator" (see below). Figure 6 gives coherence and phase differences for velocity oscillations in a photospheric and a chromospheric spectral line (after Lites and Thomas, 1985).

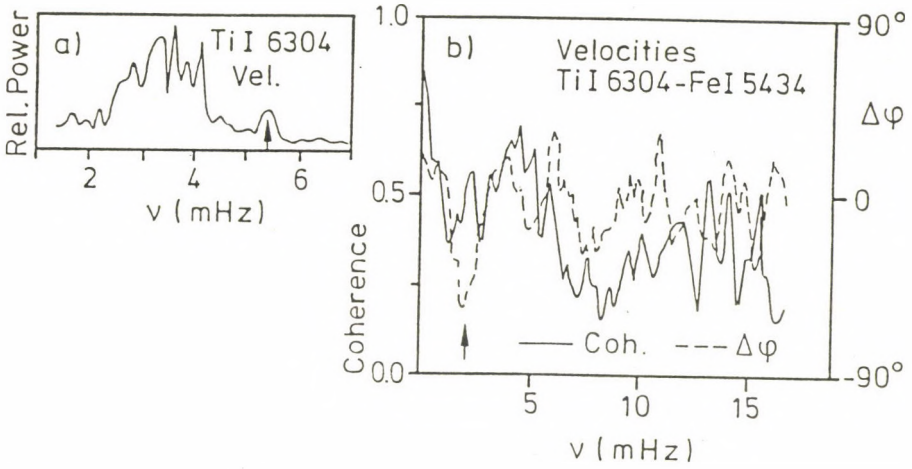

Fig. 6: a) "Chromospheric" oscillation at 5.5 mHz (arrow) seen in the velocity signal of a photospheric line. After Abdelatif et al. (1986). b) coherence and phase difference between photospheric and chromospheric oscillations; arrow: negative phase difference as for gravity waves. After Lites and Thomas (1985).

The coherence at "chromospheric" oscillation frequencies (4.5 mHz $\leq \nu \leq$ 8 mHz) is not high, yet it should be remembered that the photospheric signal is very low, $v \approx 30$ m s $^{-1}$, much affected by moise. The negative phase difference at 2 mHz (arrow in Figure 6b) is noteworthy, as it indicates the presence of gravity waves.

4.8. Models of Chromospheric Oscillations

The following review by Zhugzhda (1990, this volume) gives in-depth treatment of the theory of waves in sunspots. Here, only the concepts of two different models are sketched. In the one model (Figure 7a, Scheuer and Thomas, 1981, Thomas and Scheuer, 1982), Alfvénic fast oscillations, with predominantly horizontal motions in the photosphere, are excited by overstable convection in subphotospheric layers. Resonances occur when the reflected waves match in phase. The chromospheric oscillations are pressure waves which couple to the photospheric waves.

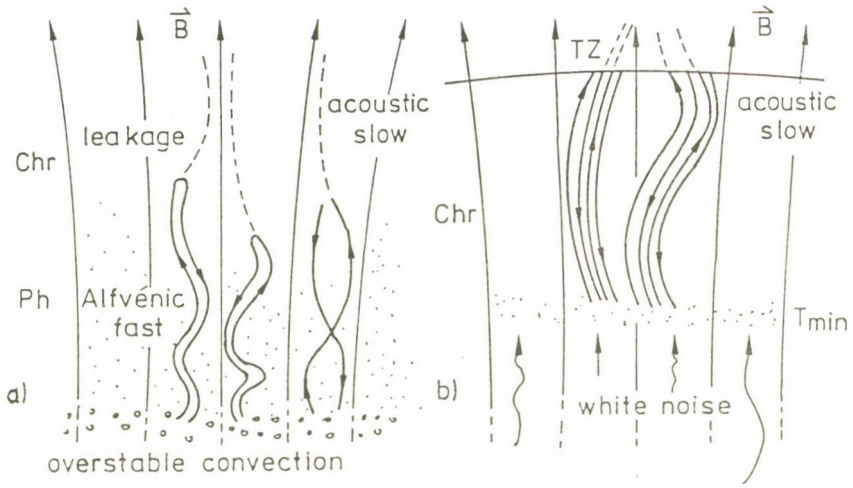

Fig. 7: a) Chromospheric pressure waves couple to photospheric transverse oscillations (after Thomas and Scheuer, 1982); Ph = photosphere, Chr = chromosphere. b) Chromospheric resonator after Zhugzhda et al. (1984), multiple reflections at TZ and T_{min} region. See text.

The chromospheric resonator model (Figure 7b) has been proposed by Zhugzhda et al. (1984, 1985) and Staude et al. (1985), to mention only few papers in a long series. There, waves enter from the photosphere into the chromospheric resonator, essentially defined by the atmosphere between the region of the temperature minimum and the TZ. When multiple reflections with matching phases occur the transmission is high and the resonator acts similarly as a (non-ideal) Fabry-Perot étalon. This model allows to reproduce observed phase differences between different chromospheric lines (Lites, 1984). It allows also the probing of sunspot chromospheres, i. e. the value of T_{min}, the temperature gradient, and the vertical extent of the chromosphere through the width, height, and frequency position of the resonance peaks.

4.9. Waves in the Penumbra

In penumbrae, waves are best seen in "unperturbed" structures, with little "activity" and simple geometry. In the chromosphere, the "running penumbral waves" (Zirin and Stein, 1972) appear

to be excited from waves at the umbra penumbra border and die out halfway to the outer penumbra. However, their frequency is lower than that of umbral chromospheric oscillations, the periods being P = 200 - 300 s. The phase velocity is about 20 km s^{-1} (e. g. Kneer et al., 1981, Thomas et al., 1984). Lites (1988) finds an "attenuation ring" for the oscillatory amplitude in the penumbra which is often most pronounced at the direction towards the disc centre. Close to the umbra one sees, after Lites, penumbral pressure waves propagating parallel to the magnetic field. At the outer border, 3 - 5 min oscillations of the quiet Sun become dominant. Figure 8 depicts the idea.

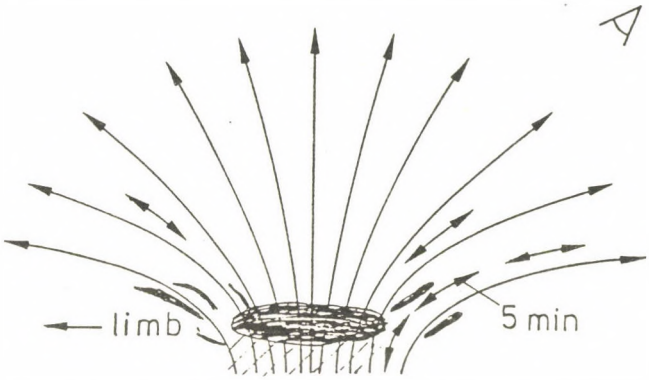

Fig. 8: Chromospheric penumbral waves, after Lites (1988), and photospheric 5 min oscillations, after Balthasar and Wiehr (1990).

With regard to the penumbral photosphere, Balthasar and Wiehr (1990) searched for preferential directions of motion of the 5 min oscillation, i. e. whether they follow the magnetic field (Figure 8). The observations are, however, not yet conclusive.

4.10. Observational Needs

From the above description of present knowledge and open questions several wishes for observational clarification can be noted:

- The role of the magnetic field for the nature of the waves is unclear and magnetic field fluctuations, if they exist, may contribute substantially to the chromospheric and coronal energy budget. Thus it is important to know the amplitude and frequency of magnetic field fluctuations and their relation to velocity and intensity fluctuations.
- Thomas and Scheuer (1982) have predicted predominantly horizontal velocity oscillations in umbral photospheres at about 3 min period. These have not yet been observed.
- It is still unclear whether different parts of umbrae oscillate coherently, i. e. in modes covering the total umbra, or whether each oscillating patch builds up its own resonances.
- The wave excitation mechanism has not been identified. It would be necessary to observe the temporal evolution of umbral finestructure and its relation to oscillatory amplitudes as well as the relation between the amplitudes of chromospheric and photospheric amplitudes.

- One must expect an effect of the sunspot geometric structure on the horizontal wavenumber, amplitude and frequency.

5. CONCLUSION

Waves in active regions are far from being understood. Substantial observational needs can be identified. They range from measurement of propagation properties of p modes in active regions in comparison with the quiet Sun to high-resolution observation of the oscillations in small-scale magnetic fluxtubes and their non-magnetic surrounding, from determination of magnetic field fluctuation in sunspots to the characterization of the temporal evolution of umbral finestructure, from measurements of horizontal umbral oscillations to the sorting out of oscillatory modes by coherence- and phase analyses. Many of these observations require high spatial and/or high spectral resolution, in addition to the need for temporal sequences. But the data, once obtained with high signal to noise ratio, together with an interpretation procedure using radiative transfer theory in dynamic model atmospheres, will help to develop a deeper insight and better understanding of wave phenomena in magnetic field regions.

Acknowledgements. Helpful discussions with Drs. H. Balthasar, E. Wiehr, and A.D. Wittmann are gratefully acknowledged. Also, I have shamelessly profitted from discussions with colleagues during the meeting. This contribution was supported by the Deutsche Forschungsgemeinschaft.

References

Abdelatif, T.E., Lites, B.W., Thomas, J.H.: 1986, Astrophys. J. **311**, 368
Abdelatif, T.E., Thomas. J.H.: 1987, Astrophys. J. **320**, 884
Alamanni, N., Cavallini, F., Ceppatelli, G., Righini, A.: 1990, Astron. Astrophys. **228**, 517
Bachmann, G.: 1983, Phys. Solariterr. **20**, 29
Ballester, J.L., Priest, E.R. (eds.): 1988, "Dynamics and Structure of Solar Prominences", workshop proceedings, Universitat de les Illes Balears
Balthasar, H., Knölker, M., Stellmacher, G., Wiehr, E.: 1986, Astron. Astrophys. **163**, 343
Balthasar, H., Küveler, G., Wiehr, E.: 1987, Solar Phys. **112**, 37
Balthasar, H., Stellmacher, G., Wiehr, E.: 1988, Astron. Astrophys. 204, 286
Balthasar, H., Wiehr, E.: 1990, Astron. Astrophys., in press
Beckers, J.M., Tallant, P.E.: 1969, Solar Phys. **7**, 351
Bogdan, T.J.: 1989, Astrophys. J. **345**, 1042
Bonet, J.A., Márquez, I., Vázquez, M., Wöhl, H.: 1988, Astron. Astrophys. **198**, 322
Braun, D.C., Duvall, T.L., Jr., LaBonte, B.J.: 1987, Astrophys. J. **319**, L27
Braun, D.C., Duvall, T.L., Jr., LaBonte, B.J.: 1988, Astrophys. J. **335**, 1015
Bray, R.J., Loughhead, R.E.: 1974, "The Solar Chromosphere", Chapman and Hall, London
Fleck, B., Deubner, F.-L.: 1990, these proceedings
Giovanelli, R.G.: 1972, Solar Phys. **27**, 71
Giovanelli, R.G., Livingston, W.C., Harvey, J.W.: 1978, Solar Phys. **59**, 49
Gurman, J.B., House, L.L.: 1981, Solar Phys. **71**, 5
Gurman, J.B., Leibacher, J.W., Shine, R.A., Woodgate, B.E., Henze, W.: 1982, Astrophys. J. **253**, 939

Henze, W., Tandberg-Hanssen, E.A., Reichmann, E.J., Athay, R.G.: 1984, Solar Phys. **91**, 33
Hollweg, J.V.: 1988, Astrophys. J. **335**, 1005
Kleczek, J., Kuperus, M.: 1969, Solar Phys. **6**, 72
Kneer, F., Mattig, W.: 1978, Astron. Astrophys. **65**, 17
Kneer, F., Mattig, W., von Uexküll, M.: 1981, Astron. Astrophys. **102**, 147
Lites, B.W.: 1984, Astrophys. J. **277**, 874
Lites, B.W.: 1986a, Astrophys. J. **301**, 992
Lites, B.W.: 1986b, Astrophys. J. **301**, 1005
Lites, B.W.: 1988, Astrophys. J. **334**, 1054
Lites, B.W., Thomas, J.H.: 1985, Astrophys. J. **294**, 682
Lites, B.W., White, O.R., Packman, D.: 1982, Astrophys. J. **253**, 386
Malherbe, J.-M., Schmieder, B., Mein, P., Tandberg-Hanssen, E.: 1987, Astron. Astrophys. **172**, 316
Mattig, W., von Uexküll, M., Kneer, F.: 1984, in "The Hydromagnetics of the Sun", Proceedings of 4th European Meeting on Solar Physics, ESA SP-220, p. 59
Mein, N., Schmieder, B.: 1981, Astron. Astrophys. **97**, 310
Mogilevskii, E.L. Obridko, V.N., Shelting, B.D.: 1973, Radiofizika **13**, 1357
Moore, R.L.: 1981, in "The Physics of Sunspots", L.E. Cram and J.H. Thomas (eds.), workshop proceedings, Sunspot, N.M., p. 319
Moore, R.L., Rabin, D.: 1985, Ann. Rev. Astron. Astrophys. **23**, 239
Ruzdjak, V., Tandberg-Hanssen, E. (eds.): 1990, "Dynamics of Prominences", IAU Colloquium 117 (in press)
Ryutov, D.D., Ryutova, M.P.: 1976, Soviet Phys. - JETP **43**, 491
Scheuer, M.A., Thomas, J.H.: 1981, Solar Phys. **71**, 21
Schmieder, B., Thompson, W.T., Mein, P.: 1990, these proceeding
Solanki, S.K.: 1986, Astron. Astrophys. **168**, 311
Soltau, D., Wiehr, E.: 1984, Astron. Astrophys. **141**, 159
Staude, J., Zhugzhda, Y.D., Locans, V.: 1985, Solar Phys. **95**, 37
Tarbell, T., Peri, M., Frank, Z., Shine, R., Title, A.: 1988, in "Seismology of the Sun and Sun-like Stars", E.J. Rolfe (ed.), proceedings of ESA symp., ESA SP-286, p. 315
Thomas, J.H.: 1978, Astrophys. J., **225**, 275
Thomas, J.H., Cram, L.E., Nye, A.H.: 1984, Astrophys. J. **285**, 368
Thomas, J.H., Lites, B.W., Gurman, J.B., Ladd, E.F.: 1987, Astrophys. J. **312**, 457
Thomas, J.H., Scheuer, M.A.: 1982, Solar Phys. **79**, 19
Tsubaki, T., Ohnishi, Y., Suematsu, Y.: 1987, Publ. Astron. Soc. Japan **39**, 179
Tsubaki, T., Takeuchi, A.: 1986, Solar Phys. **104**, 313
Tsubaki, T., Toyoda, M., Suematsu, Y.: 1988, Publ. Astron. Soc. Japan **40**, 121
Turova, I.P., Teplitskaya, R.B., Kuklin, G.V.: 1983, Solar Phys. **87**, 7
von Uexküll, M., Kneer, F., Mattig, W.: 1983, Astron. Astrophys. **123**, 263
Wiehr, E.: 1988, in "Seismology of the Sun and Sun-like Stars", E.J. Rolfe (ed.), proceedings of ESA-Symp., ESA SP-286, p. 269
Wiehr, E., Stellmacher, G., Balthasar, H.: 1984, Solar Phys. **94**, 285
Wittmann, A.D.: 1969, Solar Phys. **7**, 366
Zayer, I., Solanki, S.K., Stenflo, J.O.: 1989, Astron. Astrophys. **211**, 463
Zhugzhda, Y.D.: 1990, these proceedings
Zhugzhda, Y.D., Locans, V., Staude, J.: 1985, Astron. Astrophys. **143**, 201
Zhugzhda, Y.D., Staude, J., Locans, V.: 1984, Solar Phys. **91**, 33
Zirin, H., Stein, A.: 1972, Astrophys. J. **178**, L85

WAVES IN SUNSPOTS AND ACTIVE REGIONS: THEORY

(Extended Abstract)

Y.D. Zhugzhda

Inst.of Terrestrial Magnetism,Ionosphere, and Radio Wave Propagation
USSR Academy of Sciences,(IZMIRAN)
SU-142092 Troitsk

The main problem of wave theory in active regions is connected with influence of stratification and non-uniformity of plasma and magnetic field in active regions and sunspots. Effects of stratification and non-uniformity have been considered separately as a rule. The general theory of wave propagation in stratified plasma with magnetic field developed for an isothermal atmosphere,linear MHD waves cannot propagate independently. There are coupling of different modes (Alfvénic, slow and fast) in a stratified atmosphere.There are layers, where it is impossible to separate wave field to usual Alfvénic, slow and fast modes.The separation on elementary modes is possible in layers of weak and strong magnetic fields. An exchange of energy between different modes takes place in layers of strong modes coupling. It means that at many cases the consideration for example of slow waves in active regions is impossible without taking into account of a wave coupling.

The non-uniformity of magnetic fields is manifested first of all in a separation of active region magnetic fields on flux tubes. For exception of special cases of thin tubes the theory of waves in flux tubes has developed for non-stratified atmosphere.There are detailed investigation of different wave modes in flux tubes.Slow, fast and kink modes have been considered. Modes are subdivided on bulk and surface.The results of the wave theory for a stratified atmosphere show that wave modes in flux tubes should be coupled in a stratified atmosphere.The coupling between flux tube modes and general modes should exist too.

It is obvious that a general linear theory of waves in a stratified non-uniform atmosphere is far from the completion.

Moreover, the non-adiabacity of waves in the solar photosphere should be taken into account. In a non-adiabatic case temperature waves arise and a coupling between temperature and MHD waves exists. It is clear that interpretation of waves in sunspots could be founded on simplified models, which should be improved only step by step.

The main wave phenomenon in sunspots is 3 min oscillations. First of all it is clear that 3 min oscillations are resonance oscillations.The chromosphere of sunspot is resonator tuned on 3 min oscillations. But it is impossible to explain 3 min oscillations only by the chromospheric resonance. One or two resonances in photospheric and subphotospheric layers are possible. All resonances are coupled due to linear interaction of MHD waves. From our point of view many of proposed models used boundary conditions which were not carefully approved.Also, it is needed to take into account non-adiabatic effects in photospheric layers.

The second phenomenon, which is on consideration in sunspots, is absorption of 5 min oscillations. In comparison with 3 min oscillations there is not explanation of this effect. It is possible to consider two ways of explanation, the first one is real absorption and dissipation of waves in sunspots. But it is difficult to explain extremely effective wave dissipation. The second explanation is connected with the possibility of secondary emission of absorbed waves. The absorption of 5 min oscillations in sunspots should be explained together with running penumbral waves which transport energy outside sunspots in chromospheric layers.

One of interesting phenomenon is resonance absorption in horizontal magentic field. Many authors have considered resonance in horizontal magnetic field as an effective mechanism of absorption but the exactly horizontal fields are absent in solar atmosphere. It is needed to be careful with involving of resonances in horizontal magnetic field in solar atmosphere.

HEATING OF THE SOLAR CHROMOSPHERE BY MHD WAVES

R. Erdélyi and M. Marik
Eötvös University, Department of Astronomy
Budapest, Kun Béla tér 2, H-1083 Hungary

Abstract. We calculate a semi-theoretical model of the lower part of the chromosphere with the aid of the Vernazza *et al.*(1981) emission coefficients. The equality of the radiative emission coefficient and the absorption coefficient of weak MHD shock waves is assumed. The results show an increase of temperature with height in close agreement with observations and other models (Kalkofen, (1989) and Anderson *et al.*, (1989)). For the period of the shocks about 45 s is found.

1. The emission coefficient in the chromosphere

The emission coefficient of the solar matter in the chromosphere has been taken from VAL81. In Fig. 1. we plot the total contribution to the net radiative cooling rate due to the CaII K, H and infrared triplet lines, the MgII h and k lines, the H^- ion, the MgI b and NaI D lines, the lines SiII 181,6 nm and the HeI 58,4 nm, and the continua of SiI at 152,4 nm and 168,1 nm, FeI at 157,5 nm and 176,8 nm, Mg I at 162,2 nm, and HeI at 50,4 nm, all from VAL81.

The total net radiative cooling rate of the lower chromosphere is shown separately in Fig. 2.

2. The absorption coefficient

The absorption coefficient for weak magneto-acoustic shock waves may be written as follows (cf. Marik 1974)

$$\frac{dF_{mech}}{dh} = \frac{1}{4}2^{1/2}\rho^{-1/2}v_s^{-5/3}t_0^{-1}F_0^{3/2}\left[1+\frac{1}{8}2^{1/2}F_0^{1/2}t_0^{-1}\int_0^h v_s^{-5/2}\rho^{-1/2}dh\right]^{-3} \quad (1)$$

where F_0 is the energy flux of the shock waves at the level of the temperature minimum region, and t_0 is the characteristic time of the shock waves and v_s is the sound velocity.

Let us assume that the chromosphere is in hydrostatic equilibrium. Then we can rewrite Eq. (1) in the form

$$\frac{dF_{mech}}{dh} = \frac{1}{4}2^{1/2}t_0^{-1}\gamma^{-5/4}F_0^{3/2}g^{-3/4}p^{-5/4}(-p')^{3/4} \times\left[1+\frac{1}{8}2^{1/2}F_0^{1/2}t_0^{-1}\gamma^{-5/4}g^{-3/4}\int_0^h p^{-5/4}(-p')^{3/4}dh\right]^{-3} \quad (2)$$

where γ is the ratio of the specific heats, p is the gas pressure, $p' = dp/dh$ and g is the gravitational acceleration in the chromosphere.

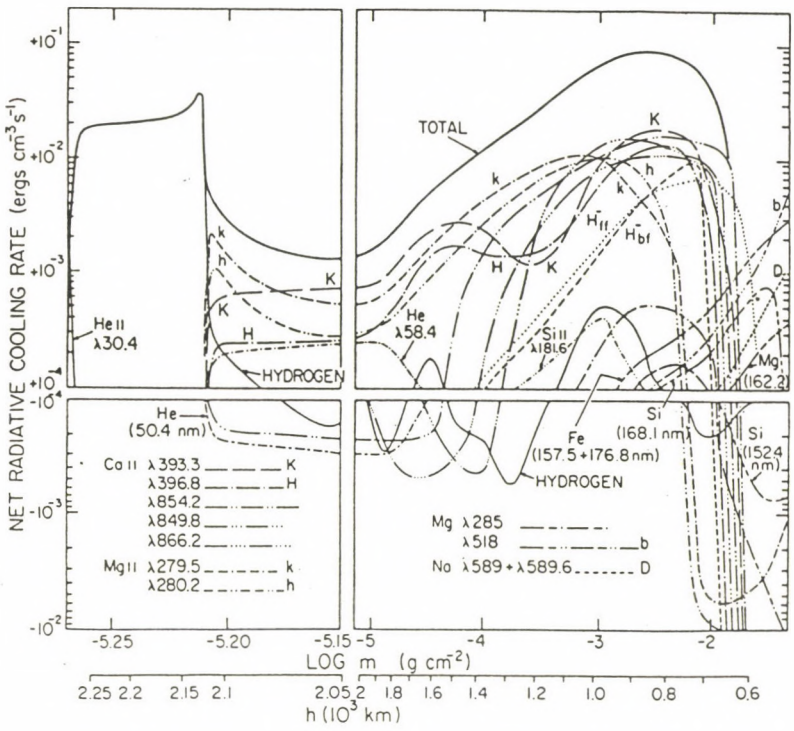

Fig. 1. Net radiative cooling rates for CaII, MgII, H^-, H and other constituents (Vernazza *et al.*,1981).

3. Radiative equilibrium

In the present context we are evidently concerned with mechanical, radiative and conductive energy fluxes only. Ignoring spatial fluctuations in the horizontal direction, we obtain the basic equation of energy balance at any given point in the chromosphere

$$-\frac{dF_{mech}}{dh} - \frac{dF_{cond}}{dh} = \frac{dF_{rad}}{dh} \tag{3}$$

where h is the vertical height, measured from the base of the chromosphere. In the lower region we can ignore the second term on the left hand side because of the small gradient of the temperature (Ulmschneider, 1970).

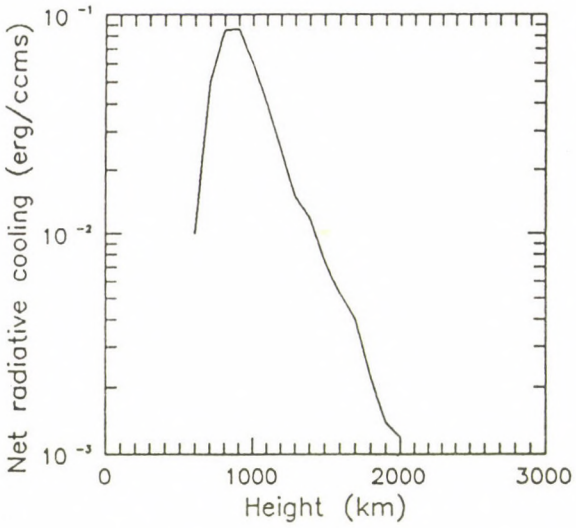

Fig. 2. Total net radiative cooling rate.

4. Calculations

From Eq. (2) and Eq. (3) after some algebra we get

$$p'' = \frac{5}{3}\frac{(p')^2}{p} + \frac{4}{3}p'\frac{d^2F_{rad}}{dh^2}\left(\frac{dF_{rad}}{dh}\right)^{-1} - (-p')^{3/2}\left(\frac{dF_{rad}}{dh}\right)^{1/3} t_0^{-2/3}\gamma^{-5/6}g^{-1/2}p^{-5/6} \qquad (4)$$

Given an initial value of p and dp/dh one can integrate Eq. (4) with the input parameter t_0. The functions $p(h)$ obtained in this way yield the temperature $T(h)$ as a function of height, assuming an ideal gas. Fig. 3. shows the temperature $T(h)$ as a function of height in the lower chromosphere for several t_0 values.

5. Conclusions

The curves plotted in Fig. 3. show the increase of the temperature in the lower part of the chromosphere with height. There is an increase of the temperature but its magnitude depends on the characteristic time of the shocks (Bray *et al.*, 1974).

The best agreement with other models (Kalkofen, 1989, Anderson *et al.*, 1989) is found in the case of a short period of about 45 s. This result agrees with that found from acoustic heatng theory (Erdélyi, these proceedings, Narain et al., 1990).

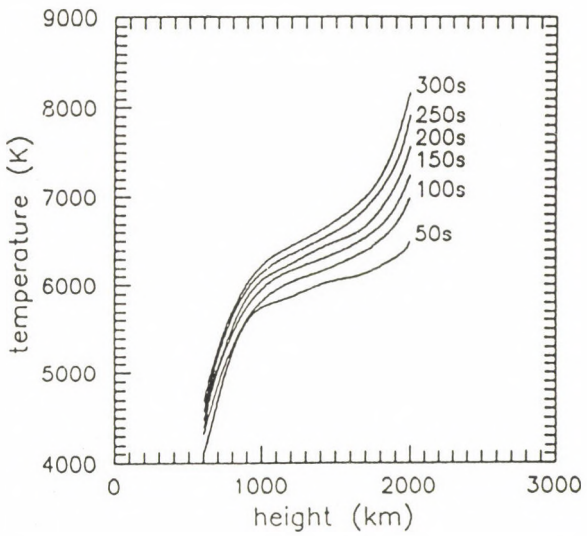

Fig. 3. Temperature as a function of height for different characteristic times

References

Anderson, L. S. *et al.*: 1989, *Ap. J.*, **336** , 1089.

Bray, R. J. *et al.*: 1974, The Solar Chromosphere, Chapman and Hall, London

Erdélyi, R. : On the strength of shock waves in the Sun (in this Proc.)

Kalkofen, W. : 1989, The heating of the solar chromosphere (preprint)

Marik, M. : 1975, *BAIC.*, **26** , 317.

Narain, U. *et al.*: 1990, *Space Sci. Rew.* (in press)

Ulmschneider, P. : 1970, *Solar Phys.* **12** , 403.

Vernazza, J. E. *et al.*: 1981, *Ap. J. Suppl.*, **45**, 635.

OSCILLATIONS DETECTED IN Hα FILAMENTS

B.Schmieder *, W.T.Thompson **, P.Mein *.

* Observatoire de Paris, Section de Meudon, F-92195 Meudon France
** Applied Research Corporation, 8201 Corporate Drive, Landover, MD 20785, USA

Abstract

We will report some new observations of oscillations in filaments observed at different positions on the disk using the MSDP spectrograph operating at Meudon. The velocity power spectra made over whole filament regions show a smooth maximum around 200s period. Oscillations are detected principally in discrete areas in the filaments and in chromospheric fibrils, with well defined periods around 250 s, 200 s and 150 s.
The oscillations could be interpreted by Alfvén waves generated in the chromosphere and propagating through magnetic filamentary structures or by eigenmodes of filamentary structures excited by chromospheric p-modes.

Introduction

Reviews of this topic (Tsubaki 1988, Schmieder 1989) show that two kinds of oscillations are detected in prominences: long period waves (40-80 min) and short period ones ($\leq$ 10 min). Long period waves are more or less related to transient phenomena. Different short periods of oscillations in the frequency range 150 - 400 s are well detected in prominences observed at the limb but not, up to now, in filaments observed at the disk center. It seems that if the oscillations in filaments exist they concern more the horizontal velocity field than the vertical one. To test this hypothesis, we have selected two filaments, a polar crown one (A) consisting in loops (May 16 1988), the other one (B) close to the meridian consisting of threads gathered along the filament axis (May 5 1989).

Observations

The two sets of data lasting 1200 s and 1050 s respectively were obtained at Meudon with the Multichannel Subtractive Double Pass (MSDP) spectrograph. This instrument provides 9 images of a solar region at 9 wavelengths in the Hα line. We reconstruct the line profile for each pixel. The displacement of the middle of the chord at a given $\Delta\lambda$ gives the Dopplershift. Differences in the intensity are referenced to the mean chromosphere. These observations are fully described by Thompson and Schmieder (1990). The pixels concerning the filament and the fibrils have been selected by using the histograms (Figure 1 a); the filaments correspond to values of the intensities lower than a certain limit (-0.024 for 16 May 1988, -0.045 for 5 May 1989). We checked this against selections made visually from the intensity maps. The results were qualitatively equivalent.

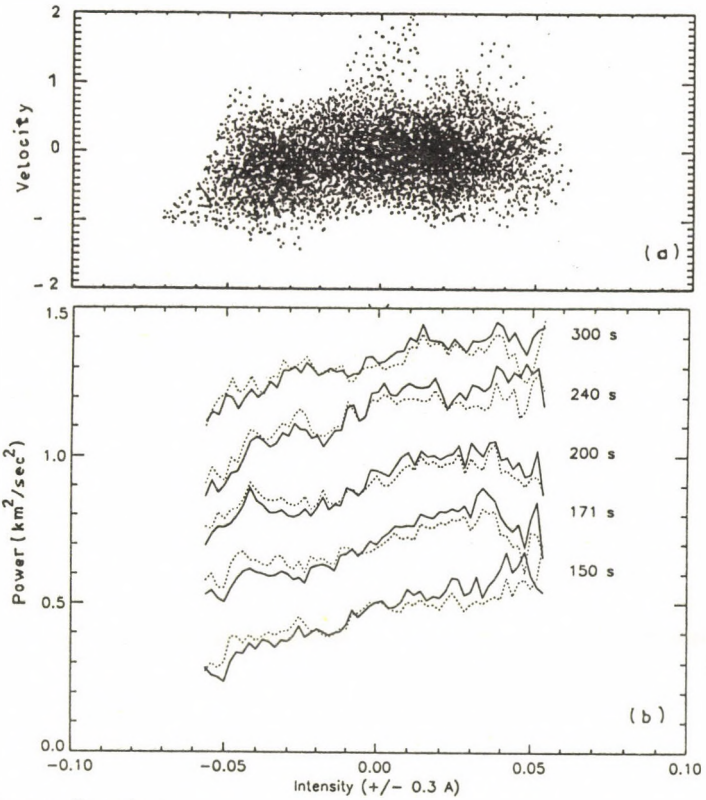

Figure 1

(a) Histogram I/V

(b) Variation of the energy power

Power Spectra

The time sequences have been apodized by a cosine bell function, after subtracting a linear baseline at each pixel location. The Fourier transform analysis has been made using the sum of the squares of the sine and the cosine terms.

The power spectrum of the *chromosphere* oberved near the disk center on May 5 (Figure 2 b) shows high energy in the low frequencies (longward of 260 s). Energy in the low frequency range could be due to convective energy generated in subphotospheric layers; von Uexküll *et al.* (1989) interpret such energy visible in the network cell boundary spectra by stochastic processes. Nevertheless we have to be careful in our interpretation because our data sets are relatively short. Near the limb the energy in the chromosphere is reduced by a factor of ~2 or more and the power spectrum presents a smooth peak around 200 s (Figure 2 a). It looks similar to the power spectra of both *filaments* which present only some energy around 200 s (Figure 2 a) or at 2 different periods 260 s and 130 s (Figure 2 b). Due to the orientation of the fine structures of the filaments, perpendicular (filament A) or parallel to the solar surface (filament B), the energy concerns mostly horizontal velocities. The oscillations are transverse.

With observations made on the disk, a main problem is to determine whether the

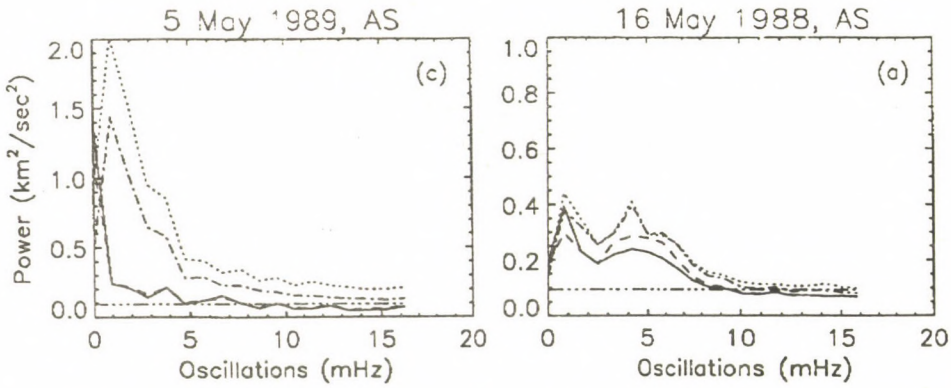

Figure 2 Power spectra in the chromosphere (dotted and dot-dashed lines) and in the filament (continuous and dashed lines).

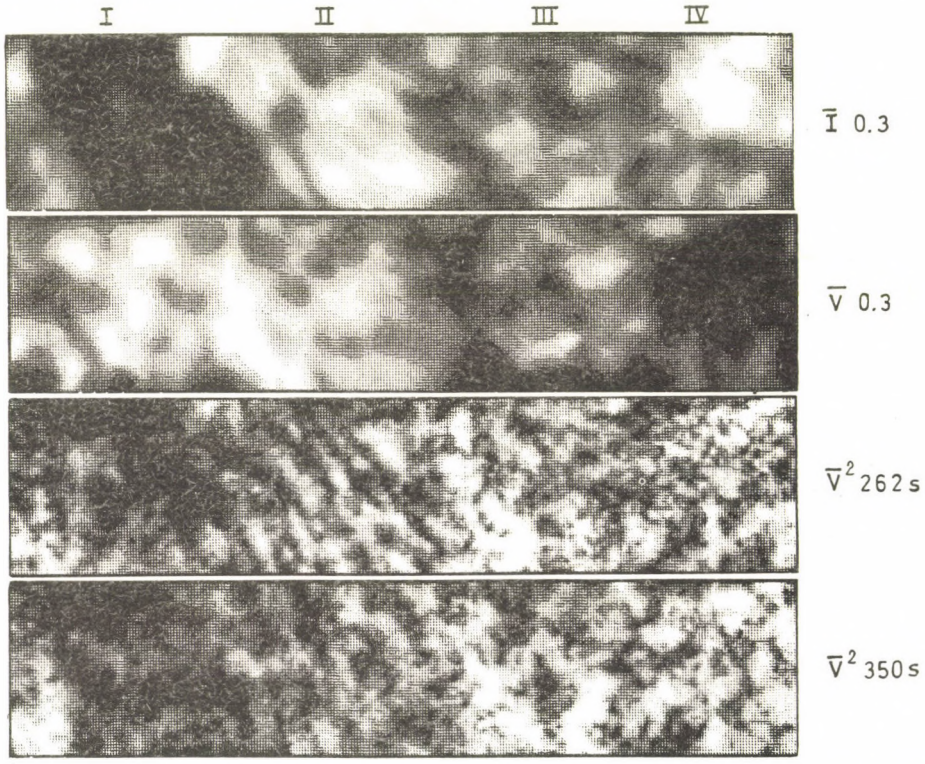

Figure 3 Intensity, Velocity at Hα ±0.3Å Energy at different frequencies. The filament is located in section I, the fibrils in section II

observations of the filaments are not contaminated by the chromospheric oscillations. To check this, we have computed the optical thickness of pixels located in the filaments using the "cloud model" technique presented first by Beckers (1964) and developed by Mein *et al.* (1985). The central values of the contrast profiles are between 0.225 and 0.4. Assuming a source function normalized by the minimum intensity equal to 0.5, we find a optical thickness τ_0 between 0.6 and 1.6 at $\Delta\lambda = 0$. With a larger value of S (0.7) as proposed by Cram (1989), τ_0 is larger than 1.3. Then for $\Delta\lambda = 0.3$ Å, $\tau(\Delta\lambda)$ is larger than 0.5. We can therefore estimate that the oscillations observed are mostly associated with the filament (Figure 1 b).

In the chromosphere close to the filament of 5 May 1989, a region containing horizontal fibrils, the power spectrum shows principally a large maximum around 250 s. That peak of energy is comparable with those observed in cell interiors (Deubner and Fleck, 1990 and von Uexküll *et al.* 1989). It corresponds to the chromospheric oscillations. The maps indicating the spatial distribution of the oscillatory power (Figure 3 section II) reveals that the energy is in fact well concentrated along the direction of the fibrils for some selected frequencies.

Results and Discussion

The Dopplershifts that we measure concern velocity perpendicular to the filamentary structures. The oscillations are principally transverse to the direction of the fine structures. That appears clearly in the fibrils. The situation in the filamentas is more confused, perhaps because of the large number of threads integrated along the line of sight.

These oscillations could be eigenmodes of the filamentary structures. Convection generates waves which propagate through the atmosphere. They excite surface waves in high gradient regions (temperature or density gradient at fibril boundaries) and a resonance phenomena occurs for discrete frequencies between these surface waves and body waves which could be Alfven waves. Another interpretation could be eigenmodes of the atmosphere, such as p-modes.

References

Beckers, J. M. (1964). PhD thesis, Utrecht University.

Cram, L. E. (1986). *Astrophys. J.* **300**, 830.

Deubner, F, I. and Fleck, B. (1990). *Astron. Astrophys.* **228**, 506.

Mein, P., Mein, N., and Malherbe, J. M. (1985). In *MPA/LPARL Workshop in Munchen*, page 303.

Schmieder, B. (1989). In Priest, E., editor, *Dynamics and Structure Of Quiescent Solar Prominences*, page 15. Kluwer Academic Publishers.

Thompson, W.T. and Schmieder,B. (1990). *Astron. Astrophys.* , , submitted.

Tsubaki, T. (1988). In Altrock, R. C., editor, *Solar and Stellar Coronal Structure and Dynamics, Sac Peak*, page 140.

von Uexkúll, M., Kneer, F., Malherbe, J. M., and Mein, P. (1989). *Astron. Astrophys.* **208**, 290.

OSCILLATIONS IN A COMPLEX UMBRA

Aballe Villero M.A.[1], García de la Rosa J.I.[1], Marco E.[2], Vázquez M.[1]

[1] *Instituto de Astrofísica de Canarias. 38200 La Laguna, Tenerife. Spain.*
[2] *Dept. Matemática Aplicada i Astronomía. Univ. Valencia. Spain*

1. Introducción

The study of the oscillatory behaviour of a complex umbra has been carried out with a particular emphasis on time evolution and spatial inhomogeneities.

2. Data

The observations were carried out at the Gregory-Coudé Telescope of the Observatorio del Teide (Tenerife), using a Reticon Diode Array (100 x 100 px) and with a spectral resolution of 14.5 mÅ/px. The studied spectral line was TiI 8396,9 Å, which shows umbral enhancement and a nearby telluric line. Series of spectra along two hours were recorded with 31.6 sec interval.

The spot, a part of active region NOAA 5047, was observed along five days (June 18 to 23, 1988) around its Central Meridian Passage. The Vacuum Newton Telescope, at the same observatory, provided high resolution pictures of the spot.

3. Results

After the process of reduction (see Aballe et al. 1989), power contours are obtained for each serie of observations. In Figure 1 those contours are represented in front of the corresponding draw of the slit-jaw picture. The ordinates represent angular distances along the slit with the position of the umbral cores clearly limited.

The main results are:

(1) The spectra of the oscillations show noticeable power at 3mHz (5 min) and less prominent peaks at 5-7 mHz ($\approx$ 3 min.).

(2) Different parts of the umbra show a distinct behaviour. Even the two different dark cores behave quite independently of each other.

(3) Following evolutionary changes of the spot, there are variations in the oscillation spectrum, with cases of redistribution of power between neighbouring frequencies.

References

Aballe Villero, M.A., García de la Rosa, J.I., Marco, E. and Vázquez, M.: 1990, *Astrophys. Space Sci.* in press.

SPOT AND SLIT POSITION

POWER SPECTRA CONTOURS

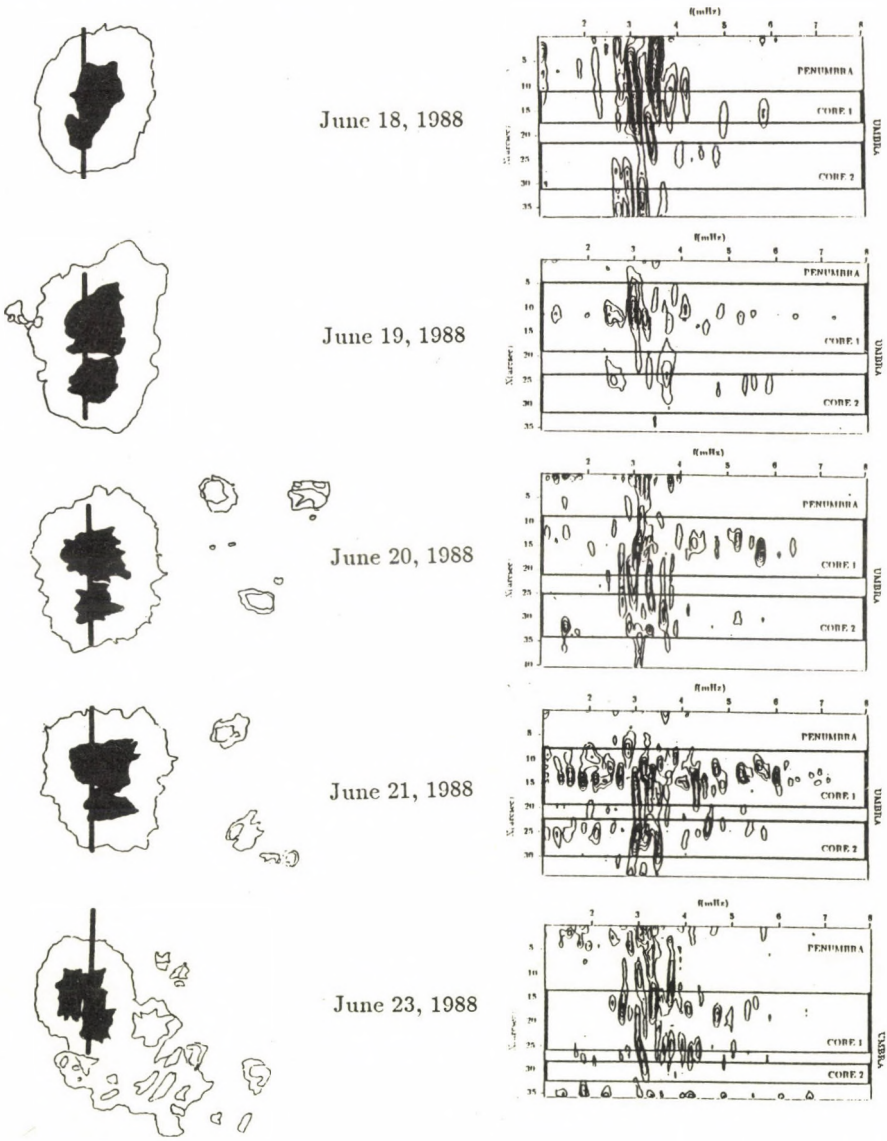

Figure 1. On the left hand side draws of the slit-jaw pictures. On the right hand side the corresponding power spectra contours are presented.

SEISMOLOGICAL DIAGNOSTICS OF SUNSPOT UMBRAL STRUCTURE

Jürgen Staude
Central Institute for Astrophysics of the GDR Academy of Sciences, Solar Observatory 'Einsteinturm', DDR-1560 Potsdam

Sunspot oscillations have attracted attention of astronomers for many years: Magneto-atmospheric waves are likely candidates for energy transport and heating in stellar atmospheres, moreover, they provide means of sounding the structure of atmospheric and subphotospheric layers. Sunspot provide a unique example of a magnetized atmosphere where up-to-date observational techniques enable us to resolve many details of such periodic disturbances and of the basic atmospheric structure as well, thus models of both waves and atmospheres can be tested. A long debate in the literature demonstrated that the observations of sunspot umbral oscillations are difficult to interpret. Only recently detailed model calculations of the propagation of magneto-atmospheric waves through realistic models of an umbral atmosphere and subphotosphere have solved many problems. The derived complex model as well as the underlying observations have been summarized by Staude et al. (1987) and Žugžda et al. (1987); the basic features of this model are now generally accepted (Campos, 1989; Evans and Roberts, 1990). The umbra seems to consist of a system of cavities or resonators which are more or less coupled and where various modes of magneto-atmospheric waves are partly trapped and partly transmitted. Immediately below the photosphere we have a region of linear transformation of different wave modes. At larger depths and heights we have a plasma parameter (ratio of sound speed and Alfvén speed) of $\beta \gg 1$ and $\beta \ll 1$, respectively; the different modes are decoupled and can be considered separately. In the photosphere and chromosphere we have a resonator for longitudinal, slow waves which are similar to sound waves but propagate only parallel to the strong vertical magnetic field. The predicted properties agree with those which are observed in the '3 min band' of closely packed sharp resonance peaks in

the power spectrum of velocity and intensity oscillations measured in umbral spectral lines. At subphotospheric depths two independent resonators are acting: A resonator for slow, quasi-transverse waves can explain the oscillations with periods $\gtrsim$ 20 min, while a resonator for fast (acoustic), quasi-longitudinal waves could result in the umbral 5 min oscillations. In the modelling details of the predicted oscillations depend critically on the assumed umbral structure. In this way we obtain a useful method of probing the basic umbral model by seismology, thus completing customary spectroscopic diagnostics. For instance,

- the extent between the temperature minimum (T_{min}) and the chromosphere-corona transition region (TR) determines the spectrum of resonance frequencies, thus providing a method to determine the temperature gradient in the umbral chromosphere (Žugžda et al., 1984);
- the values of T_{min} in umbral fine structures can be estimated by investigating the spectrum and the quality of their resonators (Locans et al., 1988);
- observations of UV lines provide information on the umbral TR, where the observed oscillations are probably concentrated in cold fine structure elements which occupy only a few percent of the volume (Staude et al., 1985).

References

Campos, L.M.B.C.: 1989, Mon. Not. R. astr. Soc. 241, 215.
Evans, D.J., Roberts, B.: 1990, Astrophys. J. 348, 346.
Locans, V., Škerse, D., Staude, J., Žugžda, Y.D.: 1988, Astron. Astrophys. 204, 263.
Staude, J., Žugžda, Y.D., Locans, V.: 1985, Solar Phys. 95,37.
Staude, J., Žugžda, Y.D., Locans, V.: 1987, in: 'The Sun', 10th ERAM, Praha 1987, Proc. Vol. 1, 161.
Žugžda, Y.D., Locans, V., Staude, J.: 1987, Astron.Nachr.308, 257.
Žugžda, Y.D., Staude, J., Locans, V.: 1984, Solar Phys. 91,219.

ON THE STRENGTH OF SHOCK WAVES IN THE SUN

Róbert Erdélyi
Eötvös University, Department of Astronomy
Budapest, Kun Béla tér 2, H-1083 Hungary

Abstract. We calculate the strength of weak shock waves with the aid of the Vernazza *et al.*(1981) model. For the period of the shocks about 45 s is found.

1. Introduction

It is well known that the high temperature of the solar chromosphere must be supported by some heating mechanism. Above the temperature minimum region the observations show a first slow, and then extremely steep increase in the temperature (Kalkofen 1989, Anderson *et al.*, 1989). For the calculations we accept a model where the net radiative cooling rate is equal to the dissipated energy of weak acoustic shock waves.

In order to derive an expression for the energy of the shocks we assumed that the waves have a roughly sawtooth shaped profile and we used the post shock termodynamical cycle given by Brinkley and Kirkwood (1947) and modified by Schatzman (1949) and Ulmschneider (1967, 1970, 1971).

In the limiting case of weak shocks, taking refraction into account (Osterbrock, 1961), this theory yields an expression for the height variation of the energy flux carried by a train of shocks of frequency ν:

$$\frac{dF_{mech}}{dh} = -2\frac{d\ln c_1}{dh}F_{mech} - \frac{1}{12}\gamma(\gamma+1)p_1\eta^3\nu \tag{1}$$

where γ is the ratio of specific heats, p_1 is the unperturbed pressure, c_1 is the sound speed and η is the strength of the shock.

On the other hand, on the basis of the Rankine-Hugoniot relation we have

$$F_{mech} = \rho_1 c_1^3 \eta^2 \nu t_0 \tag{2}$$

where t_0 is the characteristic time of the shock wave.

Substituting (2) into (1), in the particular case of hydrostatic equilibrium the expression for the strength of weak shocks is

$$\frac{d\eta}{dh} = -\frac{\eta}{2}\left[\frac{d\ln\gamma}{dh} - \frac{\gamma g}{2c_1^2} + \frac{3d\ln c_1}{dh} - \frac{1}{12t_0}\frac{(\gamma+1)\eta}{c_1}\right] \tag{3}$$

This equation is identical to the results of Ulmschneider (1970, 1971,), Bray *et al.*, (1974), Narain *et al.*, (1990) for shocks.

2.Results

Given an initial value of η one can integrate equation (3) numerically with the aid of an appropriate chromospheric model. We used the Vernazza *et al.*, (1981) model. Although the differences among the empirical models are quite large, in this analysis we find that the energy dissipated by weak shocks is enough to balance the net radiative losses in the low chromospheric region. The best agreement was found in the model 'C' (Fig. 1.), with a period of weak shocks of about 45 s (Fig. 2). A similar result for the period was found by Narain *et al.*, (1990) .

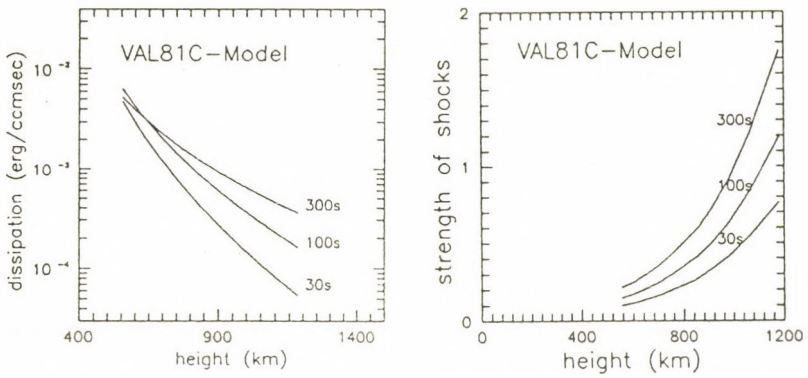

Fig. 1. The dissipated energy versus height for different periods.

Fig. 2. The strength of the shock versus height for different periods.

References

Anderson, L. S. *et al.*: 1989, *Ap. J.*, **336** , 1089.

Bray, R. J. *et al.*: 1974, The Solar Chromosphere, Chapman and Hall, London

Brinkley, S. R. *et al.*: 1947, *Phys . Rev.* **71** , 606.

Kalkofen, W. : 1989, The heating of the solar chromosphere (preprint)

Narain, U. *et al.*: 1990, *Space Sci. Rew.* (in press)

Osterbrock, D. E. : 1961, *Ap. J.* **134** , 347.

Schatzman, E. : 1949, *Ann. Astrophys.* **12** , 303.

Ulmschneider, P. : 1967, *Z. Astrophys.* **67** , 193.

Ulmschneider, P. : 1970, *Solar Phys.* **12** , 403.

Ulmschneider, P. : 1971, *Astron Astrophys* **14** , 275.

Vernazza, J. E. *et al.*: 1981, *Ap. J. Suppl.*, **45**, 635.

OBSERVATIONS OF WAVES AND OSCILLATIONS IN SOLAR FLUXTUBE CONCENTRATIONS

BERNHARD FLECK and FRANZ-LUDWIG DEUBNER
Institut für Astronomie und Astrophysik
Universität Würzburg
Am Hubland, D-8700 Würzburg, F.R.Germany

ABSTRACT. We investigate the dynamical behaviour of magnetic fluxtube concentrations by analyzing a high spatial resolution time series of spectra taken simultaneously in left-hand and right-hand circularly polarized light. The spectral range covered the lines of Fe 6302.5Å and Fe 6301.5Å. All parameters we have extracted from the Stokes V and Stokes I profiles reveal significant spatio-temporal variations. The dominant velocity signal derived from the Stokes I central wavelength and Stokes V zero-crossing wavelength are the 5 minute oscillations. We find large spatially and temporally varying differences between these two parameters (up to ±1 km/s), whereas their spatio-temporal averages are almost identical.

1. Introduction

Small-scale magnetic field concentrations play a fundamental role for almost all forms of solar activity and are considered to act as the most likely energy channels to heat the corona and the upper chromosphere (see e.g. Spruit and Roberts, 1983). A detailed insight into their dynamical behaviour is therefore of crucial importance for a proper understanding of all activity phenomena not only on the sun but also on other stars. With the new telescopes now being fully operational on the Canary Islands — a site where on can expect extended intervals of excellent seeing conditions — we started a novel project to study the physics of magnetic fluxtube concentrations. Our approach is complemetary to the one of the Zürich group who used FTS data obtained with the Mc Math telescope at Kitt Peak (Stenflo et al., 1984). While Stenflo, Solanki and coworkers have analyzed temporally and spatially averaged Stokes V and I spectra of hundreds of Fe I and II lines to derive information about the internal structure of fluxtubes (e.g. Solanki, 1986; Pantellini et al., 1988; Zayer et al., 1989), we address the problem of the *dynamical behaviour* of fluxtube concentrations by investigating *time series* of strictly simultaneously taken right-hand (I+V) and left-hand (I–V) circularly polarized spectra of several selected Fraunhofer lines with the *highest spatial* and *spectral resolution* achievable.

2. Observations and data reduction

The observations were obtained in October 1989 with the Vacuum Tower Telescope at Izaña, Tenerife, using the RCA CCD-camera and the Echelle spectrograph with an achromatic $\lambda/4$–plate and two calcites at $\pm 45^{\circ}$ immediately behind the entrance slit. The slit was positioned on a very active plage near disk center ($\mu \approx 0.98$). The projected slit width and length were 0.5 and 19.6 arcsec, respectively. The time series consists of 520 frames taken in intervals of 18.1 s with an exposure time of 1.75 s. The spatial and spectral resolution were 0.14 arcsec/pixel and 2.4 mÅ/pixel, respectively.

The spectra were corrected carefully for dark current and flat-field effects. Then the oppositely circularly polarized spectra were aligned in the spatial and spectral direction using

Fourier shift techniques, and after calibration they were added and subtracted to obtain Stokes I and Stokes V, respectively.

3. Results and discussion

In Fig.1 we have displayed the spatio-temporal behaviour of the Stokes V zero-crossing wavelength (left diagram) and of the difference between the core intensities of the (I+V) and (I–V) spectra (right diagram), a parameter which can be considered a measure of the asymmetry between the two polarization states. There were two fluxtube concentrations lying on the slit centered at about 5" and 11" where the Stokes V amplitude was high enough (> 1.5%) for a reliable interpretation. In the grey background no significant Stokes V signal has been detected. Note that, in this paper, we refer to fluxtube concentrations as clusters of fluxtubes, which Beckers and Schröter (1968) called "magnetic knots", rather than isolated concentrated structures ("solitary" fluxtubes).

The dominant oscillatory signal of the Stokes zero-crossing V_0 (as well as in all the other velocity data sets) are the 5-min oscillations (see Fig.1). The RMS of the Stokes I velocity and V_0 amounts to approximately 200 m/s and 150 m/s, respectively, which is about a factor of 2 to 3 less than the velocity RMS derived from the quiet sun. The signature of the 5-min oscillations in the zero-crossing wavelength has been reported earlier already by Giovanelli et al. (1978) and Wiehr (1985). Their observations, however, sampled an area of a few arcsec square. Here, we also present the spatial structure of these oscillations: The two magnetic concentrations do not oscillate in phase, and, more importantly, the left and the right edges of each structure reveal very often significant phase differences (see Fig.1). This leads to high spatial velocity gradients of up to 1 km/s across the magnetic fluxtubes concentrations, which demonstrate the presence of physically and dynamically independent substructures within them. These spatial gradients certainly cannot be accounted for by seeing effects.

A surprising result are the strong differences found between the (I+V) and (I–V) spectra in the magnetic structures (see the right diagram in Fig.1). These differences reveal a 300 s periodicity and vary significantly in the two structures (in the right structure the red Zeeman shifted profile is the deeper one most of the time). These fluctuations also lead to significant spatio-temporally varying differences between the Stokes I velocity and the Stokes V zero-crossing wavelength of up to $\pm$ 1 km/s by causing highly asymmetric Stokes I profiles. Such effects would not have been noticed by the previous investigations since only parts of the line profile were used to determine the velocity or V_0. The spatio-temporal averages of the Stokes I velocity and V_0, on the other hand, are almost identical: for Fe 6302.5Å we obtain a red shift of V_0 of approximately -150 m/s, and for Fe 6301.5Å only -10 m/s (in good agrement with the FTS observations of Solanki (1986)). From these findings we conclude that it is important to disentangle the various effects producing this asymmetry. Hence, in order to fully exploit the diagnostic value of the velocity information it is necessary to observe the complete (I+V) and (I–V) profiles with the highest spatial and temporal resolution achievable, otherwise essential information is lost.

Another interesting feature we have found are the strong spatial (and temporal) variations of the relative amplitude and area asymmetry δa_r and δA_r. In most spectra, the amplitude asymmetry typically increases from about 3 to 5% in the center of the magnetic structure to more than 15% towards the edges. This finding is in good agreement with theoretical predictions of Solanki (1989).

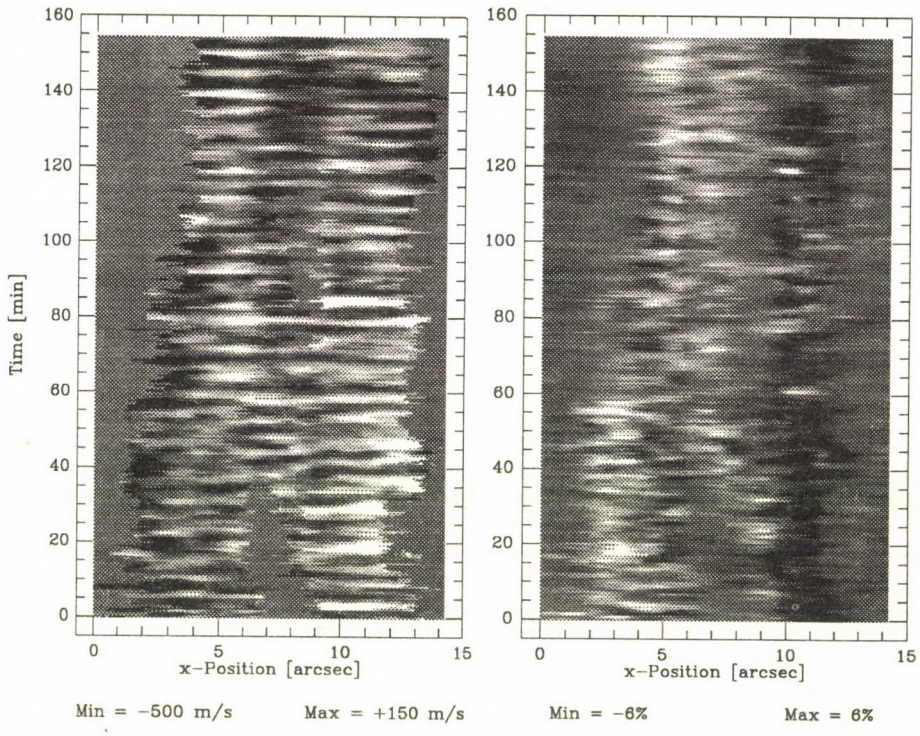

Fig.1: Spatio-temporal behaviour of the Stokes V zero-crossing wavelength V_0 (left diagram) and of the core intensity difference between (I+V) and (I–V) (right diagram). The Min/Max numbers are not the absolute minimum or maximum values of the corresponding data sets but the limits of the grey scale mapping.

A more detailed paper including also a comprehensive power and phase analysis is in preparation for Astronomy and Astrophysics.

4. References

Beckers, J.M., Schröter, E.H.: 1968, Solar Phys. **4**, 142

Giovanelli, R.G., Livingston, W.C., Harvey, J.W.: 1978, Sol. Phys. **59**, 49

Pantellini, F.G.E., Solanki, S., Stenflo, J.O.: 1988, Astron. Astrophys. **189**, 263

Solanki, S.: 1986, Astron. Astrophys. **168**, 311

Solanki, S.: 1989, Astron. Astrophys. **224**, 225

Spruit, H.C., Roberts, B.: 1983, Nature **304**, 401

Stenflo, J.O., Harvey, J.W., Brault, J.W., Solanki, S.: 1984, Astron. Astrophys. **131**, 333

Wiehr, E.: 1985, Astron. Astrophys. **149**, 217

Zayer, I., Solanki, S., Stenflo, J.O.: 1989, Astron. Astrophys. **211**, 463

Author Index

A MAGYAR TUDOMÁNYOS AKADÉMIA
CSILLAGÁSZATI KUTATÓINTÉZETE
DEBRECENI
NAPFIZIKAI OBSZERVATÓRIUMÁNAK
KÖZLEMÉNYEI

7. KÖTET (1990)

"A dinamikus Nap"
címmel
Debrecenben, 1990 május 21-24 között
rendezett konferencia anyaga

Felelös kiadó: Szeidl Béla igazgató

Hozott anyagról sokszorosítva

9019516 MTA Sokszorosító, Budapest. F. v.: dr. Héczey Lászlóné

Group Photo of Participants

EPS SOLAR MEETING, DEBRECEN, MAY 21-24,1990

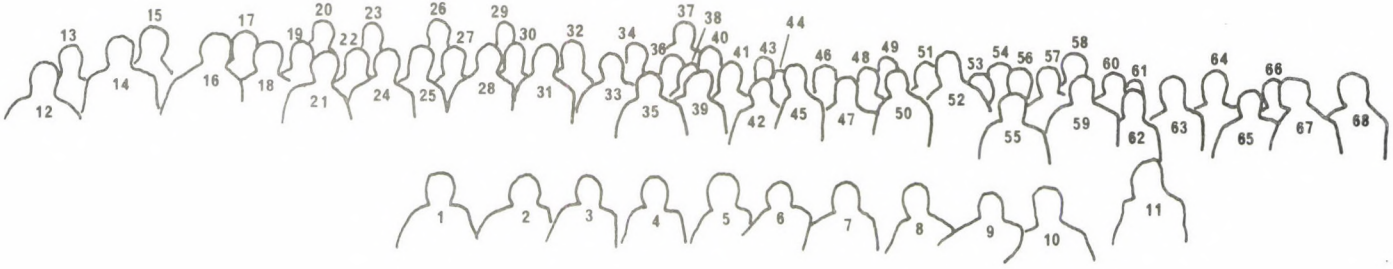

1 Garcia de la Rosa,J.I.
2 Faurobert-Scholl,M.
3 van Driel-Gesztelyi,L.
4 Rutten,R.J.
5 Mason,H.E.
6 Erdélyi,R.
7 Muller,R.
8 Marik,M.
9 Kurths,J.
10 Oncica,A.
11 Aboudarham,J.
12 Baranyi,T.
13 Ludmány,A.
14 Maltby,P.
15 Kálmán,B.
16 Fleck,B.
17 Bumba,V.
18 Hofmann,A.
19 Kliem,B.
20 Auffret,H.
21 Gabriel,A.
22 Cugnon,P.
23 Scholl,H.
24 Foing,B.
25 Galsgaard,K.
26 Pintér,T.
27 Nagelis,J.
28 Wöhl,H.
29 Petrovay,K.
30 Deubner,F.-L.
31 De Bruyne,P.J.I.
32 Fludra,A.
33 Belvedere,G.
34 Kneer,F.
35 Mattig,W.
36 Ballester,J.L.
37 Pettauer,T.
38 Lemaire,Ph.
39 Kurt,V.
40 Greimel,R.
41 Benz,A.O.
42 Dezső,L.
43 Messerotti,M.
44 Pohjolainen,S.
45 Chiuderi,C.
46 Nesis,A.
47 Schmieder,B.
48 Krüger,A.
49 Ruždjak,V.
50 Trottet,G.
51 Zlobec,P.
52 Seehafer,N.
53 Bely-Dubau,F.
54 Rušin,V.
55 Ambrož,P.
56 Dumitrache,C.
57 Altas,L.
58 Zwaan,C.
59 Lantos,P.
60 Heinzel,P.
61 Edwin,P.
62 Rigaud,D.
63 Kovács,Á.
64 McClements,K.G.
65 Marmolino,C.
66 Arena,P.
67 Abuzeid,B.
68 Staude,J.

Publications of Debrecen Heliophysical Observatory

Vol.	*No.*	Topic	Year	Page
1	*1 - 4*	Statistical Investigation of Sunspots	1964	1-108
	5 et seq. follows			
2	-	Proceedings of the 6th Regional Consultation on Solar Physics	1971	1-217
3	-	Proceedings of the Intercosmos Symposium on Solar Physics	1977	1-310
4	*1 - 2*	Sunspot Group Development	1980-1981	1 - 60
	3 et seq. follows			
5	-	Proceedings of the 11th Regional Consultation on Solar Physics (in two parts)	1983	1-666
6	*1*	(Solar spectral line profiles)	1986	1 - 38
	2 et seq. follows			
7	-	Proceedings of the EPS 6th Solar Meeting The Dynamic Sun	1990	1-312

Heliographic Series

No.1	Debrecen Photoheliographic Results for the Year 1977	1987	1-242

No.2 et seq. follows